James M. Kelly
Dimitrios A. Konstantinidis

MECHANICS OF RUBBER BEARINGS FOR SEISMIC AND VIBRATION ISOLATION

WILEY

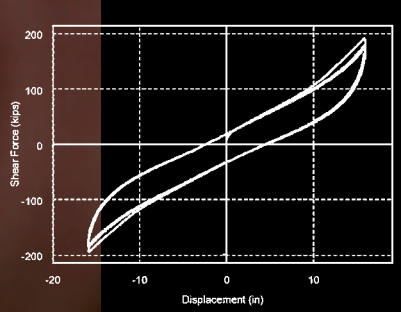

Mechanics of Rubber Bearings for Seismic and Vibration Isolation

Mechanics of Rubber Bearings for Seismic and Vibration Isolation

James M. Kelly

University of California, Berkeley, USA

Dimitrios A. Konstantinidis

McMaster University, Hamilton, Canada

WILEY

A John Wiley & Sons, Ltd., Publication

This edition firs published 2011

Registered offic
John Wiley & Sons Ltd, The Atrium, Southern Gate, Chichester, West Sussex, PO19 8SQ, United Kingdom

Library of Congress Cataloging-in-Publication Data

Kelly, James M.
Mechanics of rubber bearings for seismic and vibration isolation / James M. Kelly, Dimitrios A. Konstantinidis.
p. cm.
Includes bibliographical references and index.
ISBN 978-1-119-99401-5 (hardback)
1. Seismic waves – Damping. 2. Vibration. 3. Rubber bearings. I. Konstantinidis, Dimitrios. II. Title.
TJ1073.R8K45 2011
620.3′7–dc23 2011013205

A catalogue record for this book is available from the British Library.

Print ISBN: 9781119994015
ePDF ISBN: 9781119971887
oBook ISBN: 9781119971870
ePub ISBN: 9781119972808
Mobi ISBN: 9781119972815

Set in 10/12.5pt Palatino by Aptara Inc., New Delhi, India.

Contents

About the Authors

James M. Kelly is Professor Emeritus at the University of California at Berkeley. His undergraduate education was completed at the University of Glasgow, his Master's degree at Brown University and his PhD at Stanford University. He has been a faculty member in the Department of Civil and Environmental Engineering at U.C. Berkeley since 1965. He did pioneering work in dislocation mechanics, dynamic plasticity, impact, and wave propagation. He has carried out numerous large-scale experimental studies of isolation systems, structures with energy-absorbing devices, and structures with piping systems on the large shaking table at the Earthquake Engineering Research Center (EERC) of U.C. Berkeley. In 1971 he developed the firs energy-dissipating devices to be used in earthquake-resistant structures. Since then he has led the way in experimental investigations of seismic-isolation rubber bearings, conducting many pioneering studies of seismically isolated structures. In testing hundreds of bearings, he achieved numerous advances, including the application of high-damping rubber for seismic-isolation bearings—used in the firs U.S. isolated building and in many buildings and bridges around the world. He has developed theoretical analyses of the dynamic and ultimate behavior of elastomeric seismic isolation at large deformation. He led the development of energy-absorbing devices for the seismic protection of tall structures for which base isolation is not feasible. His test programs have included the firs U.S. shake-table investigations of the response of structures containing energy dissipaters, and he has conducted component and system-level experimental and analytical research on many concepts, including yielding steel, friction, viscoelastic, viscous, shape-memory alloy and electro-rheological systems.

Professor Kelly was instrumental in several of the early U.S. energy dissipation applications, consulted on the implementation of viscous dampers for the suspended spans of the Golden Gate Bridge and for the firs major U.S. building damper project, the Santa Clara County Civic Center Building, which was retrofitte with viscoelastic dampers following the Loma Prieta earthquake. He worked to develop seismic isolation for low-cost housing in developing countries as a consultant to the United Nations (UNIDO), and has consulted on projects in Armenia, Chile, China, India, and Indonesia, where isolation has been used for residential construction. He was the firs in the U.S. to start teaching university-level courses on seismic isolation and energy dissipation. He has conducted short courses and seminars on isolation and energy dissipation worldwide.

His work, which formed the basis for significan advances in the analysis and design of seismic isolation and energy-dissipation systems, is the foundation for many of the base-isolation design codes used today, including UBC, IBC, and CBC. Base isolation has been used for seismic retrofi of major buildings in the U.S., including important historic structures such as the city halls of Salt Lake City, Oakland, San Francisco, Los Angeles, and the Hearst Memorial Mining Building in Berkeley, on all of which he was a peer reviewer.

Professor Kelly, well recognized as an outstanding teacher and lecturer, has directed over thirty doctoral students in their PhD thesis research who have gone on to become noted practitioners, university professors, and researchers worldwide. Many Fulbright Visiting Scholars have come to Berkeley to work with him. In 1996 he published the second edition of his book based on his many years of research and testing at EERC (*Earthquake-resistant Design with Rubber*, 2nd edn Springer-Verlag). In 1999 he published with Dr Farzad Naeim a textbook on the design of seismic isolated buildings (*Design of Seismic Isolated Structures*, John Wiley). He has published over 360 papers over the course of his career.

Dimitrios A. Konstantinidis is an Assistant Professor at McMaster University. He received his Bachelor's (1999), Master's (2001), and PhD (2008) degrees from the Department of Civil and Environmental Engineering at U.C. Berkeley. His research interests and experience lie in the fiel of engineering mechanics and earthquake engineering with a primary emphasis on seismic isolation, energy dissipation devices, rocking structures, response and protection of building equipment and contents, and structural health monitoring.

As a masters student he became interested in the study of rocking structures and conducted research that led to the co-development, with Professor Nicos Makris, of the *rocking spectrum*—a concept analogous to the response spectrum for the single-degree-of-freedom oscillator. He has investigated the seismic response of multi-drum columns, such as those found in ancient temples in Greece, Western Turkey, and Southern Italy, and proposed recommendations against accepted, but unconservative, standard practice in the restoration world. In the earlier stages of his doctoral work, as part of a multi-disciplinary effort to assess the seismic vulnerability of biological research facilities, he investigated the seismic response of freestanding and anchored laboratory equipment, which included an extensive experimental program of shaking table tests of full-scale prototypes and quarter-scale models of equipment. In the later stages of his doctoral work, he begun working with Professor James M. Kelly. He has studied the effect of the isolation type on the response of internal equipment in a base-isolated structure. He has conducted research on the seismic response of bridge bearings which are traditionally used to accommodate various non-seismic translations and rotations of the bridge deck. These included *steel-reinforced rubber bearings*, *steel-reinforced rubber bearings with Teflo sliding disks*, and *woven-Teflo spherical bearings*. The work included seismic-demand-level dynamic tests at U.C. San Diego and U.C. Berkeley, as well analytical investigations and nonlinear finit element analyses utilizing adaptive remeshing techniques to study the behavior of bonded and unbonded rubber bearings under different loading actions. The finding of the study are being used by Caltrans to develop a new

Memo to Designers guideline and support the development of LRFD-based analysis and design procedures for bridge bearings and seismic isolators. The excellent seismic behavior of rubber bridge bearings, which cost less than a tenth of what rubber seismic isolations cost, has prompted him and Professor Kelly to actively promote the use of these bearing as a low-cost alternative for seismic isolation in developing countries, where the cost of conventional isolators is prohibitive.

He has conducted postdoctoral research at U.C. Berkley focusing on the development of a health monitoring scheme for viscous flui dampers in bridges using wireless and wired communication. The study involved indoor and outdoor experiments on instrumented flui dampers. The monitoring system that was developed is being assessed by Caltrans for deployment on testbed bridges.

Before joining the civil engineering faculty at McMaster University in 2011, he was Postdoctoral Fellow at the Lawrence Berkeley National Laboratory, University of California. His work there concentrated on the base isolation of nuclear power plants and on the evaluation of the U.S. Nuclear Regulatory Commission's current regulations and guidance for large, conventional Light-water Reactor (LWR) power plants to a new generation of small modular reactor (SMR) plants.

Professor Konstantinidis is a member of various professional societies and a reviewer in technical journals, including *Earthquake Engineering and Structural Dynamics* and *Journal of Earthquake Engineering*. He has authored 30 publications in refereed journals, in conference proceedings and as technical reports.

Preface

The multilayer rubber bearing is an apparently simple device that is used in a wide variety of industries that include civil, mechanical and automotive engineering. It is so ubiquitous that it may be difficul to believe that it is a relatively recent development, having been used for only about fift years. The idea of reinforcing rubber blocks by thin steel plates was firs proposed by the famous French engineer Eugène Freyssinet (1879–1962). He recognized that the vertical capacity of a rubber pad was inversely proportional to its thickness, while its horizontal flexibilit was directly proportional to it. He is best known for the development of prestressed concrete and for the discovery of creep in concrete. It is possible that his invention of the reinforced rubber pad was driven by the need to accommodate the shrinkage of the deck due to creep and prestress load, while sustaining the weight of a prestressed bridge deck. He obtained a French patent in 1954 for his invention, and within a few years the concept was adopted worldwide and led to the extraordinary variety of applications in which multilayer rubber bearings are used today.

These reinforced rubber bearings in their various forms are a source of fascinating problems in solid mechanics. It is the combination of vertical stiffness and horizontal flexibilit , achieved by reinforcing the rubber by thin steel plates perpendicular to the vertical load, that enables them to be used in many applications, including the seismic protection of buildings and bridges and the vibration isolation of buildings and machinery. The horizontal, vertical, and bending stiffnesses are important to the design of bearings for these applications and for predicting the buckling load, the interaction between vertical load and horizontal stiffness, and the dynamic response of structures and equipment mounted on the bearings.

We will cover the theory for vertical stiffness in Chapter 2 and for bending stiffness in Chapter 3. Some of the results in these two chapters are new. The results of Chapters 2 and 3 are used to predict the stresses in the steel reinforcing plates in Chapter 4. The analysis used to calculate these stresses is new to this text and was only recently developed by the authors. Also new and original to this text is the development of a theory for these stresses when the effect of the bulk compressibility of the rubber is included, which is necessary for seismic isolation bearings, but usually not for vibration isolation bearings. In Chapter 5 we study the stability of these bearings, showing

how to estimate buckling loads and the interaction between vertical load and horizontal stiffness as well as a new way to calculate the effect of horizontal displacement on the vertical stiffness. One unexpected aspect of these bearings is that they can buckle in tension, and this is covered in Chapter 6. Chapter 7 is concerned with the influenc of the flexibilit of the reinforcing plates on the buckling load. This could be important in efforts to reduce the weight of bearings in the possible application to low-cost housing. Chapters 8 and 9 present some recent research work by the authors on the mechanics of bearings that are not bonded to their supports, but are held in place by friction. This research includes some experimental work on bearings of this type used as bridge bearings.

The original work on the mechanics of rubber bearings was done at the Malaysian Rubber Producers Research Association (MRPRA, now the Tun Abdul Razak Research Centre) in the United Kingdom in the 1960s under the leadership of Dr A.G. Thomas and Dr P.B. Lindley and applied firs to bridge bearings and then to the vibration isolation of residences, hospitals and hotels in the United Kingdom.

The firs building to be isolated from low-frequency ground-borne vibration using natural rubber was an apartment block built in 1966 directly above a station of the London Underground. Many such projects have been completed in the United Kingdom using natural rubber isolators, including a low-cost public housing complex adjacent to two eight-track railway lines that carry 24-hour traffic Several hotels have been completed using this technology, and a number of hospitals have been built with this approach. More recently, vibration isolation has been applied to concert halls.

Some time later MRPRA suggested the use of bearings for the protection of buildings against earthquakes. Dr C.J. Derham, of MRPRA, approached Professor J.M. Kelly and asked him if he was interested in conducting shaking table tests at the Earthquake Simulator Laboratory at the Earthquake Engineering Research Center (EERC), University of California at Berkeley, to see to what extent natural rubber bearings could be used to protect buildings from earthquakes. Very quickly they conducted such a test using a 20-ton model and handmade isolators. The results from these early tests were very promising and led to the firs base-isolated building in the United States, also the firs building in the world to use isolation bearings made from high-damping natural rubber developed for this project by MRPRA.

The mathematical complexity in the text varies in different parts of the book, depending on which aspects of the bearings are being studied, but the reader should be assured that no more complicated mathematics than absolutely necessary to address the problem at hand has been used.

This text has been written for structural engineers, acoustic engineers and mechanical engineers with an interest in applying isolation methods to buildings, bridges and industrial equipment. If they have a background in structural dynamics and an interest in structural mechanics, they will fin that much of the analysis in the text may be applied to their work. The text can be used as supplementary reading for graduate courses and as a introduction to dissertation research.

It will also be useful to those who are charged with preparing or updating design rules and design guidelines for isolated bridges and buildings. The text is the firs that attempts to bring together in one place the mechanics of rubber bearings now widely scattered in many journals and reports.

www.wiley.com/go/kelly

James M. Kelly
Dimitrios A. Konstantinidis
Berkeley, California

1

History of Multilayer Rubber Bearings

Multilayer rubber bearings are widely used in civil, mechanical and automotive engineering. They have been used since the 1950s as thermal expansion bearings for highway bridges and as vibration isolation bearings for buildings in severe acoustic environments. Since the early 1980s, they have been used as seismic isolation devices for buildings in highly seismic areas in many countries. Their appeal in these applications is the ability to provide a component with high stiffness in one direction and high flexibilit in one or more orthogonal directions. The idea of using thin steel plates as reinforcement in rubber blocks was apparently suggested by the famous French engineer Eugène Freyssinet (1879–1962). He recognized that the vertical capacity of a rubber pad was *inversely* proportional to its thickness, while its horizontal flexibilit was *directly* proportional to the thickness. He is of course best known for the development of prestressed concrete, but also for the discovery of creep in concrete. It is possible that his invention of the reinforced rubber pad was driven by the need to accommodate the shrinkage of the deck due to creep and the prestress load while sustaining the weight of a prestressed bridge deck. In any case, he obtained a French patent in 1954 for "Dispositif de liaison élastique à un ou plusieurs degrés de liberté" (translated as "Elastic device of connection to one or more degrees of freedom"; Freyssinet 1954; the patent, with an English translation, is given in the Appendix). It seems from his patent that he envisaged that the constraint on the rubber sheets by the reinforcing steel plates be maintained by friction. However, in practical use a more positive connection was desired, and by 1956 bonding of thin steel plates to rubber sheets during vulcanization was adopted worldwide and led to the extraordinary variety of applications in which rubber pads are used today.

This combination of horizontal flexibilit and vertical stiffness, achieved by reinforcing the rubber by thin steel shims perpendicular to the vertical load, enables them to be used in many applications, including seismic protection of buildings and bridges and vibration isolation of machinery and buildings.

Mechanics of Rubber Bearings for Seismic and Vibration Isolation, First Edition. James M. Kelly and Dimitrios A. Konstantinidis.

The isolation of equipment from vibration via anti-vibration mounts is a well-established technology, and the theory and practice are covered in several books, papers, and reviews; the survey by Snowden (1979) is an example. Although the isolated machine is usually the source of the unwanted vibrations, the procedure can also be used to protect either a sensitive piece of equipment or an entire building from external sources of vibration. The use of vibration isolation for entire buildings originated in the United Kingdom and is now well accepted throughout Europe and is beginning to be used in the United States. Details of this method of building construction can be found in Grootenhuis (1983) and Crockett (1983).

The predominant disturbance to a building by rail traffi is a vertical ground motion with frequencies ranging from 25 to 50 Hz, depending on the local soil conditions and the source. To achieve a degree of attenuation that takes the disturbance below the threshold of perception or below the level that interferes with the operation of delicate equipment (e.g., an electron microscope), rubber bearings are designed to provide a vertical natural frequency for the structure about one-third of the lowest frequency of the disturbance.

The firs building to be isolated from low-frequency ground-borne vibration using natural rubber was an apartment block built in London in 1966. Known as Albany Court, this building is located directly above the St James' Park Station of the London Underground. This project was experimental to a certain extent, and the performance and durability of the isolation system in the years since its construction was monitored for several years by the Malaysian Rubber Producers Research Association (MRPRA, now the Tun Abdul Razak Research Centre) in conjunction with Aktins Research and Development (Derham and Waller 1975).

Since then, many projects have been completed in the United Kingdom using natural rubber isolators. These have included Grafton 16, a low-cost public housing complex that was built on a site adjacent to two eight-track railway lines that carry 24-hour traffic In this project the isolators produced a vertical frequency of 6.5 Hz to isolate against ground motion in the 20 Hz range. Several hotels have been completed using this technology, for example, the Holiday Inn in Swiss Cottage in London. In addition, a number of hospitals have been built with this approach, which is particularly advantageous when precision diagnostic equipment is present.

More recently, vibration isolation has been applied for use in concert halls. In 1990, the Glasgow Royal Concert Hall, which is sited directly above two underground railway lines, was completed in Glasgow, Scotland. The building has a reinforced concrete structural frame that is supported on 450 natural rubber bearings. In addition to housing the 2850-seat concert hall, it also contains a conference hall and a number of restaurants.

Another concert hall is the International Convention Centre in Birmingham, England, which was completed in 1991. Home of the City of Birmingham Symphony Orchestra, the building comprises ten conference halls and a 2211-seat concert hall. The entire complex was built at a cost of £121 million and is supported on 2000 natural rubber bearings to isolate it from noise from a main line railway running in a tunnel near the site.

The International Congress Center (ICC) in Berlin (Figure 1.1), Germany, constructed between 1970 and 1979, was Berlin's largest post-war project. It is 320 m (1050 ft) long, 80 m (260 ft) across and 40 m (130 ft) high. It has a cubic content of 800 000 m^3 (1 000 000 yd^3), and the total weight of steel in the roof is 8500 tons (18700 kips). A

Figure 1.1 The International Congress Center (ICC) in Berlin, Germany. Reproduced from Hans-Georg Weimar, Wikimedia

"box-in-box" construction, developed specially for this center, permits several functions to be held simultaneously under one roof. The building is supported on neoprene bearings (Figure 1.2) which range in size up to 2.5 m in diameter that can carry loads of 8000 tons (17600 kips; Freyssinet International 1977). They were constructed in segments which were placed in position with space between the segments to allow for bulging of the neoprene layers – described in the literature on the center as *a kind of architectural*

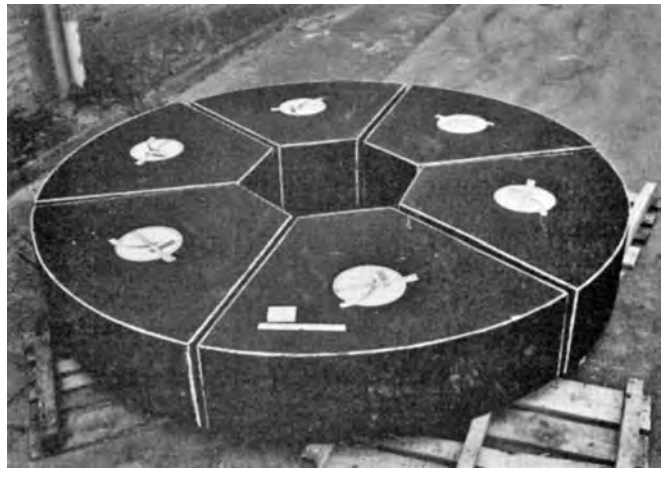

Figure 1.2 2.5-m diameter bearing for the ICC Berlin. Reproduced by permission of Freyssinet, Inc.

shock absorber – and were intended to exclude outside noise and absorb vibrations from an adjacent highway and railway. ICC Berlin has over 80 halls and conference rooms, with seating capacities ranging from 20 to 5000, with a sophisticated information and direction system. The largest hall (Hall 1) can seat up to 5000 and has the second-largest stage in Europe.

Two recent applications of vibration isolation to concert halls in the United States are the Benaroya Concert Hall in Seattle, Washington, completed in 1999 and the Walt Disney Concert Hall in Los Angeles, California, completed in 2003. The firs uses rubber bearings to mitigate ground-borne noise from trains in a tunnel below the hall. The Walt Disney Concert Hall is built directly above a loading dock for an immediately adjacent building. The interesting thing about these two buildings is that they are located in highly seismic areas, yet there was no attempt on the part of the structural engineers for either project to combine both vibration isolation and seismic isolation in the same system. Experimental results of tests done at the shake table at the Earthquake Engineering Research Center of the University of California, Berkeley, many years before the construction of these two concert halls, demonstrated that it was possible to design a rubber bearing system that would provide both vibration isolation and seismic protection. In the concert hall projects, lateral movement of the bearings that support the buildings is prevented by a system of many vertically located bearings, the additional cost of which is substantial and could have been avoided by appropriate design.

Seismic isolation can also be provided by multilayer rubber bearings that, in this case, decouple the building or structure from the horizontal components of the ground motion through the low horizontal stiffness of the bearings, which give the structure a fundamental frequency that is much lower than both its fixed-bas frequency and the predominant frequencies of the ground motion. The firs dynamic mode of the isolated structure involves deformation only in the isolation system, the structure above being to all intents and purposes rigid. The higher modes that produce deformation in the structure are orthogonal to the firs mode and, consequently, to the ground motion (Kelly 1997). These higher modes do not participate, so that if there is high energy in the ground motion at these higher frequencies, this energy cannot be transmitted into the structure. The isolation system does not absorb the earthquake energy, but rather deflect it through the dynamics of the system. This type of isolation system works when the system is linear, and even when undamped; however, a certain level of damping is beneficia to suppress any possible resonance at the isolation frequency. This damping can be provided by the rubber compound itself through appropriate compounding. The rubber compounds in common engineering use have an intrinsic energy dissipation equivalent to 2–3% of linear viscous damping, but in compounds referred to as *high-damping rubber* this can be increased to 10–20% (Naeim and Kelly 1999).

The firs use of rubber for the earthquake protection of a structure was in an elementary school, completed in 1969 in Skopje, in the Former Yugoslav Republic of Macedonia (see Figure 1.3). The building is a three-story concrete structure that rests on large blocks of natural rubber (Garevski *et al.* 1998). Unlike more recently developed rubber bearings, these blocks are completely unreinforced so that the weight of the building causes them to bulge sideways (see Figure 1.4). Because the vertical and horizontal stiffnesses of the system are about the same, the building will bounce and rock backwards and forwards in an earthquake. These bearings were designed when the technology for reinforcing

Figure 1.3 The firs rubber isolated building: the Pestalozzi elementary school completed in 1969 in Skopje. Courtesy of James M. Kelly. NISEE Online Archive, University of California, Berkeley

rubber blocks with steel plates – as in bridge bearings – was neither highly developed nor widely known, and this approach has not been used again. More recent examples of isolated buildings use multilayered laminated rubber bearings with steel reinforcing layers as the load-carrying component of the system. These are easy to manufacture, have

Figure 1.4 Unreinforced bearing in the Pestalozzi school building in Skopje. Courtesy of James M. Kelly. NISEE Online Archive, University of California, Berkeley

Figure 1.5 Foothill Communities Law and Justice Center, Rancho Cucamonga, California. Courtesy of James M. Kelly. NISEE Online Archive, University of California, Berkeley

no moving parts and are extremely durable. Many manufacturers guarantee lifetimes of around 50 or 60 years.

The firs base-isolated building to be built in the United States was the Foothill Communities Law and Justice Center (FCLJC), a legal services center for the County of San Bernardino that is located in the city of Rancho Cucamonga, California, about 97 km (60 miles) east of downtown Los Angeles (see Figure 1.5). In addition to being the firs base-isolated building in the United States, it is also the firs building in the world to use isolation bearings made from high-damping natural rubber (Derham and Kelly 1985) (Figure 1.6). The FCLJC was designed with rubber isolators at the request of the County of San Bernardino. The building is only 20 km (12 miles) from the San Andreas fault, which is capable of generating very large earthquakes on its southern branch. This fault runs through the county, and, as a result, the county has had for many years one of the most thorough earthquake-preparedness programs in the United States. Approximately 15 794 m^2 (170 000 ft^2), the building is four stories high with a full basement and was designed to withstand an earthquake with a Richter magnitude 8.3 on the San Andreas fault. A total of 98 isolators were used to isolate the building, and these are located in a special sub-basement. The construction of the building began in early 1984 and was completed in mid-1985 at a cost of $38 million (Tarics *et al.* 1984). Since then, many new buildings have been built in the United States on seismic isolation systems.

The same high-damping rubber system was adopted for a building commissioned by Los Angeles County, the Fire Command and Control Facility (FCCF), shown in Figure 1.7. This building houses the computer and communications systems for the fi e emergency services program of the county and is required to remain functional

Figure 1.6 Natural rubber isolator for the Foothill Communities Law and Justice Center showing laminated construction. Courtesy of James M. Kelly. NISEE Online Archive, University of California, Berkeley

during and after an extreme earthquake. The decision to isolate this building was based on a comparison between conventional and isolation schemes designed to provide the same degree of protection. On this basis the isolated design was estimated to cost 6% less than the conventional design (Anderson 1989). For most projects an isolated design generally costs around 5% more when compared with a conventional code

Figure 1.7 Fire Command and Control Facility, Los Angeles, California. Courtesy of James M. Kelly. NISEE Online Archive, University of California, Berkeley

design; however, the design code provides a minimum level of protection against strong ground shaking, guaranteeing only that the building will not collapse. It does not protect the building from structural damage. When equivalent levels of design performance are compared, an isolated building is always more cost effective. Additionally, these are the primary costs when contemplating a structural system and do not address the life-cycle costs, which are also more favorable when an isolation system is used as compared to conventional construction.

A second base-isolated building, also built for the County of Los Angeles, is at the same location as the FCCF. The Emergency Operations Center (EOC) is a two-story steel braced-frame structure isolated using 28 high-damping natural rubber bearings provided by the Bridgestone Engineered Products Co., Inc.

The most recent example of an isolated emergency center is the two-story Caltrans/CHP Traffi Management Center in Kearny Mesa near San Diego, California (Walters *et al.* 1995). The superstructure has a steel frame with perimeter concentrically braced bays. The isolation system, also provided by Bridgestone, consists of 40 high-damping natural rubber isolators. The isolators are 60 cm (24 in) in diameter.

The use of seismic isolation for emergency control centers is clearly advantageous since these buildings contain essential equipment that must remain functional during and after an earthquake. They are designed to a much higher level of performance than conventional buildings, and the increased cost for the isolators is easily justified Other examples are the San Francisco 911 Center and the Public Safety Building in the city of Berkeley, California.

Other base-isolated building projects in California include a number of hospitals. The M. L. King Jr–C. R. Drew Diagnostics Trauma Center in Willowbrook, California, is a 13 006 m^2 (140 000 ft^2), five-stor structure supported on 70 high-damping natural rubber bearings and 12 sliding bearings with lead–bronze plates that slide on a stainless steel surface. Built for the County of Los Angeles, the building is located within 5 km (3 miles) of the Newport–Inglewood fault, which is capable of generating earthquakes with a Richter magnitude of 7.5. The isolators are 100 cm (40 in) in diameter, and at the time of their manufacture were the largest isolation bearings fabricated in the United States. Many other hospitals have been built in California since then on rubber isolation systems, some with lead–rubber bearings (i.e., multilayered rubber bearings featuring a cylindrical lead core) and some with high-damping rubber bearings. They include the University of Southern California Teaching hospital, using lead–rubber bearings, completed in 1991. This hospital, which was instrumented with strong-motion seismic acceleration instruments was impacted by the 1994 Northridge Earthquake and performed remarkably well. The peak ground acceleration in the free fiel (the parking lot) was 0.49g, which was reduced within the building to around 0.10–0.11g by the isolation system. The Arrowhead Regional Medical Center, part of the County of San Bernardino, was completed in 1998, and the St Johns Medical Center, a private hospital in Santa Monica, in 2001. Two hospitals owned by Hoag Presbyterian in Irvine, one a retrofi and one new, were built on high-damping rubber bearings in the mid 2000s.

In addition to new buildings, there are a number of very large retrofi projects in California using base isolation, including the retrofi of the Oakland City Hall and the

Figure 1.8 The Oakland City Hall, Oakland, California. Courtesy of James M. Kelly. University of California, Berkeley

San Francisco City Hall, both of which were badly damaged in the 1989 Loma Prieta earthquake, and the Los Angeles City Hall.

When it was built in 1914, Oakland City Hall was the tallest building on the west coast. Its height was later surpassed by the Los Angeles City Hall, which was completed in 1928. The seismic rehabilitation of Oakland City Hall (Figure 1.8) using base isolation was completed in 1995, and it was at the time the tallest seismically isolated building in the world. It was once again surpassed when the seismic rehabilitation of the Los Angeles City Hall retrofi was completed in 1998, making that structure now the tallest seismically isolated building in the world. The Oakland City Hall isolation system uses 110 bearings ranging from 74 cm (29 in) to 94 cm (37 in) in diameter. A moat was constructed around the building to provide a seismic gap of 51 cm (20 in). Installing the isolators proved to be very complicated and required shoring up of the columns, cutting of the columns, and transferring of the column loads to temporary supports. In order to protect the interior, the columns were raised not more than 2.5 mm (0.1 in) during the jacking process. The cost of the retrofi was very

Figure 1.9 The Los Angeles City Hall, Los Angeles, California. Reproduced from Brion Vibber, Wikimedia

substantial – about $84 million – with the isolators comprising around 2.5% of that figu e. Details of the retrofi are given in Walters *et al.* (1995).

The Los Angeles City Hall, shown in Figure 1.9, is a 28-story steel frame building completed in 1928. The total floo area is close to 82 728 m^2 (912 000 ft^2). The lateral resistance is provided by several different elements, including steel cross-bracing, reinforced concrete walls, and interior clay hollow core tile walls, with the most of the superstructure stiffness provided by masonry infil perimeter walls. The building was damaged in the 1994 Northridge earthquake, with the most severe damage occurring on the 25th and 26th floors which have the characteristic of soft stories. The base isolation retrofi scheme (Youssef 2001) uses 416 high-damping natural rubber isolators in combination with 90 sliders and is supplemented by 52 mechanical viscous dampers at the isolation level. In addition, 12 viscous dampers were installed between the 24th and 25th floor to control

Figure 1.10 The San Francisco City Hall, San Francisco, California. Courtesy of James M. Kelly. University of California, Berkeley

interstory drifts at the soft-story levels. The total cost of this retrofi was estimated to be around $150 million, with the isolators comprising $3.5 million of that figu e.

The San Francisco City Hall, shown in Figure 1.10, was built in 1912 to replace the original city hall that was destroyed in the 1906 San Francisco Earthquake and was itself damaged in the 1989 Loma Prieta Earthquake. The repair and retrofi of the building included an isolation system with 530 lead–rubber bearings. The project involved a great deal of internal restoration and redecoration and was very expensive, but the isolation system and its installation accounted for only a small portion of the cost.

Other major base isolation retrofi projects using natural rubber bearings are the City of Berkeley administration building called the Martin Luther King Jr Civic Center and the Hearst Memorial Mining Building on the University of California, Berkeley campus (see Figures 1.11 and 1.12).

The use of isolation for earthquake-resistant design has been very actively pursued in Japan, from the completion of the firs large base-isolated building in 1986. Up to the late 1990s, all base-isolation projects in Japan had to be approved by a standing committee of the Ministry of Construction. As of June 30, 1998, 550 base-isolated buildings had been approved by the Ministry of Construction, but nowadays this approval is no longer necessary, and it is quite difficul to keep account of the number of base-isolated buildings. Many of the completed buildings have experienced earthquakes, and, in some cases, their response has been compared with adjacent conventionally designed structures. In every case where such a comparison has been made, the response of the isolated building has been highly favorable, particularly for ground motions with high levels of acceleration. The system most commonly used in the past has been undamped natural rubber

Figure 1.11 Hearst Memorial Mining Building on the University of California, Berkeley campus. Courtesy of Ian D. Aiken. SIE, Inc.

bearings with additional mechanical dampers using steel, lead or friction. However, there has been an increasing use of high-damping natural rubber isolators. There are now many large buildings that use high-damping natural rubber bearings. An example is the computer center for Tohoku Electric Power Co. in Sendai, Miyako Province.

The building houses the computers for the billing and production records of the electric power utility. It is a six-story, 10 000 m^2 (108 000 ft^2) structure and is one of the

Figure 1.12 Bearings for Hearst Memorial Mining Building on the University of California, Berkeley campus. Courtesy of James M. Kelly. University of California, Berkeley

larger base-isolated buildings in Japan. To accommodate a large number of mainframe computers and hard disk data storage equipment, the building was designed with large internal clear spans to facilitate location of this equipment. As a result of its height, the large column spacing, and the type of equipment in the building, the column loads are very large. Bridgestone provided a total of 40 bearings of three different sizes – 90 cm (35 in), 100 cm (39 in), and 120 cm (46 in) in diameter – to isolate the building. The vertical loads range from 400 tons (880 kips) to 800 tons (1760 kips). Construction of this building began in March 1989 and was completed in March 1990. The isolation system proved simple to install. All of the bearings were placed within three days and their base plates grouted after a further six days. The total construction cost, not including the internal equipment, was $20 million; the cost of the isolators was $1 million. This building represents a significan example of buildings housing expensive and critical equipment, and many more such structures were built in Japan in the following years.

One of the largest base-isolated buildings in the world is the West Japan Postal Computer Center, which is located in Sanda, Kobe Prefecture. This six-story, 47 000 m^2 (500 000 ft^2) structure is supported on 120 rubber isolators with a number of additional steel and lead dampers. The building, which has an isolated period of 3.9 s, is located approximately 30 km (19 miles) from the epicenter of the 1995 Hyogo-Ken Nanbu (Kobe) earthquake and experienced severe ground motion in that earthquake. The peak ground acceleration under the isolators was 400 cm/s^2 (0.41g) and was reduced by the isolation system to 127 cm/s^2 (0.13g) at the sixth floo . The estimate of the displacement of the isolators is around 12 cm (4.8 in). There was no damage to the isolated building; however, a fixed-base building adjacent to the computer center experienced some damage.

The use of isolation in Japan continues to increase, especially in the aftermath of the Kobe earthquake. As a result of the superior performance of the West Japan Postal Computer Center, there has been a rapid increase in the number of applications of base isolation, including many apartments and condominiums. In recent years the number of base-isolated buildings in Japan built each year has been around 100, and the total number is probably around 1500 (Kamada and Fujita 2007). This does not include single family homes of which there are around 3000, but not all of these use rubber bearings, although rubber bearings play an auxiliary role in many. The latest concept to be applied in Japan is the idea of *isolated ground*. In Sagamihara City near Tokyo an artificia ground, in fact a large concrete slab, with 21 separate buildings of 6–14 stories has been built on 150 isolation devices which include many very large rubber bearings (Terashima and Miyazaki 2001). With this approach any concerns for overturning and unacceptably large displacements are eliminated. It seems to be a very promising method of extending this technology to large complexes of high-rise condominium buildings.

The emphasis in most base isolation applications up to this time has been on large structures with sensitive or expensive contents, but there is increasing interest in applying this technology to public housing, schools, and hospitals in developing countries where the replacement cost due to earthquake damage could be a significan part of the country's Gross National Product (GNP). Several projects are under way for such applications. The challenge in such applications is to develop low-cost isolation systems that can be used in conjunction with local construction methods, such as masonry block and lightly reinforced concrete frames. The United Nations Industrial Development

Organization (UNIDO) partially finance a joint effort between the Malaysian Rubber Producers' Research Association (MRPRA, now the Tun Abdul Razak Research Centre) of the United Kingdom and the Earthquake Engineering Research Center (EERC) of the University of California at Berkeley to research and promote the use of rubber bearings for base-isolated buildings in developing countries.

To date, a number of base-isolated demonstration projects have been completed. In most cases an identical structure of fixed-bas construction was built adjacent to the isolated building to compare their behavior during earthquakes. There are demonstration projects in Reggio Calabria, Italy; Santiago, Chile; Guangdong Province, China; and Pelabuhan Ratu, Indonesia.

One of the demonstration projects completed under this program is a base-isolated apartment building in the coastal city of Shantou, Guangdong Province, an earthquake-prone area of southern China. Completed in 1994, this building is the firs rubber base-isolated building in China. This demonstration project involved the construction of two eight-story housing blocks. Two identical and adjacent buildings were built; one building is of conventional fixed-bas construction, and the other is base-isolated with high-damping natural rubber isolators. The design, testing, and manufacture of the isolators was funded by the MRPRA from a grant provided by the UNIDO. The demonstration project was a joint effort by the MRPRA, the EERC, and Nanyang University, Singapore. Details of this project can be found in Taniwangsa and Kelly (1996).

As part of the UNIDO support, several rubber technologists from a rubber company in Shantou went to the MRPRA laboratory and were trained in the manufacture of rubber isolators. The city of Shantou provided a site, and a factory producing rubber isolators was established in this city. This company has supplied isolators for projects all over China, many of them large complexes of perhaps 30–40 identical eight-story multi-family housing blocks. It also supplied isolators for buildings in Japan and in Russia.

In 1994 construction of a base-isolated four-story reinforced concrete building in Java, Indonesia, was completed (Figure 1.13). The construction of this demonstration building was part of the same UNIDO-sponsored program to introduce base isolation technology to developing countries. In order for this new technology to be readily adopted by building officials it was essential that the design and construction of the superstructure of the isolated building did not deviate substantially from common building practice and building codes used for fixed-bas buildings.

The demonstration building in Indonesia is located in the southern part of West Java, about 1 km (0.6 miles) southwest of Pelabuhan Ratu. The building is a four-story moment-resisting reinforced concrete structure, accommodating eight low-cost apartment units. The building is 7.2 × 18.0 m (24 × 59 ft) in plan, and the height to the roof above the isolators is 12.8 m (42 ft). The walls that enclose each apartment unit are made out of unreinforced masonry with special seismic gaps fille with soft mortar. A common building practice in Indonesia, this type of seismic gap separates the walls from the main structure. This building is supported by 16 high-damping natural rubber bearings. The isolation bearings are located at the ground level and are connected to the superstructure using an innovative recessed end-plate connection, as

Figure 1.13 Demonstration building in Pelabuhan Ratu, West Java, Indonesia. Courtesy of James M. Kelly. University of California, Berkeley

opposed to the more usual bolted connection. This use of a recessed end-plate connection proved to be cost-effective and very easy to install. The bearings were designed and manufactured by the MRPRA in the United Kingdom. To achieve overall economy of fabrication, installation, and maintenance of the isolation system, two different high-damping natural rubber compounds were used, and a single bearing size was selected so that only one mold was necessary for the fabrication process. The dynamic properties of the bearings were confirme by full-size bearing tests. Details of this project can be found in Taniwangsa and Kelly (1996).

Nuclear power plants are another example of a type of structure for which seismic isolation can be extremely beneficial Nuclear structures are generally very stiff and heavy, thus the benefit of a large-period shift can be obtained easily without resorting to long-period isolation systems. Also, as will be shown later, it is much easier to design stable isolators for heavier loads than light loads. Because the response of a base-isolated structure is dominated by the lowest mode, i.e., the structure moves in an approximately rigid-body manner, the stress analysis of the structure is greatly simplified A substantial level of design effort in nuclear facilities is devoted to the dynamic analysis of equipment and piping systems. The conventional design involves computing floo spectra for each

level, and, in some cases, multiple input spectra when piping systems or equipment items are attached at more than one level, and then broadening these spectra to account for uncertainties in the analysis.

In an isolated structure, however, because the dominant mode is a rigid-body mode with all the deformation concentrated at the isolation level, all parts of the building move in the same way at the low isolation frequency. The response uncertainties are reduced, multiple input spectra are not needed, and the peaks in all the floo spectra are at the low frequency of the isolation system, which is generally much lower than equipment or piping frequencies (Yang *et al.* 2010).

Thus using an isolation system allows a high degree of standardization, with equipment qualificatio processes simplifie through reduced seismic levels. A further benefi is that if the regulatory environment changes during the life of the plant, mandating an upgrade of the seismic input, the response of the equipment may not be greatly affected. If there is more than a negligible increase in the design forces at the isolation frequency, it is a relatively simple matter to reduce the overall stiffness of the isolation system and maintain the original equipment standards.

Because nuclear plants are a natural application of base isolation technology, it is no surprise that one of the earliest applications of the technology was a nuclear facility. Completed in 1980, the Koeberg Power Plant in South Africa was both the firs base-isolated nuclear power plant and one of the firs base-isolated buildings (Renault *et al.* 1979; Plichon *et al.* 1980). The power plant, designed by Électricité de France and built by Spie Batignolles, has two 900 MW_e standardized units, which had been qualifie for seismic inputs up to 0.2*g*. The nuclear island is constructed on 1829 aseismic bearings on concrete pedestals. Standard bridge bearings were used, consisting of multilayer neoprene bearings topped by bronze slip plates which slide on stainless steel plates attached to the underside of the upper base mat. These bearings were designed in the early 1970s when the technology of rubber isolators was such that the maximum lateral displacements were quite small, of the order of 5 cm (2 in). If the bearings reach this displacement, the sliding plates are expected to slip and provide further displacement. Because of subsequent developments in isolator design and manufacturing, it is unlikely that this design will be used again; in fact, a subsequent isolated nuclear power plant building by Électricité de France at Cruas uses only rubber pads.

The Cruas Nuclear Power Plant (Postollec 1982), shown in Figure 1.14, comprised four 900 MW_e PWR units supported on 3600 neoprene isolators, was constructed on an isolated nuclear island. The designers decided to isolate Cruas because the seismicity of the site exceeded that for which all previous examples of this standardized plant had been designed. The buildings and equipment of the standardized plant were designed for the basic EDF spectrum anchored at 0.2*g*, whereas at Cruas the required spectrum was 0.3*g*. In order to utilize the standardized plant design, the use of an isolation system was necessary.

Another French nuclear application of isolation consists of three large, spent-fuel storage tanks at a reprocessing plant at La Hague, France, built by COGEMA (Bouchon 1988). The three tanks are on a single reinforced concrete base mat, 1.65 m (5.4 ft) thick, supported on rubber pads on pedestals. The use of the isolators produced simplification in the design process as compared with conventional construction.

Figure 1.14 The Cruas-Meysse nuclear power plant. Courtesy of James M. Kelly. University of California, Berkeley

Other countries besides France were also interested in applying isolation technology to their nuclear facilities. During 1987–1993, the Japanese Ministry of International Trade and Industry (MITI) funded a large program of seismic isolation research for nuclear applications. Directed by the Central Research Institute of Electric Power Industry (CRIEPI) and involving the CRIEPI research laboratory at Abiko, numerous construction companies, plant manufacturers, and rubber companies, this program covered all aspects of seismic isolation and focused primarily on the application of seismic isolation to liquid-metal fast breeder reactors (FBR). The program was extremely comprehensive, and the results are available in a great many reports, mainly in Japanese. A number of these reports have been translated into English, generally appearing in the proceedings of SMiRT and Post-SMiRT Symposia.

In the United Kingdom, the use of isolation for a nuclear facility specificall for seismic protection is limited to a pipe bridge at a British Nuclear Fuels reprocessing facility in the north of England. Although a gas-cooled reactor with a prestressed concrete containment built on rubber pads, the primary goal of this application was to control stresses due to shrinkage and thermal effects. The Central Electricity Generating Board (CEGB) sponsored a program of isolation studies in the late 1980s intending to develop an isolation system for a standardized plant design. The proposed system used both natural rubber bearings and viscous dampers. The natural rubber bearings were to be made of a compound which was exactly linear in its shear response and without damping; the viscous dampers (provided by GERB of Germany) were intended to be entirely linear in velocity, thus producing a system which exactly matched the linear mechanical model used in the dynamic analysis of the plant.

The material to be covered in this book focuses on the mechanics of rubber bearings used in isolation systems. The analysis will be mainly linear and will emphasize the simplicity of these systems. Many of the results are new and are needed for a proper understanding of these bearings and for the design and analysis of vibration isolation or seismic isolation systems. It is hoped that the advantages afforded by adopting these natural rubber systems – their cost effectiveness, simplicity, and reliability – will become apparent to designers and their use will continue to expand.

2

Behavior of Multilayer Rubber Bearings under Compression

2.1 Introduction

The vertical frequency of an isolation system, often an important design criterion in a seismic isolation project, is the most important design quantity for the vibration isolation of a piece of equipment or a structure. This vertical frequency is controlled by the vertical stiffness of the bearings that comprise the system. In order to predict it, the designer need only compute the vertical stiffness of the bearings under a specifie dead load, and for this a linear analysis is adequate. The initial response of a bearing under vertical load is very nonlinear and depends on several factors. Normally, bearings have a substantial run-in before the full vertical stiffness is developed. This run-in, which is strongly influence by the alignment of the reinforcing shims and other aspects of the workmanship in the molding process, cannot be predicted by analysis, but is generally of little importance in predicting the vertical response of a bearing.

Another important bearing property that must be analyzed for design is the buckling behavior of the isolator. In order to conduct this analysis, the response of the compressed bearing to bending moment is necessary. Referred to as the *bending stiffness*, this can be ascertained by an extension of the same analysis that is done to determine the vertical stiffness. The bending stiffness of rubber pads is examined in the following chapter.

2.2 Pure Compression of Bearing Pads with Incompressible Rubber

The vertical stiffness of a rubber bearing is given by the formula

$$K_V = \frac{E_c A}{t_r} \tag{2.1}$$

Mechanics of Rubber Bearings for Seismic and Vibration Isolation, First Edition. James M. Kelly and Dimitrios A. Konstantinidis.

where A is the loaded area of the bearing, t_r is the total thickness of rubber in the bearing (i.e., the sum of the thicknesses of the individual layers), and E_c is the instantaneous compression modulus of the rubber-steel composite under the specifie level of vertical load. The value of E_c, which is computed for a single rubber layer, is controlled by the shape factor S, define as

$$S = \frac{\text{loaded area}}{\text{force-free area}} \tag{2.2}$$

which is a dimensionless measure of the aspect ratio of the single layer of the rubber. For example, for an infinit strip of width $2b$ and thickness t,

$$S = \frac{b}{t} \tag{2.3}$$

for a circular pad of radius R and thickness t,

$$S = \frac{R}{2t} \tag{2.4}$$

for a rectangular pad of side dimensions $2b$ and l and thickness t,

$$S = \frac{bl}{(l + 2b)\, t} \tag{2.5}$$

and for an annular pad of inner radius a, outer radius b, and thickness t,

$$S = \frac{b - a}{2t} \tag{2.6}$$

In order to predict the compression stiffness and the bending stiffness, a linear elastic theory is used. The firs analysis of the compression stiffness was done using an energy approach by Rocard (1937), and further developments were made by Gent and Lindley (1959b) and Gent and Meinecke (1970). The theory given here is a version of these analyses and is applicable to bearings with shape factors greater than about five

The analysis for the compression and bending stiffnesses is an approximate one based on two sets of assumptions, the firs relating to the kinematics of the deformation and the second to the stress state. For direct compression, the kinematic assumptions are as follows:

(i) points on a vertical line before deformation lie on a parabola after loading;
(ii) horizontal planes remain horizontal.

Consider an arbitrarily shaped pad of thickness t and locate, as shown in Figure 2.1(a), a rectangular Cartesian coordinate system (x, y, z) in the middle surface of the pad. As

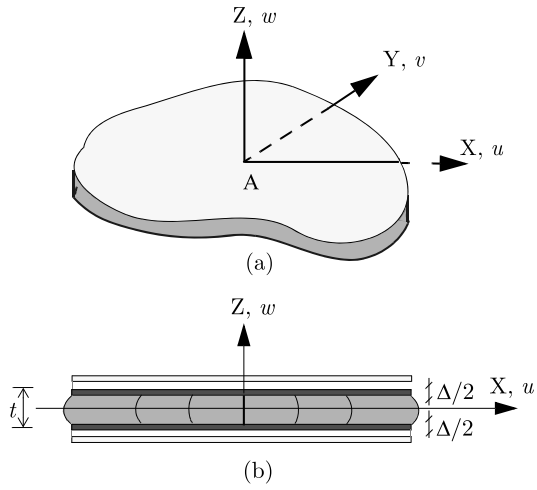

Figure 2.1 (a) Cartesian coordinate system on an arbitrarily shaped pad; (b) displacement field of an arbitrarily shaped pad

shown in Figure 2.1(b) under the kinematic assumptions described above, the displacements (u, v, w) in the coordinate directions are

$$\begin{aligned} u(x, y, z) &= u_0(x, y)\left(1 - \frac{4z^2}{t^2}\right) \\ v(x, y, z) &= v_0(x, y)\left(1 - \frac{4z^2}{t^2}\right) \\ w(x, y, z) &= w(z) \end{aligned} \tag{2.7}$$

This displacement fiel satisfie the constraint that the top and bottom surfaces of the pad are bonded to rigid layers. The assumption of incompressibility produces a further constraint on the three components of strain, $\varepsilon_{xx} = \partial u/\partial x$, $\varepsilon_{yy} = \partial v/\partial y$, $\varepsilon_{zz} = \partial w/\partial z$, in the form

$$\varepsilon_{xx} + \varepsilon_{yy} + \varepsilon_{zz} = 0 \tag{2.8}$$

which leads to

$$\left(\frac{\partial u_0}{\partial x} + \frac{\partial v_0}{\partial y}\right)\left(1 - \frac{4z^2}{t^2}\right) + \frac{\mathrm{d}w}{\mathrm{d}z} = 0 \tag{2.9}$$

Rearranging this to read

$$\frac{\partial u_0}{\partial x} + \frac{\partial v_0}{\partial y} = -\frac{1}{1 - \dfrac{4z^2}{t^2}}\frac{\mathrm{d}w}{\mathrm{d}z} \tag{2.10}$$

we see that we have a function of x and y on the left-hand side and a function of z on the right, and since the equation is an identity that holds everywhere, both sides must equal a constant k. To determine k, we solve

$$\frac{\mathrm{d}w}{\mathrm{d}z} = -k\left(1 - \frac{4z^2}{t^2}\right) \tag{2.11}$$

to get

$$w(z) = -k\left(z - \frac{4z^3}{3t^2}\right) + c \tag{2.12}$$

where c is a constant of integration. Using the boundary conditions $w(t/2) = -\Delta/2$ and $w(-t/2) = \Delta/2$, we fin that $c = 0$ and $k = 3\Delta/(2t) = 3\,\varepsilon_c/2$, where the compression strain ε_c is define by

$$\varepsilon_c = -\frac{w\,(t/2) - w\,(-t/2)}{t}, \quad \left(\varepsilon_c > 0 \text{ in compression}\right) \tag{2.13}$$

From this we obtain the distribution of the displacement w through the thickness of the pad, if this is needed, and the integrated form of the compressibility constraint as

$$\frac{\partial u_0}{\partial x} + \frac{\partial v_0}{\partial y} = \frac{3\,\varepsilon_c}{2} \tag{2.14}$$

The stress state is assumed to be dominated by the internal pressure, p, such that the normal stress components, σ_{xx}, σ_{yy}, σ_{zz}, differ from $-p$ only by terms of order $(t^2/l^2)p$ (where l is a characteristic length in the $x-y$ plane), i.e.,

$$\sigma_{xx} \approx \sigma_{yy} \approx \sigma_{zz} \approx -p\left(1 + O\left(\frac{t^2}{l^2}\right)\right) \tag{2.15}$$

This stress assumption gives the solution its name: *pressure solution*. The shear stress components, τ_{xz} and τ_{yz}, which are generated by the constraints at the top and bottom of the pad, are assumed to be of order $(t/l)p$; the in-plane shear stress, τ_{xy}, is assumed to be of order $(t^2/l^2)p$.

The complete equations of equilibrium for the stresses are

$$\begin{aligned}
\frac{\partial \sigma_{xx}}{\partial x} + \frac{\partial \tau_{xy}}{\partial y} + \frac{\partial \tau_{xz}}{\partial z} &= 0 \\
\frac{\partial \tau_{xy}}{\partial x} + \frac{\partial \sigma_{yy}}{\partial y} + \frac{\partial \tau_{yz}}{\partial z} &= 0 \\
\frac{\partial \tau_{xz}}{\partial x} + \frac{\partial \tau_{yz}}{\partial y} + \frac{\partial \sigma_{zz}}{\partial z} &= 0
\end{aligned} \tag{2.16}$$

and the firs two, if we identify σ_{xx} and σ_{yy}, with $-p$, reduce under these assumptions to

$$\begin{aligned} \frac{\partial \tau_{xz}}{\partial z} &= \frac{\partial p}{\partial x} \\ \frac{\partial \tau_{yz}}{\partial z} &= \frac{\partial p}{\partial y} \end{aligned} \tag{2.17}$$

The third of the equations of equilibrium can be differentiated with respect to z, the order of differentiation inverted, and Equation (2.17) substituted into the resulting equation, to give

$$\frac{\partial^2 p}{\partial x^2} + \frac{\partial^2 p}{\partial y^2} = \nabla^2 p = \frac{\partial^2 \sigma_{zz}}{\partial z^2} \tag{2.18}$$

Assuming that the material is linearly elastic, the shear stresses, τ_{xz} and τ_{yz}, are related to the shear strains, γ_{xz} and γ_{yz}, by

$$\tau_{xz} = G\gamma_{xz}, \quad \tau_{yz} = G\gamma_{yz} \tag{2.19}$$

with G being the shear modulus of the rubber; since $\gamma_{xz} = \partial u/\partial z + \partial w/\partial x$ and $\gamma_{yz} = \partial v/\partial z + \partial w/\partial y$,

$$\tau_{xz} = -\frac{8\,G}{t^2} z u_0, \quad \tau_{yz} = -\frac{8\,G}{t^2} z v_0 \tag{2.20}$$

From the equilibrium equations, therefore,

$$\frac{\partial p}{\partial x} = -\frac{8\,G}{t^2} u_0, \quad \frac{\partial p}{\partial y} = -\frac{8\,G}{t^2} v_0 \tag{2.21}$$

which, when inverted to give u_0 and v_0 and inserted into the incompressibility condition, give

$$\frac{t^2}{8\,G}\left(\frac{\partial^2 p}{\partial x^2} + \frac{\partial^2 p}{\partial y^2}\right) = -\frac{3\,\varepsilon_c}{2} \tag{2.22}$$

and this, in turn, reduces to

$$\frac{\partial^2 p}{\partial x^2} + \frac{\partial^2 p}{\partial y^2} = \nabla^2 p = -\frac{12\,G\varepsilon_c}{t^2} \tag{2.23}$$

as the partial differential equation to be satisfie by $p(x, y)$ over the area of the pad. The boundary condition, $p = 0$, on the edge of the pad completes the system for $p(x, y)$.

To use this to determine E_c, we solve for p and integrate over the area of the pad A to determine the resultant normal load, P. E_c is then given by

$$E_c = \frac{P}{A\varepsilon_c} \tag{2.24}$$

The significanc of the third equation of equilibrium is now clear: with the substitution of Equation (2.23), we have an equation for the distribution of σ_{zz} through the thickness of the pad in the form

$$\frac{\partial^2 \sigma_{zz}}{\partial z^2} = \frac{12\,G\varepsilon_c}{t^2} \tag{2.25}$$

2.2.1 Infinit Strip Pad

For an infinit strip of width $2b$ (Figure 2.2), Equation (2.23) reduces to

$$\nabla^2 p = \frac{\mathrm{d}^2 p}{\mathrm{d}x^2} = -\frac{12\,G\varepsilon_c}{t^2} \tag{2.26}$$

which, with $p(\pm b) = 0$, gives

$$p = \frac{6\,G\varepsilon_c}{t^2}\left(b^2 - x^2\right) \tag{2.27}$$

In this case the load per unit length of the strip, P, is given by

$$P = \int_{-b}^{+b} p\,\mathrm{d}x = \frac{8\,G\varepsilon_c b^3}{t^2} \tag{2.28}$$

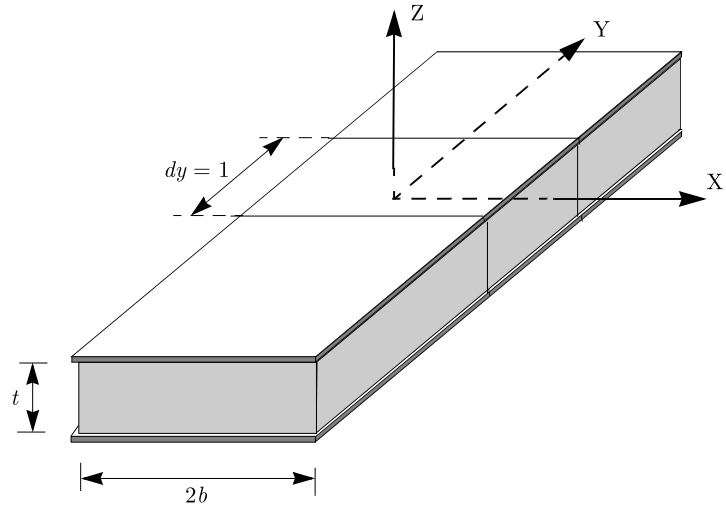

Figure 2.2 Coordinate system for an infinit strip pad of width $2b$

Because the shape factor, S, is b/t, and the area per unit length, A, is $2b$,

$$E_c = \frac{P}{A\varepsilon_c} = 4GS^2 \tag{2.29}$$

2.2.2 Circular Pad

For a circular pad of radius, R (Figure 2.3), the equation for p becomes

$$\nabla^2 p = \frac{\mathrm{d}^2 p}{\mathrm{d}r^2} + \frac{1}{r}\frac{\mathrm{d}p}{\mathrm{d}r} = -\frac{12\,G\varepsilon_c}{t^2}, \quad r = \sqrt{x^2 + y^2} \tag{2.30}$$

The general solution of Equation (2.30) is

$$p = A\,\ln r + B - \frac{3\,G\varepsilon_c}{t^2} r^2 \tag{2.31}$$

and because p is bounded at $r = R$, and $p = 0$ at $r = R$, the solution for the complete pad becomes

$$p = \frac{3\,G\varepsilon_c}{t^2}\left(R^2 - r^2\right) \tag{2.32}$$

and

$$P = 2\pi \int_0^R p\,(r)\,r\,\mathrm{d}r = \frac{3\,G\varepsilon_c \pi R^4}{2t^2} \tag{2.33}$$

Recalling that $S = R/(2t)$ and $A = \pi R^2$, we have

$$E_c = 6GS^2 \tag{2.34}$$

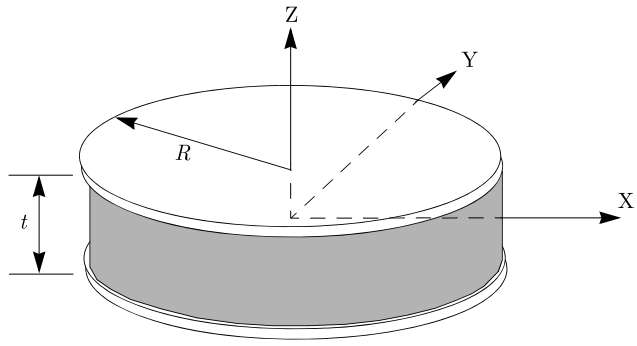

Figure 2.3 Coordinate system for a circular pad of radius R

2.2.3 Rectangular Pad (with Transition to Square or Strip)

For a rectangular pad with width $2b$ and length l as shown in Figure 2.4, Equation (2.23) can be solved using Fourier series. We let $p(x, y) = \sum_{m=1}^{\infty} P_m(y) \sin\left(\frac{m\pi x}{2b}\right)$ with the coordinate system as shown in Figure 2.4, which automatically satisfie the boundary conditions at $x = 0$ and $x = 2b$. The Fourier coeff cients, P_m, satisfy

$$\frac{\mathrm{d}^2 P_m}{\mathrm{d}y^2} - \left(\frac{m\pi}{2b}\right)^2 P_m = -\frac{12\,G\varepsilon_c}{t^2} a_m \tag{2.35}$$

where

$$a_m = \begin{cases} \dfrac{4}{m\pi}; & m = 1, 3, 5 \ldots \\ 0; & m = 2, 4, 6 \ldots \end{cases} \tag{2.36}$$

Symmetry over $-l/2 \leq y \leq +\,l/2$ and the boundary condition $P_m = 0$ at $y = \pm l/2$ give

$$P_m = \frac{12\,G\varepsilon_c}{t^2} a_m \left(\frac{2b}{m\pi}\right)^2 \left(1 - \frac{\cosh\left(\frac{m\pi y}{2b}\right)}{\cosh\left(\frac{m\pi l}{4b}\right)}\right) \tag{2.37}$$

and, therefore,

$$p\,(x, y) = \frac{12\,G\varepsilon_c}{t^2} \sum_{m=1}^{\infty} a_m \left(\frac{2b}{m\pi}\right)^2 \left(1 - \frac{\cosh\left(\frac{m\pi y}{2b}\right)}{\cosh\left(\frac{m\pi l}{4b}\right)}\right) \sin\left(\frac{m\pi x}{2b}\right) \tag{2.38}$$

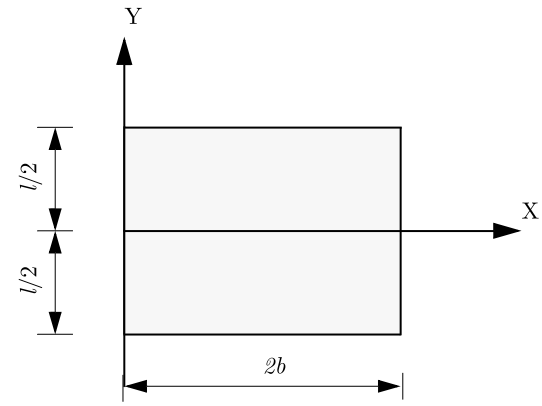

Figure 2.4 Coordinate system for a rectangular pad with side lengths l and $2b$

We note that the series associated with the firs term in the parenthesis is the solution of

$$\frac{\mathrm{d}^2 p(x)}{\mathrm{d}x^2} = -\frac{12\,G\varepsilon_c}{t^2} \tag{2.39}$$

on $0 \le x \le 2b$ and can be summed separately to give

$$p(x) = \frac{12\,G\varepsilon_c}{t^2} 2b^2 \left(\frac{x}{2b} - \frac{x^2}{4b^2}\right) \tag{2.40}$$

giving the fina result

$$p(x,\,y) = \frac{12\,G\varepsilon_c}{t^2}\left[2b^2\left(\frac{x}{2b} - \frac{x^2}{4b^2}\right) - \sum_{m=1,3,5\ldots}^{\infty} \frac{16b^2}{m^3\pi^3} \frac{\cosh\left(\dfrac{m\pi\,y}{2b}\right)}{\cosh\left(\dfrac{m\pi\,l}{4b}\right)} \sin\left(\frac{m\pi\,x}{2b}\right)\right] \tag{2.41}$$

The corresponding result for $E_c = P/(A\varepsilon_c)$ is

$$E_c = \frac{G\,(2b)^2}{t^2}\left(1 - \sum_{m=1,3,5\ldots}^{\infty} \frac{192\,(b/l)}{m^5\pi^5} \tanh\left(\frac{m\pi l}{4b}\right)\right) \tag{2.42}$$

The shape factor for a rectangular pad is given by $S = bl/[(l + 2b)t]$, and the compression modulus can also be expressed in terms of the shape factor S and the aspect ratio of the bearing $\rho = 2b/l$ as

$$E_c = \frac{384}{\pi^4} GS^2\,(1+\rho)^2 \sum_{m=\mathrm{odd}}^{\infty} \frac{1}{m^4}\left(1 - \frac{2\rho}{m\pi}\tanh\left(\frac{m\pi}{2\rho}\right)\right) \tag{2.43}$$

Figure 2.5 is a graph of the compression modulus as a $E_c/(GS^2)$ ratio. The graph shows that for a square pad, $E_c = 6.748\,GS^2$, while for an infinit strip, $E_c = 4\,GS^2$, which is in agreement with Equation (2.29).

2.2.4 Annular Pad

Consider an annular pad with inner radius a, outer radius b, and thickness t. The shape factor in this case is

$$S = \frac{\pi\left(b^2 - a^2\right)}{2\pi\,(a+b)\,t} = \frac{b-a}{2t} \tag{2.44}$$

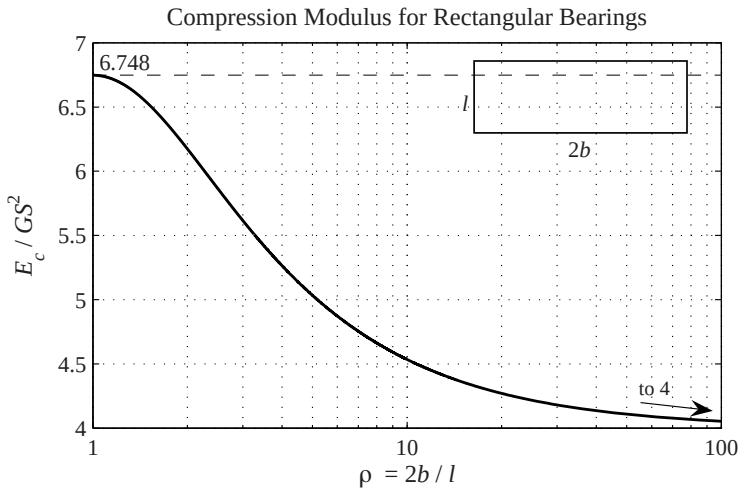

Figure 2.5 Compression modulus for a rectangular bearing with side lengths l and $2b$

The solution of Equation (2.30), with $p(a) = 0$ and $p(b) = 0$, is

$$p(r) = \frac{3G\varepsilon_c}{t^2}\left(\frac{(b^2 - a^2)\ln(r/a)}{\ln(b/a)} - (r^2 - a^2)\right) \tag{2.45}$$

The total load, P, is given by

$$P = 2\pi \int_a^b p(r)\, r\, \mathrm{d}r = \frac{3G\varepsilon_c}{2t^2}\pi(b^2 - a^2)\left(b^2 + a^2 - \frac{b^2 - a^2}{\ln(b/a)}\right) \tag{2.46}$$

from which we have

$$E_c = \frac{P}{A\varepsilon_c} = \frac{3G}{2t^2}\left(b^2 + a^2 - \frac{b^2 - a^2}{\ln(b/a)}\right) \tag{2.47}$$

Using the expression for S, we can write this in the form

$$E_c = 6GS^2\lambda \tag{2.48}$$

where

$$\lambda = \frac{b^2 + a^2 - \dfrac{b^2 - a^2}{\ln(b/a)}}{(b - a)^2} \tag{2.49}$$

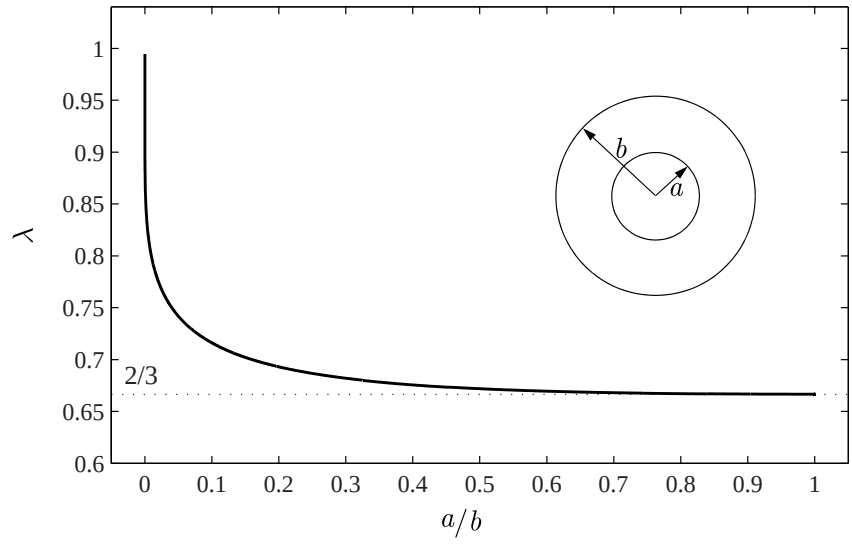

Figure 2.6 Reduction of compression modulus for an annular pad

which, in terms of the ratio a/b, becomes

$$\lambda = \frac{1 + (a/b)^2 + \dfrac{1 - (a/b)^2}{\ln (a/b)}}{(1 - a/b)^2} \tag{2.50}$$

The solution for λ that is plotted versus the ratio a/b from $0 \leq a/b \leq 1$ in Figure 2.6 shows that E_c drops very rapidly from the value of $6\,GS^2$, which corresponds to a circular pad, to the value of $4\,GS^2$, which corresponds to an infinit strip pad.

If we let $a = \varepsilon b$ with $\varepsilon \ll 1$ and assume that the hole is small enough that its effect on the compression modulus can be ignored, then we would assume that $E_c = 6\,GS^2$, where S is given by $b/(2t)$, so that Equation (2.50) becomes

$$\lambda = \frac{E_c}{6\,GS^2} = 1 + \varepsilon^2 + \frac{1 - \varepsilon^2}{\ln\,\varepsilon} \tag{2.51}$$

Clearly as $\varepsilon \to 0$, $\lambda \to 1$, but for $\varepsilon \neq 0$ we have the unexpected result that the modulus drops rapidly with ε. If we denote $\lambda = f(\varepsilon)$, the fact is that the derivative of f at $\varepsilon = 0$ is negative infinit , and it is this that causes the sensitivity. For example if the hole diameter is only 5% of the full diameter, the value of $f(\varepsilon)$ is 0.67, implying a drop in the modulus of one third for such a small hole. This shows that the presence of a small hole cannot be ignored.

At the other extreme, when $a/b \to 1$, by writing $a/b = 1 - \varepsilon$ in Equation (2.50) and letting $\varepsilon \to 0$, we fin that $\lambda \to 2/3$ and $E_c \to 4\,GS^2$, which is the result for the infinit strip. In fact, the solution goes very rapidly to this value. Clearly for the case when

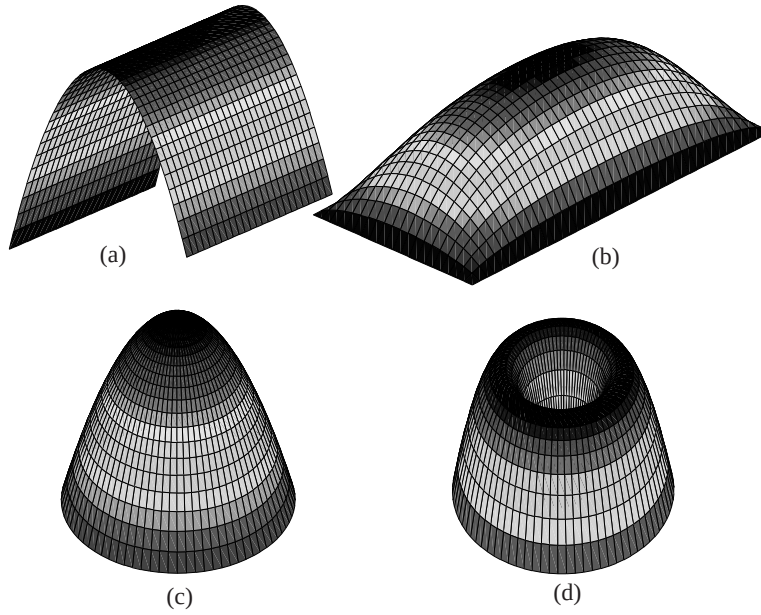

Figure 2.7 Pressure distributions for various pad geometries: (a) infinit strip; (b) rectangular; (c) circular; (d) annular

$a/b > 0.10$, the value of λ is almost two-thirds, indicating that the presence of even a small hole has a large effect on E_c; therefore, in most cases for bearings with central holes, the value of E_c should be taken as $4\,GS^2$ rather than $6\,GS^2$.

Figure 2.7 plots pressure distributions for the four pad geometries presented in this chapter.

2.3 Shear Stresses Produced by Compression

The shear stresses (or shear strains) that develop under direct compression by the constraint of the rigid steel layers to which the rubber is bonded (Figure 2.8) are also very important for design purposes. From Equation (2.20), we have

$$\begin{aligned} \tau_{xz} &= -\frac{8\,G}{t^2} z u_0 \\ \tau_{yz} &= -\frac{8\,G}{t^2} z v_0 \end{aligned} \tag{2.52}$$

but from the equilibrium equation, Equation (2.17), and the assumptions that led to Equation (2.23), we get

$$\begin{aligned} \frac{\partial \tau_{xz}}{\partial z} &= -\frac{\partial \sigma_{xx}}{\partial x} = \frac{\partial p}{\partial x} \\ \frac{\partial \tau_{yz}}{\partial z} &= -\frac{\partial \sigma_{yy}}{\partial y} = \frac{\partial p}{\partial y} \end{aligned} \tag{2.53}$$

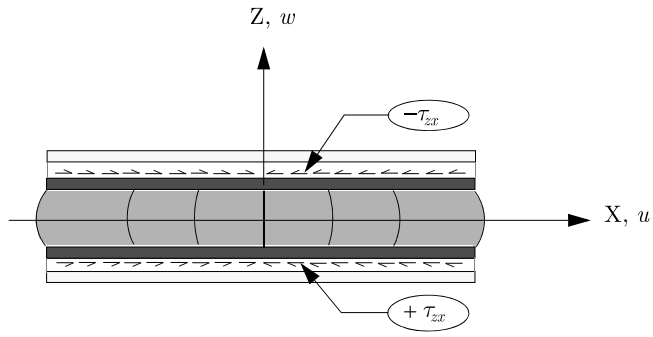

Figure 2.8 Shear stresses produced by pure compression

Given p, these equations can be used to determine the shear stress or shear strain distribution, particularly the maximum shear stress and shear strain.

For the infinit strip of width $2b$, where

$$p = \frac{6\,G\varepsilon_c}{t^2}\left(b^2 - x^2\right) \tag{2.54}$$

we have

$$\tau_{xz} = -\frac{12\,G\varepsilon_c}{t^2}xz \tag{2.55}$$

and the maximum value occurs at $x = b$, $z = t/2$, giving

$$\tau_{\max} = 6\,G\varepsilon_c\frac{b}{t} \tag{2.56}$$

In terms of S, the maximum shear strain is given by

$$\gamma_{\max} = 6\,S\varepsilon_c = \gamma_c \tag{2.57}$$

Thus, the compression strain causes a shear strain with a peak value $6S$ times greater, and since S can be quite large for a thin pad, the multiplying factor will be correspondingly large.

For a circular pad, we have

$$p = \frac{3\,G\varepsilon_c}{t^2}\left[R^2 - \left(x^2 + y^2\right)\right] \tag{2.58}$$

and

$$\tau_{xz} = -\frac{6\,G\varepsilon_c}{t^2}xz,\ \tau_{yz} = -\frac{6\,G\varepsilon_c}{t^2}yz \tag{2.59}$$

The maximum shear stress occurs at the top and bottom edges of the periphery of the pad and is

$$\tau_{\max} = \frac{3\,G\varepsilon_c R}{t} \tag{2.60}$$

which is equivalent to

$$\gamma_c = 6\,S\varepsilon_c \tag{2.61}$$

as before. These results can be used to establish a maximum strain criterion for the rubber. For example, some bridge-bearing design codes denote the shear strain due to shear deformation of the pad by γ_s, which when added to the shear strain produced by compression, γ_c, is used to defin a maximum strain unit, such as, for example,

$$\gamma_s + \gamma_c \leq 0.5\varepsilon_{br} \tag{2.62}$$

where ε_{br} is the elongation to break of the rubber.

The maximum shear strain due to compression is not the only shear strain quantity of interest to the designer. It is also useful to have an estimate of the average strain for the following reason: because rubber is somewhat strain sensitive, G is often modifie according to the strain level, particularly in highly fille rubbers. In compression, the shear strain varies from positive to negative over the volume of the pad in such a way that the simple average is zero; therefore, the appropriate average is the square root of the integrated squared strains. We defin γ_{ave} through the integral

$$\gamma_{\text{ave}}^2 = \frac{1}{At}\int_{Vol}\left(\gamma_{xz}^2 + \gamma_{yz}^2\right)\mathrm{d}V \tag{2.63}$$

On the other hand the total elastic stored energy, U, in the pad is given by

$$U = \frac{1}{2\,G}\int_A\int_t\left(\tau_{xz}^2 + \tau_{yz}^2\right)\mathrm{d}z\,\mathrm{d}A \tag{2.64}$$

so that the average shear strain, γ_{ave}, can be obtained from

$$U = \frac{1}{2}G\gamma_{\text{ave}}^2 At \tag{2.65}$$

But the total elastic stored energy is in turn equal to the external work $P\Delta/2$, from which

$$U = \frac{1}{2}G\gamma_{\text{ave}}^2 = At = \frac{1}{2}\left(E_c A\varepsilon_c\right)\left(\varepsilon_c t\right) \tag{2.66}$$

Therefore,

$$\gamma_{\text{ave}}^2 = \frac{E_c}{G}\varepsilon_c^2 \tag{2.67}$$

For the strip, we have

$$\gamma_{\text{ave}} = 2\,S\varepsilon_c \tag{2.68}$$

and for the circular pad,

$$\gamma_{\text{ave}} = \sqrt{6}\,S\varepsilon_c \tag{2.69}$$

Although a certain degree of trial and error is needed, computations of this kind allow the designer to estimate the appropriate value of G, which can then be used to estimate the vertical stiffness. First, we must assume a value of G in order to calculate ε_c, and from that calculate γ_{ave}; we then modify G and iterate as necessary. Because the modulus is not very sensitive to strain above about 20%, few iterations are needed.

2.4 Pure Compression of Single Pads with Compressible Rubber

The theory for the compression of a rubber pad given in this section is based on two assumptions: first the displacement pattern determined in Equation (2.7); second, the normal stress components in all three directions can be approximated by the pressure, p, in the material. Integration through the thickness of the pad of the equation of incompressibility leads to an equation for $p(x,y)$. To include the influenc of bulk compressibility, we need only replace the equation of incompressibility constraint, Equation (2.8), by

$$\varepsilon_{xx} + \varepsilon_{yy} + \varepsilon_{zz} = -\frac{p}{K} \tag{2.70}$$

where K is the bulk modulus. Integration through the thickness leads to

$$\nabla^2 p - \frac{12\,G}{K\,t^2}\,p = -\frac{12\,G\varepsilon_c}{t^2} \tag{2.71}$$

that is solved, as before, with $p = 0$ on the edge of the pad.

2.4.1 Infinit Strip Pad

For an infinit strip, $-b \le x \le b$, of thickness t, the solution for p is of the form (Chalhoub and Kelly 1991)

$$p = K\varepsilon_c\left(1 - \frac{\cosh(\lambda x)}{\cosh(\lambda b)}\right) \tag{2.72}$$

where $\lambda^2 = 12\,G/(Kt^2)$. Integrating p over the area of the pad gives

$$P = \int_{-b}^{+b} p(x)\,\mathrm{d}x = 2K\varepsilon_c b\left(1 - \frac{1}{\lambda b}\tanh(\lambda b)\right) \tag{2.73}$$

and

$$E_c = K\left(1 - \frac{1}{\lambda b}\tanh(\lambda b)\right) \tag{2.74}$$

In terms of the shape factor, S, here taken as b/t, we have

$$\lambda b = \sqrt{\frac{12\,G}{K}}S \tag{2.75}$$

and then Equation (2.74) can be expressed as

$$E_c = K\left(1 - \frac{\tanh\left(\sqrt{\frac{12\,G}{K}}S\right)}{\sqrt{\frac{12\,G}{K}}S}\right) \tag{2.76}$$

For small values of the parameter x, $\tanh x$ can be approximated by

$$\tanh x = x - \frac{x^3}{3} + \frac{2x^5}{15} + \cdots$$

Thus,

$$1 - \frac{1}{x}\tanh x = \frac{x^2}{3} - \frac{2x^4}{15}$$

and from this, E_c can be approximated by

$$E_c = 4\,GS^2\left(1 - \frac{24\,GS^2}{5K}\right) \tag{2.77}$$

For example, for a fille rubber with $G = 1.0$ MPa (145 psi), $K = 2000$ MPa (289 855 psi), and a shape factor of 10, the contribution provided by the second term in Equation (2.77) is 24%.

The recommended *ad hoc* modificatio (Lindley 1966) for the effect of bulk compressibility is

$$\frac{1}{E_c} = \frac{1}{E_c^{\infty}} + \frac{1}{K} \tag{2.78}$$

where E_c^{∞} is the effective compression modulus assuming incompressibility. The approximation for small S can be inverted to give

$$\frac{1}{E_c} = \frac{1}{4GS^2\left(1 - \dfrac{24GS^2}{5K}\right)} \tag{2.79}$$

which, in turn, can be approximated by

$$\frac{1}{E_c} = \frac{1}{4GS^2} + \frac{6}{5K} \tag{2.80}$$

indicating that the *ad hoc* modificatio is not completely correct. For very large values of S, where $(12GS^2/K)^{1/2} \geq 1$,

$$E_c = K\left[1 - \sqrt{\frac{K}{12GS^2}}\right] \tag{2.81}$$

showing that K is an upper bound to E_c.

The effect of the shape factor on the pressure distribution also confirm this result. If we set $\lambda b \ll 1$, and approximate $\cosh(\lambda x)$ and $\cosh(\lambda b)$ by Taylor's series, clearly, the previously noted parabolic distribution of pressure occurs; however, if $\lambda b \gg 1$, we can approximate $\cosh(\lambda b)$ by $e^{\lambda b}/2$ and $\cosh(\lambda x)$ by $e^{\lambda x}/2$, from which

$$p = K\varepsilon_c\left(1 - e^{-\lambda(b-x)}\right) \tag{2.82}$$

implying a constant distribution of pressure across the width of the strip (except on the edges, where $x = \pm b$, therefore, the pressure must go to zero).

When the pressure, $p(x)$ of Equation (2.72), is normalized with the average pressure, $P/(2b)$, then

$$\bar{p} = \frac{p}{P/(2b)} = \frac{1 - \dfrac{\cosh(\lambda x)}{\cosh(\lambda b)}}{1 - \dfrac{\tanh(\lambda b)}{\lambda b}} \tag{2.83}$$

Figure 2.9 shows the normalized pressure distribution, $\bar{p}$, due to pure compression for different shape factors ($S = 10$, 50, 500) for a strip with $G = 1.0$ MPa (145 psi) and $K = 2000$ MPa (289 855 psi).

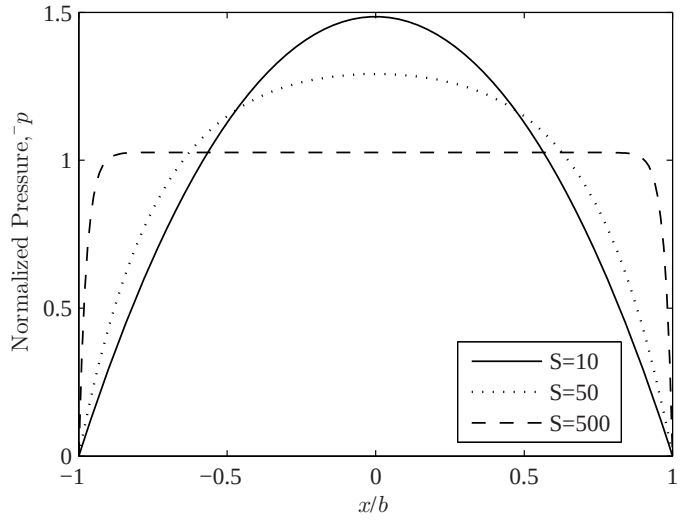

Figure 2.9 Normalized pressure distribution on an infinit strip pad under pure compression

2.4.2 Circular Pad

Consider a circular pad with a large shape factor, an external radius, R, and thickness, t. The pressure in the pad is axisymmetrical, i.e., $p = p(r)$, where $0 \leq r \leq R$, therefore, Equation (2.71) becomes

$$\begin{aligned} &\frac{\mathrm{d}^2 p}{\mathrm{d}r^2} + \frac{1}{r}\frac{\mathrm{d}p}{\mathrm{d}r} - \lambda^2 (p - K\varepsilon_c) = 0 \\ &\lambda^2 = \frac{12\,G}{Kt^2} \end{aligned} \tag{2.84}$$

with $p = 0$ at $r = R$.

The general solution of the homogeneous part of this modifie Bessel equation of order 0, $r^2 p'' + rp' - \lambda^2 r^2 p = 0$, has the form $p(r) = C_1 \mathrm{I}_0(\lambda r) + C_2 \mathrm{K}_0(\lambda r)$, where I_0 is the modifie Bessel function of the firs kind of order 0, and K_0 is the modifie Bessel function of the second kind of order 0. The complete solution, together with the constraint that $p(0)$ is bounded, is

$$p\,(r) = K\varepsilon_c \left(1 - \frac{\mathrm{I}_0\,(\lambda r)}{\mathrm{I}_0\,(\lambda R)}\right) \tag{2.85}$$

Integrating p over the area of the pad gives

$$P = K\varepsilon_c \pi R^2 \left(1 - \frac{2}{\lambda R}\frac{\mathrm{I}_1\,(\lambda R)}{\mathrm{I}_0\,(\lambda R)}\right) \tag{2.86}$$

where I_1 is the modifie Bessel function of the firs kind of order 1.

The resulting expression for the compression modulus is

$$E_c = K\left(1 - \frac{2}{\lambda R}\frac{\mathrm{I}_1(\lambda R)}{\mathrm{I}_0(\lambda R)}\right) \tag{2.87}$$

where

$$\lambda R = \frac{\sqrt{12\,GR^2}}{Kt^2} = \sqrt{\frac{48\,G}{K}}S \tag{2.88}$$

and the shape factor, S, is $R/(2t)$. In terms of S, Equation (2.87) can be expressed as

$$E_c = K\left(1 - \frac{2}{\sqrt{\frac{48\,G}{K}}S}\frac{\mathrm{I}_1\left(\sqrt{\frac{48\,G}{K}}S\right)}{\mathrm{I}_0\left(\sqrt{\frac{48\,G}{K}}S\right)}\right) \tag{2.89}$$

Figure 2.10 shows graphs of $E_c/(GS^2)$ as a function of S for different K/G values.

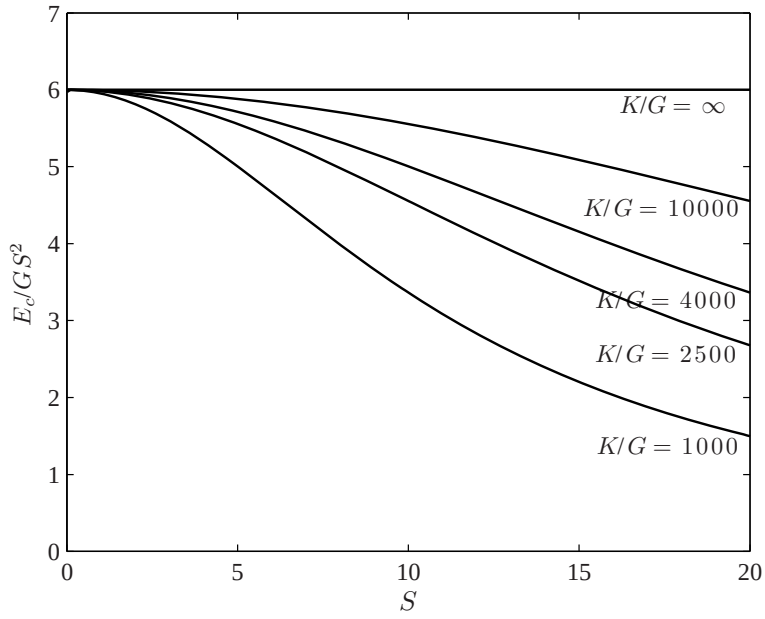

Figure 2.10 Effect of bulk compressibility on E_c for circular pads

When the argument of the modified Bessel functions is small, the functions may be approximated by

$$\mathrm{I}_1(x) = \frac{x}{2}\left(1 + \frac{x^2}{8} + \frac{x^4}{192} + \cdots\right)$$
$$\mathrm{I}_0(x) = \left(1 + \frac{x^2}{4} + \frac{x^4}{64} + \cdots\right)$$

from which

$$\frac{2}{x}\frac{\mathrm{I}_1(x)}{\mathrm{I}_0(x)} = 1 - \frac{x^2}{8} + \frac{x^4}{48}$$

Thus, for small values of S, the compression modulus may be estimated by

$$E_c = 6GS^2\left(1 - \frac{8GS^2}{K}\right) \tag{2.90}$$

The first term is the standard result from the incompressibility analysis given in Equation (2.34), and the second term is the correction for compressibility at moderately large shape factors. For typical values of G and K for filled rubbers, e.g., $G = 1.0$ MPa (145 psi), $K = 2000$ MPa (289 855 psi), and $S = 10$, the second term is of order 40%. We also note that

$$\frac{1}{E_c} = \frac{1}{6GS^2\left(1 - \dfrac{8GS^2}{K}\right)} = \frac{1}{6GS^2}\left(1 + \frac{8GS^2}{K}\right) = \frac{1}{6GS^2} + \frac{4}{3}\frac{1}{K} \tag{2.91}$$

demonstrating again that the *ad hoc* modification to include compressibility is not quite correct. For a more exact result, K must be replaced by $3K/4$ in the empirical formula.

For very large values of the argument, the modified Bessel functions can be approximated by the asymptotic expansions

$$\mathrm{I}_1(x) = \frac{e^x}{\sqrt{2\pi x}}\left(1 - \frac{3}{8x} - \frac{15}{128}\frac{1}{x^2} - \cdots\right)$$
$$\mathrm{I}_0(x) = \frac{e^x}{\sqrt{2\pi x}}\left(1 + \frac{1}{8x} + \frac{9}{128}\frac{1}{x^2} + \cdots\right)$$

from which

$$\frac{2}{x}\frac{\mathrm{I}_1(x)}{\mathrm{I}_0(x)} = \frac{2}{x}\left(1 - \frac{1}{2x} - \frac{1}{8x^2}\right)$$

giving

$$E_c = K\left(1 - \frac{1}{\sqrt{\frac{12\,G}{K}}S} + \frac{1}{\frac{48\,G}{K}S^2}\right) \tag{2.92}$$

This equation is useful when values for the modifie Bessel functions at large arguments are not available, and it can be used with negligible error when the shape factor is greater than 25.

There are two points that should be mentioned about these results. The firs is that the effect of compressibility on the compression modulus happens at such a low value of the shape factor. It is clear that bulk compressibility must be included for pads with shape factors a low as 10. In current practice, bearings tend to have shape factors in the range 30–40, where the compressibility will play a very large role. The other point is that the *ad hoc* approximation is not very accurate and that the designer should use the Bessel function solution, which is not the usual practice. There is the further complication that we need a good estimate of the value of the bulk modulus, K, when designing these high-shape-factor bearings, but this quantity is very difficul to measure, and estimates in the literature vary widely, for example from 1000 to 3500 MPa. To provide accurate estimates of the vertical frequency or the buckling load, covered in Chapters 5 and 6, a better estimate is needed, although it is not yet available.

2.4.3 Rectangular Pad

To compute the effective stiffness, E_c, for a rectangular pad (as shown in Figure 2.4) with a large shape factor, we f rst solve Equation (2.71) by using the same rapidly convergent single series solution, $p(x, y) = \sum_{m=1}^{\infty} P_m(y) \sin\left(\frac{m\pi x}{2b}\right)$, used to develop the earlier result for incompressible rubber. The Fourier coefficients $P_m(y)$, must satisfy

$$\frac{\mathrm{d}^2 P_m}{\mathrm{d}y^2} - \beta_m^2 P_m = -\frac{12\,G\varepsilon_c}{t^2} a_m \tag{2.93}$$

where $a_m = 4/(m\pi)$ for odd m and zero otherwise, and $\beta_m^2 = [m\pi/(2b)]^2 + 12\,G/(Kt^2)$. After solving for P_m, the pressure distribution takes the fina form

$$p = (x, y) = \frac{12\,G\varepsilon_c}{t^2} \sum_{m=1}^{\infty} \frac{a_m}{\beta_m^2}\left(1 - \frac{\cosh(\beta_m y)}{\cosh\left(\frac{\beta_m l}{2}\right)}\right) \sin\left(\frac{m\pi x}{2b}\right) \tag{2.94}$$

Integrating over the domain,

$$P = \int_{-l/2}^{l/2} \int_{0}^{2b} p\,(x,\, y)\,\mathrm{d}x\,\mathrm{d}y = \frac{12\,G\varepsilon_c}{t^2} \sum_{m=\text{odd}}^{\infty} \frac{ba_m^2}{\beta_m^2} \left(l - \frac{2}{\beta_m} \tanh\left(\frac{\beta_m l}{2} \right) \right) \tag{2.95}$$

and using $S = lb/[t(l + 2b)]$ and $E_c = P/(A\varepsilon_c)$, we obtain

$$E_c = \frac{384}{\pi^4} GS^2 (1 + \rho)^2 \sum_{m=\text{odd}}^{\infty} \frac{1}{m^4 \xi_m^2} \left(1 - \frac{2\rho}{m\pi\,\xi_m} \tanh\left(\frac{m\pi\,\xi_m}{2\rho} \right) \right) \tag{2.96}$$

where $\rho = 2b/l$ is the aspect ratio of the pad, and

$$\xi_m = \sqrt{1 + \frac{48\,GS^2\,(1 + \rho)^2}{K\,(m\pi)^2}} \tag{2.97}$$

Figure 2.11 shows $E_c/(GS^2)$ as a function of the shape factor, S, for different K/G values. The effect of bulk compressibility is pronounced, even for bearings with moderate shape factors. For example, for a rectangular pad with aspect ratio $\rho = 3$, shape factor $S = 20$, shear modulus $G = 1.0$ MPa, and bulk modulus $K = 2000$ MPa, (i.e., $K/G = 2000$), Equation (2.43) which ignores bulk-compressibility effects gives $E_c/(GS^2) = 5.62$, while Equation (2.96) which takes bulk-compressibility effects into account gives only $E_c/(GS^2) = 2.32$.

2.4.4 Annular Pad

Consider a annular pad of thickness t, inner radius a, and outer radius b. The boundary value problem for pressure p is

$$\begin{aligned} &\frac{\mathrm{d}^2 p}{\mathrm{d}r^2} + \frac{1}{r}\frac{\mathrm{d}p}{\mathrm{d}r} - \lambda^2\,(p - K\varepsilon_c) = 0 \\ &p\,(a) = 0, \quad p\,(b) = 0 \end{aligned} \tag{2.98}$$

where $\lambda^2 = 12G/(Kt^2)$. The problem was studied by Chalhoub and Kelly (1987) and Constantinou *et al.* (1992). The solution of the homogeneous part of the modifie Bessel equation, $r^2p'' + rp' - \lambda^2 r^2 p = 0$, has the form $p(r) = C_1\mathrm{I}_0(\lambda r) + C_2\mathrm{K}_0(\lambda r)$, where I_0 is the modifie Bessel function of the firs kind of order 0, and K_0 is the modifie Bessel function of the second kind of order 0. This, together with the boundary conditions $p(a) = 0$ and $\mathrm{p}(b) = 0$, gives the complete solution to Equation (2.98) as

$$p\,(r) = K\varepsilon_c\,(1 + C_1\mathrm{I}_0\,(\lambda r) + C_2\mathrm{K}_0\,(\lambda r)) \tag{2.99}$$

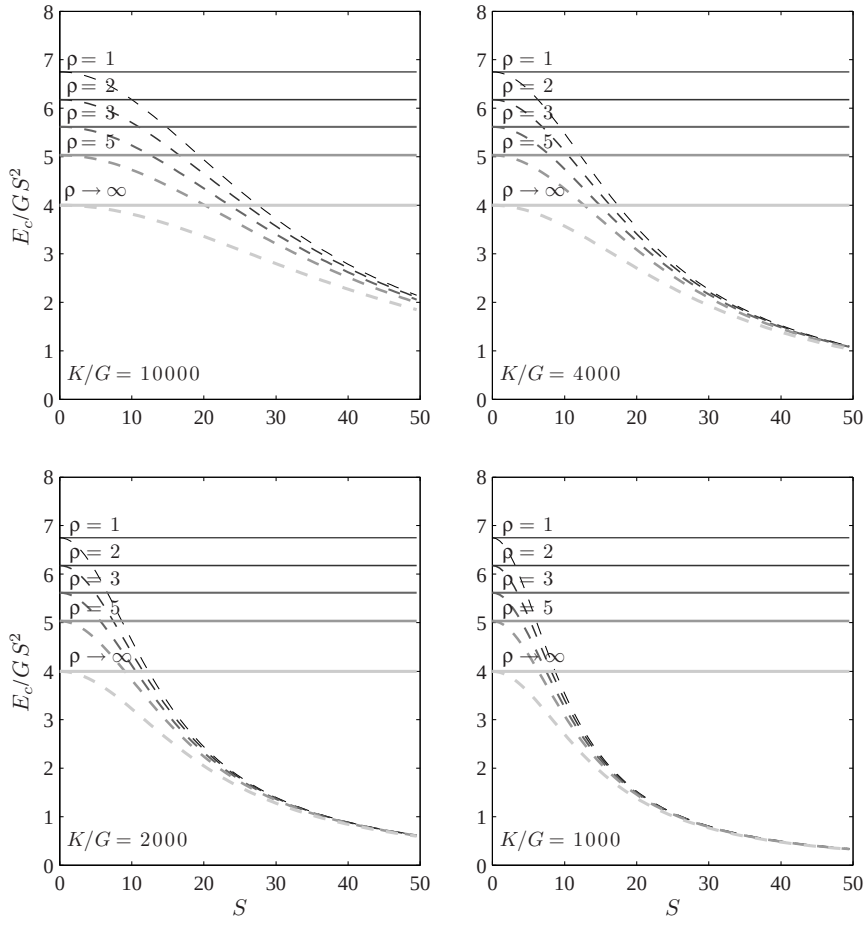

Figure 2.11 Effect of bulk compressibility on E_c for rectangular pads with different length-to-width ratios, ρ

where

$$C_1 = \frac{\mathrm{K}_0(\lambda b) - \mathrm{K}_0(\lambda a)}{\mathrm{I}_0(\lambda b)\,\mathrm{K}_0(\lambda a) - \mathrm{I}_0(\lambda a)\,\mathrm{K}_0(\lambda b)}$$
$$C_2 = -\frac{\mathrm{I}_0(\lambda b) - \mathrm{I}_0(\lambda a)}{\mathrm{I}_0(\lambda b)\,\mathrm{K}_0(\lambda a) - \mathrm{I}_0(\lambda a)\,\mathrm{K}_0(\lambda b)} \tag{2.100}$$

Integrating p over the area of the pad gives the total load P

$$P = \int_0^{2\pi}\int_a^b p(r) r\,\mathrm{d}r\,\mathrm{d}\theta = 2\pi K\varepsilon_c \left[\frac{b^2 - a^2}{2} + \frac{C_1}{\lambda}\left(b\mathrm{I}_1(\lambda b) - a\mathrm{I}_1(\lambda a)\right) - \frac{C_2}{\lambda}\left(b\mathrm{K}_1(\lambda b) - a\mathrm{K}_1(\lambda a)\right)\right] \tag{2.101}$$

and since $E_c = P/(A\varepsilon_c)$,

$$E_c = K\left[1 + \frac{2C_1}{\lambda^2(b^2-a^2)}(\lambda b \mathrm{I}_1(\lambda b) - \lambda a \mathrm{I}_1(\lambda a)) - \frac{2C_2}{\lambda^2(b^2-a^2)}(\lambda b \mathrm{K}_1(\lambda b) - \lambda a \mathrm{K}_1(\lambda a))\right] \tag{2.102}$$

where I_1 is the modifie Bessel function of firs kind of order 1, and K_1 is the modifie Bessel function of the second kind of order 1. Using $S = (b-a)/(2t)$ and $\eta = a/b$ (the ratio of the inner diameter to the outer diameter), we can express the compression modulus as

$$E_c = K\left[1 + C_1'(\mathrm{I}_1(\vartheta) - \eta \mathrm{I}_1(\eta\vartheta)) + C_2'(\mathrm{K}_1(\vartheta) - \eta \mathrm{K}_1(\eta\vartheta))\right] \tag{2.103}$$

where

$$\vartheta = \sqrt{\frac{48\,G}{K}}\frac{S}{1-\eta} \tag{2.104}$$

and

$$\begin{aligned} C_1' &= \frac{1}{\sqrt{\frac{12\,G}{K}}(1+\eta)\,S}\frac{\mathrm{K}_0(\vartheta) - \mathrm{K}_0(\eta\vartheta)}{\mathrm{I}_0(v)\,\mathrm{K}_0(\eta\vartheta) - \mathrm{I}_0(\eta\vartheta)\,\mathrm{K}_0(\vartheta)} \\ C_2' &= \frac{1}{\sqrt{\frac{12\,G}{K}}(1+\eta)\,S}\frac{\mathrm{I}_0(\vartheta) - \mathrm{I}_0(\eta\vartheta)}{\mathrm{I}_0(\upsilon)\,\mathrm{K}_0(\eta\vartheta) - \mathrm{I}_0(\eta\vartheta)\,\mathrm{K}_0(\vartheta)} \end{aligned} \tag{2.105}$$

Figure 2.12 shows graphs of the normalized compression modulus of an annular pad as a function of the shape factor, S, for different η and K/G values. The f gure shows that for realistic values of K/G (e.g., $K/G = 2000$), neglecting bulk-compressibility effects may grossly overestimate the compression modulus even for moderate shape factors.

We now seek to investigate the effect of a small hole on a circular pad. We firs normalize E_c with respect to $6\,GS^2$, the value for a complete pad based on the radius R (here $= b$), when incompressibility is assumed and note that $(\lambda R)^2 = (48\,GS^2)/K$, so that

$$\frac{K}{6\,GS^2} = \frac{8}{(\lambda R)^2} \tag{2.106}$$

We now consider small η (i.e., <0.1) and denote it as ε. Using $y = E_c/(6\,GS^2)$ and $x = \lambda R$, Equation (2.102) can be approximated by

$$y = \frac{8}{x^2}\left(1 - \frac{2}{x}\frac{(\mathrm{K}_0(x) - \mathrm{K}_0(\varepsilon x))(\mathrm{I}_1(x) - \varepsilon \mathrm{I}_1(\varepsilon x)) + (\mathrm{K}_1(x) - \varepsilon \mathrm{K}_1(\varepsilon x))(\mathrm{I}_0(x) - \mathrm{I}_0(\varepsilon x))}{\mathrm{I}_0(\varepsilon x)\,\mathrm{K}_0(x) - \mathrm{I}_0(x)\mathrm{K}_0(\varepsilon x)}\right) \tag{2.107}$$

We now consider the particular case with $G = 1.0$ MPa, $K = 2000$ MPa and $S = 20$, for which $x = 3.098$. The value of the normalized modulus y when $\varepsilon = 0$ is 0.3936, and the

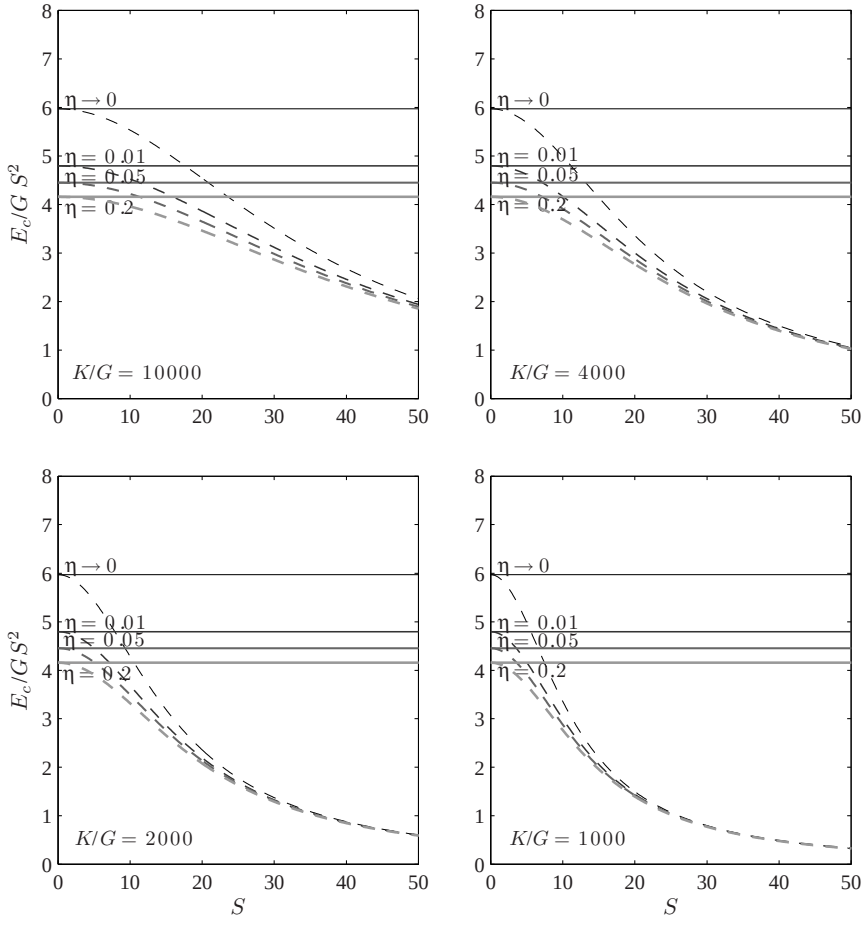

Figure 2.12 Effect of bulk compressibility on E_c for annular pads with different inner-to-outer radius ratios, η

curve of y as a function of ε over the range $0 < \varepsilon \leq 0.10$ is shown in Figure 2.13. As with the analysis conducted for incompressible material, the solution exhibits a singularity at $\varepsilon = 0$, where the tangent is negative infinity however, the value of the compression modulus does not drop as dramatically as it does for the incompressible material. For example, for $\varepsilon = 0.1$, $y = 0.320$ (while the exact solution, Equation (2.103), gives 0.351 for $\eta = 0.1$). For comparison, $E_c/(6\,GS^2)$ for the incompressible material drops from 1 for $\eta = 0$ to 0.716 for $\eta = 0.1$. Therefore, the effect that a small hole in a circular bearing has on the compression modulus decreases as the compressibility increases. This is evident in Figure 2.13 which shows both the solution for compressible and incompressible material.

This chapter has provided results for the behavior of a wide variety of bearings under pure compression which will form the basis of further analysis in later chapters. One of the most interesting aspects of the analyses in this chapter has been the unexpected result that bulk compressibility plays an important role, even at shape factors as low as 10. It means that for the bearings used in seismic isolation systems which tend

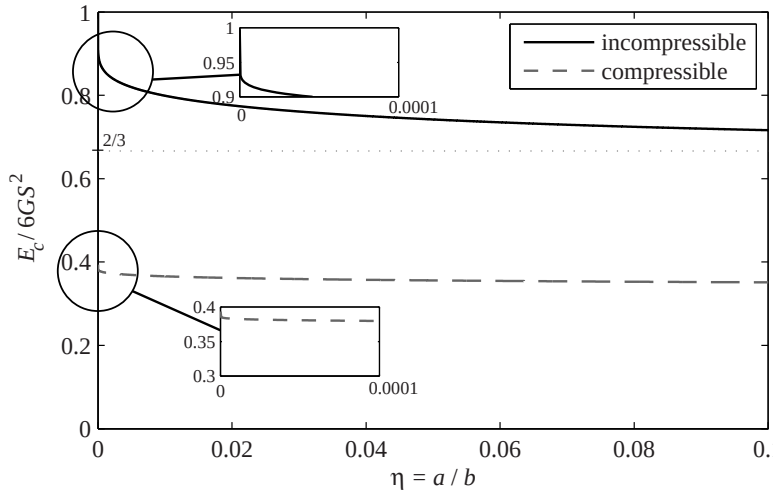

Figure 2.13 Effect of small hole on the compression modulus of a circular pad ($G = 1.0$ MPa, $K = 2000$ MPa, $S = 20$)

to have shape factors in the range of 30–40, compressibility of the rubber cannot be ignored. The bulk modulus of elastomeric materials is an extremely difficul property to measure. Elastomers, such as natural rubber, have a bulk modulus that is several orders of magnitude larger than their shear modulus so that the material will deform only in shear—if at all possible. In most other types of applications, the deformation can be assumed to be a constant volume one, and the material be assumed to be incompressible, but for seismic isolators the design formula based on the incompressible model can seriously over-predict the vertical stiffness and the buckling load of a bearing.

It is accordingly essential to have an accurate estimate of the bulk modulus. A quick review of the data available on this property for natural rubber in particular reveals that an accurate estimate is difficul to find For example, the widely used handbook *Engineering Design with Natural Rubber* (Lindley 1978) published by the Malaysian Rubber Producers Research Association (now the Tun Abdul Razac Research Center) provides a table of bulk modulus values based on the International Rubber Hardness Degrees (IRHD) that range from 1000 to 1330 MPa as the hardness varies from 30 to 75 IRHD. On the other hand the reference *Engineering Use of Natural Rubber* (Fuller *et al.* 1988) published by Oxford University Press gives values in the range from 2000 to 3500 MPa.

The analysis given in this chapter suggests that a possible way to determine the bulk modulus even if in a somewhat indirect way is to use the measured vertical stiffness of isolators to estimate its value. Seismic isolators are usually made with high damping rubber compounds that are nonlinear and have large hysteresis which can make interpretation of the measurements difficult but in some projects the compounds used (LNR) have almost no hysteresis and are very linear in shear up to very large shear strains. For these, the results of horizontal shear tests can be used to infer the shear modulus, and the results of vertical stiffness tests can be used to obtain an estimate of the bulk modulus.

3

Behavior of Multilayer Rubber Bearings under Bending

3.1 Bending Stiffness of Single Pad with Incompressible Rubber

An important bearing property that must be analyzed for design is the buckling behavior of the isolator. For this analysis, the response of the compressed bearing to bending moment is necessary. Referred to as the *bending stiffness*, this can be ascertained by an extension of the same analysis that is done to determine the vertical stiffness. The bending stiffness plays an important role in the estimate of the buckling load in a bearing and also is needed to determine the influenc of the vertical load on the horizontal (shear) stiffness of a bearing. In addition, when the isolator is subject to shear deformation, a bending moment is generated by the unbalanced shear forces at the top and bottom of the bearing. These bending moments cause shear strains in the rubber that are important for design, and they also affect the stresses in the steel shims. In contrast to the case of pure compression, these stresses can be compressive and could produce buckling of the shims.

The bending stiffness of a single pad is computed using an approach similar to that for compression stiffness; however, the displaced configuratio is obtained in two stages. First visualize the deformation that would occur if the bending conformed to elementary beam theory (shown dotted in Figure 3.1). Because this cannot satisfy the incompressibility constraint, a further pure shear deformation is superimposed. The displacement fiel is given by

$$\begin{aligned} u(x, y, z) &= u_0(x, y)\left(1 - \frac{4z^2}{t^2}\right) - \frac{\alpha z^2}{2t} \\ v(x, y, z) &= v_0(x, y)\left(1 - \frac{4z^2}{t^2}\right) \\ w(x, y, z) &= \frac{\alpha z x}{t} \end{aligned} \tag{3.1}$$

Mechanics of Rubber Bearings for Seismic and Vibration Isolation, First Edition. James M. Kelly and Dimitrios A. Konstantinidis.

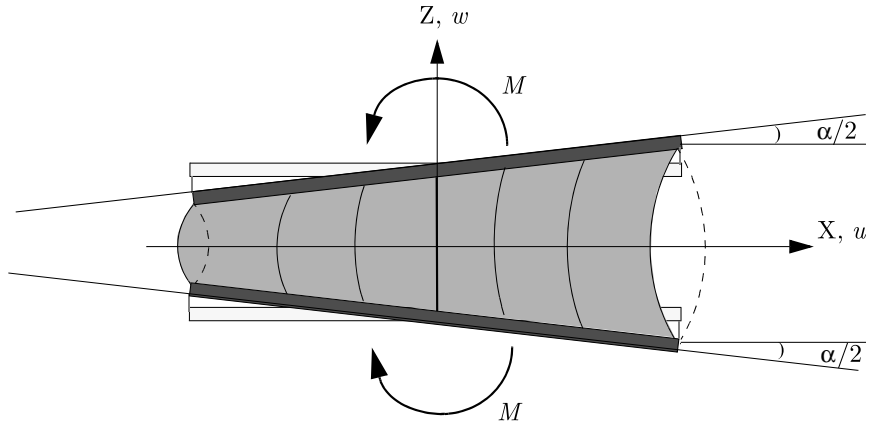

Figure 3.1 Rubber pad between rigid plates in pure bending

Here, α is the angle between the rigid plates in the deformed configuration and the bending is about the y-axis. The radius of curvature, ϱ, generated by the deformation is related to α by

$$\frac{1}{\varrho} = \frac{\alpha}{t} \tag{3.2}$$

When integrated through the thickness, the incompressibility condition

$$\varepsilon_{xx} + \varepsilon_{yy} + \varepsilon_{zz} = 0 \tag{3.3}$$

gives

$$\frac{\partial u_0}{\partial x} + \frac{\partial v_0}{\partial y} + \frac{3\alpha}{2t}x = 0 \tag{3.4}$$

The shear stresses, $\tau_{xz} = G\gamma_{xz} = G(\partial u/\partial z + \partial w/\partial x)$ and $\tau_{yz} = G\gamma_{yz} = G(\partial v/\partial z + \partial w/\partial y)$, are given by

$$\begin{aligned} \tau_{xz} &= -\frac{8\,G}{t^2} z u_0 \\ \tau_{yz} &= -\frac{8\,G}{t^2} z v_0 \end{aligned} \tag{3.5}$$

and substitution into the equations of equilibrium,

$$\begin{aligned} \frac{\partial \sigma_{xx}}{\partial x} + \frac{\partial \tau_{xz}}{\partial z} &= 0 \\ \frac{\partial \sigma_{yy}}{\partial y} + \frac{\partial \tau_{yz}}{\partial z} &= 0 \end{aligned} \tag{3.6}$$

gives

$$u_0 = -\frac{t^2}{8\,G}\,\frac{\partial p}{\partial x},\, v_0 = -\frac{t^2}{8\,G}\,\frac{\partial p}{\partial y} \tag{3.7}$$

which, with the incompressibility condition, leads to

$$\frac{\partial^2 p}{\partial x^2} + \frac{\partial^2 p}{\partial y^2} = \nabla^2 p = \frac{12\,G\alpha}{t^3} x \tag{3.8}$$

with $p = 0$ on the edges.

The solution technique is to solve Equation (3.8) for p and to compute the bending moment M from

$$M = -\int_A p(x, y) x \mathrm{d}A \tag{3.9}$$

Using the analogy with beam theory, where

$$M = EI\frac{1}{\varrho} \tag{3.10}$$

we compute the bending stiffness

$$(EI)_{\mathit{eff}} = \frac{M}{\alpha/t} \tag{3.11}$$

3.1.1 Infinit Strip Pad

For the example of the infinit strip of width $2b$, shown in Figure 2.2, we have

$$\frac{\mathrm{d}^2 p}{\mathrm{d}x^2} = \frac{12\,G\alpha}{t^3} x \tag{3.12}$$

or

$$p = -\frac{2\,G\alpha}{t^3}(b^2 - x^2)x \tag{3.13}$$

The resultant moment M is given by

$$M = -\int_{-b}^{+b} px\mathrm{d}x = \frac{8\,G\alpha b^5}{15t^3} \tag{3.14}$$

If we compare this with the usual bending equation for a beam, namely, $M = EI(1/\varrho)$, where $I = 2b^3/3$ is the moment of inertia of a beam cross-section with the shape of the pad, we can obtain an *effective* bending stiffness $(EI)_{eff}$,

$$(EI)_{eff} = M\varrho = \frac{M}{\alpha/t} = \frac{8\,Gb^5}{15t^2} = \frac{4}{5}GS^2\left(\frac{2}{3}b^3\right) = \frac{4}{5}GIS^2 \tag{3.15}$$

As seen in Chapter 2, $E_c = 4\,GS^2$, then $(EI)_{eff} = E_cI/5$. Thus, the effective I for the strip is $I/5$. This reduction is caused by the pressure distribution that varies cubically across the width of the strip, whereas in a beam the bending stress distribution varies linearly through the thickness.

3.1.2 Circular Pad

For a circular pad of radius R (see Figure 2.3), the equation to be solved, using polar coordinates r and θ, is

$$\frac{\partial^2 p}{\partial r^2} + \frac{1}{r}\frac{\partial p}{\partial r} + \frac{1}{r^2}\frac{\partial^2 p}{\partial \theta^2} = \frac{12\,G\alpha}{t^3} r\cos\theta \tag{3.16}$$

The solution is

$$p(r,\theta) = \left(Ar + B\frac{1}{r} + Cr^3\right)\cos\theta \tag{3.17}$$

where

$$C = \frac{3\,G\alpha}{2t^3}$$

For the complete circle, $0 \le r \le R$, B has to be zero for p to be bounded at $r = 0$, and using $p = 0$ at $r = R$ gives

$$p = \frac{3\,G\alpha}{2t^3}(r^2 - R^2)r\cos\theta \tag{3.18}$$

and

$$M = -\int_0^{2\pi}\int_0^R pr^2\cos(\theta)\mathrm{d}r\,\mathrm{d}\theta = \frac{G\alpha}{8t^3}\pi R^6 \tag{3.19}$$

The effective moment of inertia in this case, taking $E = E_c = 6\,GS^2$ and $I = \pi R^4/4$, is one-third of the conventional moment of inertia,

$$(EI)_{eff} = \frac{M}{\alpha/t} = \frac{G}{8t^2}\pi R^6 = 2\,GS^2\left(\frac{\pi R^4}{4}\right) = 2\,GIS^2 \tag{3.20}$$

Also, since for a circular pad, $E_c = 6\,GS^2$, $(EI)_{eff} = E_cI/3$.

3.1.3 Rectangular Pad

We consider the bending of a rectangular pad of sides $2b$ and l about the y-axis as shown in Figure 3.2. The result for a rectangular pad can be determined by assuming a single Fourier series solution of the form

$$p(x, y) = \sum_{m=1}^{\infty} P_m(y) \sin\left(\frac{m\pi x}{b}\right) \tag{3.21}$$

Substituting into Equation (3.8) gives

$$\sum_{m=1}^{\infty} \left[\frac{\mathrm{d}^2 P_m(y)}{\mathrm{d}y^2} - \left(\frac{m\pi}{b}\right)^2 P_m(y)\right] \sin\left(\frac{m\pi x}{b}\right) = \frac{12\,G\alpha}{t^3} x \tag{3.22}$$

Multiplying by $\sin(n\pi x/b)$ and integrating from $-b$ to b gives

$$P_n''(y) - \left(\frac{n\pi}{b}\right)^2 P_n(y) = \frac{24\,G\alpha}{t^3} \frac{b}{n\pi} (-1)^{n-1} \tag{3.23}$$

Symmetry and the boundary condition $P_n(\pm l/2) = 0$ (from $p(x, \pm l/2) = 0$) give the solution to this ordinary differential equation as

$$P_n(y) = \frac{24\,G\alpha}{t^3} \left(\frac{b}{n\pi}\right)^3 (-1)^n \left(1 - \frac{\cosh\left(\frac{n\pi y}{b}\right)}{\cosh\left(\frac{n\pi l}{2b}\right)}\right) \tag{3.24}$$

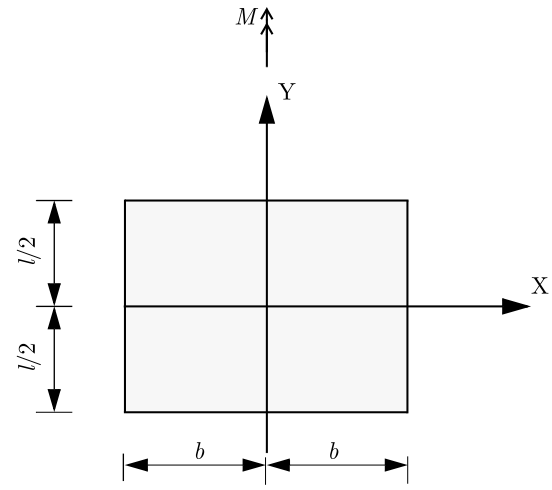

Figure 3.2 Coordinate system of a rectangular pad under bending

The complete solution for the pressure then becomes

$$p(x,y) = \frac{24\,Gb^3\alpha}{\pi^3 t^3}\sum_{n=1}^{\infty}\frac{(-1)^n}{n^3}\left(1-\frac{\cosh\left(\frac{n\pi y}{b}\right)}{\cosh\left(\frac{n\pi l}{2b}\right)}\right)\sin\left(\frac{n\pi x}{b}\right) \tag{3.25}$$

which can also be expressed in terms of the shape factor $S = bl/[(2\,b + l)t]$ as

$$p(x,y) = \frac{24\,GS^2 b\alpha}{\pi^3 t}\left(1+\frac{2b}{l}\right)^2\sum_{n=1}^{\infty}\frac{(-1)^n}{n^3}\left(1-\frac{\cosh\left(\frac{n\pi y}{b}\right)}{\cosh\left(\frac{n\pi l}{2b}\right)}\right)\sin\left(\frac{n\pi x}{b}\right) \tag{3.26}$$

Then

$$\begin{aligned}(EI)_{\mathit{eff}} &= \frac{M}{\alpha/t} = -\frac{1}{\alpha/t}\int_{-l/2}^{l/2}\int_{-b}^{b} p(x,y)\,x\,\mathrm{d}x\,\mathrm{d}y \\ &= \frac{48\,GS^2 lb^3}{\pi^4}\left(1+\frac{2b}{l}\right)^2\sum_{n=1}^{\infty}\frac{1}{n^4}\left(1-\frac{2b}{n\pi l}\tanh\left(\frac{n\pi l}{2b}\right)\right)\end{aligned} \tag{3.27}$$

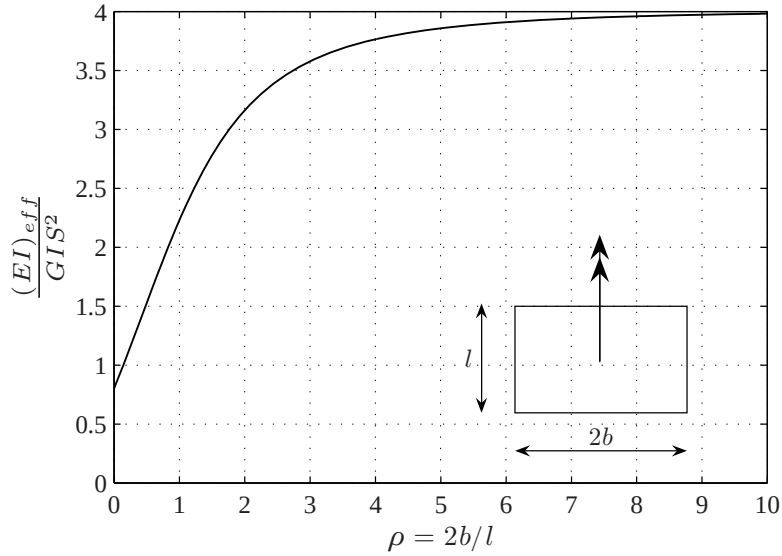

Figure 3.3 Effective *EI* of a rectangular pad

With $I = 2lb^3/3$, the effective bending stiffness can be expressed as

$$(EI)_{eff} = \frac{72\,GIS^2}{\pi^4}(1+\rho)^2 \sum_{n=1}^{\infty} \frac{1}{n^4}\left(1 - \frac{\rho}{n\pi}\,\tanh\left(\frac{n\pi}{\rho}\right)\right) \tag{3.28}$$

where $\rho = 2b/l$. Figure 3.3 shows the effective EI of a rectangular pad as a function of ρ.

For a square pad,

$$(EI)_{eff} = \frac{288\,GIS^2}{\pi^4} \sum_{n=1}^{\infty} \frac{1}{n^4}\left(1 - \frac{1}{n\pi}\,\tanh(n\pi)\right) \approx 2.228\,GIS^2 \tag{3.29}$$

3.1.4 Annular Pad

For an annular pad of inner radius, a, outer radius, b, where $a \le r \le b$, we have

$$p = \frac{3\,G\alpha}{2t^3}\left(\frac{a^2b^2}{r} + r^3 - (b^2+a^2)r\right)\cos\theta \tag{3.30}$$

and

$$M = -\frac{3\,G\alpha}{2t^3}\int_0^{2\pi}\left[\int_a^b \left(\frac{a^2b^2}{r} + r^3 - (b^2+a^2)r\right) r^2 \mathrm{d}r\right]\cos^2\theta\,\mathrm{d}\theta = \frac{G\alpha\pi}{8t^3}(b^2-a^2)^3 \tag{3.31}$$

which leads to

$$\begin{aligned}(EI)_{eff} &= \frac{\pi}{8}G\frac{(b^2-a^2)^3}{t^2}\\ &= \frac{\pi}{2}GS^2(b-a)(b+a)^3\\ &= \frac{\pi}{2}GS^2I\left(4\frac{(b-a)(b+a)^3}{\pi(b^4-a^4)}\right)\\ &= 2\,GS^2I\frac{(b+a)^2}{b^2+a^2} = 2\,GS^2I\frac{(1+\rho)^2}{1+\rho^2}\end{aligned} \tag{3.32}$$

where here $\rho = a/b$ is the ratio of the inner radius to the outer radius. Figure 3.4 shows a graph of $(EI)_{eff}/(2\,GS^2I)$ as a function of ρ.

There are two ways to express this result. One is to assume that a/b is greater than about 0.1, in which case the effective compression modulus is $4\,GS^2$ where $S = (b-a)/(2t)$, giving

$$\frac{(EI)_{eff}}{EI} = \frac{1}{2}\frac{\left(1+\frac{a}{b}\right)^2}{1+\left(\frac{a}{b}\right)^2} \tag{3.33}$$

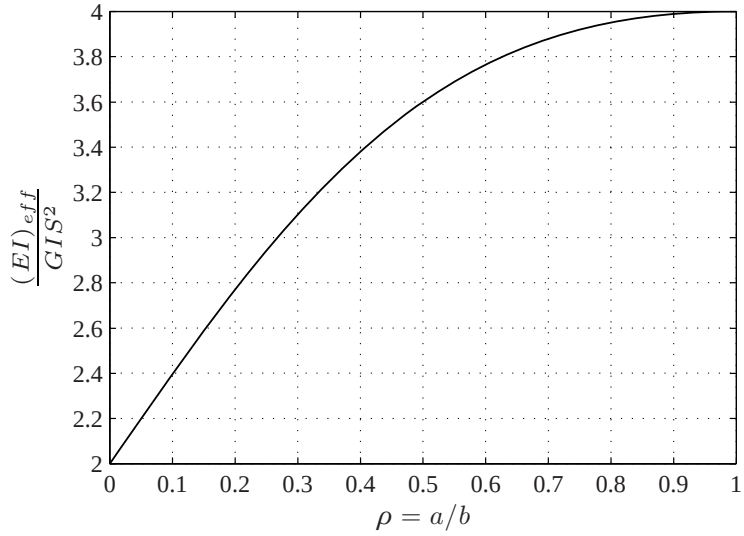

Figure 3.4 Effective *EI* of an annular pad with inner radius *a* and outer radius *b*

On the other hand, if $a \to 0$, then $(EI)_{\mathit{eff}} \to 6\,GS^2(I/3)$. In addition, if we write $a = b\varepsilon$ and let $\varepsilon \to 0$, we get $(EI)_{\mathit{eff}} \to 4\,GS^2(1 + 2\varepsilon)\,(I/2)$, showing that in contrast to case of the compression modulus, the presence of a small hole has a negligible effect on the bending stiffness. The reason, of course, is that the pressure at the edge of the hole, if it is small, is very close to zero anyway, and the boundary condition of zero pressure is already met.

3.2 Bending Stiffness of Single Pads with Compressible Rubber

If we take into account the bulk compressibility when estimating the bending stiffness, the equation to be solved is

$$\nabla^2 p - \lambda^2 p = \frac{\lambda^2 K\alpha}{t} x \tag{3.34}$$

where $\lambda^2 = 12\,G/(Kt^2)$ and $p = 0$ at the edge of the pad.

3.2.1 Infinit Strip Pad

For an infinit strip of width $2b$, Equation (3.34) becomes

$$\frac{\mathrm{d}^2 p}{\mathrm{d}x^2} - \lambda^2 p = \frac{\lambda^2 K\alpha}{t} x \tag{3.35}$$

with $p(\pm b) = 0$. The solution is

$$p(x) = \frac{K\alpha b}{t}\left(\frac{\sinh(\lambda x)}{\sinh(\lambda b)} - \frac{x}{b}\right) \tag{3.36}$$

The moment per unit length generated by this pressure distribution is

$$M = -\int_{-b}^{+b} xp(x)\mathrm{d}x = \frac{2\,K\alpha b}{\lambda^2 t}\left(1 + \frac{\lambda^2 b^2}{3} - \lambda b\coth(\lambda b)\right) \tag{3.37}$$

Because $1/\varrho = \alpha/t$, the effective bending stiffness is

$$(EI)_{eff} = \frac{2\,Kb}{\lambda^2}\left(1 + \frac{\lambda^2 b^2}{3} - \lambda b\coth(\lambda b)\right) \tag{3.38}$$

The effective EI of the compressible rubber, given by Equation (3.38), can be expressed as a ratio of the effective EI of the incompressible rubber, given by Equation (3.15),

$$\frac{(EI)_{eff}^{\text{comp}}}{(EI)_{eff}^{\text{inc}}} = \frac{\dfrac{2\,Kb}{\lambda^2}\left(1 + \dfrac{\lambda^2 b^2}{3} - \lambda b\coth(\lambda b)\right)}{\dfrac{8\,Gb^5}{15t^2}} = \frac{45}{\lambda^4 b^4}\left(1 + \frac{\lambda^2 b^2}{3} - \lambda b\coth(\lambda b)\right) \tag{3.39}$$

which, with $\lambda b = \sqrt{12\,G/K}S$, can also be expressed as

$$\frac{(EI)_{eff}^{\text{comp}}}{(EI)_{eff}^{\text{inc}}} = \frac{5\,K^2}{16\,G^2 S^4}\left(1 + \frac{4\,GS^2}{K} - \sqrt{\frac{12\,G}{K}}\mathrm{S}\coth\left(\sqrt{\frac{12\,G}{K}}S\right)\right) \tag{3.40}$$

Figure 3.5, which is a graph of the ratio given by Equation (3.40) for various values of K/G, shows that compressibility can have a significan effect even for pads with moderate shape factors.

For small values of λb, an approximation of Equation (3.38) can be obtained from the power series for coth for small x by

$$\coth x = \frac{1}{x}\left(1 + \frac{x^2}{3} - \frac{x^4}{45} + \frac{2x^6}{945}\cdots\right)$$

from which we obtain

$$(EI)_{eff} = \frac{4\,GIS^2}{5}\left(1 - \frac{8}{7}\frac{GS^2}{K}\right) \tag{3.41}$$

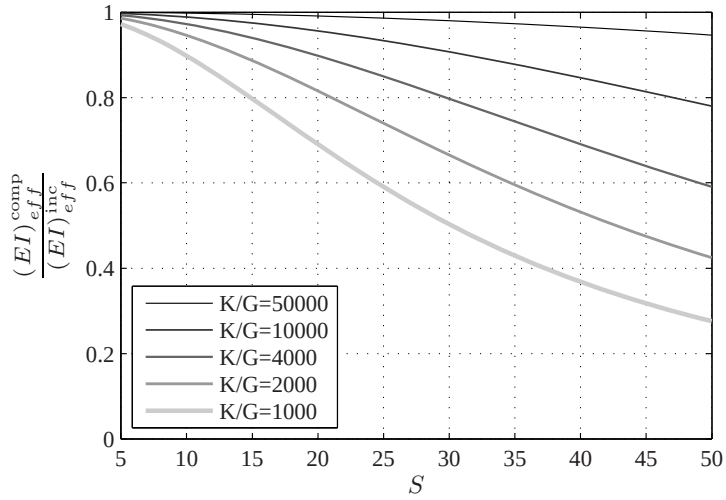

Figure 3.5 Ratio of the effective bending stiffness with compressible rubber to the effective bending stiffness with incompressible rubber for a strip pad

For large values of λb, $\coth(\lambda b)$ tends to 1 and $(EI)_{eff}$ tends to $2Kb^3/3$, implying that the effective I tends to the actual I, which, in turn, implies that the pressure distribution is linear across the strip. In fact, for large λb, we can approximate p by

$$p(x) = \frac{K\alpha b}{t}\left(e^{-\lambda(b-x)} - \frac{x}{b}\right) \tag{3.42}$$

which means that the distribution is linear except when x is close to $\pm b$.

When the pressure, $p(x)$, of Equation (3.36) is normalized with the maximum pressure due to the moment M of Equation (3.37), we get

$$\bar{p} = \frac{p}{M\Big/\left(\frac{2}{3}b^2\right)} = \frac{\lambda^2 b^2\left(\frac{\sinh(\lambda x)}{\sinh(\lambda b)} - \frac{x}{b}\right)}{3\left(1 + \frac{\lambda^2 b^2}{3} - \lambda b\coth(\lambda b)\right)} \tag{3.43}$$

Figure 3.6 shows the normalized pressure distribution, $\bar{p}$, of Equation (3.43) under pure bending for different shape factors ($S = 10, 50, 500$) for a strip using $G = 1.0$ MPa (145 psi) and $K = 2000$ MPa (289 855 psi).

3.2.2 Circular Pad

For a circular pad, the equation to be solved is

$$\frac{\partial^2 p}{\partial r^2} + \frac{1}{r}\frac{\partial p}{\partial r} + \frac{1}{r^2}\frac{\partial^2 p}{\partial \theta^2} - \lambda^2 p = \frac{\lambda^2 K\alpha}{t} r\cos\theta \tag{3.44}$$

with $p(r = R) = 0$.

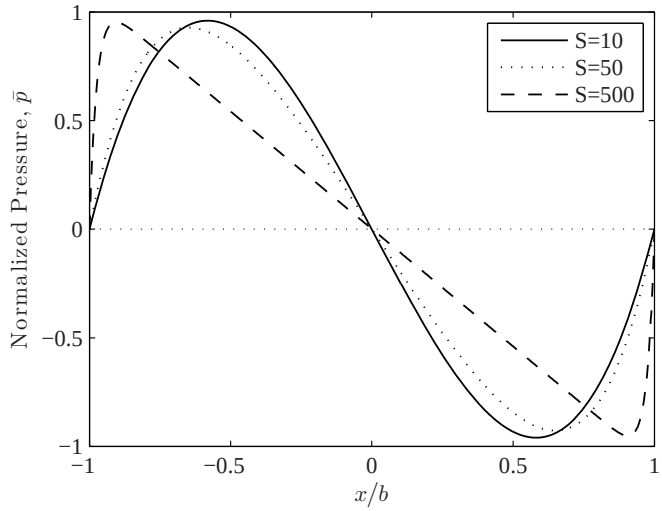

Figure 3.6 Normalized pressure distribution of infinit strip pad under pure bending

The result for $p(r, \theta)$ is

$$p = \frac{K\alpha R}{t}\left(\frac{\mathrm{I}_1(\lambda r)}{\mathrm{I}_1(\lambda R)} - \frac{r}{R}\right)\cos\theta \tag{3.45}$$

where I_1 is the modifie Bessel function of the firs kind of order 1. The moment produced by this pressure distribution is

$$\begin{aligned} M &= -\int_0^{2\pi}\int_0^{R} p(r,\theta) r^2 \cos\theta \,\mathrm{d}r\,\mathrm{d}\theta \\ &= \pi K \frac{\alpha}{t}\frac{R^2}{\lambda^2}\left(\frac{(\lambda R)^2}{4} - \lambda R\frac{\mathrm{I}_2(\lambda R)}{\mathrm{I}_1(\lambda R)}\right) \end{aligned} \tag{3.46}$$

where I_2 is the modifie Bessel function of the firs kind of order 2. Then the effective bending stiffness is

$$(EI)_{\mathit{eff}} = \frac{\pi K R^2}{\lambda^2}\left(\frac{(\lambda R)^2}{4} - \lambda R\frac{\mathrm{I}_2(\lambda R)}{\mathrm{I}_1(\lambda R)}\right) \tag{3.47}$$

The result in Equation (3.47) is most conveniently used as a ratio to the bending stiffness in the incompressible case, which is given by Equation (3.20). Dividing Equation (3.47) by this gives

$$\frac{(EI)_{\mathit{eff}}^{\mathrm{comp}}}{(EI)_{\mathit{eff}}^{\mathrm{inc}}} = \frac{24}{\lambda^2 R^2}\left(1 - \frac{4}{\lambda R}\frac{\mathrm{I}_2(\lambda R)}{\mathrm{I}_1(\lambda R)}\right) \tag{3.48}$$

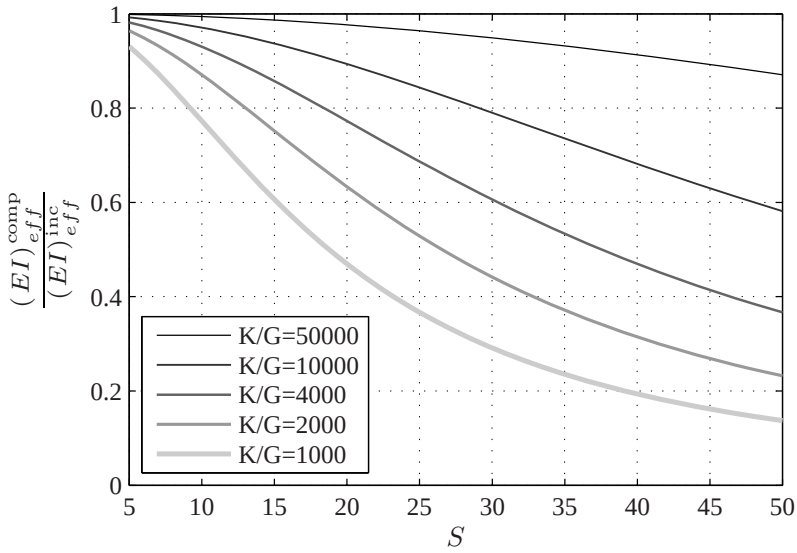

Figure 3.7 Ratio of the effective bending stiffness with compressible rubber to the effective bending stiffness with incompressible rubber for a circular pad

Or, since $\lambda R = \sqrt{48\,G/K}S$,

$$\frac{(EI)^{\text{comp}}_{eff}}{(EI)^{\text{inc}}_{eff}} = \frac{K}{2\,GS^2}\left(1 - \frac{4}{\sqrt{\frac{48\,G}{K}}S}\frac{\mathrm{I}_2\left(\sqrt{\frac{48\,G}{K}}S\right)}{\mathrm{I}_1\left(\sqrt{\frac{48\,G}{K}}S\right)}\right) \tag{3.49}$$

The form of this ratio as a function of shape factor S for various K/G in Figure 3.7, where it is clear that the bending stiffness is affected by compressibility at surprisingly low values of S.

An approximation of the bending stiffness for the compressible rubber can be obtained by expanding the modifie Bessel functions for small x. We get

$$\mathrm{I}_1(x) = \frac{x}{2} + \frac{x^3}{16} + \frac{x^5}{384} + \cdots$$
$$\mathrm{I}_2(x) = \frac{x^2}{8} + \frac{x^4}{96} + \frac{x^6}{3072} + \cdots$$

and

$$\lambda R\frac{\mathrm{I}_2(\lambda R)}{\mathrm{I}_1(\lambda R)} = \frac{(\lambda R)^2}{4} - \frac{(\lambda R)^4}{96} + \frac{(\lambda R)^6}{1536}$$

leading to

$$(EI)_{eff} = 2GIS^2\left(1 - \frac{3GS^2}{K}\right) \tag{3.50}$$

For very large values of x, both I_1 and I_2 tend to $e^x/\sqrt{2\pi x}$, and the asymptotic value of $(EI)_{eff}$ is KI, which is what would be expected if the pressure distribution was linear and the compression modulus was K. In fact, for large values of S, the pressure distribution does tend to be linear, as shown by Equation (3.45), which when $\lambda \to \infty$, tends to

$$p = -\frac{K\alpha}{t} r\cos\theta \tag{3.51}$$

3.2.3 Rectangular Pad

The result for a rectangular pad (Figure 3.2) can be determined by assuming a single Fourier series solution of the form

$$p(x, y) = \sum_{m=1}^{\infty} P_m(y)\sin\left(\frac{m\pi x}{b}\right) \tag{3.52}$$

Substituting this into Equation (3.34) gives

$$\sum_{m=1}^{\infty}\left\{\frac{\mathrm{d}^2 P_m(y)}{\mathrm{d}y^2} - \left[\left(\frac{m\pi}{b}\right)^2 + \lambda^2\right] P_m(y)\right\}\sin\left(\frac{m\pi x}{b}\right) = \frac{\lambda^2 K\alpha}{t}x \tag{3.53}$$

Multiplying by $\sin(n\pi x/b)$ and integrating from $-b$ to b gives

$$\frac{\mathrm{d}^2 P_n(y)}{\mathrm{d}y^2} - \beta_n^2 P_n(y) = \frac{2\lambda^2 K\alpha b}{n\pi t}(-1)^{n-1} \tag{3.54}$$

where $\beta_n^2 = (n\pi/b)^2 + \lambda^2$. Symmetry and the boundary condition $P_n(\pm l/2) = 0$ (from $p(x, \pm l/2) = 0$) give the solution to this ordinary differential equation as

$$P_n(y) = \frac{2\lambda^2 K\alpha b}{n\pi t\beta_n^2}(-1)^n\left(1 - \frac{\cosh(\beta_n y)}{\cosh(\beta_n l/2)}\right) \tag{3.55}$$

The complete solution for the pressure becomes

$$p(x, y) = \frac{2\lambda^2 K\alpha b}{t}\sum_{n=1}^{\infty}\frac{(-1)^n}{n\pi\beta_n^2}\left[1 - \frac{\cosh(\beta_n y)}{\cosh(\beta_n l/2)}\right]\sin\left(\frac{n\pi x}{b}\right) \tag{3.56}$$

Then

$$(EI)_{eff} = \frac{M}{\alpha/t} = -\frac{1}{\alpha/t}\int_{-l/2}^{l/2}\int_{-b}^{b} p(x,y)x\,dx\,dy$$
$$= \frac{4\lambda^2 K l b^3}{\pi^2}\sum_{n=1}^{\infty}\frac{1}{n^2\beta_n^2}\left(1-\frac{2}{\beta_n l}\tanh\left(\frac{\beta_n l}{2}\right)\right)$$
$$= \frac{48\,GS^2 lb}{\pi^2}\left(1+\frac{2b}{l}\right)^2\sum_{n=1}^{\infty}\frac{1}{n^2\beta_n^2}\left(1-\frac{2}{\beta_n l}\tanh\left(\frac{\beta_n l}{2}\right)\right) \tag{3.57}$$

To examine the effect of compressibility on the bending stiffness, we can express Equation (3.57) as a ratio to the effective EI for incompressible material, Equation (3.27), obtaining

$$\frac{(EI)_{eff}^{\text{comp}}}{(EI)_{eff}^{\text{inc}}} = \frac{\sum_{n=1}^{\infty}\dfrac{1}{n^4\left(1+\dfrac{12\,GS^2}{n^2\pi^2 K}(1+\rho)^2\right)}\left[1-\dfrac{\rho}{n\pi}\dfrac{\tanh\left(\dfrac{n\pi}{\rho}\sqrt{1+\dfrac{12\,GS^2}{n^2\pi^2 K}(1+\rho)^2}\right)}{\sqrt{1+\dfrac{12\,GS^2}{n^2\pi^2 K}(1+\rho)^2}}\right]}{\sum_{n=1}^{\infty}\dfrac{1}{n^4}\left(1-\dfrac{\rho}{n\pi}\tanh\left(\dfrac{n\pi}{\rho}\right)\right)} \tag{3.58}$$

where $\rho = 2b/l$. Figure 3.8 shows graphs of $(EI)_{eff}^{\text{comp}}/(EI)_{eff}^{\text{inc}}$ versus S for different K/G and ρ values.

3.2.4 Annular Pad

For an annular pad of inner radius a, outer radius b, where $a \le r \le b$, Equation (3.34) becomes

$$\frac{\partial^2 p}{\partial r^2} + \frac{1}{r}\frac{\partial p}{\partial r} + \frac{1}{r^2}\frac{\partial^2 p}{\partial \theta^2} - \lambda^2 p = \lambda^2\frac{K\alpha}{t} r\cos\theta \tag{3.59}$$

with boundary conditions $p(a,\theta) = p(b,\theta) = 0$. Assuming a solution of the form

$$p(r,\theta) = f(r)\cos\theta \tag{3.60}$$

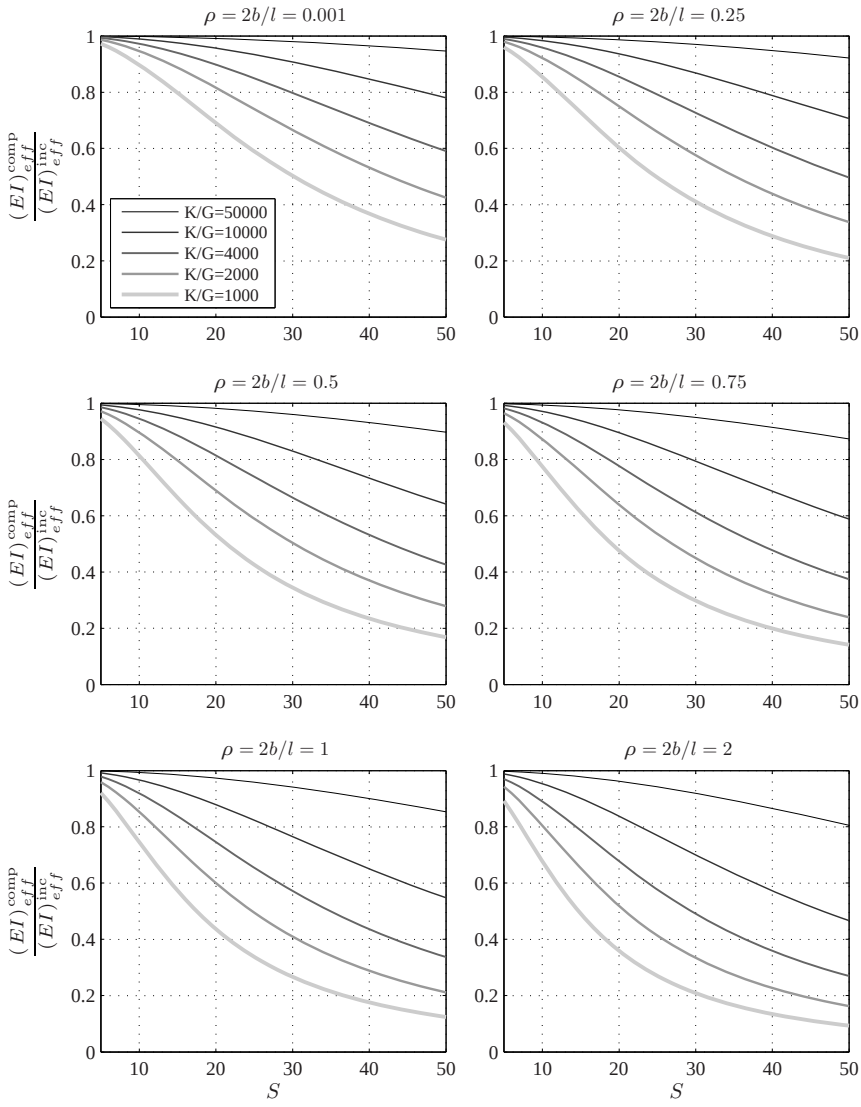

Figure 3.8 Ratio of the effective bending stiffness with compressible rubber to the effective bending stiffness with incompressible rubber for a rectangular pad

and substituting into Equation (3.59) gives the ordinary differential equation

$$r^2 \frac{\mathrm{d}^2 f}{\mathrm{d}r^2} + r \frac{\mathrm{d}f}{\mathrm{d}r} - (1 + \lambda^2 r^2) f = \frac{\lambda^2 K \alpha}{t} r^3 \tag{3.61}$$

The solution has the form

$$f(r) = \frac{K\alpha}{t} (B_1 \mathrm{I}_1(\lambda r) + B_2 \mathrm{K}_1(\lambda r) - r) \tag{3.62}$$

where K_1 is the modifie Bessel function of the second kind of order 1. Using the boundary conditions $f(a) = f(b) = 0$, we obtain the constants B_1 and B_2,

$$\begin{aligned} B_1 &= \frac{-b\mathrm{K}_1(\lambda a) + a\mathrm{K}_1(\lambda b)}{\mathrm{I}_1(\lambda a)\mathrm{K}_1(\lambda b) - \mathrm{I}_1(\lambda b)\mathrm{K}_1(\lambda a)} \\ B_2 &= \frac{b\mathrm{I}_1(\lambda a) - a\mathrm{I}_1(\lambda b)}{\mathrm{I}_1(\lambda a)\mathrm{K}_1(\lambda b) - \mathrm{I}_1(\lambda b)\mathrm{K}_1(\lambda a)} \end{aligned} \tag{3.63}$$

Then

$$p(r,\theta) = \frac{K\alpha}{t}(B_1\mathrm{I}_1(\lambda r) + B_2\mathrm{K}_1(\lambda r) - r)\cos\theta \tag{3.64}$$

and

$$\begin{aligned} M &= -\int_0^{2\pi}\int_a^b p(r,\theta)r^2\cos\theta \mathrm{d}r\,\mathrm{d}\theta \\ &= -\pi\frac{K\alpha}{t}\left[B_1\frac{r^2}{\lambda}\mathrm{I}_2(\lambda r) - B_2\frac{r^2}{\lambda}\mathrm{K}_2(\lambda r) - \frac{r^4}{4}\right]_a^b \\ &= -\pi\frac{K\alpha}{t}\left[\frac{B_1}{\lambda}(b^2\mathrm{I}_2(\lambda b) - a^2\mathrm{I}_2(\lambda a)) - \frac{B_2}{\lambda}(b^2\mathrm{K}_2(\lambda b) - a^2\mathrm{K}_2(\lambda a)) - \frac{b^4 - a^4}{4}\right] \end{aligned} \tag{3.65}$$

where I_2 and K_2 are order-1 modifie Bessel functions of the firs and of the second kind respectively. The bending stiffness of the pad is

$$(EI)_{eff} = -\pi K\left[\frac{B_1}{\lambda}(b^2\mathrm{I}_2(\lambda b) - a^2\mathrm{I}_2(\lambda a)) - \frac{B_2}{\lambda}(b^2\mathrm{K}_2(\lambda b) - a^2\mathrm{K}_2(\lambda a)) - \frac{b^4 - a^4}{4}\right] \tag{3.66}$$

Using $S = (b - a)/(2t)$, $\eta = a/b$ (the ratio of the inner radius to the outer radius), and $I = \pi(b^4 - a^4)/4$, we can express the bending stiffness as

$$(EI)_{eff} = KI[1 - B_1'(\mathrm{I}_2(\vartheta) - \eta^2\mathrm{I}_2(\eta\vartheta)) + B_2'(\mathrm{K}_2(\vartheta) - \eta^2\mathrm{K}_2(\eta\vartheta))] \tag{3.67}$$

where

$$\vartheta = \sqrt{\frac{48\,G}{K}}\frac{S}{1-\eta} \tag{3.68}$$

and

$$\begin{aligned} B_1' &= \frac{4}{\vartheta(1-\eta^4)}\frac{-\mathrm{K}_1(\eta\vartheta) + \eta\mathrm{K}_1(\vartheta)}{\mathrm{I}_1(\eta\vartheta)\mathrm{K}_1(\vartheta) - \mathrm{I}_1(\vartheta)\mathrm{K}_1(\eta\vartheta)} \\ B_2' &= \frac{4}{\vartheta(1-\eta^4)}\frac{\mathrm{I}_1(\eta\vartheta) - \eta\mathrm{I}_1(\vartheta)}{\mathrm{I}_1(\eta\vartheta)\mathrm{K}_1(\vartheta) - \mathrm{I}_1(\vartheta)\mathrm{K}_1(\eta\vartheta)} \end{aligned} \tag{3.69}$$

The result in Equation (3.67) is most conveniently used as a ratio to the bending stiffness in the incompressible case, which is given by Equation (3.32). We obtain,

$$\frac{(EI)_{\mathit{eff}}^{\mathrm{comp}}}{(EI)_{\mathit{eff}}^{\mathrm{inc}}} = \frac{K}{2GS^2}\frac{1+\eta^2}{(1+\eta)^2}[1 - B_1'(\mathrm{I}_2(\vartheta) - \eta^2\mathrm{I}_2(\eta\vartheta)) + B_2'(\mathrm{K}_2(\vartheta) - \eta^2\mathrm{K}_2(\eta\vartheta))] \tag{3.70}$$

Figure 3.9 shows graphs of $(EI)_{\mathit{eff}}^{\mathrm{comp}}/(EI)_{\mathit{eff}}^{\mathrm{inc}}$ versus S for different K/G and η values.

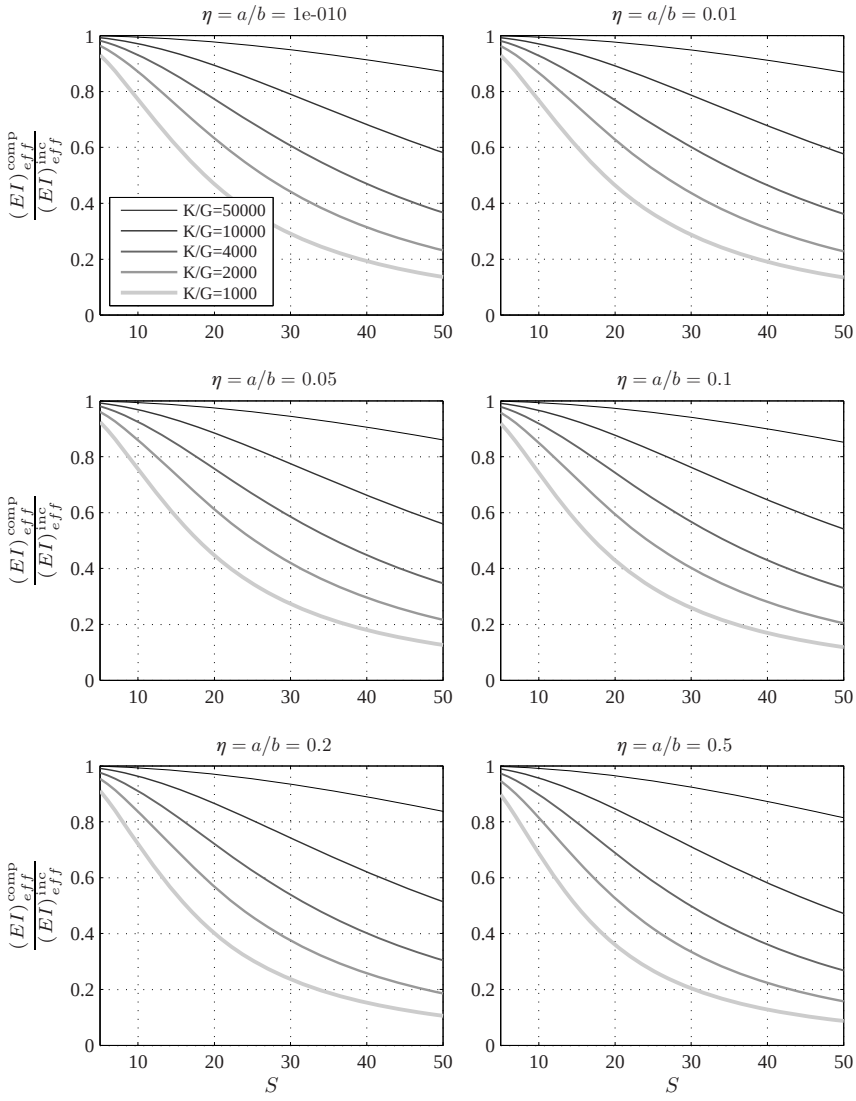

Figure 3.9 Ratio of the effective bending stiffness with compressible rubber to the effective bending stiffness with incompressible rubber for an annular pad

The analysis given in this chapter has focused on the bending stiffness for a wide variety of isolator shapes. The bending stiffness of a rubber isolator is an important bearing property that must be available for design in estimating the buckling behavior of the isolator. It allows us to assess the response of the compressed bearing to an externally applied bending moment and is needed to estimate the influenc of the vertical load on the horizontal stiffness of a bearing. In addition, when the isolator is subject to shear deformation, a bending moment is generated by the unbalanced shear forces at the top and bottom of the bearing. These bending moments cause shear strains in the rubber that are important for design. Also, the moments produce compressive stresses in the shims that can result in buckling. The bending stiffness analyses that were presented in this chapter for many shapes of isolators and which include bulk-compressibility effects are entirely new and are essential for a complete analysis of the types of bearings that are used in current design practise, where very large shape-factor rubber layers are preferred by the manufacturers.

4

Steel Stress in Multilayer Rubber Bearings under Compression and Bending

The essential characteristic of the rubber isolator is the very large ratio of the vertical stiffness to the horizontal stiffness. This is produced by the reinforcing plates, which in current industry standard are thin steel plates called *shims*. The shims prevent lateral bulging of the rubber, but allow the rubber to shear freely. The vertical stiffness of the bearing can be several hundred times the horizontal stiffness. The steel reinforcement has the effect of generating shear stresses in the rubber, and these stresses act on the steel plates to cause tensile stresses which, if they were to become large enough, could result in failure of the steel shims through yielding or fracture. The external pressure on the isolator at which this might happen is an important design quantity, and it is therefore necessary to be able to estimate these tensile stresses under the applied external load.

In this chapter, solutions are developed for the tensile stresses in the steel reinforcing shims of rubber isolators. The method makes use of generalized plane stress and uses a stress function approach, treating the shim as a thin plate with body forces generated by surface shears on the top and bottom of the plate. It is shown that the pressure in the rubber acts as a potential for these body forces. Solutions are presented for the case of rubber bearings with low and moderate shape factors, where it is acceptable to assume that the rubber is incompressible, and also for the more common case in current practice where the shape factor is so large that the assumption of incompressibility cannot be made, and the effect of the bulk modulus of the rubber must be included. The stress state in the steel reinforcing plates is calculated for pure compression and for

The material in Sections 4.2 and 4.3 firs appeared in the article by Kelly, J. M. and Konstantinidis, D. (2009). "Steel Shim Stresses in Multilayer Bearings under Compression and Bending." *Journal of Mechanics of Materials and Structures*, **4**(6), 1109–1125, DOI: 10.2140/jomms.2009.4.1109. Reproduced by permission of Mathematical Sciences Publishers.

Mechanics of Rubber Bearings for Seismic and Vibration Isolation, First Edition. James M. Kelly and Dimitrios A. Konstantinidis.

pure bending of the bearing. These two cases, separately and their combination, are the typical situation in current practice. While a solution for the stress state in the shims of a circular isolator, assuming incompressibility and under pure compression, has been available using an analogy with the stresses in a rotating circular plate, the use of the stress function method is new (Kelly and Konstantinidis 2009a) and suggests a method to extend the solutions to isolators with shapes other than circular.

In the later part of the chapter we look into the yielding of the steel shims, and we show that the result for the pressure that causes full yielding throughout the steel shim in the incompressible case is a conservative estimate of the pressure to produce full yield in the case of the larger-shape-factor isolator, for which the compressibility of the rubber must be taken into account.

4.1 Review of the Compression and Bending of a Pad

In Chapters 2 and 3, the pure compression and pure bending of a single pad were investigated, and the results important for the developments in this chapter are restated here for convenience to the reader. The pressure solution for the case of a circular bearing of radius R with incompressible rubber, which applies to low and moderate shape factors, is

$$p(r) = \frac{3\,G\varepsilon_c}{t^2}(R^2 - r^2) \tag{4.1}$$

The compressive load is then given by

$$P = 2\pi \int_0^R p\,(r)\,r\,\mathrm{d}r \;= \frac{3\,G\varepsilon_c \pi\, R^4}{2t^2} \tag{4.2}$$

and, with $S = R/(2t)$ and $A = \pi R^2$, the compression modulus, $E_c = P/(A\varepsilon_c)$, becomes

$$E_c = 6\,GS^2 \tag{4.3}$$

Under pure bending, the pressure solution for the circular pad with incompressible rubber is

$$p(r) = \frac{3\,G}{2t^2}\frac{\alpha}{t}(r^2 - R^2) r\cos\theta \tag{4.4}$$

It is useful to defin a bending strain ε_b, analogous to the compression strain ε_c, as

$$\varepsilon_b = \frac{\alpha}{t} R \tag{4.5}$$

Then Equation (4.4) becomes

$$p(r) = \frac{3\,G\varepsilon_b}{2Rt^2}(r^2 - R^2)\, r\cos\theta = 6\,GS^2\varepsilon_b \left(\frac{r^2}{R^2} - 1\right)\frac{r}{R}\cos\theta \tag{4.6}$$

In the case of compressible rubber, which applies to bearings with larger shape factors, the pressure solution for a circular bearing under pure compression is

$$p(r) = K\varepsilon_c \left(1 - \frac{\mathrm{I}_0(\lambda r)}{\mathrm{I}_0(\lambda R)}\right) \tag{4.7}$$

where I_0 is the zero-order modifie Bessel function of the firs kind. Integrating p over the area of the pad gives $P = K\varepsilon_c R^2[1 - 2\mathrm{I}_1(\lambda R)/(\lambda R \mathrm{I}_0(\lambda R))]$ where I_1 is the modifie Bessel function of the firs kind of order 1. The resulting expression for the compression modulus is

$$E_c = K\left(1 - \frac{2}{\lambda R}\frac{\mathrm{I}_1(\lambda R)}{\mathrm{I}_0(\lambda R)}\right) \tag{4.8}$$

where $\lambda R = \sqrt{12\,GR^2/(Kt^2)} = \sqrt{48\,G/K}\,S$.

For a circular pad with compressible rubber under pure bending, it was shown in Chapter 3 that the pressure distribution takes the form

$$p(r) = \frac{K\alpha}{t}\left(R\frac{I_1(\lambda r)}{I_1(\lambda R)} - r\right)\cos\theta = K\varepsilon_b\left(\frac{\mathrm{I}_1(\lambda r)}{\mathrm{I}_1(\lambda R)} - \frac{r}{R}\right)\cos\theta \tag{4.9}$$

4.2 Steel Stresses in Circular Bearings with Incompressible Rubber

The state of stress in a rubber layer, within a multilayer bearing under compression or bending, or a combination of the two, is assumed to be a state of pressure that would induce a bulging of the rubber were it not restrained by the thin steel reinforcing shims that are bonded to the rubber (see Figure 1.4). The restraint of the rubber by the steel causes shear stresses in the rubber which act on each side of the steel plate to induce tensile or compressive stresses in the plane of the plate. It is possible to solve for these in-plane stresses using two-dimensional elasticity theory, assuming that the plate is in a state of generalized plane stress and that the surface shear stresses are equivalent to in-plane body forces. While it is possible to formulate the plane-stress problem for an arbitrarily shaped plate, we will consider only the circular bearing. We will use the notations for the stresses and the stress function from Timoshenko and Goodier (1970).

In polar coordinates (r, θ), the equations of equilibrium for the stresses in the rubber are

$$\begin{aligned}
&\frac{\partial\sigma_r}{\partial r} + \frac{1}{r}\frac{\partial\tau_{r\theta}}{\partial\theta} + \frac{\partial\tau_{rz}}{\partial z} + \frac{\sigma_r - \sigma_\theta}{r} = 0\\
&\frac{\partial\tau_{r\theta}}{\partial r} + \frac{1}{r}\frac{\partial\sigma_\theta}{\partial\theta} + \frac{\partial\tau_{\theta z}}{\partial z} + \frac{2\tau_{r\theta}}{r} = 0\\
&\frac{\partial\tau_{rz}}{\partial r} + \frac{1}{r}\frac{\partial\tau_{\theta z}}{\partial\theta} + \frac{\partial\sigma_z}{\partial z} + \frac{\tau_{rz}}{r} = 0
\end{aligned} \tag{4.10}$$

It is assumed that $\sigma_r = \sigma_\theta = \sigma_z = -p$, and are independent of z, and also that the inplane shear stress $\tau_{r\theta}$ is negligible. Hence the firs of the equilibrium equations yields

$$\frac{\partial \tau_{rz}}{\partial z} = \frac{\partial p}{\partial r} \tag{4.11}$$

and the second

$$\frac{\partial \tau_{\theta z}}{\partial z} = \frac{1}{r}\frac{\partial p}{\partial \theta} \tag{4.12}$$

Inserting these equilibrium equations into the third equation in (4.10), differentiating with respect to z, and interchanging the order of differentiation, changes it to

$$\frac{\partial^2 p}{\partial r^2} + \frac{1}{r}\frac{\partial p}{\partial r} + \frac{1}{r^2}\frac{\partial^2 p}{\partial \theta^2} + \frac{\partial \sigma_z}{\partial z} = 0 \tag{4.13}$$

This equation, with substitution from either Equation (4.11) or (4.12), allows us, if necessary, to calculate the distribution of σ_z through the thickness of the pad. Within the stress assumptions above, we have $p = p(r, \theta)$, which means that we can write

$$\begin{aligned} \tau_{rz} &= \frac{\partial p}{\partial r} z \\ \tau_{\theta z} &= \frac{1}{r}\frac{\partial p}{\partial \theta} z \end{aligned} \tag{4.14}$$

The shear stresses at the bottom of the rubber layer $\tau_{rz}|_{z=-t/2}$ and $\tau_{\theta z}|_{z=-t/2}$ become the shear stresses on the top surface of the plate, and the shear stresses at the top of the rubber layer $\tau_{rz}|_{z=t/2}$ and $\tau_{\theta z}|_{z=t/2}$ are the shear stresses on the lower surface of the plate (Figure 4.1).

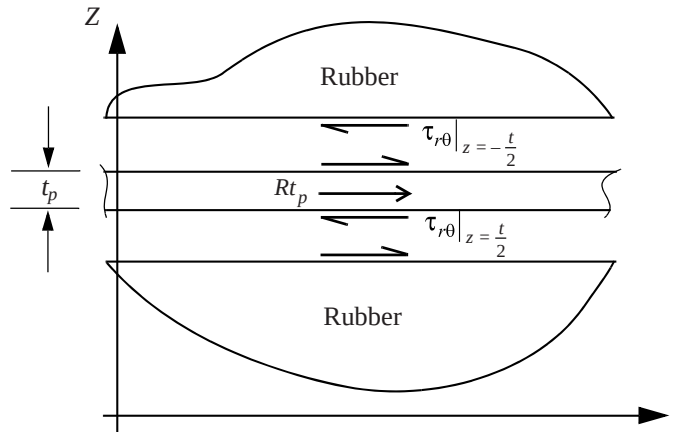

Figure 4.1 Shear stresses producing equivalent body forces in the plate

The internal stresses in the steel shims satisfy the equilibrium equations

$$\begin{aligned}\frac{\partial \sigma_r}{\partial r}+\frac{1}{r}\frac{\partial \tau_{r\theta}}{\partial \theta}+\frac{\sigma_r-\sigma_\theta}{r}+R=0\\ \frac{\partial \tau_{r\theta}}{\partial r}+\frac{1}{r}\frac{\partial \sigma_\theta}{\partial \theta}+\frac{2\tau_{r\theta}}{r}+S=0\end{aligned} \tag{4.15}$$

where R and S are the equivalent body forces per unit volume created by the surface shear stresses and are given by

$$\begin{aligned}t_p R &= \tau_{rz}|_{z=-t/2}-\tau_{rz}|_{z=t/2}\\ t_p S &= \tau_{\theta z}|_{z=-t/2}-\tau_{\theta z}|_{z=t/2}\end{aligned} \tag{4.16}$$

where t_p is the thickness of the steel shim, leading to

$$\begin{aligned}R&=-\frac{t}{t_p}\frac{\partial p}{\partial r}\\ S&=-\frac{t}{t_p}\frac{1}{r}\frac{\partial p}{\partial \theta}\end{aligned} \tag{4.17}$$

It follows that the pressure plays the role of a potential, V, for the body forces in the form

$$V(r,\theta)=\frac{t}{t_p}p(r,\theta) \tag{4.18}$$

with

$$R=-\frac{\partial V}{\partial r}\quad\text{and}\quad S=-\frac{1}{r}\frac{\partial V}{\partial \theta} \tag{4.19}$$

The equations of equilibrium for the plate then become

$$\begin{aligned}\frac{\partial(\sigma_r-V)}{\partial r}+\frac{1}{r}\frac{\partial \tau_{r\theta}}{\partial \theta}+\frac{(\sigma_r-V)-(\sigma_\theta-V)}{r}=0\\ \frac{\partial \tau_{r\theta}}{\partial r}+\frac{1}{r}\frac{\partial(\sigma_\theta-V)}{\partial \theta}+\frac{2\tau_{r\theta}}{r}=0\end{aligned} \tag{4.20}$$

These equations are satisfie by a stress function $\Phi(r, \theta)$ for the stresses, such that

$$\begin{aligned} \sigma_r - V &= \frac{1}{r}\frac{\partial \Phi}{\partial r} + \frac{1}{r^2}\frac{\partial^2 \Phi}{\partial \theta^2} \\ \sigma_\theta - V &= \frac{\partial^2 \Phi}{\partial r^2} \\ \tau_{r\theta} &= -\frac{\partial}{\partial r}\left(\frac{1}{r}\frac{\partial \Phi}{\partial \theta}\right) \end{aligned} \tag{4.21}$$

and under the assumption of plane stress, the equation for Φ is

$$\nabla^2 \nabla^2 \Phi + (1 - \nu)\nabla^2 V = 0 \tag{4.22}$$

where ν is the Poisson's ratio of the steel. In the case of pure compression, the pressure satisfie

$$\nabla^2 p = -\frac{12\, G \varepsilon_c}{t^2} \tag{4.23}$$

and for bending

$$\nabla^2 p = \frac{12\, G \varepsilon_b}{t^2}\frac{r}{R}\cos\theta \tag{4.24}$$

4.2.1 Stress Function Solution for Pure Compression

The stress function Φ for pure compression is given by the solution of

$$\nabla^2 \nabla^2 \Phi + \overline{C} = 0 \tag{4.25}$$

where $\overline{C}$ is a constant having the value

$$\overline{C} = -(1 - \nu)\frac{12\, G \varepsilon_c}{t_p t} \tag{4.26}$$

In this case the stress function depends only on r, and we look for a solution of that form. The result is (Timoshenko and Goodier 1970)

$$\Phi = A \ln r + B r^2 \ln r + C r^2 + D - \frac{\overline{C} r^4}{64} \tag{4.27}$$

The resulting stresses are given by

$$\begin{aligned} \sigma_r - \frac{t}{t_p} p(r) &= \frac{A}{r^2} + B(1 + 2\ln r) + 2C - \frac{1}{16}\overline{C} r^2 \\ \sigma_\theta - \frac{t}{t_p} p(r) &= -\frac{A}{r^2} + B(3 + 2\ln r) + 2C - \frac{3}{16}\overline{C} r^2 \end{aligned} \tag{4.28}$$

It is clear that both A and B must vanish for the completely circular plate, and using $\sigma_r(R) = 0$ and the fact that the pressure is also zero at $r = R$, we have

$$2C = \frac{\overline{C}R^2}{16} \tag{4.29}$$

Using the pressure from Equation (4.1) and $\overline{C}$ from Equation (4.26), the solution for the tensile stresses becomes

$$\begin{aligned}
\sigma_r &= \frac{3G\varepsilon_c}{tt_p}\frac{3+\nu}{4}(R^2 - r^2) = 3GS^2\varepsilon_c\frac{t}{t_p}(3+\nu)\left(1 - \frac{r^2}{R^2}\right) \\
\sigma_\theta &= \frac{3}{4}\frac{G\varepsilon_c}{tt_p}\left[(3+\nu)R^2 - (1+3\nu)r^2\right] = 3GS^2\varepsilon_c\frac{t}{t_p}\left(3+\nu-(1+3\nu)\frac{r^2}{R^2}\right)
\end{aligned} \tag{4.30}$$

The distribution of the stresses in the plate with $\nu = 0.3$ under pure compression is shown in Figure 4.2, where

$$S_r = \frac{\sigma_r}{3GS^2\varepsilon_c(t/t_p)} \quad \text{and} \quad S_\theta = \frac{\sigma_\theta}{3GS^2\varepsilon_c(t/t_p)} \tag{4.31}$$

At the center of the plate, we have

$$\sigma_{\max} = \sigma_r = \sigma_\theta = 3GS^2\varepsilon_c\frac{t}{t_p}(3+\nu) \tag{4.32}$$

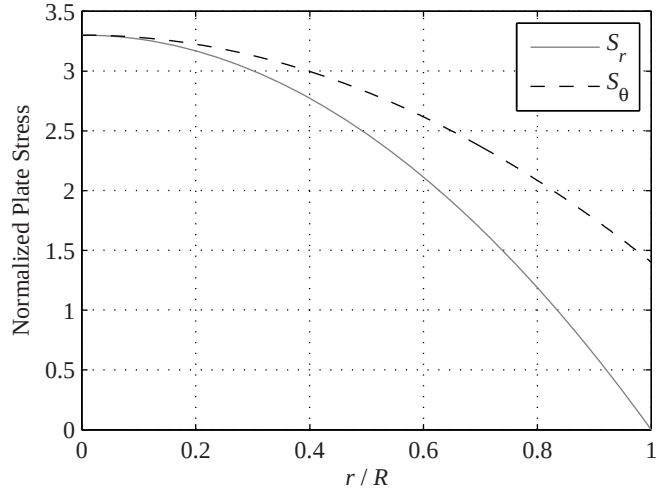

Figure 4.2 Plate stresses in compression, assuming incompressibility

By expressing the maximum stresses in terms of the average pressure over the plate, p_{ave}, given by

$$p_{\text{ave}} = E_c \varepsilon_c = 6GS^2 \varepsilon_c \tag{4.33}$$

we obtain

$$\frac{\sigma_{\max}}{P_{\text{ave}}} = \frac{3+\nu}{2}\frac{t}{t_p} \tag{4.34}$$

which can be used to determine the maximum pressure needed to cause yield in the shim at the center. It shows why, under normal circumstances, the stresses in the shims due to the pressure are not considered important. For example, if we have steel shims 3-mm (0.118 in.) thick and 15-mm (0.591 in.) thick rubber layers, the stresses in the steel due to a pressure of 7.0 MPa (1.0 ksi), which is standard, are only 58 MPa (8.4 ksi), well below the yield level of the plate material. If the tension stress at the center is in fact the yield stress of the material σ_o, then the average pressure to initiate yield is

$$p_{\text{ave}} = \frac{2}{3+\nu}\frac{t_p}{t}\sigma_o \tag{4.35}$$

This is only the start of yield, but the plate will experience further yielding as the pressure increases. The zone of yielding will spread from the center to the outer radius so that the pressure can increase further until the entire plate has yielded, that is, until the region $0 \le r \le R$ is fully plastic.

It is interesting to note that the problem in this case is the same as that for the stresses in a thin disk due to centrifugal forces. That solution was given in Timoshenko and Goodier (1970) using an entirely different approach based on displacements, and, except for constants, is identical to this. Timoshenko and Goodier (1970) also provide the solution for a circular plate of radius b with a central hole of radius a, which for $a \le r \le b$ is

$$\begin{aligned}
\sigma_r &= \frac{3}{4}\frac{G\varepsilon_c}{tt_p}(3+\nu)\left(b^2 + a^2 - \frac{a^2b^2}{r^2} - r^2\right) \\
\sigma_\theta &= \frac{3}{4}\frac{G\varepsilon_c}{tt_p}(3+\nu)\left(b^2 + a^2 + \frac{a^2b^2}{r^2} - \frac{1+3\nu}{3+\nu}r^2\right)
\end{aligned} \tag{4.36}$$

The maximum radial stress is at $r = \sqrt{ab}$, where

$$\sigma_r = \frac{3}{4}\frac{G\varepsilon_c}{tt_p}(3+\nu)(b-a)^2 \tag{4.37}$$

and the maximum tangential stress is at the inner boundary, where

$$\sigma_\theta = \frac{3}{4}\frac{G\varepsilon_c}{tt_p}(3+\nu)\left(b^2 + \frac{1-\nu}{3+\nu}a^2\right) \tag{4.38}$$

This is always larger than the maximum radial stress. When the radius a of the hole becomes very small, the maximum tangential stress approaches a value twice as large as the complete circular plate. This is another example of a stress concentration at a small hole.

4.2.2 Stress Function Solution for Pure Bending

For the case of pure bending on the pad, the equation for the stress function takes the form

$$\nabla^2\nabla^2\Phi + \overline{C} r\cos\theta = 0 \tag{4.39}$$

where now

$$\overline{C} = (1-\nu)\frac{12\,G\varepsilon_b}{Rtt_p} \tag{4.40}$$

We look for a solution of the form

$$\Phi(r,\theta) = f(r)\cos\theta \tag{4.41}$$

From Timoshenko and Goodier (1970), the ordinary differential equation for f is

$$\frac{\mathrm{d}^4 f}{\mathrm{d}r^4} + \frac{2}{r}\frac{\mathrm{d}^3 f}{\mathrm{d}r^3} - \frac{3}{r^2}\frac{\mathrm{d}^2 f}{\mathrm{d}r^2} + \frac{3}{r^3}\frac{\mathrm{d}f}{\mathrm{d}r} - \frac{3}{r^4}f + \overline{C}r = 0 \tag{4.42}$$

The solution is

$$f(r) = Ar^3 + \frac{B}{r} + Cr + Dr\ln r - \frac{\overline{C}r^5}{192} \tag{4.43}$$

The resulting stresses are

$$\begin{aligned}
\sigma_r - \frac{t}{t_p}p &= \left(2Ar - \frac{2B}{r^3} + \frac{D}{r}\right)\cos\theta + \overline{R} \\
\sigma_\theta - \frac{t}{t_p}p &= \left(6Ar + \frac{2B}{r^3} + \frac{D}{r}\right)\cos\theta + \overline{S} \\
\tau_{r\theta} &= \left(2Ar - \frac{2B}{r^3} + \frac{D}{r}\right)\sin\theta + \overline{T}
\end{aligned} \tag{4.44}$$

where

$$\begin{aligned}
\overline{R} &= \left(\frac{1}{r}\frac{\partial}{\partial r} + \frac{1}{r^2}\frac{\partial^2}{\partial\theta^2}\right)\left(-\frac{\overline{C}r^5}{192}\cos\theta\right) = -\frac{\overline{C}r^3}{48}\cos\theta \\
\overline{S} &= \frac{\partial^2}{\partial r^2}\left(-\frac{\overline{C}r^5}{192}\cos\theta\right) = -\frac{5\overline{C}r^3}{48}\cos\theta \\
\overline{T} &= -\frac{\partial}{\partial r}\left[\frac{1}{r}\frac{\partial}{\partial\theta}\left(-\frac{\overline{C}r^5}{192}\cos\theta\right)\right] = -\frac{\overline{C}r^3}{48}\sin\theta
\end{aligned} \tag{4.45}$$

For the complete plate, $0 \le r \le R$, both B and D must vanish, giving

$$\sigma_r = \frac{t}{t_p}p(r,\theta) + 2Ar\cos\theta - \frac{\overline{C}r^3}{48}\cos\theta \tag{4.46}$$

and since $p(r, \theta)$ is zero on the boundary, the requirement that $\sigma_r(R, \theta) = 0$ gives $2A = \overline{C}R^2/48$, leading, with Equation (4.6), to the fina results

$$\begin{aligned}
\sigma_r(r,\theta) &= -\frac{G\varepsilon_b}{4\,tt_pR}(5+\nu)(R^2-r^2)r\cos\theta \\
\sigma_\theta(r,\theta) &= \frac{G\varepsilon_b}{4\,tt_pR}\left[(1+5\nu)r^2-3(1+\nu)R^2\right]r\cos\theta \\
\tau_{r\theta}(r,\theta) &= -\frac{G\varepsilon_b}{4\,tt_pR}(1-\nu)(R^2-r^2)r\sin\theta
\end{aligned} \tag{4.47}$$

These results are plotted as nondimensional stresses in Figure 4.3, where

$$\begin{aligned}
S_r &= \frac{\sigma_r(r,\theta)}{GS^2\varepsilon_b\dfrac{t}{t_p}} = -(5+\nu)\left[1-\left(\frac{r}{R}\right)^2\right]\frac{r}{R}\cos\theta \\
S_\theta &= \frac{\sigma_\theta(r,\theta)}{GS^2\varepsilon_b\dfrac{t}{t_p}} = \left[(1+5\nu)\left(\frac{r}{R}\right)^2-3(1+\nu)\right]\frac{r}{R}\cos\theta \\
T_{r\theta} &= \frac{\tau_{r\theta}(r,\theta)}{GS^2\varepsilon_b\dfrac{t}{t_p}} = (1-\nu)\left[1-\left(\frac{r}{R}\right)^2\right]\frac{r}{R}\sin\theta
\end{aligned} \tag{4.48}$$

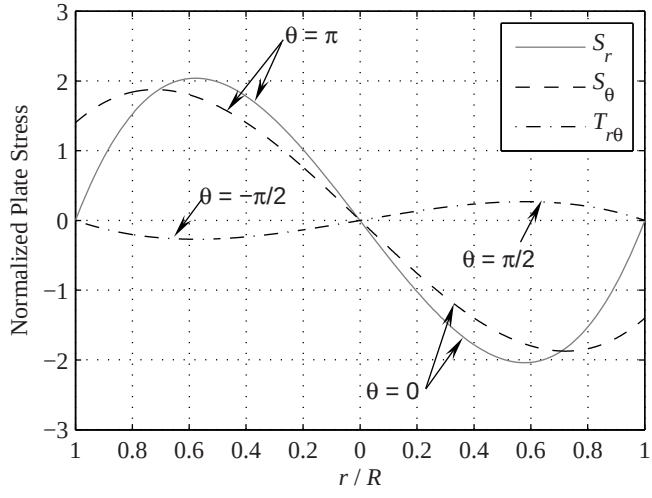

Figure 4.3 Plate stresses under bending moment for the incompressible case

4.3 Steel Stresses in Circular Bearings with Compressible Rubber

4.3.1 Stress Function Solution for Pure Compression

The tension stresses in the steel reinforcing plates can be calculated in the same way as before by using the stress function method. The equation for the stress function remains the same, $\nabla^2\nabla^2\Phi + (1-\nu)\nabla^2 V = 0$, and the definitio of the potential $V(r,\theta)$ is the same, $V = (t/t_p)p(r,\theta)$, but the pressure now satisfie the equation

$$\nabla^2 p - \frac{12\,G}{Kt^2}p = -\frac{12\,G\varepsilon_c}{t^2} \tag{4.49}$$

Thus the stress function now must satisfy the equation

$$\nabla^2\nabla^2\Phi + (1-\nu)\frac{t}{t_p}\frac{12\,G}{t^2}\left(\frac{p}{K} - \varepsilon_c\right) = 0 \tag{4.50}$$

With p given by Equation (4.7), we have

$$\nabla^2\nabla^2\Phi - (1-\nu)\frac{t}{t_p}\frac{12\,G}{t^2}\frac{\mathrm{I}_0(\lambda r)}{\mathrm{I}_0(\lambda R)}\varepsilon_c = 0 \tag{4.51}$$

The solution for pure compression is rotationally symmetric, and the complementary part of the solution remains the same, but it is necessary to determine the particular integral that corresponds to the term $\mathrm{I}_0(\lambda r)$. To develop this, we recall that in radial symmetry,

$$\nabla^2\nabla^2(f) = \frac{1}{r}\frac{\mathrm{d}}{\mathrm{d}r}\left(r\frac{\mathrm{d}}{\mathrm{d}r}\left(\frac{1}{r}\frac{\mathrm{d}}{\mathrm{d}r}\left(r\frac{\mathrm{d}f}{\mathrm{d}r}\right)\right)\right) \tag{4.52}$$

By taking $f = \mathrm{I}_0(\lambda r)$, changing the variable to $x = \lambda r$, and recalling that x so define is dimensionless and that λ is a reciprocal length, we have $\nabla^2\nabla^2\Phi|_r = (1/\lambda^4)\nabla^2\nabla^2\Phi|_x$.

Thus, we have successively

$$\begin{aligned}
\frac{1}{x}\frac{\mathrm{d}}{\mathrm{d}x}\left(x\frac{\mathrm{d}}{\mathrm{d}x}\left(\frac{1}{x}\frac{\mathrm{d}}{\mathrm{d}x}\left(x\frac{\mathrm{d}f}{\mathrm{d}x}\right)\right)\right) &= \mathrm{I}_0(x)\\
x\frac{\mathrm{d}}{\mathrm{d}x}\left(\frac{1}{x}\frac{\mathrm{d}}{\mathrm{d}x}\left(x\frac{\mathrm{d}f}{\mathrm{d}x}\right)\right) &= \int x\mathrm{I}_0(x)\,\mathrm{d}x = x\mathrm{I}_1(x)\\
\frac{1}{x}\frac{\mathrm{d}}{\mathrm{d}x}\left(x\frac{\mathrm{d}f}{\mathrm{d}x}\right) &= \int \mathrm{I}_1(x)\,\mathrm{d}x = \mathrm{I}_0(x)\\
x\frac{\mathrm{d}f}{dx} &= \int x\mathrm{I}_0(x)\,\mathrm{d}x = x\mathrm{I}_1(x)\\
f &= \mathrm{I}_0(x)
\end{aligned}$$

The result for the stress function Φ is

$$\Phi = A\ln r + Br^2\ln r + Cr^2 + D + \frac{1}{\lambda^4}\overline{C}\,\mathrm{I}_0(\lambda r) \tag{4.53}$$

where now the constant $\overline{C}$ is given by

$$\overline{C} = (1-\nu)\frac{t}{t_p}\frac{12\,G\varepsilon_c}{t^2}\frac{1}{\mathrm{I}_0(\lambda R)} \tag{4.54}$$

and the stresses are

$$\begin{aligned}
\sigma_r - \frac{t}{t_p}p(r) &= \frac{A}{r^2} + B(1+2\ln r) + 2C + \frac{\overline{C}}{\lambda^2}\frac{\mathrm{I}_1(\lambda r)}{\lambda r}\\
\sigma_\theta - \frac{t}{t_p}p(r) &= -\frac{A}{r^2} + B(3+2\ln r) + 2C + \frac{\overline{C}}{\lambda^2}\left(\mathrm{I}_0(\lambda r) - \frac{\mathrm{I}_1(\lambda r)}{\lambda r}\right)
\end{aligned} \tag{4.55}$$

Since, in the case of a complete plate, A and B must vanish, and the pressure is zero at the outside radius, the condition that $\sigma_r(R) = 0$ means that

$$C = -\frac{\overline{C}}{2\lambda^2}\frac{\mathrm{I}_1(\lambda R)}{\lambda R} \tag{4.56}$$

and, with $p(r)$ given by Equation (4.7), we have

$$\begin{aligned}
\sigma_r &= \frac{t}{t_p}K\varepsilon_c\left[1 - \frac{\mathrm{I}_0(\lambda r)}{\mathrm{I}_0(\lambda R)} - \frac{1-\nu}{\mathrm{I}_0(\lambda R)}\left(\frac{\mathrm{I}_1(\lambda R)}{\lambda R} - \frac{\mathrm{I}_1(\lambda r)}{\lambda r}\right)\right]\\
\sigma_\theta &= \frac{t}{t_p}K\varepsilon_c\left[1 - \frac{\mathrm{I}_0(\lambda r)}{\mathrm{I}_0(\lambda R)} - \frac{1-\nu}{\mathrm{I}_0(\lambda R)}\left(\frac{\mathrm{I}_1(\lambda R)}{\lambda R} + \frac{\mathrm{I}_1(\lambda r)}{\lambda r} - \mathrm{I}_0(\lambda r)\right)\right]
\end{aligned} \tag{4.57}$$

At the center of the plate, the stresses become

$$\sigma_r = \sigma_\theta = \frac{t}{t_p}K\varepsilon_c\left[1 - \frac{1}{\mathrm{I}_0(\lambda R)} - \frac{1-\nu}{\mathrm{I}_0(\lambda R)}\left(\frac{\mathrm{I}_1(\lambda R)}{\lambda R} - \frac{1}{2}\right)\right] \tag{4.58}$$

To illustrate these results we look at the case when the shape factor is 30, the rubber shear modulus is 0.42 MPa (60.9 psi) and the bulk modulus is 2000 MPa (289 855 psi), giving $\lambda R = 3$. The normalized plate stresses denoted by

$$S_r = \frac{\sigma_r}{K\varepsilon_c(t/t_p)} \quad \text{and} \quad S_\theta = \frac{\sigma_\theta}{K\varepsilon_c(t/t_p)} \tag{4.59}$$

are shown as functions of r/R in Figure 4.4.

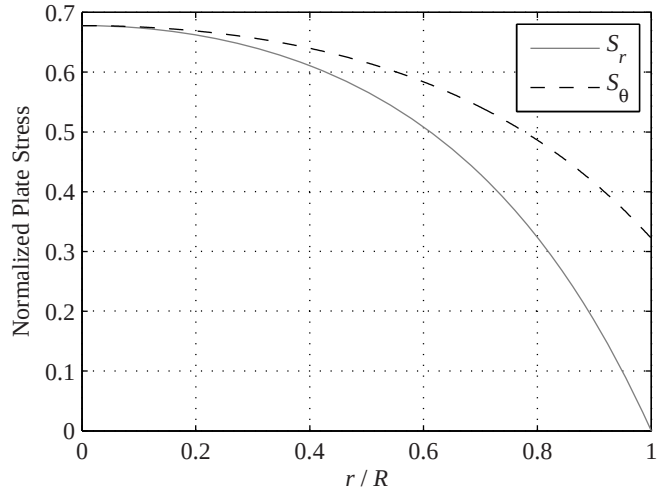

Figure 4.4 Plate stresses in compression for the large-shape-factor case

If we compare the maximum value of the stress at the center of the plate of this solution with the same result for the incompressible case, we can use Equation (4.8) to determine the average pressure and Equation (4.58) to get

$$\frac{\sigma_{\max}}{p_{\text{ave}}} = \frac{t}{t_p} \frac{\mathrm{I}_0(\lambda R) - 1 - (1-\nu)\left(\dfrac{\mathrm{I}_1(\lambda R)}{\lambda R} - \dfrac{1}{2}\right)}{\mathrm{I}_0(\lambda R) - \dfrac{2}{\lambda R}\mathrm{I}_1(\lambda R)} \tag{4.60}$$

Figure 4.5 is a graph of Equation (4.60) for a range of values of λR from zero to fiv (zero being the incompressible case). It shows that for the same value of ε_c and t/t_p, the

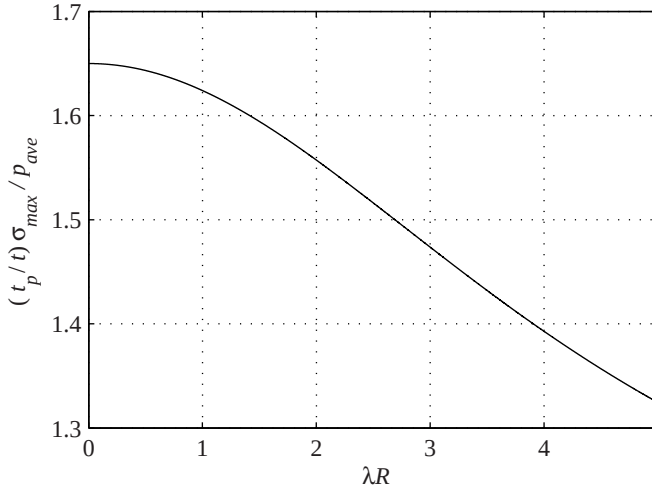

Figure 4.5 Ratio of maximum plate stresses for compressible and incompressible cases

peak stresses get smaller as compressibility increases. This implies that the result for the incompressible computation is a conservative estimate of the stresses in the large-shape-factor case, which, if it can be used, greatly simplifie the prediction of the maximum value of the tension stress.

4.3.2 Stress Function Solution for Pure Bending

For a circular pad under pure bending with an angle of rotation α between the shims (see Figure 3.1), Equations (4.9) and (4.22) give the equation to be solved for the stress function

$$\nabla^2\nabla^2\Phi + (1-\nu)\frac{t}{t_p}\frac{12\,G\varepsilon_b}{t^2}\frac{\mathrm{I}_1(\lambda r)}{\mathrm{I}_1(\lambda R)}\cos\theta = 0 \tag{4.61}$$

We look for a solution of the form

$$\Phi(r,\theta) = f(r)\cos\theta \tag{4.62}$$

Substitution into Equation (4.61) results in the ordinary differential equation for f

$$\frac{\mathrm{d}^4 f}{\mathrm{d}r^4} + \frac{2}{r}\frac{\mathrm{d}^3 f}{\mathrm{d}r^3} - \frac{3}{r^2}\frac{\mathrm{d}^2 f}{\mathrm{d}r^2} + \frac{3}{r^3}\frac{\mathrm{d}f}{\mathrm{d}r} - \frac{3}{r^4}f + \overline{C}\mathrm{I}_1(\lambda r) = 0 \tag{4.63}$$

where

$$\overline{C} = (1-\nu)\frac{t}{t_p}\frac{12\,G\varepsilon_b}{t^2}\frac{1}{\mathrm{I}_1(\lambda R)} \tag{4.64}$$

The complementary part of the solution is

$$f(r) = Ar^3 + \frac{B}{r} + Cr + Dr\ln r \tag{4.65}$$

and the particular integral can be shown (after considerable algebraic manipulation) to be $-(\overline{C}/\lambda^4)\mathrm{I}_1(\lambda r)$.

The resulting stresses are

$$\begin{aligned}
\sigma_r - \frac{t}{t_p}p &= \left(2Ar - \frac{2B}{r^3} + \frac{D}{r}\right)\cos\theta + \overline{R}\\
\sigma_\theta - \frac{t}{t_p}p &= \left(6Ar + \frac{2B}{r^3} + \frac{D}{r}\right)\cos\theta + \overline{S}\\
\tau_{r\theta} &= \left(2Ar - \frac{2B}{r^3} + \frac{D}{r}\right)\sin\theta + \overline{T}
\end{aligned} \tag{4.66}$$

where

$$\overline{R} = \left(\frac{1}{r}\frac{\partial}{\partial r} + \frac{1}{r^2}\frac{\partial^2}{\partial \theta^2}\right)\left(-\frac{(\overline{C}\mathrm{I}_1(\lambda r)\cos\theta)}{\lambda^4}\right) = \frac{2\mathrm{I}_1(\lambda r) - \mathrm{I}_0(\lambda r)\lambda r}{\lambda^2 r^2}\frac{\overline{C}}{\lambda^2}\cos\theta$$

$$\overline{S} = \frac{\partial^2}{\partial r^2}\left(-\frac{(\overline{C}\mathrm{I}_1(\lambda r)\cos\theta)}{\lambda^4}\right) = \frac{\mathrm{I}_0(\lambda r)\lambda r - \mathrm{I}_1(\lambda r)\left(2+\lambda^2 r^2\right)}{\lambda^2 r^2}\frac{\overline{C}}{\lambda^2}\cos\theta \tag{4.67}$$

$$\overline{T} = -\frac{\partial}{\partial r}\left(\frac{1}{r}\frac{\partial}{\partial \theta}\left(-\frac{(\overline{C}\mathrm{I}_1(\lambda r)\cos\theta)}{\lambda^4}\right)\right) = \frac{2\mathrm{I}_1(\lambda r) - \mathrm{I}_0(\lambda r)\lambda r}{\lambda^2 r^2}\frac{\overline{C}}{\lambda^2}\sin\theta$$

For the complete plate, $0 \le r \le R$, both B and D must vanish and $\sigma_r(R,\theta) = 0$, giving

$$A = \frac{1}{2R}\frac{\mathrm{I}_0(\lambda R)\lambda R - 2\mathrm{I}_1(\lambda R)}{\lambda^2 R^2}\frac{\overline{C}}{\lambda^2} \tag{4.68}$$

Substituting for $p(r,\theta)$ from Equation (4.9) and $\overline{C}$ from Equation (4.64), and making use of $\lambda^2 = 12G/(Kt^2)$ leads to

$$\sigma_r = K\varepsilon_b\frac{t}{t_p}\left[\frac{\mathrm{I}_1(\lambda r)}{\mathrm{I}_1(\lambda R)} - \frac{r}{R} + \frac{1-\nu}{\mathrm{I}_1(\lambda R)}\left(\frac{\mathrm{I}_0(\lambda R)\lambda R - 2\mathrm{I}_1(\lambda R)}{\lambda^2 R^2}\frac{r}{R} - \frac{\mathrm{I}_0(\lambda r)\lambda r - 2\mathrm{I}_1(\lambda r)}{\lambda^2 r^2}\right)\right]\cos\theta$$

$$\sigma_\theta = K\varepsilon_b\frac{t}{t_p}\left[\frac{\mathrm{I}_1(\lambda r)}{\mathrm{I}_1(\lambda R)} - \frac{r}{R} + \frac{1-\nu}{\mathrm{I}_1(\lambda R)}\left(3\frac{\mathrm{I}_0(\lambda R)\lambda R - 2\mathrm{I}_1(\lambda R)}{\lambda^2 R^2}\frac{r}{R} + \frac{\mathrm{I}_0(\lambda r)\lambda r - \mathrm{I}_1(\lambda r)\left(\lambda^2 r^2 + 2\right)}{\lambda^2 r^2}\right)\right]\cos\theta \tag{4.69}$$

$$\tau_{r\theta} = K\varepsilon_b\frac{t}{t_p}\frac{1-\nu}{\mathrm{I}_1(\lambda R)}\left(\frac{\mathrm{I}_0(\lambda R)\lambda R - 2\mathrm{I}_1(\lambda R)}{\lambda^2 R^2}\frac{r}{R} - \frac{\mathrm{I}_0(\lambda r)\lambda r - 2\mathrm{I}_1(\lambda r)}{\lambda^2 r^2}\right)\sin\theta$$

These results are plotted in Figure 4.6 for the case when $\lambda R = 3$.

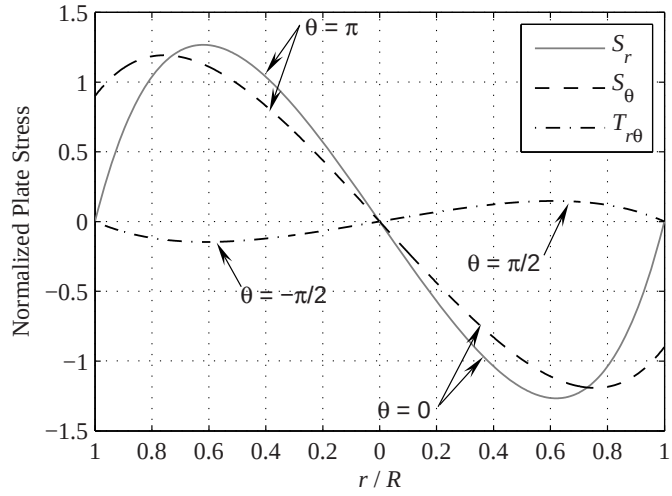

Figure 4.6 Plate stresses for bending in the large-shape-factor case

4.4 Yielding of Steel Shims under Compression

The analysis in this section will show that the pressure that causes full yielding throughout the steel shim in the incompressible case is a conservative estimate of the pressure to produce full yield in the case of the larger-shape-factor isolator when the compressibility of the rubber must be included.

4.4.1 Yielding of Steel Shims for the Case of Incompressible Rubber

While the previous analyses have concentrated on the tensile stresses in the shims, assuming that the plates were completely elastic, it is possible in the case of pure compression to estimate the pressure that will produce fully plastic yielding of the shims. Making use of the Tresca yield condition (Prager and Hodge 1951), which is shown in Figure 4.7, allows a particularly simple solution for the prediction of the pressure necessary to cause complete yield. We denote the yield force in the plate by N_o, where $N_o = \sigma_o t_p$, with σ_o being the yield stress of the steel. It is reasonable to assume both the force in the radial direction, N_r, and the force in the tangential direction, N_θ, to be tensile and to take $N_\theta = N_o$ and $0 \le N_r \le N_o$, for which the equation of equilibrium for the plate is

$$\frac{\mathrm{d}N_r}{\mathrm{d}r} + \frac{N_r - N_\theta}{r} + \tau_{rz}\big|_{z=-t/2} - \tau_{rz}\big|_{z=t/2} = 0 \tag{4.70}$$

or when the shear stresses from Equation (4.14), with p from Equation (4.1), are inserted

$$\frac{\mathrm{d}N_r}{\mathrm{d}r} + \frac{N_r - N_\theta}{r} = -\frac{6\,G\varepsilon_c}{t} r \tag{4.71}$$

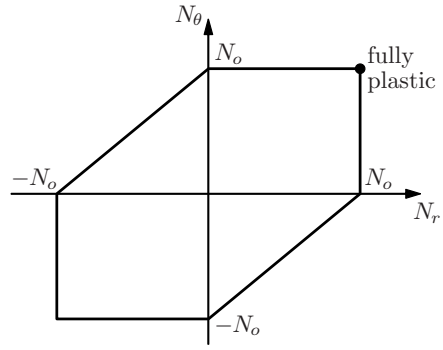

Figure 4.7 Tresca yield condition

If the plate is assumed to be rigid, there is no unique solution of the equilibrium equation. But if we assume the plate to be deformable, even if the deformations are negligible, we can obtain a unique solution. Rearranging the expression and using $N_\theta = N_o$,

$$\frac{\mathrm{d}\,(r\,N_r)}{\mathrm{d}r} = N_o - \frac{6\,G\varepsilon_c}{t}r^2 \tag{4.72}$$

Integrating this equation with the boundary condition that $N_r = N_\theta = N_o$ at $r = 0$ gives

$$N_r\,(r) = N_o - \frac{2\,G\varepsilon_c}{t}r^2 \tag{4.73}$$

and the other boundary condition that $N_r = 0$ at $r = R$ provides the maximum value of ε_c. In turn, using $p_{\text{ave}} = E_c\varepsilon_c = 6\,GS^2\varepsilon_c$ gives

$$p_{\text{ave}} = \frac{3}{4}\frac{t_p}{t}\sigma_o \tag{4.74}$$

as the value of the average pressure needed to produce full yielding of the plate. Thus the ratio of the pressure at full yielding to that when yield is initiated is around 1.23. It should be emphasized that this computation is based on the assumption that the rubber is incompressible and, in most cases, in practice the shape factors used are much larger than those for which this assumption can be made. Accordingly, it is necessary to extend the calculation to cases where the compressibility of the rubber is taken into account.

4.4.2 Yielding of Steel Shims for the Case of Compressible Rubber

The theory for the compression of a rubber pad given in the preceding section is based on two assumptions: first the displacement pattern is that given by Equation (2.7); second, the normal stress components in all three directions can be approximated by the

pressure, p, in the material. To include the influenc of bulk compressibility, we need only replace the equation of incompressibility constraint by

$$\varepsilon_{xx} + \varepsilon_{yy} + \varepsilon_{zz} = -\frac{p}{K} \tag{4.75}$$

where K is the bulk modulus. Integration through the thickness leads to an equation for $p(x,y)$ of the form

$$\nabla^2 p - \frac{12\,G}{K t^2}\,p = -\frac{12\,G\varepsilon_c}{t^2} \tag{4.76}$$

that is solved, as before, with $p = 0$ on the edge of the pad.

As shown in Section 2.4.2, the pressure distribution is given by

$$p\,(r) = K\varepsilon_c \left(1 - \frac{\mathrm{I}_0\,(\lambda r)}{\mathrm{I}_0\,(\lambda R)}\right) \tag{4.77}$$

The tensile stresses in the steel reinforcing plates can be calculated in the same way as before by using the pressure distribution given in Equation (4.77). Here we will only calculate the fully plastic state of the plate when yielding has reached the outer edge of the plate.

The equilibrium equation in the rubber becomes

$$\frac{\partial \tau_{rz}}{\partial z} = \frac{\partial p}{\partial r} = -\lambda K \varepsilon_c \frac{\mathrm{I}_1\,(\lambda r)}{\mathrm{I}_0\,(\lambda R)} \tag{4.78}$$

and the equation of equilibrium for the plate becomes

$$\frac{\mathrm{d}N_r}{\mathrm{d}r} + \frac{N_r - N_\theta}{r} = -\lambda K \varepsilon_c t \frac{\mathrm{I}_1\,(\lambda r)}{\mathrm{I}_0\,(\lambda R)} \tag{4.79}$$

Using, as before, the Tresca yield condition and assuming $N_\theta = N_o$ and $0 \le N_r \le N_o$, we have

$$\frac{\mathrm{d}\,(r\,N_r)}{\mathrm{d}r} = N_o - K\varepsilon_c t \frac{\lambda r \mathrm{I}_1\,(\lambda r)}{\mathrm{I}_0\,(\lambda R)} \tag{4.80}$$

which by integration and use of the boundary condition $N_r = N_\theta = N_o$ at $r = 0$, results in

$$r\,N_r\,(r) = N_o r - K\varepsilon_c t \int_0^r \frac{\lambda r \mathrm{I}_1\,(\lambda r)}{\mathrm{I}_0\,(\lambda R)}\,\mathrm{d}r \tag{4.81}$$

This can, in turn, be written in the form

$$N_r(r) = N_o - \frac{K\varepsilon_c t}{\lambda r \mathrm{I}_0(\lambda R)} \mathrm{L}(\lambda r) \tag{4.82}$$

where

$$\mathrm{L}(\lambda r) = \int_0^{\lambda r} x \mathrm{I}_1(x)\, \mathrm{d}x \tag{4.83}$$

The boundary condition that $N_r = 0$ at $r = R$ provides the maximum value of ε_c from

$$\frac{K\varepsilon_c t}{\lambda R \mathrm{I}_0(\lambda R)} \mathrm{L}(\lambda R) = N_o \tag{4.84}$$

and, in turn, using $p_{\text{ave}} = E_c \varepsilon_c$, where the compression modulus is given by Equation (4.8), gives the value of the average pressure needed to fully yield the plate

$$\frac{t p_{\text{ave}}}{\lambda R \mathrm{I}_0(\lambda R) - 2\mathrm{I}_1(\lambda R)} \mathrm{L}(\lambda R) = N_o \tag{4.85}$$

The integral for L(λR) can be expressed in terms of Bessel Functions and Struve Functions (McLachlan 1955) in the form

$$\int x \mathrm{I}_1(x)\, \mathrm{d}x = \frac{1}{2}\pi x \left(\mathrm{I}_1(x) \mathrm{H}_0(x) - \mathrm{I}_0(x) \mathrm{H}_1(x)\right) \tag{4.86}$$

where H_0, H_1 are the Struve functions.

The four functions that appear in the integral can be expressed as series in x as follows

$$\mathrm{I}_1(x) = \frac{x}{2}\left(1 + \frac{x^2}{8} + \frac{x^4}{192} + O\left(x^6\right)\right)$$

$$\mathrm{I}_0(x) = \left(1 + \frac{x^2}{4} + \frac{x^4}{64} + O\left(x^6\right)\right)$$

$$\mathrm{H}_1(x) = \frac{2}{3\pi}\left(x^2 - \frac{x^4}{15} + \frac{x^6}{525} + O\left(x^8\right)\right)$$

$$\mathrm{H}_0(x) = \frac{2}{\pi}\left(x - \frac{x^3}{8} + \frac{x^5}{225} + O\left(x^7\right)\right)$$

Substituting all of these into Equation (4.85) gives as the firs approximation for small values of λR the result

$$p_{\text{ave}} = \frac{3}{4}\sigma_o \frac{t_p}{t}\left(1 + \frac{(\lambda R)^2}{120} + O\left((\lambda R)^4\right)\right) \tag{4.87}$$

The firs term corresponds to the incompressible solution, and since $(\lambda R)^2 = 48\,G/(KS^2)$, it shows that for increasing shape factor the multiplier increases; in fact, by using the asymptotic expressions for the four functions, it can be shown that the multiplier monotonically increases to the asymptotic value of unity. The point of this result is that the estimate of the average pressure needed to fully yield the plate is bounded from below by the value for the incompressible case, so that for design purposes it is really only necessary to take for the maximum pressure

$$p_{\text{ave}} = \frac{3}{4}\frac{t_p}{t}\sigma_o \tag{4.88}$$

The solution for the pressure to initiate yield within the assumption of incompressibility has been well known, but the fully plastic case is new (Kelly and Konstantinidis 2009a). It had been a point of concern until recently that the known result might not be conservative for bearings with large shape factors, the analysis of which requires the inclusion of compressibility in the rubber. However, the analysis in this chapter shows that the solution for the incompressible case can be used as a conservative estimate of the limiting pressure in the more general case of large-shape-factor bearings.

5

Buckling Behavior of Multilayer Rubber Isolators

5.1 Stability Analysis of Bearings

A multilayered rubber bearing can be susceptible to a buckling type of instability similar to that of an ordinary column, but dominated by the low-shear stiffness of a bearing. The previous analysis of the overall deformation of a single pad can be used in a buckling analysis that treats the bearing as a continuous composite system. This analysis considers the bearing to be a beam, and the deformation is assumed to be such that plane sections normal to the undeformed central axis remain plane, but not necessarily normal to the deformed axis.

The theory for the buckling of isolation bearings is an outgrowth of work by Haringx in 1947 on the mechanical characteristics of helical steel springs and rubber rods used for vibration mountings. This work was published in a series of reports, the third of which (Haringx 1949) covers the stability of solid rubber rods. The Haringx theory was later applied by Gent (1964) to the problem of the stability of multilayered rubber compression springs, and it is this application that forms the basis for the theory given here.

The deformation pattern, shown in Figure 5.1, is define by two quantities: $v(x)$ is the displacement of the middle surface of the bearing, and $\psi(x)$ is the rotation of a face originally normal to the undeformed axis. The overall shear deformation, γ, is the difference between the rotation of the horizontal axis, $v'(x)$, and the rotation of the normal face, ψ (i.e., $\gamma = v' - \psi$). Figure 5.2 shows the internal and external forces on the bearing in the deformed position. The shear force, V, and the axial force, N, are shown parallel and perpendicular, respectively, to the rotated face. The end loads, including the axial load, P, are define by a lateral reaction, H_0, and bending moment, M_0, which may be specifie or unknown, depending on the problem.

The internal shear force, V, is related to the shear deformation through

$$V = GA_S(v' - \psi)$$

Mechanics of Rubber Bearings for Seismic and Vibration Isolation, First Edition. James M. Kelly and Dimitrios A. Konstantinidis.

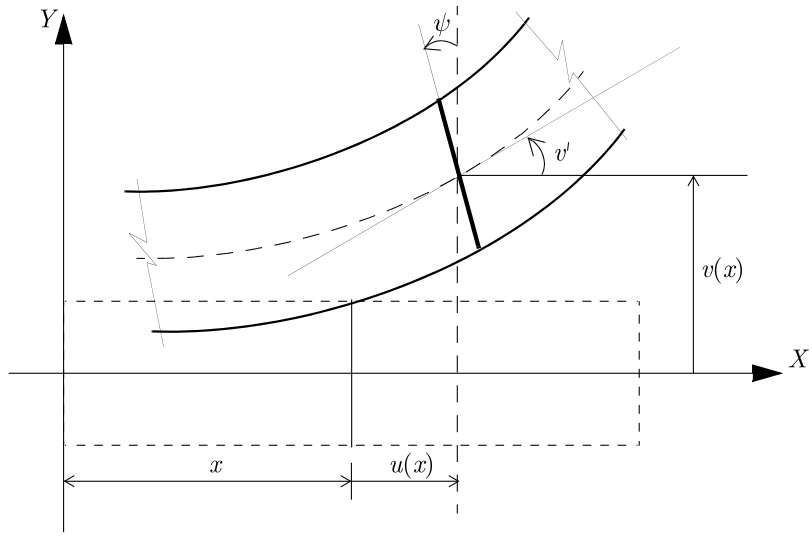

Figure 5.1 Deformation pattern for a bearing (plane sections remain plane after deformation, but not necessarily perpendicular to the deformed axis)

where A_S is not exactly the total cross-sectional area, A, but $A(h/t_r)$, where h is the total height of the bearing (rubber plus steel) and t_r is the total height of rubber. The increase in A is needed to account for the fact that the steel does not deform in the composite system.

Here, the curvature, which for a single pad was α/t, becomes ψ'; the relationship between the curvature and bending moment, M, which for a single pad was $EI = E_c I/3$,

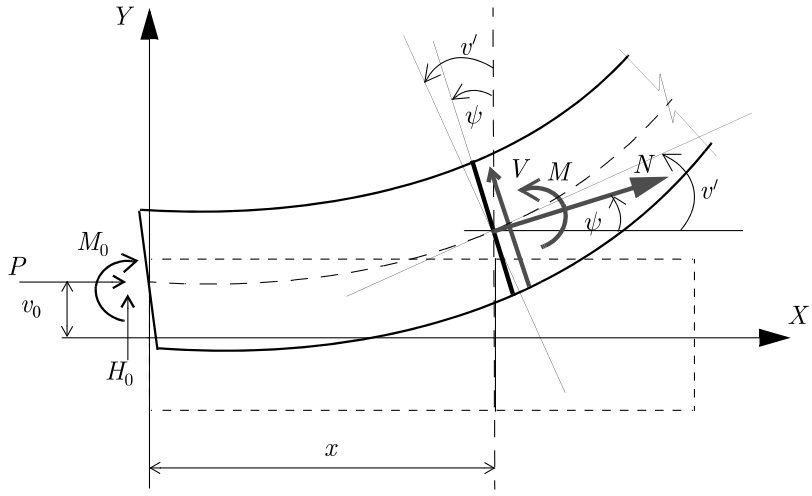

Figure 5.2 Internal forces and external loads on a deformed bearing (shear force V is parallel and axial force N is perpendicular to the deformed section)

must now be modifie in the same way as was the shear stiffness to account for the presence of the steel plates. In the following we denote the shear and bending stiffnesses of the composite system by GA_S, as define above, and $EI_S = (1/3)E_c I(h/t_r)$, with shear force V, and bending moment M, given by

$$V = GA_S(v' - \psi) \tag{5.1a}$$

$$M = EI_S\psi' \tag{5.1b}$$

The equations of equilibrium for bending moment and shear force in the deformed state, shown in Figure 5.2, are

$$M + P\,(v - v_0) - M_0 - H_0 x = 0 \tag{5.2a}$$

$$V + H_0 - P\psi = 0 \tag{5.2b}$$

and with the constitutive equations, we have

$$EI_S\psi' + Pv = Pv_0 + M_0 + H_0 x \tag{5.3a}$$

$$GA_S(v' - \psi) - P\psi = -H_0 \tag{5.3b}$$

Equation (5.3b) gives

$$\psi = \frac{GA_S v' + H_0}{GA_S + P} \tag{5.4}$$

and

$$\psi' = \frac{GA_S}{GA_S + P} v'' \tag{5.5}$$

If ψ' is substituted in Equation (5.3a), we get

$$EI_S \frac{GA_S}{GA_S + P} v'' + Pv = Pv_0 + M_0 + H_0 x \tag{5.6}$$

We can also write Equation (5.3b) in the form

$$v' = \frac{GA_S + P}{GA_S}\psi - \frac{H_0}{GA_S} \tag{5.7}$$

and when v' is inserted into the derivative of Equation (5.3a), we get

$$EI_S\psi'' + \frac{P\,(GA_S + P)}{GA_S}\psi = H_0 + \frac{P}{GA_S}H_0 \tag{5.8}$$

or

$$EI_S \frac{GA_S}{GA_S + P} \psi'' + P\psi = H_0 \tag{5.9}$$

Thus, the two equations to be solved for the two kinematic variables, v and ψ, are

$$EI_S \frac{GA_S}{GA_S + P} v'' + Pv = Pv_0 + M_0 + H_0 x \tag{5.10a}$$

$$EI_S \frac{GA_S}{GA_S + P} \psi'' + P\psi = H_0 \tag{5.10b}$$

It is useful to defin two parameters α and β as

$$\alpha^2 = \frac{P\,(GA_S + P)}{EI_S GA_S} \quad \text{and} \quad \beta = \frac{GA_S}{GA_S + P} \tag{5.11}$$

The solutions for the two differential equations in Equations (5.10a) and (5.10b) are

$$\begin{aligned} v &= A\cos(\alpha x) + B\sin(\alpha x) + v_0 + \frac{M_0}{P} + \frac{H_0}{P} x \\ \psi &= C\cos(\alpha x) + D\sin(\alpha x) + \frac{H_0}{P} \end{aligned} \tag{5.12}$$

The constants A, B, C, D are not independent, but are interrelated through Equation (5.7), which can be written in the form

$$v' = \frac{1}{\beta}\psi - \frac{H_0}{GA_S} \tag{5.13}$$

and by substitution of Equation (5.12), leads to

$$-\alpha A\sin(\alpha x) + \alpha B\cos(\alpha x) + \frac{H_0}{P} = \frac{1}{\beta} C\sin(\alpha x) + \frac{1}{\beta} D\sin(\alpha x) + \frac{1}{\beta}\frac{H_0}{P} - \frac{H_0}{GA_S} \tag{5.14}$$

giving the relationship between the constants as

$$C = \alpha\beta B \quad \text{and} \quad D = -\alpha\beta A \tag{5.15}$$

The most general form of solution of Equations (5.10a) and (5.10b) becomes

$$v = A\cos(\alpha x) + B\sin(\alpha x) + v_0 + \frac{M_0}{P} + \frac{H_0}{P} x \tag{5.16a}$$

$$\psi = \alpha\beta B\cos(\alpha x) - \alpha\beta A\sin(\alpha x) + \frac{H_0}{P} \tag{5.16b}$$

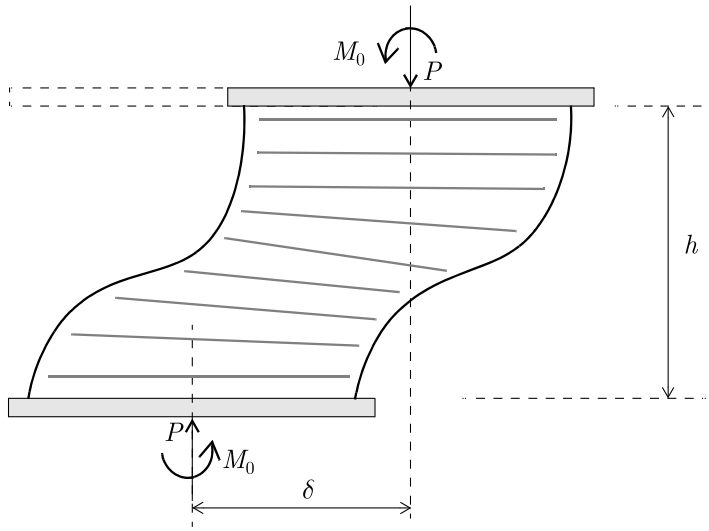

Figure 5.3 Boundary conditions for an isolation bearing under a vertical load P (the bearing buckles with no lateral force constraint but is prevented from rotating at each end)

We now turn our attention to the specifi example of a bearing in an isolation system. As shown in Figure 5.3, the bearing is constrained against displacement at the bottom, rotation at the top and bottom, and is free to move laterally at the top. Setting $x = 0$ at the bottom of the bearing and $x = h$ at the top, we have

$$v(0) = 0, \quad \psi(0) = 0, \quad \psi(h) = 0, \quad H_0 = 0 \tag{5.17}$$

thus Equation (5.16a) gives

$$A + \frac{M_0}{P} = 0 \tag{5.18}$$

and Equation (5.16b) yields

$$\begin{aligned} \psi(0) &= \alpha\beta B = 0 \\ \psi(h) &= -\alpha\beta A \sin(\alpha h) = 0 \end{aligned} \tag{5.19}$$

Therefore, $\alpha h = \pi$, and the general solution becomes

$$\begin{aligned} v(x) &= \frac{1}{2}\delta\left(1 - \cos\left(\frac{\pi x}{h}\right)\right) \\ \psi(x) &= \frac{1}{2}\alpha\beta\delta \sin\left(\frac{\pi x}{h}\right) \end{aligned} \tag{5.20}$$

and $M_0 = P\delta/2$, where $\delta = v(h)$.

The result $\alpha h = \pi$ means

$$\alpha^2 = \frac{\pi^2}{h^2} \tag{5.21}$$

If we substitute the definitio of α^2 from Equation (5.11), we get

$$\frac{P\,(GA_S + P)}{GA_S} = \frac{\pi^2 EI_S}{h^2} = P_E \tag{5.22}$$

where P_E is the Euler load for the standard column. If we denote $GA_S = P_S$, the above equation for the critical load, P, becomes

$$P^2 + P_S P - P_S P_E = 0 \tag{5.23}$$

from which the critical load, P_{crit}, is given by

$$P_{crit} = \frac{-P_S + \sqrt{P_S^2 + 4P_S P_E}}{2} \tag{5.24}$$

If we now assume that $P_S \approx GA$ and

$$P_E \approx \frac{\pi^2}{h^2}\frac{1}{3}6\,GS^2 I \approx GA\left(\frac{2\pi^2 S^2 I}{Ah^2}\right) \tag{5.25}$$

then, for most types of bearings where S is 5 or greater, $P_E \gg P_S$, the critical load can be approximated by

$$P_{crit} = \sqrt{P_S P_E} \tag{5.26}$$

Using this expression and recalling that

$$\begin{aligned} P_S &= GA\frac{h}{t_r} \\ P_E &= \frac{\pi^2}{h^2}\frac{1}{3}E_c I\frac{h}{t_r} \end{aligned} \tag{5.27}$$

we have

$$\begin{aligned} P_{crit} &= \sqrt{\left(GA\frac{h}{t_r}\right)\left(\frac{\pi^2}{h^2}\frac{1}{3}6\,GS^2 Ar^2\frac{h}{t_r}\right)} \\ &= \frac{\sqrt{2}\pi GASr}{t_r} \end{aligned} \tag{5.28}$$

where r is the radius of gyration, which is $r = \sqrt{I/A} = a/(2\sqrt{3})$ for a square bearing with side dimension a, and $\Phi/4$ for a circular bearing with diameter Φ.

The critical pressure, $p_{crit} = P_{crit}/A$, can be expressed in terms of S and the quantity S_2, referred to as the aspect ratio or the *second shape factor*, define by

$$S_2 = \frac{\Phi}{t_r} \quad \text{for a circular bearing} \tag{5.29a}$$

$$S_2 = \frac{a}{t_r} \quad \text{for a square bearing} \tag{5.29b}$$

Thus

$$\frac{p_{crit}}{G} = \frac{\pi}{2\sqrt{2}} SS_2 \quad \text{for a circular bearing} \tag{5.30a}$$

$$\frac{p_{crit}}{G} = \frac{\pi}{\sqrt{6}} SS_2 \quad \text{for a square bearing} \tag{5.30b}$$

In actual design, the load carried by a bearing (say, W) will be less than the critical load, and neglecting the effect of the vertical load on the horizontal stiffness, K_H, of the bearing, this is given by $K_H = GA/t_r$, which in turn is related to the horizontal frequency, ω_H, through

$$\omega_H^2 = \frac{K_H}{W} g \tag{5.31}$$

Thus, the safety factor, S.F., against buckling, which is define by S.F. $= P_{crit}/W$, becomes

$$\text{S.F.} = \frac{\sqrt{2}\pi S \omega_H^2 r}{g} \tag{5.32}$$

All other things being equal, the safety factor increases with shape factor, S, frequency, ω_H, or bearing size (either a or Φ).

The bearing size will, of course, depend on the carried load. If the pressure, $p = W/A$, is specified then

$$r = \frac{1}{2\sqrt{\pi}} \left(\frac{W}{p}\right)^{1/2} \quad \text{for a circular bearing} \tag{5.33a}$$

$$r = \frac{1}{2\sqrt{3}} \left(\frac{W}{p}\right)^{1/2} \quad \text{for a square bearing} \tag{5.33b}$$

If the pressure is fixed the safety factor will diminish as $W^{1/2}$, leading to the unexpected result that buckling can become a problem for bearings that are lightly loaded.

To get a feeling for the magnitude of the quantities involved, suppose that the safety factor must be at least three, the shape factor, S, is 10, and the frequency is π rad/s (2.0 s period), all of which are typical values. In this case, r must be at least

$$r = \frac{3 \cdot 9810}{\sqrt{2 \cdot \pi \cdot 10 \cdot \pi^2}} = 67.01 \text{ mm } (2.64 \text{ in})$$

If the bearing is circular, then $\Phi = 268$ mm (10.6 in). This minimum dimension is independent of the carried load or the pressure, but if the pressure is specified say, for example, at 6.90 MPa (1000 psi), it translates to a minimum load of 39 tons (88 kips). For most buildings, the bearings will be much larger than this minimum size, and the carried loads will be in the hundreds of tons, so that buckling is not likely to be a problem for the design.

There have been cases, however, when it has been necessary to design isolators for lighter loads, for example, circuit breakers in electric power plant switch yards. These components weigh as little as a few tons, and the bearing design should be stable under loads that range from 1 to perhaps 5 tons. Bearings developed for such applications are referred to as "enhanced stability bearings." In these bearings the tilting stiffness is increased either by making the bearing an assembly of small bearings connected by steel plates (Kircher *et al.* 1979) or by individual rubber discs connected by steel plates (Tyler 1991). The firs application of a bearing of this kind was carried out by Kircher *et al.* (1979) for circuit breakers at the Edmunson Power Plant near Bakersfield California. The stability analysis given here for the single bearing is applicable to these enhanced stability bearings.

5.2 Stability Analysis of Annular Bearings

Another way to improve the stability of a bearing that is intended to support a light load is to use an annular bearing. The presence of a large central hole reduces the horizontal stiffness, but has only a small effect on the bending stiffness. Using the analysis developed in the previous chapter, the bending stiffness of a single annular pad is given by

$$(EI)_{eff} = \frac{\pi G}{8t^2}\left(b^2 - a^2\right)^3 \tag{5.34}$$

where a and b are the inside and outside radii of the pad, and t is the pad thickness. If this is substituted into the approximate form for the buckling load, i.e., $P_{crit} = \sqrt{P_S P_E}$, with

$$P_S = GA\frac{h}{t_r} = G\pi\left(b^2 - a^2\right)\frac{h}{t_r} \tag{5.35}$$

and

$$P_E = \pi^2 (EI)_{eff}\frac{h}{t_r}\frac{1}{h^2} = \frac{\pi^2 \pi G}{h t_r 8t^2}\left(b^2 - a^2\right)^3 \tag{5.36}$$

we have

$$P_{crit}^2 = G\pi\left(b^2 - a^2\right)\frac{h}{t_r}\frac{\pi^2}{ht_r}\frac{\pi G}{8t^2}\left(b^2 - a^2\right)^3 = \frac{G^2\pi^4\left(b^2 - a^2\right)^4}{8t_r^2t^2}$$

$$P_{crit} = \frac{\pi^2 G\left(b^2 - a^2\right)^2}{2\sqrt{2}t_r t} \tag{5.37}$$

The specifie horizontal frequency is related to the carried load per bearing, W, by

$$\omega_H^2 = \frac{K_H}{W}g = \frac{G\pi g\left(b^2 - a^2\right)}{Wt_r} \tag{5.38}$$

so that the safety factor against buckling is given by

$$\text{S.F.} = \frac{P_{crit}}{W} = \frac{\pi^2 G\left(b^2 - a^2\right)^2}{2\sqrt{2}t_r t}\frac{\omega_H^2 t_r}{G\pi\left(b^2 - a^2\right)g} = \frac{\pi\left(b^2 - a^2\right)\omega_H^2}{2\sqrt{2}tg} \tag{5.39}$$

If we fi ω_H and layer thickness t, then the safety factor must decrease as the size of the hole increases. This apparently contradictory result occurs because if we fi b and vary a, the pressure is not kept constant. If the pressure is fixed then $(b^2 - a^2)$ is f xed, thus the safety factor remains constant. If the pressure is held constant, then the only way to increase the safety factor is to reduce the individual layer thickness t. It follows that simply replacing a circular bearing with an annular bearing does not improve stability; it is necessary to reduce the pressure and the layer thickness. An annular bearing does have merit in certain cases, however. Because the total rubber thickness, t_r, does not enter into the safety factor, a larger value of t_r can be used, thus lowering the peak shear strain and the ratio of the displacement to diameter with no reduction of the safety factor against buckling; this will certainly lead to better performance when light loads are to be isolated.

5.3 Influenc of Vertical Load on Horizontal Stiffness

If the load carried by a bearing is comparable to the buckling load, then the simple formula for horizontal stiffness, $K_H = GA/t_r$, may need to be modified The analysis that led to the buckling load can be used to determine the effective horizontal stiffness in the presence of axial load (Koh and Kelly 1987). Consider a horizontal force, F_H, at the top of a bearing. When the resulting displacement at the top, $v(h)$, is computed, then the horizontal stiffness, K_H, is given by

$$K_H = \frac{F_H}{v(h)} \tag{5.40}$$

The basic equations, Equations (5.16a) and (5.16b), are solved using the boundary conditions

$$v(0) = 0, \quad \psi(0) = 0, \quad \psi(h) = 0, \quad H_0 = -F_H \tag{5.41}$$

Thus

$$v(x) = A\cos(\alpha x) + B\sin(\alpha x) + \frac{M_0}{P} - \frac{F_H}{P}x \tag{5.42a}$$

and

$$\psi(x) = \alpha\beta B\cos(\alpha x) - \alpha\beta A\sin(\alpha x) - \frac{F_H}{P} \tag{5.42b}$$

Using the boundary conditions, we have

$$A = \frac{F_H}{P}\frac{\cos(\alpha h) - 1}{\alpha\beta\sin(\alpha h)} \tag{5.43}$$

and

$$B = \frac{F_H}{\alpha\beta P} \tag{5.44}$$

When these are substituted back into Equation (5.42a), we obtain

$$v(h) = \frac{F_H}{\alpha\beta P}\left(2\tan\left(\frac{\alpha h}{2}\right) - \alpha\beta h\right) \tag{5.45}$$

for the displacement evaluated at $x = h$. Thus the horizontal stiffness is

$$K_H = \frac{F_H}{v(h)} = \frac{\alpha\beta P}{2\tan\left(\frac{\alpha h}{2}\right) - \alpha\beta h} \tag{5.46}$$

When $\alpha h \to \pi$, the term $\tan(\alpha h/2) \to \infty$ and $K_H \to 0$. For small values of P,

$$\alpha^2 \to \frac{P}{EI_S} \quad \text{and} \quad \beta \to 1 - \frac{P}{GA_S} \tag{5.47}$$

Expanding $2\tan(\alpha h/2)$ in a Taylor series gives

$$2\tan\left(\frac{\alpha h}{2}\right) = \alpha h + \frac{1}{12}(\alpha h)^3 + \cdots$$

so that

$$\begin{aligned} K_H &= \frac{\alpha\left[1 - P/(GA_S)\right]P}{\dfrac{1}{12}\alpha^3 h^3 + \alpha h\dfrac{P}{GA_S}} \\ &\approx \frac{P}{\dfrac{1}{12}\dfrac{P}{EI_S}h^3 + \dfrac{Ph}{GA_S}} \\ &= \frac{1}{h^3/(12\,EI_S) + h/(GA_S)} \approx \frac{GA_S}{h}\left(1 - \frac{GA_S h^2}{12\,EI_S}\right) \end{aligned} \tag{5.48}$$

The second term in the brackets is the effect of the bending flexibilit on the stiffness. For circular isolators this is

$$\frac{h^2}{6\,S^2 R^2}$$

and is generally negligible compared to the firs term.

For values of P between P_S and P_E, the approximations that led to Equation (5.26) give

$$\alpha^2 = \frac{P^2}{EI_S GA_S} \tag{5.49}$$

and

$$\begin{aligned} \alpha h &= \pi\left(\frac{P}{P_{crit}}\right) \\ \beta &= \frac{GA_S}{P} = \frac{P_S}{P} \end{aligned} \tag{5.50}$$

leading to

$$K_H = \frac{GA_S}{h}\frac{\dfrac{\pi}{2}\dfrac{P}{P_{crit}}}{\tan\left(\dfrac{\pi}{2}\dfrac{P}{P_{crit}}\right) - \dfrac{\pi}{2}\dfrac{P}{P_{crit}}\dfrac{GA_S}{P}} \tag{5.51}$$

When P is close to P_{crit}, the tangent term dominates and an approximation can be made

$$K_H = \frac{GA_S}{h}\frac{\dfrac{\pi}{2}\dfrac{P}{P_{crit}}}{\tan\left(\dfrac{\pi}{2}\dfrac{P}{P_{crit}}\right)} \tag{5.52}$$

as shown in Figure 5.4, with the exact result, Equation (5.51), also shown for comparison. Although Equation (5.52) is only valid when P is near P_{crit}, it is a good

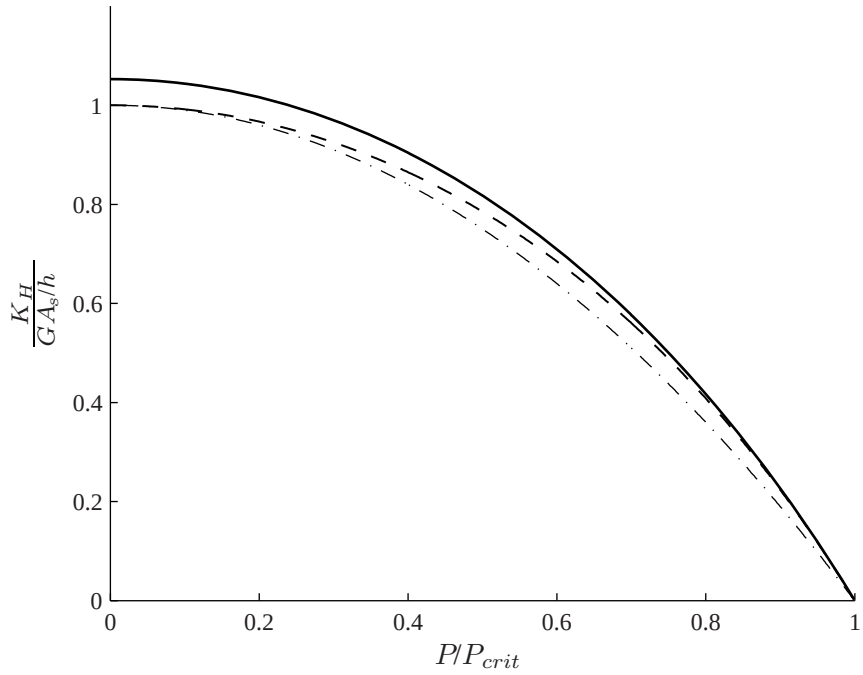

Figure 5.4 Influenc of the axial load on the horizontal stiffness. Solid line: "exact", Equation (5.51) with $GA_S/P = 0.05$; dashed line: approximation of Equation (5.52); dash-dotted line: approximation of Equation (5.53)

approximation over the entire range of P; however, an even simpler fi to the exact result is the function

$$K_H = \frac{GA_S}{h}\left[1 - \left(\frac{P}{P_{crit}}\right)^2\right] \tag{5.53}$$

which is also shown in Figure 5.4.

The exact value of K_H can be most easily expressed in terms of dimensionless quantities p and λ, if we introduce the load, P_A, by

$$P_A^2 = \frac{\pi^2 EI_S GA_S}{h^2} \tag{5.54}$$

(P_A is P_{crit} when $P_S \ll P_{crit} \ll P_E$) and $p = P/P_A$, $\lambda = GA_S/P_A$. In terms of these variables, we have

$$K_H = \frac{GA_S}{h}\frac{\frac{\pi}{2}p^{2/3}(p+\lambda)^{-1/2}}{\tan\left[\frac{\pi}{2}p^{1/2}(p+\lambda)^{-1/2}\right] - \frac{\pi}{2}p^{1/2}\lambda(p+\lambda)^{-1/2}} \tag{5.55}$$

The value of λ is $\sqrt{2}h/(\pi SR)$ and generally is small compared with one.

5.4 Downward Displacement of the Top of a Bearing

The downward displacement of the top of a bearing due to a horizontal displacement is often needed in the design process, and this can also be calculated using the buckling analysis. Suppose that the bearing is just at critical load, but undeflected and imagine the work done externally and internally as it moves to a buckled position. The external work is denoted by $P\delta_v$, where δ_v is the downward displacement, since we assume that the load remains constant during this process. The internal work, W_D, is given by

$$W_D = \frac{1}{2}\int_0^h [V(v' - \psi) + M\psi']\mathrm{d}x \tag{5.56}$$

but by equilibrium Equations (5.2a) and (5.2b),

$$\begin{aligned} V &= -H_0 + P\psi \\ M &= M_0 + H_0 x - Pv + Pv_0 \end{aligned} \tag{5.57}$$

so that

$$\begin{aligned} W_D &= \frac{1}{2}\int_0^h \left[(-H_0 + P\psi)(v' - \psi) + (M_0 + H_0 x - Pv + Pv_0)\psi'\right]\mathrm{d}x \\ &= \frac{1}{2}P\int_0^h \left(\psi v' - \psi^2 - v\psi'\right)\mathrm{d}x \\ &\quad -\frac{1}{2}H_0\int_0^h [(v' - \psi) - x\psi']\mathrm{d}x + (M_0 + Pv_0)[\psi(h) - \psi(0)] \end{aligned} \tag{5.58}$$

In the buckling problem, we have $v_0 = 0$, $\psi(0) = 0$, $\psi(h) = 0$, and $H_0 = 0$. Accordingly, the work equality becomes

$$P\delta_v = \frac{P}{2}\int_0^h \left(2\psi v' - \psi^2\right)\mathrm{d}x \tag{5.59}$$

The implication of this result is that the downward displacement is given by

$$\delta_v = \frac{1}{2}\int_0^h \left(2\psi v' - \psi^2\right)\mathrm{d}x \tag{5.60}$$

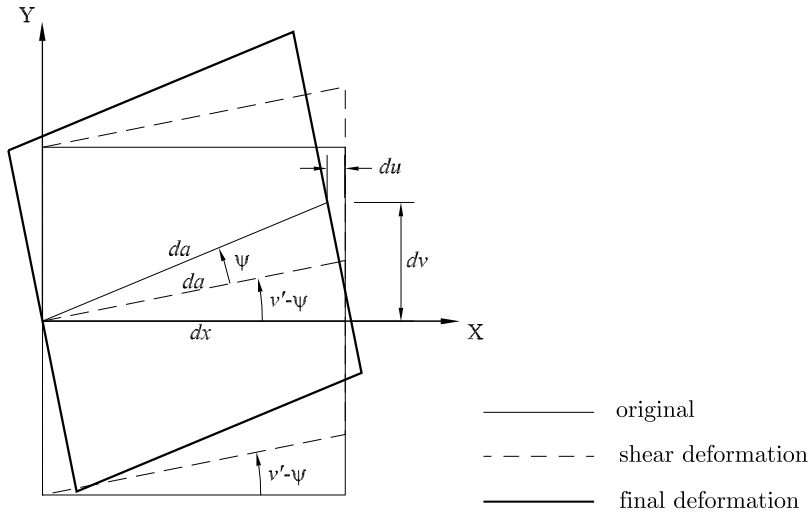

Figure 5.5 Geometry of the axial displacement of a bearing due to lateral deformation

Although somewhat counter intuitive, this result can be obtained geometrically, as shown in Figure 5.5. Here the downward displacement is represented by the displacement, u, in the x, or axial, direction. We visualize a displacement of the center line of the element through an angle of $v' - \psi$ with no downward displacement, then a further rotation of the entire element through an angle, ψ. The change in the projected length of the element, shown as du in the figu e, is given by

$$\mathrm{d}u = \mathrm{d}a(\cos(v' - \psi) - \cos v') \tag{5.61}$$

where

$$\mathrm{d}a = \frac{\mathrm{d}x}{\cos(v' - \psi)} \tag{5.62}$$

Since

$$\cos(v' - \psi) - \cos v' = -2\sin\left[\frac{1}{2}(v' - \psi + v')\right]\sin\left[\frac{1}{2}(v' - \psi - v')\right]$$

when we use small-angle approximations for sine and cosine, we have

$$\mathrm{d}u = \mathrm{d}x\left(1 + \frac{1}{2}(v' - \psi)^2\right)\left(\frac{1}{2}(2v' - \psi)\psi\right) \tag{5.63}$$

leading to

$$\delta_v = \frac{1}{2}\int_0^h (2v' - \psi)\psi \, \mathrm{d}x \tag{5.64}$$

When the bearing is buckled, the relationship between the vertical movement and the lateral displacement is given by Equation (5.64) by inserting

$$\begin{aligned} v(x) &= \frac{\delta}{2}\left(1 - \cos\frac{\pi x}{h}\right) \\ \psi(x) &= \frac{\alpha\beta\delta}{2}\sin\frac{\pi x}{h} \end{aligned} \tag{5.65}$$

giving

$$\begin{aligned} \delta_v &= \frac{1}{2}\int_0^h \left(2\frac{\alpha\beta\delta}{2}\frac{\pi}{h}\frac{\delta}{2} - \frac{\alpha^2\beta^2\delta^2}{4}\right)\sin^2\frac{\pi x}{h}\,\mathrm{d}x \\ &= \frac{\alpha\beta\pi}{8}\left(1 - \frac{\alpha\beta h}{2\pi}\right)\delta^2 \end{aligned} \tag{5.66}$$

At buckling, $\alpha h = \pi$, so

$$\delta_v = \frac{\pi^2}{8h}\beta\left(1 - \frac{\beta}{2}\right)\delta^2 \tag{5.67}$$

Since

$$\beta = \frac{GA_S}{GA_S + P_{crit}} \approx \frac{GA_S}{P_{crit}} \ll 1 \tag{5.68}$$

$$\delta_v = \frac{\pi^2 GA_S}{8\,h\,P_{crit}}\delta^2 \tag{5.69}$$

Using the approximation for P_{crit} in Equation (5.26) for a circular bearing with radius R, we have

$$\delta_v = \frac{\sqrt{2}\pi}{8\,SR}\delta^2 \tag{5.70}$$

which surprisingly does not depend on the height of the bearing. For example, suppose $R = h$, $\delta = h$, $S = 10$, then

$$\delta_v = \frac{\sqrt{2}\pi}{80}h = 0.055\,h$$

Although the same procedure can be used to estimate δ_v when $P < P_{crit}$ and the bearing is laterally displaced, the algebraic complexity has reached the point of diminishing returns. A simpler model will be developed in Section 5.5.

The previous result Equation (5.60) can be used to calculate the displacement of the top of the bearing when it is loaded by a lateral load F_H and a downward vertical load P.

The starting point for the calculation is the solution for $v(x)$ and $\psi(x)$, namely

$$v(x) = \frac{F_H}{\alpha\beta P}\left[\sin(\alpha x) - \alpha\beta x + \frac{1-\cos(\alpha h)}{\sin(\alpha h)}(1-\cos(\alpha x))\right] \tag{5.71}$$

and

$$\psi(x) = \frac{F_H}{P}\left[\frac{1-\cos(\alpha h)}{\sin(\alpha h)}\sin(\alpha x) - (1-\cos(\alpha x))\right] \tag{5.72}$$

from these, we have

$$v(h) = \delta_h = \frac{F_H}{\alpha\beta P}\left(2\frac{1-\cos(\alpha h)}{\sin(\alpha h)} - \alpha\beta h\right) \tag{5.73}$$

and

$$v'(x) = \frac{F_H}{\beta P}\left(\cos(\alpha x) + \frac{1-\cos(\alpha h)}{\sin(\alpha h)}\sin(\alpha x) - \beta\right) \tag{5.74}$$

Using Equations (5.72) and (5.74), we form the product

$$\begin{aligned} 2\psi v' - \psi^2 = \frac{F_H^2}{\beta P^2}\{&-2[\beta\cos\alpha h\cos^2\alpha x - \beta\cos\alpha h + \cos\alpha h - 2\cos\alpha h\cos^2\alpha x \\ &+ \cos\alpha h\cos\alpha x - 1 + \sin\alpha h\sin\alpha x - 2\sin\alpha h\cos\alpha x\sin\alpha x \\ &+ \beta\cos\alpha x\sin\alpha x\sin\alpha h + \cos\alpha x]/[\cos\alpha h + 1]\} \end{aligned} \tag{5.75}$$

Integrating this expression from $x = 0$ to $x = h$, and plugging into Equation (5.64) leads to

$$\delta_v = \frac{1}{2}\frac{F_H^2}{\beta P^2}\frac{\alpha h\beta\cos\alpha h - 2\sin\alpha h + 2\alpha h - \beta\sin\alpha h}{\alpha(\cos\alpha h + 1)} \tag{5.76}$$

The terms F_H and P can be eliminated by dividing this by the square of δ_h from Equation (5.73), giving

$$\delta_v = \left[\frac{\alpha h\beta}{2}\frac{\alpha h\beta\cos(\alpha h) - 2\sin(\alpha h) + 2\alpha h - \beta\sin(\alpha h)}{-4\cos(\alpha h) + \beta^2\alpha^2h^2\cos(\alpha h) + 4 + \beta^2\alpha^2h^2 - 4\beta\alpha h\sin(\alpha h)}\right]\frac{\delta_h^2}{h} \tag{5.77}$$

In Equation (5.77) the expression in the brackets is a function of the two dimensionless quantities αh and β both of which depend on the vertical load P. The result shows

that when the bearing parameters P_S and P_E are specified the vertical displacement is quadratic in the lateral displacement δ_h and can easily be computed for any value of axial load.

If we use the approximations made in the earlier section neglecting GA_S as compared with P, giving $\alpha h = \pi p$ and $\beta \approx 0$, this reduces to

$$\delta_v = \frac{\pi G A_S}{4 P_{crit}} \left(\frac{\pi p - \sin(\pi p)}{1 - \cos(\pi p)} \right) \frac{\delta_h^2}{h} = \frac{\pi G A_S}{4 P_{crit}} f(\pi p) \frac{\delta_h^2}{h} \tag{5.78}$$

The function $f(x) = (x - \sin x)/(1 - \cos x)$ varies from 0 when $x = 0$ to $\pi/2$ when $x = \pi$ and increases monotonically over the range $0 \leq x \leq \pi$. When x is replaced by $-x$, it is anti-symmetric, i.e., $f(-x) = -f(x)$. The derivative

$$f'(x) = \frac{(1 - \cos x) - x \sin x}{(1 - \cos x)^2} \tag{5.79}$$

is symmetric and varies from $1/3$ to 1 as x varies from 0 to π and monotonically increases over this range.

The vertical stiffness of the isolator in the undeformed position is given by

$$K_v^0 = \frac{E_c A_S}{h} \tag{5.80}$$

where E_c is the compression modulus given by

$$E_c = 6 G S^2 \tag{5.81}$$

The vertical stiffness when sheared through a displacement δ_h will be

$$K_v = \left(\frac{\mathrm{d}\delta_v^t}{\mathrm{d}P} \right)^{-1} \tag{5.82}$$

where

$$\delta_v^t = \frac{Ph}{E_c A_S} + \delta_v \tag{5.83}$$

Now

$$\frac{\mathrm{d}\delta_v}{\mathrm{d}P} = \frac{\mathrm{d}\delta_v}{\mathrm{d}x} \frac{\mathrm{d}x}{\mathrm{d}P} = \frac{\pi^2 G A_S}{4 P_{crit}^2} f'(\pi p) \frac{\delta_h^2}{h} \tag{5.84}$$

giving

$$K_v = K_v^0 \frac{1}{1 + \dfrac{\pi^2}{4} \dfrac{G A_S E_c A_S}{P_{crit}^2} f'(\pi p) \dfrac{\delta_h^2}{h}} \tag{5.85}$$

Since $P_{crit}^2 = GA_S EI_S(\pi^2/h^2)$, this becomes

$$K_v = K_v^0 \frac{1}{1 + \frac{3}{4} f'(\pi p) \frac{\delta_h^2}{r^2}} \tag{5.86}$$

where $r^2 = I/A$. For a circular bearing of diameter Φ, $r^2 = \Phi^2/16$ leading to

$$K_v = K_v^0 \frac{1}{1 + 12 f'(\pi p) \frac{\delta_h^2}{\Phi^2}} \tag{5.87}$$

In many cases the displacement can be a significan fraction of the diameter so that the vertical stiffness can be considerably reduced by the lateral displacement. This result has implications for the computer modelling of isolation bearings. The models of isolators in most structural analysis programs have two sets of independent springs that represent the horizontal stiffness and the vertical stiffness. This result shows that if we are to properly model an isolator, we need to include the interaction between the vertical stiffness and the horizontal displacement. In principle this could be done by a finit element model, but this is much too complicated to be included in a structural analysis program. In the next section, however, we will demonstrate a simple two-spring mechanical model that will very accurately represent the behavior of a bearing including interaction between these quantities, and that could be easily incorporated into a structural analysis program.

5.5 A Simple Mechanical Model for Bearing Buckling

There are a number of other aspects of bearing behavior that can be modelled using the shear-weak column theory, but the algebraic complexity becomes considerable and one loses the direct physical understanding of the phenomenon that is useful in design. The other aspects of bearing behavior that are useful to cover are the downward movement of the top of the bearing produced by horizontal displacement, the postbuckling behavior, and the influenc of the axial load on the damping in the bearing. To provide a simple physical interpretation of these factors, a simple mechanical model with two mechanisms of deformation has been developed that closely fit the exact theory and demonstrates these aspects of bearing behavior in a simple way.

In the model shown in Figure 5.6, two rigid elements in the shape of tees are connected by moment springs across hinges at top and bottom and by shear springs and friction-less rollers at mid-height. The two deformation variables shown are shear displacement, s, and relative rotation, θ; the two moment spring stiffnesses are shown as $K_1/2$ each (moment/radian), the shear spring stiffness as K_2 (shear force/displacement), the vertical load as P, and the horizontal load at the top of the column as F_H. The horizontal displacement, v, of the top of the column is given, in terms of s and θ, by

$$v = h \sin\theta + s \cos\theta \tag{5.88}$$

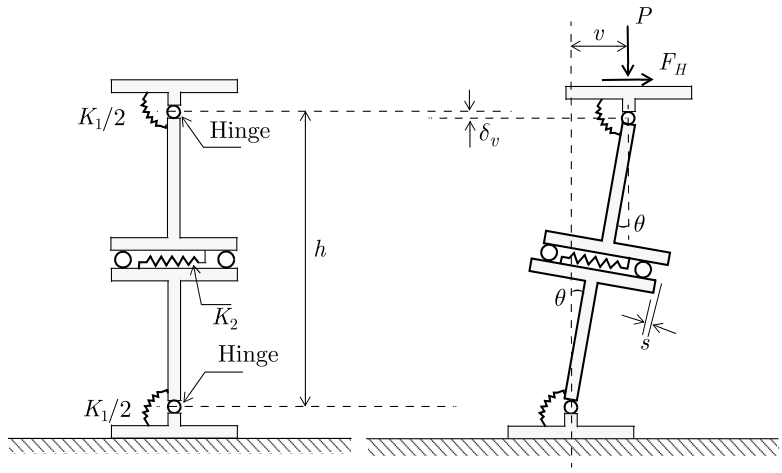

Figure 5.6 A simple two-spring model of an isolation bearing

Or, if we assume the displacements and rotations to be small, is

$$v = h\theta + s \tag{5.89}$$

To relate the quantities of this system to those of the exact theory, we recognize that if the shear stiffness, K_2, is set to infinit , the buckling load of the model is K_1/h. On the other hand, if the rotational spring stiffness, K_1, is infinit and only shear deformation is allowed, the horizontal stiffness is K_2h. It follows that K_1 should be equated to P_Eh and K_2 to GA_S/h, where $P_E = \pi^2 EI_S/h^2$ is the Euler buckling load of the column neglecting shear deformation, and GA_S and EI_S are the effective shear and bending stiffnesses of the bearing. As before, it is convenient to write GA_S as P_S.

If we assume small displacements i.e., Equation (5.89), the equilibrium equations become

$$(P_E - P)\,\theta - P\frac{s}{h} = F_H \tag{5.90}$$

and

$$-P\theta + P_S\frac{s}{h} = F_H \tag{5.91}$$

If $F_H = 0$, the possibility of nonzero values of θ and s/h leads to the determinental equation

$$(P_E - P)\,P_S = P^2 = 0 \tag{5.92}$$

This is the same equation for the buckling load as that developed for the exact theory in Equation (5.23).

When the horizontal force, F_H, is present, the solutions for θ and s are

$$\begin{aligned}\theta &= F_H \frac{P_S + P}{P_S P_E - P P_S - P^2} \\ \tfrac{s}{h} &= F_H \frac{P_E}{P_S P_E - P P_S - P^2}\end{aligned} \tag{5.93}$$

The horizontal stiffness of the model is given by

$$K_H = F_H / v \tag{5.94}$$

and

$$v = h\theta + s = \frac{h F_H (P_S + P + P_E)}{P_S P_E - P P_S - P^2} \tag{5.95}$$

so that

$$K_H = \frac{1}{h} \frac{P_S P_E - P P_S - P^2}{P_E + P + P_S} \tag{5.96}$$

To the same order of approximation that gave the buckling load as $(P_E P_S)^{1/2}$, this result reduces to

$$K_H = \frac{G A_S}{h} \left(1 - \frac{P^2}{P_S P_E}\right) \tag{5.97}$$

This result is identical to the approximate Equation (5.53) and is plotted in Figure 5.4 for comparison with the exact formula, Equation (5.51), for $GA_S/P = 0.05$.

The downward movement of the top of the bearing due to the horizontal displacement can also be derived from this model. The height reduction of a bearing is often useful to know for detailing adjacent foundation components. If we assume a small rotation, the downward movement of the top of the bearing, denoted by δ_v, is given by

$$\delta_v = s\theta + h\theta^2/2 \tag{5.98}$$

If we substitute for θ and s/h, using Equation (5.93), and eliminate F_H in terms of v from Equation (5.95), we have

$$\delta_v = \frac{v^2}{2h} \frac{(GA_S + P)(GA_S + P + 2P_E)}{(GA_S + P + P_E)^2} \tag{5.99}$$

Since P_E is very much larger than P or P_S, we can approximate this expression by

$$\delta_v = \frac{v^2}{h} \frac{GA_S + P}{P_E} \tag{5.100}$$

Koh and Kelly (1987) presented the exact form of this result. The result above, however, is considerably simpler and has been verifie by experimental work presented in the same publication. This simplifie result is very useful for practical applications and can be used to estimate the vertical stiffness of an isolator in a deformed position. This parameter is necessary for some applications, and the standard recommendation is to use the formula $K_V = E_c A/t_r$, replacing the area, A, by the area of overlap between the top plate and the bottom plate when the bearing is displaced horizontally. This very simplistic approach is not based on rational analysis; it ignores the fact that the downward movement of the top of the bearing (with respect to the bottom during lateral displacement) is caused by a tilting of the reinforcing layers at the middle of the bearing away from the end restraints. This tilting process means that some of the layers experience a shear stress produced by the component of the vertical load in the direction of the rotated plates.

Thus, if we take the horizontal displacement, v, to be f xed and vary load P, the additional displacement, δ_v, due to the column action of the bearing is given by Equation (5.100), and the total vertical displacement, which includes δ_v and the compression of the rubber, δ_v^t, is

$$\delta_v^t = \frac{Ph}{E_c A_S} + \frac{GA_S + P}{P_E}\frac{v^2}{h} \tag{5.101}$$

The instantaneous vertical stiffness is given by

$$K_V = \frac{\mathrm{d}P}{\mathrm{d}\delta_v^t} = \frac{1}{h/(E_c A_S) + v^2/(P_E h)} \tag{5.102}$$

Recalling that $P_E = \pi^2 EI_S/(3h^2)$, this reduces to

$$K_V = \frac{E_c A_S}{h}\frac{1}{1 + (3v^2)/(\pi^2 r^2)} \tag{5.103}$$

For a circular bearing, $r = \Phi/4$; therefore

$$\frac{3v^2}{\pi r^2} = 1 \tag{5.104}$$

when

$$v^2 = \frac{\pi^2}{3}\frac{\Phi^2}{16} \tag{5.105}$$

or when

$$v = \frac{1}{\sqrt{3}}\frac{\pi}{4}\Phi = 0.45\,\Phi \tag{5.106}$$

It follows that the influenc of horizontal displacement on the vertical stiffness can play a significan role at displacements that are comparable to the bearing diameter.

5.5.1 Postbuckling Behavior

The behavior of a bearing under large displacements can be described by the simple two-spring model if we do not linearize the equations of equilibrium, but retain the exact trigonometric terms. The equations of equilibrium are

$$\begin{aligned} Pv + hF_H \cos\theta &= P_E h\,\theta \\ P\sin\theta + F_H\cos\theta &= P_S\frac{s}{h} \end{aligned} \tag{5.107}$$

(where the small term $F_H s\sin\theta$ has been neglected) with displacement v related to θ and h by Equation (5.88). The second of the equations of equilibrium allows us to solve for s/h in terms of θ, which when substituted into the firs equation gives

$$P\sin\theta + \frac{P\,(F_H\cos\theta + P\sin\theta)}{P_S}\cos\theta + F_H\cos\theta = P_E\theta \tag{5.108}$$

Equations (5.88) and (5.108) can be used in two ways. We can fi F_H and solve the second as a quadratic equation for P in terms of θ, and from the first we can determine the value of v that corresponds to this value of P, thus obtaining a relationship for P as a function of horizontal displacement v. For example, to determine whether or not the postbuckled state is stable, we set $F_H = 0$ and solve for P to obtain

$$P = \frac{P_S}{2\cos\theta}\left[\left(1 + 4\frac{P_E}{P_S}\frac{\theta}{\tan\theta}\right)^{1/2} - 1\right] \tag{5.109}$$

and

$$\frac{v}{h} = \frac{\sin\theta}{2}\left[1 + \left(1 + 4\frac{P_E}{P_S}\frac{\theta}{\tan\theta}\right)^{1/2}\right] \tag{5.110}$$

The dominant term in both equations is P_E/P_S, and to the same level of approximation that gave the critical load as $(P_S/P_E)^{1/2}$, these two equations can be approximated by

$$P = \frac{(P_S P_E)^{1/2}}{\cos\theta}\left(\frac{\theta}{\tan\theta}\right)^{1/2} \tag{5.111}$$

and

$$\frac{v}{h} = \sin\theta\left(\frac{P_E}{P_S}\right)^{1/2}\left(\frac{\theta}{\tan\theta}\right)^{1/2} \tag{5.112}$$

To determine whether the bearing is stable in the postbuckled configuration it is only necessary to determine the sign of $\mathrm{d}P/\mathrm{d}v$. Now

$$\frac{\mathrm{d}P}{\mathrm{d}v} = \frac{\mathrm{d}P}{\mathrm{d}\theta}\frac{\mathrm{d}\theta}{\mathrm{d}v} \tag{5.113}$$

and

$$\begin{aligned}\frac{\mathrm{d}P}{\mathrm{d}\theta} &= (P_E P_S)^{1/2}\left(\frac{\sin(2\theta)}{2\theta}\right)^{1/2}\frac{\sin(2\theta)-2\theta\cos(2\theta)}{(\sin(2\theta))^2}\\ \frac{\mathrm{d}v}{\mathrm{d}\theta} &= h\,(P_E P_S)^{1/2}\left(\frac{2}{\theta\sin(2\theta)}\right)^{1/2}\frac{\sin(2\theta)-2\theta\cos(2\theta)}{4}\end{aligned} \tag{5.114}$$

so that

$$\frac{\mathrm{d}P}{\mathrm{d}v} = \frac{P_S}{h}\frac{\sin(2\theta)-2\theta\cos(2\theta)}{\sin(2\theta)(\sin(2\theta)+2\theta\cos(2\theta))} \tag{5.115}$$

which can be written as

$$\frac{\mathrm{d}P}{\mathrm{d}v} = \frac{P_S}{h}\frac{\tan(2\theta)-2\theta}{\sin(2\theta)(\tan(2\theta)+2\theta)} \tag{5.116}$$

Now, $\tan(2\theta) > 2\theta$ for $0 < \theta < \pi/2$, so that $\mathrm{d}P/\mathrm{d}v > 0$ over this range, therefore, the bearing is stable (i.e., the equilibrium load P increases as v increases).

Another way to interpret the equations is to assume that P is fixed solve the firs equation for F_H as a function of θ, the second equation for v as a function of θ, and then determine a relationship for F_H as a function of v for constant P. First we get

$$F_H = \frac{P_S P_E\,\theta - PP_S\sin\theta - P^2\sin\theta\cos\theta}{\cos\theta\,(P_S + P\cos\theta)} \tag{5.117}$$

and the second equation

$$\frac{v}{h} = \sin\theta\left(\frac{P}{P_S}\cos\theta + 1\right) + \frac{F_H\cos^2\theta}{P_S} \tag{5.118}$$

becomes

$$\frac{v}{h} = \frac{P_E\,\theta\cos\theta + P\cos\theta\sin\theta + P_S\sin\theta}{P_S + P\cos\theta} \tag{5.119}$$

By making the same approximations as before, these become

$$F_H = \frac{P_E P_S\,\theta - P^2\sin\theta\cos\theta}{P\cos^2\theta} \tag{5.120}$$

and

$$\frac{v}{h} = \frac{P_E\,\theta + P\sin\theta}{P} \tag{5.121}$$

Again, we are interested in the sign of the derivative $\mathrm{d}F_H/\mathrm{d}v$, for if it becomes negative, it implies that the bearing could become unstable under a lateral force, F_H, for vertical loads that do not exceed $(P_S P_E)^{1/2}$. Proceeding in the same way as before, we have

$$\frac{\mathrm{d}F_H}{\mathrm{d}\,\theta} = \frac{P_S P_E(\cos\theta + 2\,\theta\sin\theta) - P^2(\cos\theta\cos(2\theta) + \sin\theta\sin(2\theta))}{P\cos^3\theta} \tag{5.122}$$

and

$$\frac{\mathrm{d}v}{\mathrm{d}\theta} = h\frac{P_E + P\cos\theta}{P} \tag{5.123}$$

so that

$$\frac{\mathrm{d}F_H}{\mathrm{d}v} = \frac{P}{h}\frac{P_S P_E(\cos\theta + 2\theta\sin\theta) - P^2\cos\theta}{(P_E + P\cos\theta)\cos^3\theta} \tag{5.124}$$

The denominator of this expression is always positive, and the numerator is positive if

$$\frac{P_S P_E}{P^2} > \frac{\cos\theta}{\cos\theta + 2\theta\sin\theta} = \frac{1}{1 + 2\theta\tan\theta} \tag{5.125}$$

Now, $P_S P_E/P^2$ will always be greater than 1, and because $\theta\tan\theta > 0$ for $0 < \theta < \pi/2$, the right-hand side is always less than one over this range, therefore, the bearing is always stable.

5.5.2 Influenc of Compressive Load on Bearing Damping Properties

The simple two-spring model can also be used to estimate the effect of the vertical load on the damping properties of a bearing. In this case we replace E and G by $E^* = E(1 + i\tan\delta)$ and G by $G^* = G(1 + i\tan\delta)$, where δ is define as the *loss angle* of the material and $\tan\delta$ the *loss factor* of the rubber. The corresponding quantities, P_E^*, P_S^*, are define as

$$\begin{aligned} P_E^* &= P_E(1 + i\tan\delta) \\ P_S^* &= P_S(1 + i\tan\delta) \end{aligned} \tag{5.126}$$

The horizontal stiffness becomes

$$K_H^* = \frac{P_S^*}{h}\frac{P_S^* P_E^* - PP_S^* - P^2}{P_S^* P_E^* + PP_S^* + P_S^{*2}} \tag{5.127}$$

The corresponding complex rotations, θ^*, and shear deformation, s^*, are given by

$$\begin{aligned}\theta^* &= F_H \frac{P_S^* + P}{P_S^* P_E^* - P P_S^* - P^2} \\ \frac{s^*}{h} &= F_H \frac{P_E^*}{P_S^* P_E^* - P P_S^* - P^2}\end{aligned} \tag{5.128}$$

from which we see that the phase angle for θ^* and s^* differs if $\delta \neq 0$.

The dynamic shear stiffness of the bearing, K_D, is define by

$$K_D = \left| K_H^* \right| \tag{5.129}$$

and the *loss factor*, $\tan\eta$, for the *bearing*, as opposed to that for the material (e.g., $\tan\delta$), is define by

$$\tan\eta = \frac{\mathrm{Im}(K_H^*)}{\mathrm{Re}\left(K_H^*\right)} \tag{5.130}$$

The results for a number of cases can be evaluated easily. For example, if $P_E \gg GA_S > P$, which define the case when the entire deformation is shear deformation, the loss factor for the bearing becomes

$$\tan\eta = \tan\delta \tag{5.131}$$

Thus, the loss factor is unaffected by compressive load, and no amplificatio of the damping occurs. On the other hand, if $P_S = GA_S \gg P_E > P$, which is the situation that leads to flexura deformation only, the loss factor of the bearing becomes

$$\tan\eta = \frac{\tan\delta}{1 - P/P_E} \tag{5.132}$$

In this case the buckling load is P_E; therefore, although an amplificatio of the damping occurs, it is solely due to the reduction in the stiffness, i.e., $\mathrm{Re}(K_H^*)$, as a result of the axial load. There is no increase in the energy dissipated over a complete cycle.

For the typical bearing where $P_E \gg GA_S$ but $P > GA_S$, the result for the loss factor becomes

$$\tan\eta = \tan\delta \frac{1 + \tan^2\delta + P^2/P_{crit}^2}{1 + \tan^2\delta - P^2/P_{crit}^2} \tag{5.133}$$

where $P_{crit} = \sqrt{P_E P_S}$. The term in the denominator comes from the reduction in the stiffness, but the term in the numerator shows that the total energy dissipated in a cycle increases. This increase in the energy dissipation in a cycle is due to the compression load increasing the phase difference between the force, F_H, and displacement, v, through its effects on θ and s. It is also significan that the dynamic stiffness, K_D, does not vanish

at the static buckling load, $P_{crit} = \sqrt{P_E P_S}$, but at $P_{crit}(1 + \tan^2 \delta)^{1/2}$; however, since $\tan \delta$ is generally no more than about 0.20–0.30; in practice the increase can be neglected.

The accuracy of these predictions of the enhancement of damping by the axial load was verifie by a testing program on reduced-scale natural rubber bearings conducted at the Earthquake Engineering Research Center (EERC), University of California, Berkeley. The results, given in Koh and Kelly (1987) verify that the simple two-spring model can be used to accurately predict the downward movement resulting from horizontal displacement and the damping and dynamic stiffness as influence by the axial load.

5.6 Rollout Stability

An isolation bearing, even if inherently stable under its design load, can experience another form of instability if it is connected to the foundation below and the superstructure above through shear keys that cannot sustain tensile loads. Initially designers felt that rubber should not be subjected to tension, therefore, early designs of rubber bearings used dowelled shear connections rather than bolted connections. Dowelled bearings, however, can experience an unstable mode of behavior – called *rollout* – that is associated with lateral displacement and which puts a limit on the maximum displacement that the bearing can sustain. The bearing is unstable in the sense that beyond this displacement, the force–displacement curve has a decreasing slope. Because the bearing cannot sustain tension, the movement at the top and bottom of the bearing is produced by a change in the line of action of the resultant of the vertical load, as shown in Figure 5.7(a). The limit of this migration of the resultant is reached when the resultant is at the edge of the bearing, and equilibrium of the moment generated by the lateral force, F_H, with that generated by the vertical load, P, gives

$$P\,(b - \delta_{\max}) = h F_H \tag{5.134}$$

where b is the bearing width (either a if square or Φ if circular). The relationship between the lateral force, F_H, and the displacement, δ, is shown in Figure 5.7(b).

If we take $F_H = K_H \delta$, then this gives

$$\frac{\delta_{\max}}{b} = \frac{P}{P + K_H h} \tag{5.135}$$

If we take K_H as GA/t_r and the pressure, $p = P/A$, this becomes

$$\frac{\delta_{\max}}{b} = \frac{1}{1 + \dfrac{G}{p}\dfrac{h}{t_r}} \tag{5.136}$$

In typical bearings where $G \approx 0.828$ MPa (120 psi), $p \approx 6.90$ MPa (1000 psi), and $h = 1.2t_r$, for example,

$$\frac{\delta_{\max}}{b} = 0.88$$

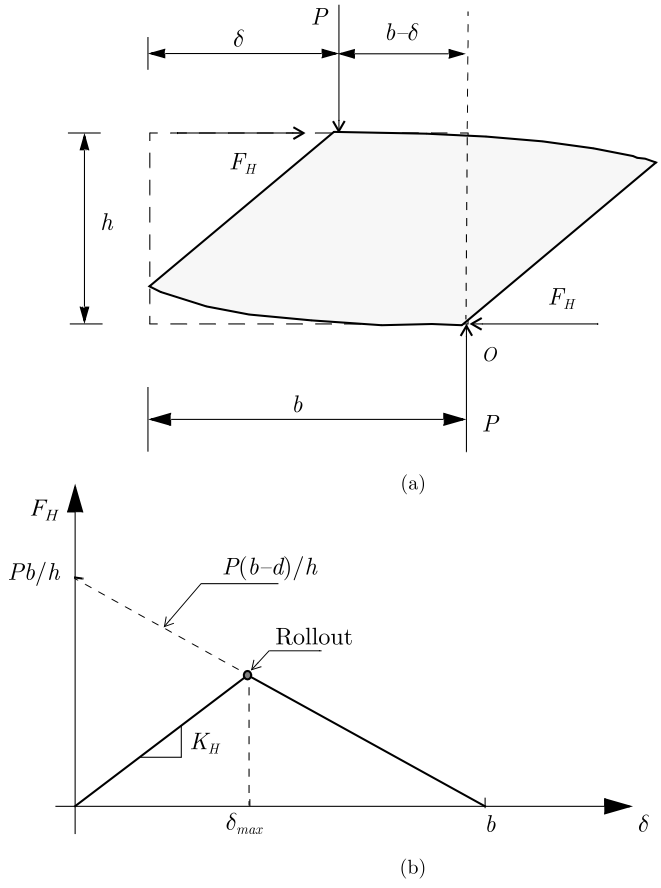

Figure 5.7 Mechanics of rollout for dowelled bearings

Thus, if the lateral displacement is less than about 88% of the least plan dimension of a dowelled bearing, it can be expected to be stable against rollout. Conversely, if a bearing is bolted into place, no significan tension will develop in the bearing until the displacement exceeds this value. Tests conducted at the EERC, and in Japan demonstrate that rubber is capable of sustaining quite high tensile stresses, and it has now become more common to use bolted rather than dowelled connections for isolation bearings. Additional research, however, needs to be done as the failure process in tension is not yet well understood; in bearings it can involve cavitation in the rubber (Gent and Lindley 1959a) or loss of bond. Although some tests (Kelly 1991) have shown that there have been cases where the displacement has exceeded the bearing diameter, it is certainly good design practice to limit the displacement to the rollout value, even when bolted connections are used.

5.7 Effect of Rubber Compressibility on Buckling

In the previous chapter, it was shown that bulk compressibility in the rubber had a surprisingly large effect on both the compression stiffness and bending stiffness of a bearing even for shape factors as low as 10. The impression given by Equation (5.32) is that it is possible to improve the stability of a bearing with a certain diameter and

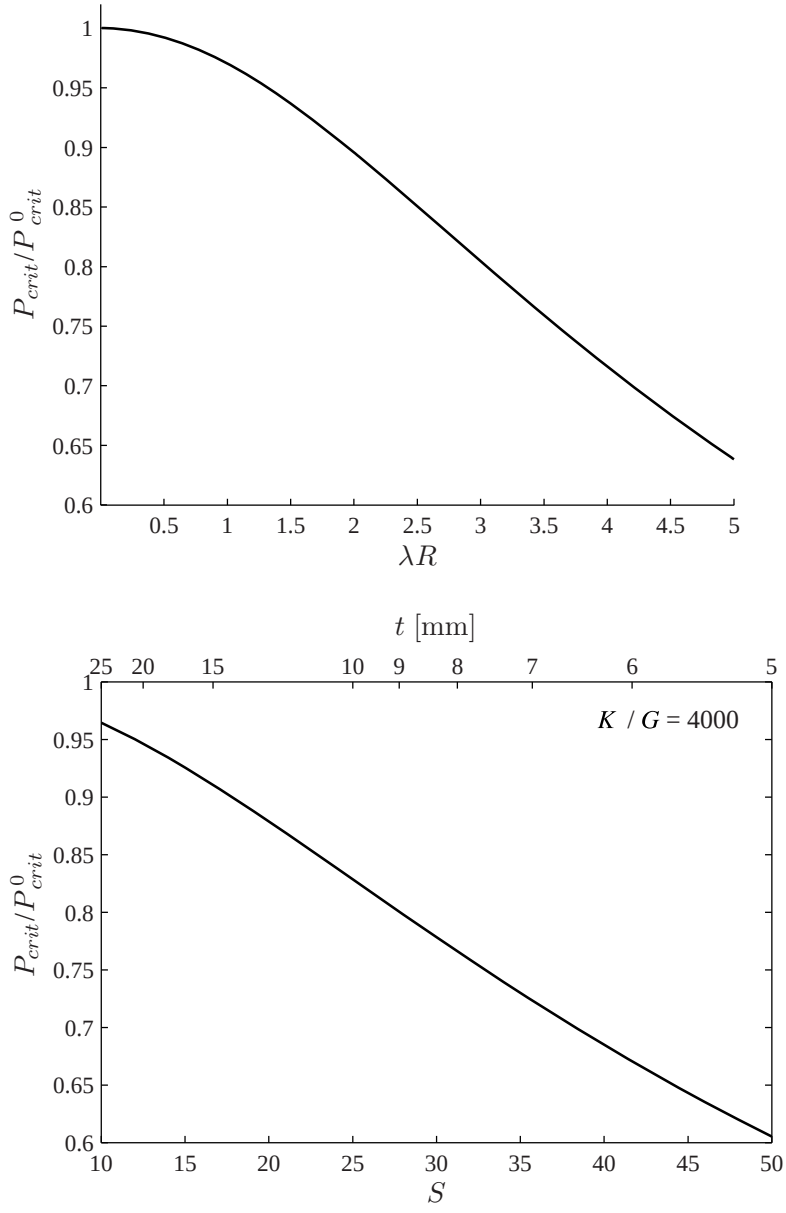

Figure 5.8 Effect of compressibility on buckling load

thickness of rubber by the simple process of increasing the shape factor, i.e., increasing the number of layers and reducing their thickness. However, because of the effect of bulk compressibility on the effective stiffness, the improvement is limited. We assume that the buckling load is given by the solution in Equation (5.26) but use

$$\begin{aligned} P_S &= GA\frac{h}{t_r} \\ P_E &= \frac{\pi^2}{h^2}(EI)_{eff}\frac{h}{t_r} \end{aligned} \tag{5.137}$$

and substitute for $(EI)_{eff}$ the expression

$$(EI)_{eff} = \frac{K\pi R^4}{4}\left(1 - \frac{4\,\mathrm{I}_2(\lambda R)}{\lambda R \mathrm{I}_1(\lambda R)}\right) \tag{5.138}$$

where $\lambda R = \sqrt{48\,GS^2/K}$. The resulting value of the critical load, P_{crit}, can be reduced to an expression that depends only on the quantity λR by dividing by the result for the critical load when the material is taken as incompressible, P^0_{crit}, leading to

$$\left(\frac{P_{crit}}{P^0_{crit}}\right)^2 = \frac{24}{\lambda^2 R^2}\left(1 - \frac{4\,\mathrm{I}_2(\lambda R)}{\lambda R \mathrm{I}_1(\lambda R)}\right) \tag{5.139}$$

or, in term of the shape factor, shear and bulk modulus,

$$\left(\frac{P_{crit}}{P^0_{crit}}\right)^2 = \frac{1}{\dfrac{2\,GS^2}{K}}\left(1 - \frac{4\,\mathrm{I}_2\left(\sqrt{\dfrac{48\,G}{K}}S\right)}{\sqrt{\dfrac{48\,G}{K}}S\mathrm{I}_1\left(\sqrt{\dfrac{48\,G}{K}}S\right)}\right) \tag{5.140}$$

The graphs in Figure 5.8 show that there is a significan reduction of the buckling load when compressibility is taken into account. They also indicate that the effort to get a higher bucking load by increasing the shape factor is self-defeating. While the incompressible analysis suggest that the bucking load will increase linearly with increasing shape factor, this result shows that this is not the case. Most bearing designs at present use very large shape factors in the range of 30–40 in an attempt to get a larger buckling load, but to no avail.

6

Buckling of Multilayer Rubber Isolators in Tension

6.1 Introduction

We recall from the last chapter that the equation for the buckling of the isolator in compression is

$$P^2 + P_S P - P_S P_E = 0 \tag{6.1}$$

where $P_S = GA_S$ and $P_E = \pi^2 E_S I/h^2$. This equation has two solutions, one of which is positive and the other negative. These solutions are given by

$$P_{crit} = \frac{-P_S \pm \sqrt{P_S^2 + 4P_S P_E}}{2}$$

The compression solution has been treated in detail in the last chapter. The negative solution

$$P_{crit} = \frac{-P_S - \sqrt{P_S^2 + 4P_S P_E}}{2} \tag{6.2}$$

implies that there exists a tensile buckling load, and the question now is the significanc of that solution. The tensile critical load, which, if the isolator has a shape factor larger

The material in Sections 6.2 and 6.3 firs appeared in the article by Kelly, J. M. (2003). "Tension Buckling in Multilayer Elastomeric Bearings." *Journal of Engineering Mechanics* (ASCE), **129**(12), 1363–1368. DOI 10.1061/(ASCE)0733-9399(2003)129:12(1363). Reproduced with permission from ASCE.

Mechanics of Rubber Bearings for Seismic and Vibration Isolation, First Edition. James M. Kelly and Dimitrios A. Konstantinidis.

than say 5, as shown in the previous chapter in Equation (5.26), is the negative of the compression critical load. We can then defin a tension critical load by

$$T_{crit} = \sqrt{P_S P_E} \tag{6.3}$$

The unexpected implication of this result is that there is a tensile buckling load for this type of rubber component that has the same numerical value as the compression buckling load. In addition, the quantities α and β when P is replaced by $-T$ become

$$\alpha^2 = \frac{T(T - GA_S)}{E I_S GA_S} \tag{6.4}$$

$$\beta = -\frac{GA_S}{T - GA_S} \tag{6.5}$$

so that if $T > GA_S$, the buckled shape in tension is the same solution as in the compression case. Since the value of β is now negative, the rotation $\psi(x)$ (Equation 5.20) is reversed, and the central layers are rotated in the direction that facilitates the upward movement of the top of the isolation through a shear deformation. Of course this buckling load could not be achieved in practice since the rubber will have cavitated before the bearing buckles, but the tensile buckling load and buckled shape are opposites of the compression case due to the fact that the deformation is entirely shear – and shear is intrinsically symmetric.

There are many examples of strange systems that buckle in tension, but these are entirely pathological in that the tension forces are always transferred to compression elements that produce the instability. This is not the case here. The buckling process is really tensile. The linear elastic model that leads to both compression and tension buckling is an extremely simple one, and it might be argued that the tensile buckling may be an artifact of the model itself and not of the isolator. For this reason it was decided to verify the results of the simple model by numerical simulation using a finit element model of a multilayer rubber bearing to show that the prediction of tensile buckling by the simple linear elastic theory is in fact accurate and not an artifact of the way the model was set up. This numerical experiment, done in two dimensions to reduce the size of the computation, simulates the behavior of a bearing in the shape of a long strip, and it shows clearly that tensile bucking is a real possibility and not an artifact of the model. The essential point is that the mechanics of the isolator in tension are the mirror image of those of the isolator in compression. In particular when the isolator is in compression below the buckling load, but laterally displaced, the layers in the center experience rotations that give the vertical load a component along the layer, causing a shear deformation. In tension the layers in the center experience rotations in the opposite direction, giving a shear deformation due to the tensile force that permits the top of the isolator to move upwards by a much larger displacement than that which could be sustained in pure tension with no lateral displacement.

6.2 Influenc of a Tensile Vertical Load on the Horizontal Stiffness

If the load carried by a bearing is comparable to the buckling load, then the simple formula for horizontal stiffness, $K_H = GA/t_r = GA_S/h$, may need to be modified The analysis that led to the buckling load can be used to determine the effective horizontal stiffness in the presence of axial load. Consider a horizontal force, F_H, at the top of a bearing. When the resulting displacement at the top, $v(h) = \delta_h$, is computed, then K_H is given by

$$K_H = \frac{F_H}{v(h)} = \frac{F_H}{\delta_h} \tag{6.6}$$

The basic equations, Equations (5.42a) and (5.42b), are solved using the boundary conditions

$$v(0) = 0,\ \psi(0) = 0,\ \psi(h) = 0,\ H_0 = -F_H \tag{6.7}$$

Thus

$$v(x) = A\ \cos(\alpha x) + B\sin(\alpha x) + \frac{M_0}{P} - \frac{F_H}{P}x \tag{6.8a}$$

and

$$\psi(x) = \alpha\beta\ B\cos\ (\alpha x) - \alpha\beta A\sin(\alpha x) - \frac{F_H}{P} \tag{6.8b}$$

Using the boundary conditions, we have

$$A = \frac{F_H}{P}(\cos(\alpha h) - 1)\frac{1}{\alpha\beta\sin(\alpha h)} = -\frac{M_0}{P} \tag{6.9}$$

and

$$B = \frac{F_H}{\alpha\beta P} \tag{6.10}$$

When these are substituted back into Equation (6.8a) we obtain

$$v(x) = \frac{F_H}{\alpha\beta P}\left[\frac{1-\cos(\alpha h)}{\sin(\alpha h)}(1-\cos(\alpha x)) + \sin(\alpha x) - \alpha\beta x\right] \tag{6.11a}$$

$$\psi(x) = \frac{F_H}{P}\left[\frac{1-\cos(\alpha h)}{\sin(\alpha h)}\sin(\alpha x) - (1-\cos(\alpha x))\right] \tag{6.11b}$$

The horizontal displacement at $x = h$ is given by

$$\delta_h = v(h) = \frac{F_H}{\alpha\beta P}\left(2\tan\left(\frac{\alpha h}{2}\right) - \beta\alpha h\right) \tag{6.12}$$

and the rotation at $x = h/2$ is

$$\psi\left(\frac{h}{2}\right) = \frac{F_H}{P}\left(\frac{1-\cos\left(\frac{\alpha h}{2}\right)}{\cos\left(\frac{\alpha h}{2}\right)}\right) \tag{6.13}$$

The horizontal stiffness K_H is given by Equation (6.6)

$$K_H = \frac{F_H}{\delta_h} = \frac{\alpha\beta P}{2\ \tan\left(\frac{\alpha h}{2}\right) - \beta\alpha h} \tag{6.14}$$

When P is replaced by $-T$, and $T > GA_S$, both β and P change sign in Equation (6.14), and the stiffness is still positive, but the rotation at the center of the isolator changes sign, facilitating the upward displacement of the top.

When $T < GA_S$, the solution for this case will involve hyperbolic instead of trigonometric functions, and, when $T = GA_S$, the firs terms in the basic Equations (5.10a) and (5.10b) become indeterminate. The solutions for $v(x)$ and $\psi(x)$ for this case are

$$v(x) = \frac{F_H}{GA_S}x \tag{6.15a}$$

$$\psi(x) = 0 \tag{6.15b}$$

Thus the deformation is one of pure shear, and it is easy to show from Equation (5.60) that there is no change in height in the bearing (Kelly 2003).

The result for the influenc of the vertical load on the horizontal stiffness does not give physical insight into the effect, but if we recall that the value of GA_S is very small as compared with P_E and P, we can approximate αh and β by $\alpha h = \pi p$ (where $p = P/P_{crit}$) and $\beta \approx GA_S/P$, which is much less than 1, giving

$$K_H = \frac{GA_S}{h}\frac{\pi p}{2\ \tan(\pi p)} \tag{6.16}$$

which leads to $K_H = GA_S/h = GA/t_r$ as $p \to 0$, and $K_H \to 0$ as $p \to 1$. When P is replaced by $-T$ and p by $-t$, where $t = T/\sqrt{P_E P_S}$, we get the same result, showing that both P and T affect the stiffness in a symmetric way.

6.3 Vertical Displacement under Lateral Load

The previous result Equation (5.60) can be used to calculate the displacement of the top of the bearing when it is loaded by a lateral load F_H and a tension load $T > GA_S$.

The starting point for the calculation is the solution for $v(x)$ and $\psi(x)$, namely Equations (6.11a) and (6.11b). Evaluating Equation (6.11a) at $x = h$ gives the horizontal displacement

$$\delta_h = v(h) = \frac{F_H}{\alpha\beta P}\left(2\frac{1-\cos(\alpha h)}{\sin(\alpha h)} - \beta\alpha h\right) \tag{6.17}$$

Differentiating (6.11a), we obtain

$$v'(x) = \frac{F_H}{\beta P}\left(\cos(\alpha x) + \frac{1-\cos(\alpha h)}{\sin(\alpha h)}\sin(\alpha x) - \beta\right) \tag{6.18}$$

and using Equation (6.11b), we form the product

$$\begin{aligned} 2\psi v' - \psi^2 = \frac{F_H^2}{\beta P^2}\{&-2[\beta\cos\alpha h\ \cos^2\alpha x - \beta\cos\alpha h + \cos\alpha h - 2\cos\alpha h\ \cos^2\alpha x \\ &+ \cos\alpha h\ \cos\alpha x - 1 + \sin\alpha h\ \sin\alpha x - 2\sin\alpha h\ \cos\alpha x\ \sin\alpha x + \beta\cos\alpha x\ \sin\alpha x\sin\alpha h \\ &+ \cos\alpha x]/[\cos\alpha h + 1]\} \end{aligned}$$

Integrating this expression from $x = 0$ to $x = h$ gives

$$\delta_v = \frac{1}{2}\int_0^h (2\psi v' - \psi^2)\,\mathrm{d}x = \frac{1}{2}\frac{F_H^2}{\beta \mathrm{P}^2}\left(\frac{\alpha h\beta\cos(\alpha \mathrm{h}) - 2\sin(\alpha \mathrm{h}) + 2\alpha h - \beta\sin(\alpha h)}{\alpha(\cos(\alpha h) + 1)}\right) \tag{6.19}$$

The terms F_H and P can be eliminated by dividing this by the square of δ_h from Equation (6.17), giving

$$\delta_v = \frac{\beta\alpha h}{2}\left(\frac{\beta\alpha h\ \cos(\alpha h) - 2\sin(\alpha h) + 2\alpha h - \beta\sin(\alpha h)}{-4\ \cos(\alpha h) + \beta^2\alpha^2h^2\ \cos(\alpha h) + 4 + \beta^2\alpha^2h^2 - 4\beta\alpha h\ \sin(\alpha h)}\right)\frac{\delta_h^2}{h} \tag{6.20}$$

In Equation (6.20), the expression in the brackets is a function of the two dimensionless quantities αh and β, both of which depend on the vertical load, P or T. The result shows that when the bearing parameters P_S and P_E are specified the vertical displacement is quadratic in the lateral displacement δ_h and can easily be computed for any value of axial load, compressive or tensile.

If we use the approximations made in the earlier section neglecting GA_S as compared to P, giving $\alpha h = \pi p$ and $\beta \approx 0$, this reduces to

$$\delta_v = \frac{\pi GA_S}{4P_{crit}}\left(\frac{\pi p - \sin(\pi p)}{1-\cos(\pi p)}\right)\frac{\delta_h^2}{h} = \frac{\pi GA_S}{4P_{crit}}f(\pi p)\frac{\delta_h^2}{h} \tag{6.21}$$

The function $f(x) = (x - \sin x)/(1 - \cos x)$ varies from 0 when $x = 0$ to $\pi/2$ when $x = \pi$ and increases monotonically over the range $0 \leq x \leq \pi$. When x is replaced by $-x$, it is antisymmetric, i.e., $f(-x) = -f(x)$. The derivative

$$f'(x) = \frac{2(1 - \cos x) - x \sin x}{(1 - \cos x)^2} \tag{6.22}$$

is symmetric and varies from 1/3 to 1 as x varies from 0 to π and monotonically increases over this range, and at say $x = \pi/2$, which corresponds to $p = 1/2$, it has the value 0.429.

The vertical stiffness of the isolator in the undeformed position is given by

$$K_v^0 = \frac{E_c A_S}{h} \tag{6.23}$$

where E_c is the compression modulus. For a circular bearing, $E_c = 6\ GS^2$. The vertical stiffness when sheared through a displacement δ_h will be

$$K_v = \left(\frac{\mathrm{d}\delta_v^t}{\mathrm{d}P}\right)^{-1} \tag{6.24}$$

where

$$\delta_v^t = \frac{P}{K_v^0} + \delta_v = \frac{h}{E_c A_S} P + \delta_v \tag{6.25}$$

Now

$$\frac{\mathrm{d}\delta_v}{\mathrm{d}P} = \frac{\mathrm{d}\delta_v}{\mathrm{d}x}\frac{\mathrm{d}x}{\mathrm{d}P} = \frac{\pi^2}{4}\frac{GA_S}{P_{crit}^2} f'(\pi p)\frac{\delta_h^2}{h} \tag{6.26}$$

giving

$$K_v = K_v^0 \frac{1}{1 + \dfrac{\pi^2}{4}\dfrac{GA_S E_c A_S}{P_{crit}^2} f'(\pi p)\dfrac{\delta_h^2}{h^2}} \tag{6.27}$$

Since $P_{crit}^2 = GA_S EI_S(\pi^2/h^2)$, this becomes

$$K_v = K_v^0 \frac{1}{1 + \dfrac{3}{4} f'(\pi p)\dfrac{\delta_h^2}{r^2}} \tag{6.28}$$

where $r^2 = I/A$. For a circular bearing of diameter Φ, $r^2 = \Phi^2/16$ leading to

$$K_v = K_v^0 \frac{1}{1 + 12 f'(\pi p) \dfrac{\delta_h^2}{\Phi^2}} \tag{6.29}$$

In many cases, the displacement that is calculated from code requirements at extreme seismic loads can be a significan fraction of the diameter so that the vertical stiffness in both compression and tension is considerably reduced by the lateral displacement. For example, if $\delta_h = 0.5\Phi$ and $p = P/P_{crit} = 0.5$, then Equation (6.29) gives $K_v = 0.437 K_v^0$. While the bearings are normally in compression, the code requirements for base-isolated tall buildings in near-fault locations can lead to situations where peripheral bearings in the isolation system can be required to take some amount of tension. This tension is caused by global overturning of the building produced by the lateral inertial force at the center of the mass of the building. The maximum inertial force and the resulting maximum overturning moment occur at the same time as the maximum lateral displacement of the isolators, which at firs sight would seem to be a critical situation. It is well known that elastomers, such as natural rubber (polyisoprene) or neoprene (polycloroprene), will cavitate at a negative pressure of around $3G$ (Gent 1990). Since the value of G is in the range 0.5 to 1.0 MPa (75 to 150 psi), and the state of internal stress in a thin layer of a multilayer isolator is virtually hydrostatic, the tension stress to produce cavitation is quite low. The tensile strain is also extremely small, since the stiffness of an isolator in tension before cavitation occurs is the same as that in compression. The effective compression modulus E_c of a circular pad of rubber is $6\,GS^2$, where S is the shape factor of an individual layer of the isolator, which can be in the range of 10 to 20, so that the tensile strain ε_t at the onset of cavitation will be $\varepsilon_t = 1/(2S^2)$, and the corresponding upward displacement will be of the order of a few millimeters or less.

So concerned are design engineers that an isolator not experience tension due to uplift, that many have resorted to a design approach called "loose bolts." This certainly solves the tension problem, but raises other questions such as the reliability of the bolts if uplift should occur, since the bolts will have to transfer the shear load to the isolator while acting as cantilever elements. Other strategies have been tried, but each approach to eliminating tension has its own disadvantages.

All current seismic isolation codes require that the prototype tests include an uplift test if uplift is predicted by analysis. In two seismic isolation projects, isolators were displaced laterally to very large displacements, and then the top of the isolator was jacked up by, in one case, 12.5 mm (0.5 inch) and, in the other, by 19.0 mm (0.75 inch). In neither case did the test isolators fail, but clearly the tensile strain greatly exceeds the strain at cavitation. The value of the buckling theory is to explain how the isolators can survive this tensile loading. The essential point is that the mechanics of the isolator in tension are the mirror image of those for the isolator in compression. In particular when the isolator is in compression below the buckling load but laterally displaced, the layers in the center experience a rotation which gives the vertical load a component along the layer and induces a shear deformation. In tension, the layers in the center experience a

rotation in the opposite direction, which allows a shear deformation caused by the tensile force and permits the top of the isolator to move upwards by a much larger displacement than that which could be sustained in pure tension with no lateral displacement. Thus the simultaneous occurrence of tension and shear allows the isolator to avoid the damage of cavitation. The rubber can sustain only small strains in the state of triaxial stress generated by pure tension on a multilayer isolator with a large shape factor, but can sustain shear strains on the order of 500 or 600%. Thus the simultaneous occurrence of tension and shear allows the isolator to avoid the damaging effects of cavitation.

6.4 Numerical Modelling of Buckling in Tension

6.4.1 Modelling Details

In order to verify that the tension buckling predicted by the simple analytical theory is real, the general purpose finit element ABAQUS (HKS 2001) was used to model a steel-reinforced multilayer bearing and to study its buckling behavior in both tension and compression. The complete details of the procedure are given in (Kelly and Takhirov 2004). Five finit element models of a bearing were created. These numerical models all have the same width, the same total rubber thickness, and all the steel shims have the same thickness. The only difference between the models is the shape factor of the rubber layers. The total thickness of rubber is the same in each model, but the thickness of the rubber layer varies from model to model. The correspondence between the model number and the layer thickness is given in Table 6.1.

The bearings are visualized as being long strip isolators, as shown in Figure 6.1, and the finit element analysis is restricted to plane strain. Thus the numerical solutions to be described in the next sections are based on a two-dimensional analysis of an isolator with infinit length.

The y-axis of the coordinate system is a vertical axis that extends across the steel shims and rubber layers, and the horizontal axis x corresponds to the lateral direction of the bearing, as shown in Figure 6.1. Generally steel-reinforced rubber bearings have a hole in the middle of the steel plates and a rubber cover on the traction-free sides of the

Table 6.1 Finite element models with various shape factors

Model name	Steel shim thickness [mm]	Total rubber thickness [mm]	Width [mm]	Rubber layer thickness [mm]	Shape factor
Model 1	2.60	80.01	160.02	5.72	14
Model 2	2.60	80.01	160.02	8.00	10
Model 3	2.60	80.01	160.02	11.43	7
Model 4	2.60	80.01	160.02	16.00	5
Model 5	2.60	80.01	160.02	26.67	3

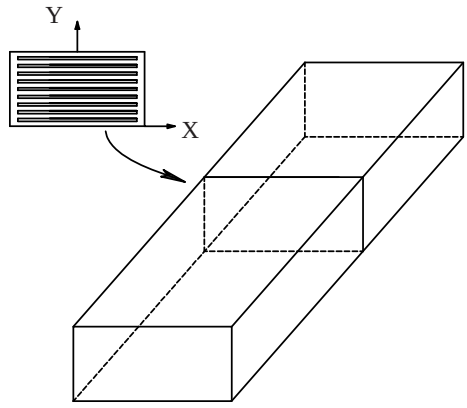

Figure 6.1 Geometry and coordinate axes of finit element simulation models

bearing. In order to create a model close to the theoretical one given earlier, the hole in the middle and the rubber cover are not included in the consideration.

The end-plates of the bearing are assumed to be undeformable; therefore, in the finit element model, the top rubber layer of the bearing is connected to a rigid surface with the reference point in the middle; the vertical load is applied to this reference point. The bottom surface of the bearing is fixed The two vertical sides of the bearing model are traction free. The top surface is restrained against rotation about the z (out-of-plane) axis, but free to move horizontally.

Linearly elastic material properties are assumed for the steel plates with Young's modulus and Poisson's ratio equal to 200 GPa (29 000 ksi) and 0.30, respectively. Rubber materials have very little compressibility compared with their shear flexibilit , and these materials are usually modeled by a hyperelastic material model. ABAQUS (HKS 2001) has a special family of "hybrid" elements to model the fully incompressible behavior seen in a rubber material. The following assumptions are made in modelling a rubber material: (1) the material is elastic, (2) the material is isotropic, (3) the material is incompressible or almost incompressible, and (4) the simulation includes nonlinear geometric effects.

Hyperelastic materials are described in terms of a strain energy potential, U, which define the strain energy stored in the material per unit of reference volume (volume in the initial configuration as a function of the strain at that point in the material. The rubber is modelled as a polynomial hyperelastic material of the second order. In this case, the strain energy potential has the following form:

$$U = \frac{1}{D_1}(J^{el} - 1)^2 + \sum_{i+j=1}^{2} C_{ij}(I_1 - 3)^i (I_2 - 3)^j \tag{6.30}$$

where C_{ij} and D_1 are the material parameters, I_1 and I_2 are the firs and the second deviatoric strain invariants, respectively, and J^{el} is the elastic volume ratio.

Table 6.2 Material parameters for the two rubber models

Rubber model	C_{10} [kPa]	C_{01} [kPa]	C_{20} [kPa]	C_{11} [kPa]	C_{02} [kPa]	D_1 [kPa^{-1}]
Polynomial	193.4	−0.1	−0.8	0.2	0	0
Neo-Hookean	345.0	0	0	0	0	9.7×10^{-7}

Two rubber models are included in the consideration: a fully incompressible model, called here *Polynomial*, and an almost incompressible model, called here *Neo-Hookean* (Gent 2001). The material parameters of the rubber can be expressed in terms of initial shear modulus, G, and initial bulk modulus, K, in the following form:

$$\begin{aligned} G &= 2(C_{10} + C_{10}) \\ K &= 2/D_1 \end{aligned} \tag{6.31}$$

The values of the material parameters for both rubber models are presented in Table 6.2. Since D_1 is not equal to zero for the Neo-Hookean model, this model allows some compressibility in the rubber material.

A supplemental study on the properties of the rubber models was conducted with ABAQUS on a rubber cylinder and a rubber layer. The cylinder was used to study the material model in compression and tension, while the layer, representing one single layer of the rubber locked between two rigid horizontal surfaces, was used to study the material model in shear with no vertical load. While both rubber materials are linearly elastic up to about 250% strain in shear, they exhibit nonlinearity in tension or compression at lower strains, as shown in Figure 6.2(a) and (b).

6.4.2 Critical Buckling Load in Compression and Tension

The model was studied by a classical buckling analysis scheme available in ABAQUS. In this approach, the buckling mode of each bearing model is determined. Very small imperfections (about 1% of the steel layer thickness) are introduced in the model, and they are based on the buckling mode obtained in the buckling mode analysis. The postbuckling behavior is followed up to about 30% shear deformation.

The buckling analysis of the numerical bearing models reveals the following results. All models have significan horizontal drift caused by a large vertical load. The curves of the compression vertical load versus horizontal drift for all numerical models are shown in Figure 6.3. The critical buckling load increases with the increase in the shape factor. All plots show similar behavior with a significantl changing part before 3% deformation, and after that they become almost fla when the bearing is buckling. Figure 6.4 presents the corresponding curves of buckling in tension. The critical load is again dependent on the shape factor and increases with increasing shape factor. The buckling in tension is more sudden, so the point at which buckling starts moves very close to the vertical axis, and the shear when the buckling starts in tension can be as low as 0.2%, as it is observed

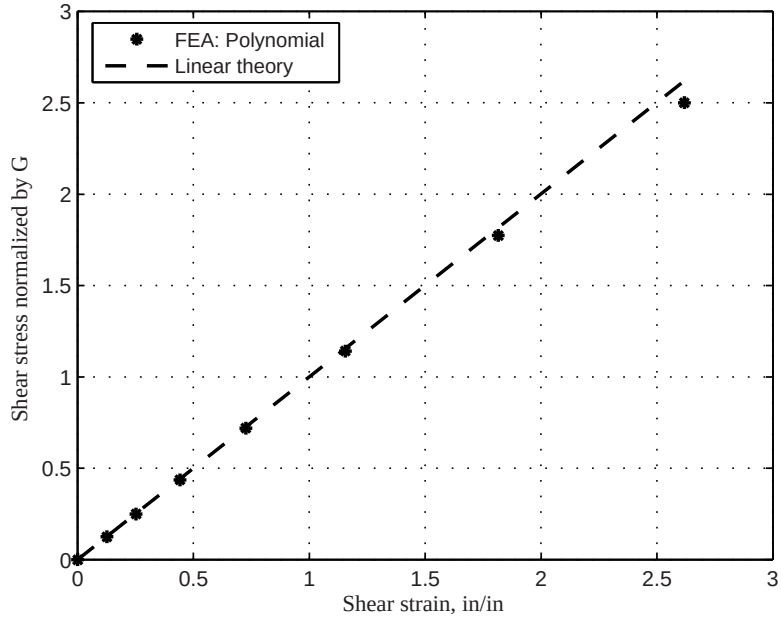

(a)

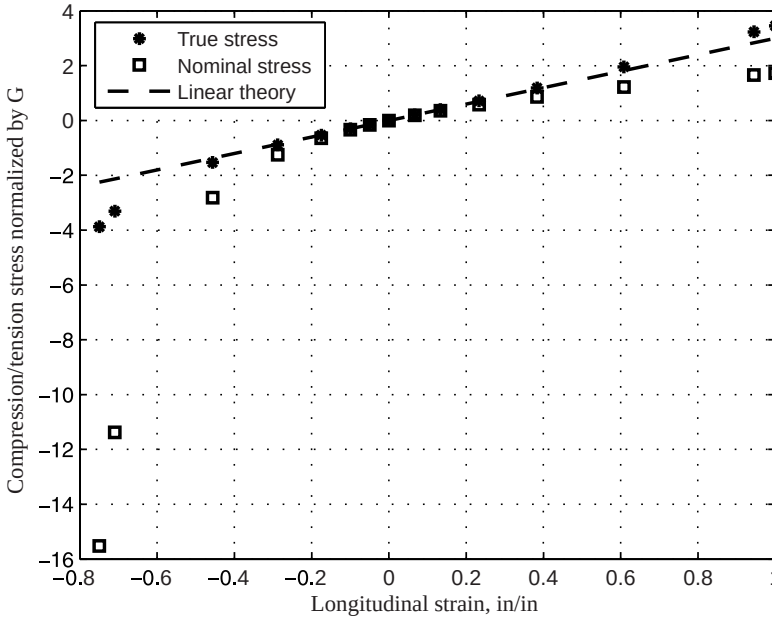

(b)

Figure 6.2 Behavior of the Polynomial rubber material model in: (a) shear; (b) compression/tension

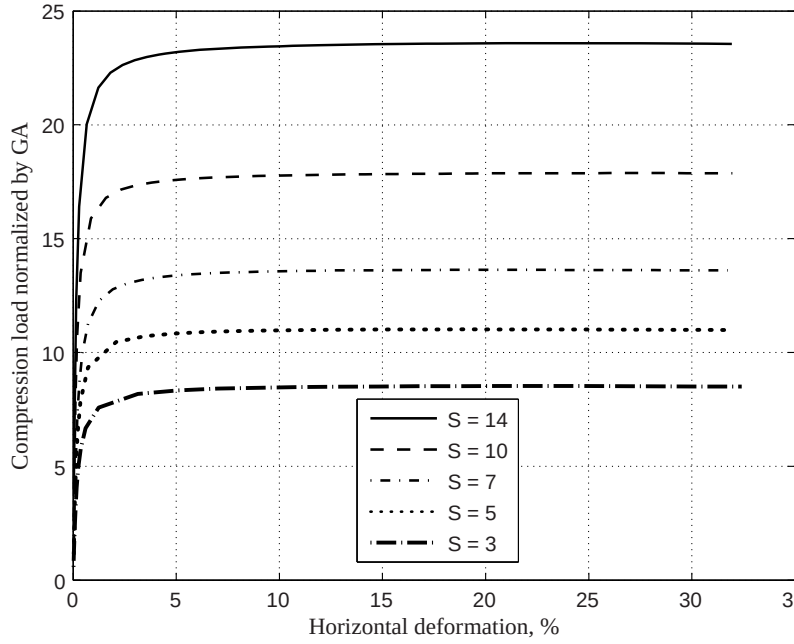

Figure 6.3 Buckling behavior in compression

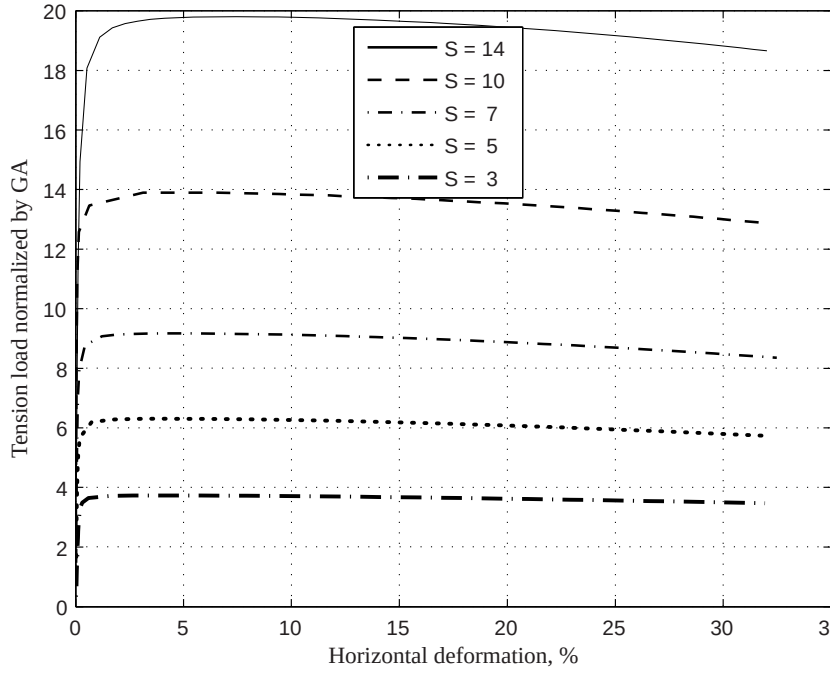

Figure 6.4 Buckling behavior in tension

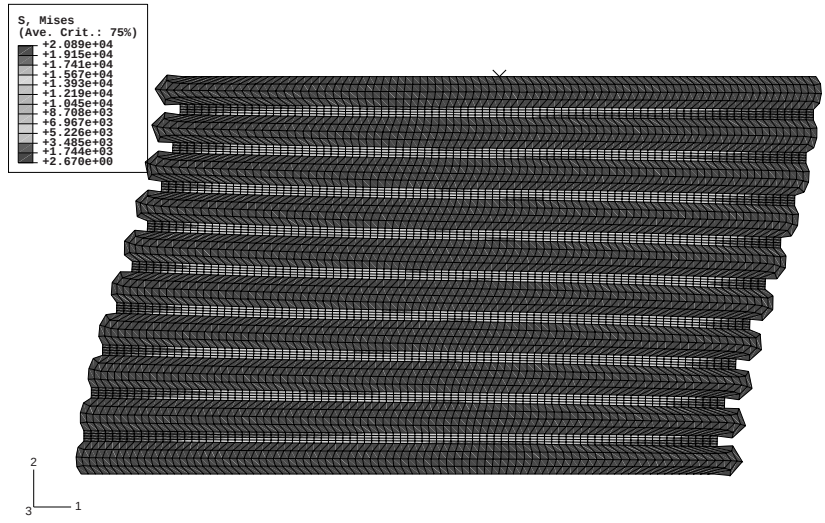

Figure 6.5 Buckled shape and von Mises stresses for Model 2 (compression)

for Model 5 with the smallest shape factor. Increase in the shape factor moves this point closer to the 3% critical strain obtained for the compression buckling.

Figures 6.5 to 6.8 show deformed shapes of two numerical models in compression and tension simulations.

The numerical results on buckling behavior of the bearing have satisfactory correlation with the theoretical solutions. The theoretical study and the finit element analyses lead

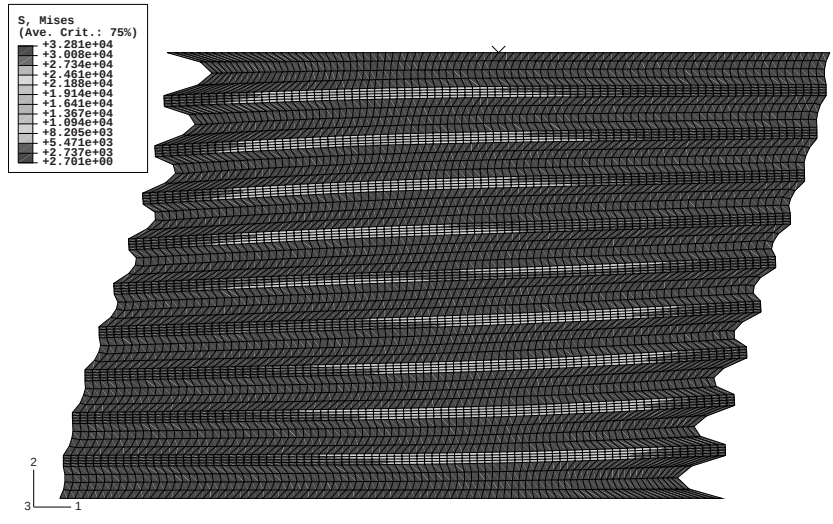

Figure 6.6 Buckled shape and von Mises stresses for Model 2 (tension)

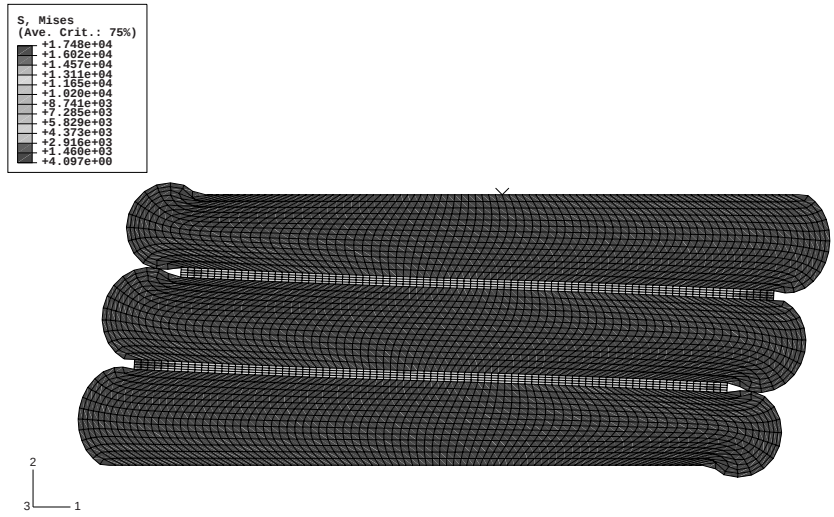

Figure 6.7 Buckled shape and von Mises stresses for Model 5 (compression)

to the following conclusions. The critical buckling load increases with increasing shape factor, and it has an almost linear behavior relative to shape factor, as predicted by the theory. The numerical compression buckling load is almost always higher than the theoretically estimated one for all bearings. The numerical models have different postbuckling behaviors in compression and tension. In compression, the vertical load remains almost the same after the buckling occurs and the bearing deflect horizontally. In contrast, the vertical load in tension slowly decreases with horizontal deflection

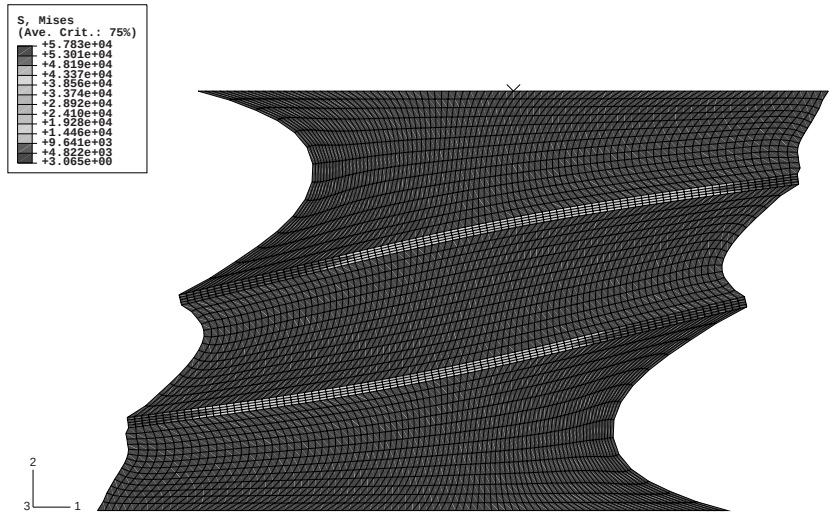

Figure 6.8 Buckled shape and von Mises stresses for Model 5 (tension)

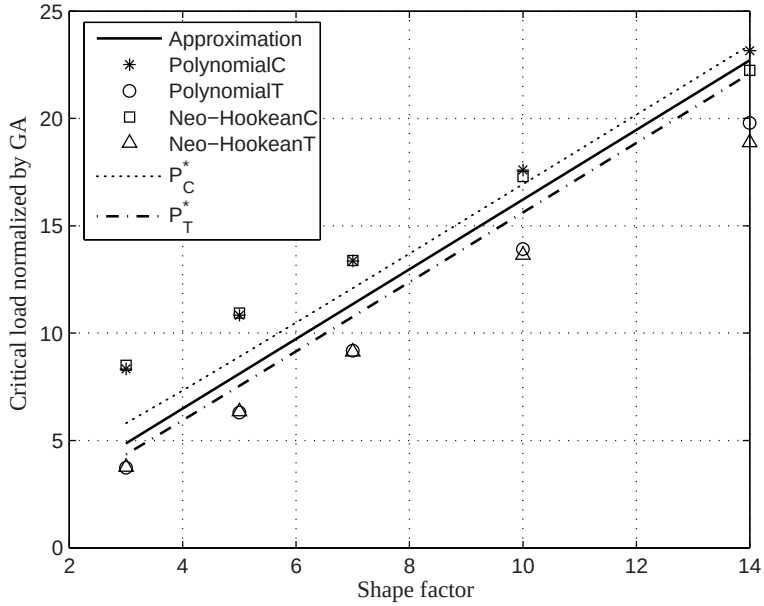

Figure 6.9 Critical buckling load (normalized by GA) versus shape factor, S

Figure 6.9, which plots the critical load as a function of shape factor, shows no significan differences between critical buckling load for incompressible (Polynomial) and compressible (Neo-Hookean) rubber materials.

The theoretical buckling compression load is always less than the absolute value of the tension load for the simple theoretical solution presented by Equation (6.2), which is not consistent with the numerical analysis results shown in Figure 6.9. The figu e shows that the compression buckling load is always greater than the absolute value of the tension buckling load for the same shape factor (shown in Figure 6.9 by dashed and dot-dashed lines, respectively). This might seem to indicate a fla in the theory, but in fact it arises from the way length is used in elementary column buckling theory. The theory neglects the change in length due to the axial load, whereas in the finit element analysis lengthening or shortening has occurred when buckling initiates. For smaller values of the shape factor, the changes in length can be significant

Using the approximations for $GA_S \ll P$ and the values of GA_S and EI_S, the critical pressures $p_{crit} = P_{crit}/A = \sqrt{P_S P_E}/A$ are given in the theoretical analysis by (Kelly and Takhirov 2007)

$$\frac{p_{crit}}{G} = \pm \frac{2\pi b S}{\sqrt{15} t_r} \tag{6.32}$$

for a long strip bearing. Here, t_r is the total thickness of rubber in the bearing. To bring the theory into conformance with the finit element simulation, we replace t_r by

$$t_r = t_r^0 \left(1 \mp \frac{p_{crit}}{4GS^2}\right) \tag{6.33}$$

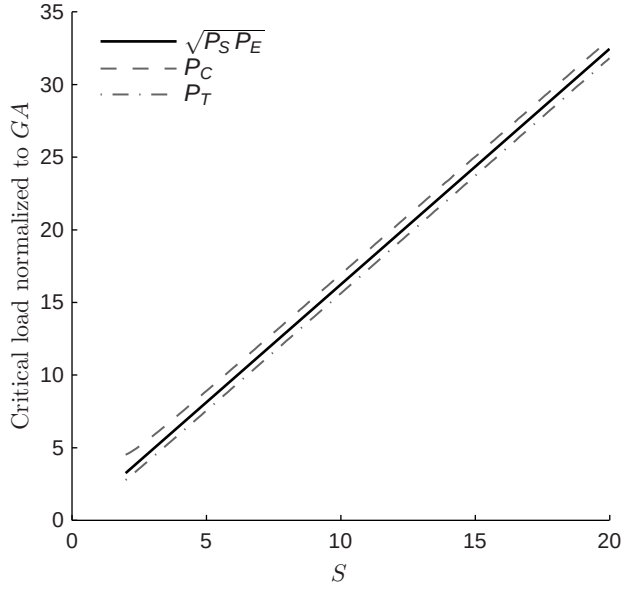

Figure 6.10 Normalized critical load versus shape factor for strip bearing (Equations 6.32, 6.35a and 6.35b)

where t_r^0 is the total thickness of the rubber in the undeformed configuration The minus sign is for compression and the plus for tension. The buckling loads are then given by (Kelly and Takhirov 2007)

$$\frac{p_{crit}}{G} = \pm \frac{2\pi b S}{\sqrt{15} t_r^0 \left(1 \mp \dfrac{p_{crit}}{4GS^2}\right)} \tag{6.34}$$

So

$$\frac{p_{crit}}{G} = 2S^2 \left[1 - \left(1 - \frac{2\pi b}{\sqrt{15}\, t_r^0} \frac{1}{S}\right)^{1/2}\right], \quad \text{in compression} \tag{6.35a}$$

$$\frac{p_{crit}}{G} = 2S^2 \left[\left(1 + \frac{2\pi b}{\sqrt{15}\, t_r^0} \frac{1}{S}\right)^{1/2} - 1\right], \quad \text{in tension} \tag{6.35b}$$

The compression and tension critical loads, $P_{crit}/(GA) = p_{crit}/G$, computed by means of Equations (6.35a) and (6.35b) are presented in Figure 6.10. It is easy to see that the value in compression is always larger than that in tension. The difference between $|p_{crit}/G|$ in compression and tension is approximately $2(\pi b/(\sqrt{15} t_r^0))^2$. For $b = t_r^0$, the difference is $4/3$ and thus becomes less important with increasing S.

7

Influenc of Plate Flexibility on the Buckling Load of Multilayer Rubber Isolators

7.1 Introduction

In the previous two chapters, the buckling behavior in compression and tension of a multilayer rubber bearing used for the seismic or vibration isolation of buildings or equipment was studied under the assumption that the reinforcing steel plates were rigid. In the buckling analysis used, the isolator was treated as a composite column with low shear stiffness. In Chapter 5, where the buckling of bearings under compression loading was studied, the bearing was modelled as a continuous beam and plane sections, normal to the undeformed axis before deformation, were assumed to remain plane, but not necessarily normal after deformation. The theory is an outgrowth of work by Haringx on the mechanical characteristics of helical steel springs and rubber rods used for vibration mountings. This work was published as a series of technical reports, the third of which (Haringx 1949), covers the stability of rubber rods. The Haringx theory was later applied by Gent (1964) to multilayer rubber bearings. In all earlier analyses of the stability of isolators the reinforcing plates have been assumed to be rigid, and there is no way to know how thick the plates must be in order for this to be a valid assumption, or, if not, how thick they must be for the effect of their flexibilit to be negligible. For seismic isolators, which are generally circular in cross-section and about 0.6 to 1 m (24 to 40 in) in diameter and about 0.3 to 0.4 m (12 to 16 in) high, the steel reinforcing shims are about 3.18 mm (1/8 in) thick as a general rule.

The application of seismic isolation to buildings in the United States, Japan and Europe has been so far to large expensive buildings with sensitive internal equipment such as computer centers, emergency operations centers and hospitals. The isolators used in these applications are large, expensive and may weigh anywhere from 0.5 to 1.5 tons

Mechanics of Rubber Bearings for Seismic and Vibration Isolation, First Edition. James M. Kelly and Dimitrios A. Konstantinidis.

(1.1 to 3.3 kips). There have been efforts to apply this approach to low-cost public housing in developing countries or poorer regions of developed countries with severe seismic problems. Examples of demonstration projects have been completed in Chile and in the southern Italian region of Reggio Calabria. Demonstration projects with partial support from United Nations Industrial Development Organization (UNIDO) were built in Guangzhou Province, China, and in Indonesia.

To make the seismic isolation useful for such applications, it is necessary to reduce the cost of the isolators and reduce their weight in order to limit the dependence on site equipment. Both aims can be met either by reducing the thickness of the reinforcing steel plates or by replacing the steel with a fabric reinforcement, such as carbon fibe (Kelly and Takhirov 2001, Tsai and Kelly 2002). It is possible that flexibilit of the shims or the lack of bending stiffness in the fibe reinforcement could have a large effect on the buckling load of a bearing. It is necessary, therefore, to have a theory for the buckling of these isolators that takes into account the flexibilit of the reinforcement; such a theory will be covered in this chapter.

This theory is similar to the compression buckling theory of Chapter 5 in that it treats the isolator as a composite beam. The warping of the cross-section, which is permitted by the flexibilit of the reinforcing sheets, is taken into account by introducing an additional kinematic displacement function, which will be referred to as the *warping function*. It will be selected to produce no additional rotation of the section, but to measure the deviation from plane of the deformed cross-section. Force resultants that arise from the presence of this kinematic quantity are also introduced, and constitutive equations for these quantities are derived. The appropriate equations of equilibrium incorporating these new force quantities are developed: first in the undeformed configuratio for non-buckling problems; secondly, in the deformed configuratio for buckling problems.

The development of the constitutive equations for rubber bearings is complicated by the fact that the mechanical response of the thin rubber layers is governed by equations that lead to a parabolic stress distribution under pure axial load and a cubic stress distribution under pure bending (both with zero stress at the free edges), and these have to be included in the buckling analysis of the isolator.

The outcome of this analysis will include completely rigid plates and completely flexibl reinforcement as special cases, and it will show that for the typical range of sizes of isolators for buildings, the reduction in buckling load from the completely rigid plate case to the completely flexibl plate case is from 25 to 50%. The analysis will also show that the 3.18 mm (1/8 in) thick steel plates have almost the same buckling load as the completely rigid case, and that 0.79 mm (1/32 in) thick steel plates have almost the same buckling load as the completely flexibl case. These results are very encouraging for the design of low-cost isolators and should encourage the development of alternative lightweight reinforcing systems.

7.2 Shearing Deformations of Short Beams

Before developing a theory for the buckling of the isolator with flexibl reinforcing plates, it is useful to develop the theory for a simple beam of rectangular cross-section

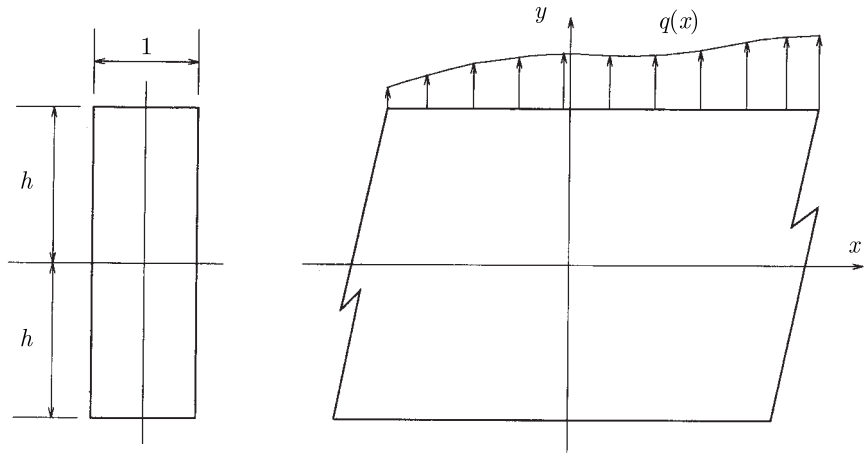

Figure 7.1 Beam model showing dimensions and shear loading

and to obtain the response of this beam model to the two cases: (i) simple shear, and (ii) column buckling. The theory could be extended to arbitrary cross-sections, albeit with a considerable increase in algebraic complexity, but for the purpose of illustration the rectangular section is adequate. The geometry of the beam is shown in Figure 7.1. Shear loading will be covered in this section and buckling under axial load will be considered in the next section.

The deformation of the beam is characterized by four displacement variables, u, v, ψ and ϕ, all of which are functions of x. The displacement field (u, v), shown in Figure 7.2, is taken to be

$$\begin{aligned} u(x, y) &= u_0(x) - \psi(x)y + \phi(x) f_w(y) \\ v(x, y) &= v(x) \end{aligned} \tag{7.1}$$

The function ψ is the average angle of rotation of the section and ϕ is the measure of the warping of the section. The functions u_0 and v are the displacement of the middle surface in the x and y directions. It is convenient to select the function $f_w(y)$ to be orthogonal to both 1 and y so that no rotation of the section is produced by $f_w(y)$; thus the product ϕf_w can be identifie as the deviation from a planar displacement field or in other words, the warping of the section.

The appropriate form of $f_w(y)$ for the rectangular section is

$$f_w(y) = \frac{y^3}{h^3} - \frac{3}{5}\frac{y}{h} \tag{7.2}$$

The selection of $f_w(y)$ to be dimensionless means the warping function, $\phi(x)$, has units of displacement.

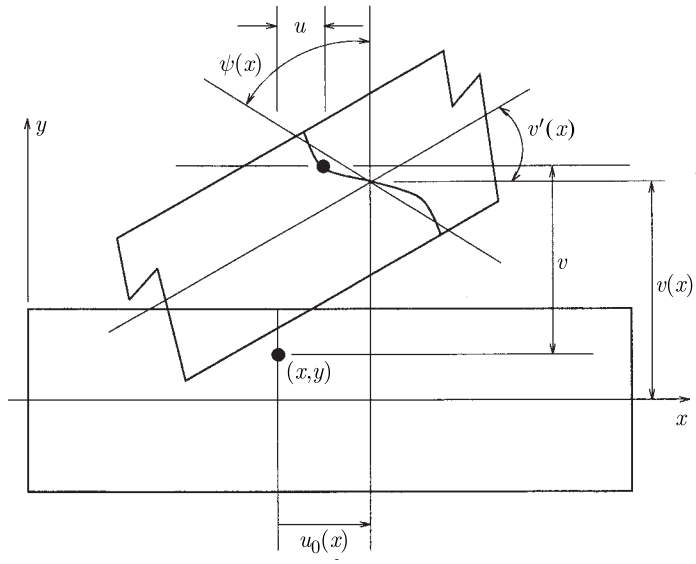

Figure 7.2 Displacement fiel of beam with shear and warping

The resulting strains are

$$\begin{aligned} \varepsilon_{xx} &= u_0' - \psi' y + \phi' f_w \\ \gamma_{xy} &= (v' - \psi) + \phi f_w' \end{aligned} \tag{7.3}$$

and assuming elastic behavior, the stresses become

$$\begin{aligned} \sigma_{xx} &= E u_0' - E\psi' y + E\phi' f_w(y) \\ \tau_{xy} &= G(v' - \psi) + G\phi f_w'(y) \end{aligned} \tag{7.4}$$

We defin a set of stress resultants by

$$N = \int_A \sigma_{xx} \mathrm{d}A \tag{7.5a}$$

$$M = -\int_A \sigma_{xx} y \mathrm{d}A \tag{7.5b}$$

$$Q = \int_A f_w(y)\sigma_{xx} \mathrm{d}A \tag{7.5c}$$

$$V = \int_A \tau_{xy} \mathrm{d}A \tag{7.5d}$$

$$R = \int_A f_w'(y)\tau_{xy} \mathrm{d}A \tag{7.5e}$$

The resultants are related to the kinematic variables by

$$N = E A u_0' \tag{7.6}$$

$$M = E I \psi' \tag{7.7}$$

$$Q = E J \phi' \tag{7.8}$$

and

$$V = G A(v' - \psi) + G B \phi \tag{7.9}$$

$$R = G B(v' - \psi) + G C \phi \tag{7.10}$$

where

$$A = \int_A \mathrm{d}A = 2h \tag{7.11a}$$

$$I = \int_A y^2 \mathrm{d}A = \frac{2}{3}h^3 \tag{7.11b}$$

$$J = \int_A f_w^2(y) \mathrm{d}A = \frac{8}{175}h \tag{7.11c}$$

$$B = \int_A f_w'(y) \mathrm{d}A = \frac{4}{5} \tag{7.11d}$$

$$C = \int_A \left(f_w'(y)\right)^2 \mathrm{d}A = \frac{48}{25h} \tag{7.11e}$$

Substitution back into the stress equations gives

$$\begin{aligned} \sigma_{xx} &= \frac{N}{A} - \frac{M}{I}y + \frac{Q}{J} f_w(y) \\ \tau_{xy} &= \frac{CV - BR}{AC - B^2} - \frac{BV - AR}{AC - B^2} f_w'(y) \end{aligned} \tag{7.12}$$

The equilibrium equations for the stress resultants are derived from the equilibrium equations for the stress, namely

$$\frac{\partial \sigma_{xx}}{\partial x} + \frac{\partial \tau_{xy}}{\partial y} = 0 \tag{7.13}$$

$$\frac{\partial \tau_{xy}}{\partial x} + \frac{\partial \sigma_{yy}}{\partial y} = 0 \tag{7.14}$$

Integrating the firs through the thickness and assuming zero external shear on $y = \pm h$ leads to

$$N' = 0 \tag{7.15}$$

Multiplying the firs by y and integrating gives

$$M' + V = 0 \tag{7.16}$$

and multiplying the firs by $f_w(y)$ and integrating through the thickness gives

$$Q' - R = 0 \tag{7.17}$$

Finally, integrating the second equation of equilibrium through the thickness gives

$$V' + q = 0 \tag{7.18}$$

where $q(x)$ is the external load per unit length on the beam.

This set of equilibrium equations derived by integration through the thickness of the beam can be verifie using virtual work. The firs variation of the internal virtual work, δW_i, is given by

$$\delta W_i = \int_0^l \int_A (\sigma_{xx}\delta\varepsilon_{xx} + \tau_{xy}\delta\varepsilon_{xy})\mathrm{d}A\,\mathrm{d}l \tag{7.19}$$

and the external virtual work, δW_e, is

$$\delta \mathrm{W}_e = \int_0^l q(x)\delta v(x)\,\mathrm{d}x \tag{7.20}$$

By expanding the virtual strains in terms of the virtual displacements and carrying out the resulting integrations over the cross-section, A, the internal virtual work in terms of the kinematic variables and the stress resultants becomes

$$\delta W_i = \int_0^l \left[N\delta u_0' + M\delta\psi' + Q\delta\phi' + V\delta v' - V\delta\psi + R\delta\phi\right]\mathrm{d}x \tag{7.21}$$

Using integration by parts and reorganizing the result into terms in each of the four virtual displacements, δu_0, δv, $\delta\psi$ and $\delta\phi$, we have

$$\begin{aligned}\delta W_i - \delta W_e &= N\delta u_0\,|_0^l + M\delta\psi\,|_0^l + V\delta v\,|_0^l + Q\delta\phi\,|_0^l \\ &- \int_0^l N'\delta u_0\mathrm{d}x - \int_0^l (M' + V)\delta\psi\,\mathrm{d}x - \int_0^l (Q' - R)\delta\phi\,\mathrm{d}x - \int_0^l (V' + q)\delta v\,\mathrm{d}x\end{aligned} \tag{7.22}$$

which for equilibrium must vanish for all kinematically acceptable virtual displacements, leading to consistent boundary conditions and the same set of equilibrium equations as before.

When the resultants are replaced by the kinematic variables, we have

$$EI\psi'' + GA(v' - \psi) + GB\phi = 0 \tag{7.23}$$

$$GA(v' - \psi)' + GB\phi' + q = 0 \tag{7.24}$$

$$EJ\phi'' - GB(v' - \psi) - GC\phi = 0 \tag{7.25}$$

These three equations can be reduced to a single equation for $v' - \psi$, ψ or ϕ by the following process. We write the three equations in matrix form using the symbol D in place of the derivative with respect to x, i.e., $\mathrm{D} = \mathrm{d}/\mathrm{d}x$. The equations then become

$$\begin{bmatrix} GA & EI\mathrm{D}^2 & GB \\ -GB & 0 & EJ\mathrm{D}^2 - GC \\ GA\mathrm{D} & 0 & GB\mathrm{D} \end{bmatrix} \begin{bmatrix} v' - \psi \\ \psi \\ \phi \end{bmatrix} = - \begin{bmatrix} 0 \\ 0 \\ 1 \end{bmatrix} q \tag{7.26}$$

The determinant of the 3×3 matrix on the left-hand side is

$$EI\mathrm{D}^2[(GB)^2\,\mathrm{D} + (EJ\mathrm{D}^2 - GC)GA\mathrm{D}] \tag{7.27}$$

This operator controls the left-hand side of the differential equations for the three variables $v' - \psi$, ψ, ϕ. The right hand sides of the equations are determined by the determinants of the matrices

$$\begin{bmatrix} 0 & EI\mathrm{D}^2 & GB \\ 0 & 0 & EJ\mathrm{D}^2 - GC \\ 1 & 0 & GB\mathrm{D} \end{bmatrix}$$

which gives the information for $v' - \psi$;

$$\begin{bmatrix} GA & 0 & GB \\ -GA & 0 & EJ\mathrm{D}^2 - GC \\ GA\mathrm{D} & 1 & GB\mathrm{D} \end{bmatrix}$$

which provides this for ψ, and

$$\begin{bmatrix} GA & EI\mathrm{D}^2 & 0 \\ -GA & 0 & 0 \\ GA\mathrm{D} & 0 & 1 \end{bmatrix}$$

which applies to ϕ.

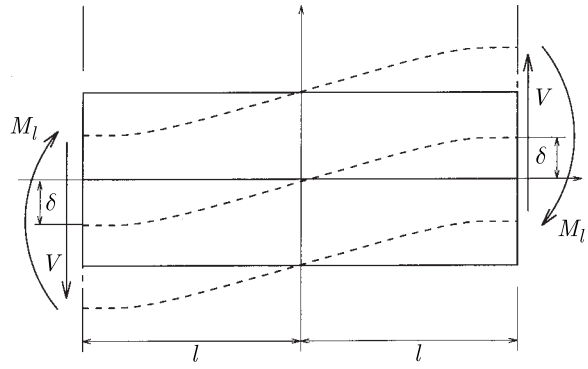

Figure 7.3 Beam model under shear end load

Using Cramer's rule, we have

$$GAEJ(v' - \psi)''' + [(GB)^2 - GAGC](v' - \psi) = -EJq'' + GCq \tag{7.28}$$

$$EIGAEJ\psi'''' + EI[(GB)^2 - GAGC]\psi'' = GAEJq'' + GA(GB - GC)q \tag{7.29}$$

$$GAEJ\phi'''' + [(GB)^2 - GAGC]\phi'' = -GAq \tag{7.30}$$

The problem to which we intend to apply these equations is that of a beam under endshears, V, only (i.e., $q = 0$) and constraints against rotation and warping at each end, as shown in Figure 7.3. The problem is clearly anti-symmetric in displacement v and symmetric in ψ and ϕ. The shear force is constant throughout the beam, and the moment is

$$M = -Vx \tag{7.31}$$

The equations for the displacement variables, $v' - \psi$, ψ and ϕ, reduce to

$$EI\psi' = -Vx \tag{7.32}$$

$$GA(v' - \psi) + GB\phi = V \tag{7.33}$$

$$EJ\phi'' - GB(v' - \psi) - GC\phi = 0 \tag{7.34}$$

From Equation (7.33), we have

$$v' - \psi = -\frac{B}{A}\phi + \frac{V}{GA} \tag{7.35}$$

and this inserted into Equation (7.34) gives

$$EJGA\phi'' - [GAGC - (GB)^2]\phi = GBV \tag{7.36}$$

The alternative form in terms of $(v' - \psi)$ is

$$EJGA(v' - \psi)'' - [GAGC - (GB)^2](v' - \psi) = -GCV \tag{7.37}$$

We note that the combination $AC - B^2$ for the rectangular section is positive, so that the solutions are hyperbolic functions. The solutions are

$$\phi = C_1 \cosh(\omega x) - \frac{GB}{GAGC - (GB)^2} V$$

and

$$v' - \psi = D_1 \cosh(\omega x) - \frac{GC}{GAGC - (GB)^2} V$$

where

$$\omega^2 = \frac{GAGC - (GB)^2}{EJGA} \tag{7.38}$$

and where C_1 and D_1 are related through Equation (7.35) as

$$D_1 \cosh(\omega x) + \frac{C}{AC - B^2}\frac{V}{G} = -\frac{B}{A}\left(C_1 \cosh(\omega x) - \frac{B}{AC - B^2}\frac{V}{G}\right) + \frac{V}{GA}$$

i.e.,

$$D_1 = -\frac{B}{A} C_1 \tag{7.39}$$

The boundary conditions at $x = \pm l$ require that both ψ and ϕ vanish, and this determines that

$$\phi(x) = -\frac{B}{AC - B^2}\left(1 - \frac{\cosh(\omega x)}{\cosh(\omega l)}\right)\frac{V}{G} \tag{7.40}$$

and

$$v' - \psi = \frac{V}{GA}\left(\frac{AC}{AC - B^2} - \frac{B^2}{AC - B^2}\frac{\cosh(\omega x)}{\cosh(\omega l)}\right) \tag{7.41}$$

From Equation (7.32), we have

$$\psi = -\frac{V}{2EI}x^2 + C_3$$

and since $\psi(\pm l) = 0$

$$\psi = \frac{V}{2EI}(l^2 - x^2) \tag{7.42}$$

To complete the solution, we substitute for ψ in Equation (7.41) and integrate, obtaining

$$v(x) = \frac{V}{2EI}\left(l^2x - \frac{x^3}{3}\right) - \frac{V}{GA}\left(\frac{B^2}{AC - B^2}\frac{1}{\omega}\frac{\sinh(\omega x)}{\cosh(\omega l)} - \frac{AC}{AC - B^2}x\right) \tag{7.43}$$

where we have set $v(0) = 0$ to maintain the anti-symmetry of the solution for $v(x)$. The deflection at each end are $\pm\delta$ where

$$\delta = \frac{Vl^3}{3EI} + \frac{Vl}{GA}\left(\frac{AC}{AC - B^2} - \frac{B^2}{AC - B^2}\frac{\tanh(\omega l)}{\omega l}\right) \tag{7.44}$$

For the rectangular section considered here

$$\frac{AC}{AC - B^2} = \frac{6}{5} \tag{7.45}$$

and

$$\frac{B^2}{AC - B^2} = \frac{1}{5} \tag{7.46}$$

so that if we suppress the warping by setting $EJ \to \infty$, i.e., ϕ everywhere zero, then $\omega l \to 0$, and δ_s, the part of δ due to shear, becomes

$$\delta_s \to \frac{Vl}{GA} \tag{7.47}$$

On the other hand, to model the case when there is no restraint on the warping at the end of the beam, the warping stiffness EJ is set to zero, then

$$\lambda l \to \infty \quad \text{and} \quad \delta_s \to \frac{6}{5}\frac{Vl}{GA} = \frac{Vl}{G\left(\frac{5A}{6}\right)} \tag{7.48}$$

which corresponds to the usual theory of shear deformation in beams. Furthermore, if ϕ is not constrained and either $EJ \to 0$ or alternatively $\phi'' \to 0$, then

$$\phi = -\frac{B}{C}(v' - \psi) \tag{7.49}$$

and

$$\tau_{xy} = G\left(1 - \frac{B}{C}f'_w(y)\right)(v' - \psi) \tag{7.50}$$

which with Equation (7.12) gives

$$\tau_{xy} = \frac{3V}{2A}\left(1 - \frac{y^2}{h^2}\right) \tag{7.51}$$

Thus, if the effect of the warping is not included, the solution reduces to the standard beam theory with shear deformation included. The influenc of the constraint of the warping depends on the parameter ωl, which is given by

$$(\omega l)^2 = \frac{G}{E}\frac{AC - B^2}{JA}l^2 = \frac{35\,G}{E}\frac{l^2}{h^2} \tag{7.52}$$

It follows that ω is likely to be large, and the solution for $\phi(x)$ near $x = \pm l$ can be written as

$$\phi(x) = -\frac{AB}{AC - B^2}[1 - e^{-\omega(l-x)}]\frac{V}{GA} \tag{7.53}$$

We can defin a penetration length l_p for the distance over which the constraint of the warping is important by setting $\omega l_p = 1$, which gives $l_p \approx h/3.5$. Clearly this means that the constraint of the warping is of no significanc in normal beams. The effective E in isolators is of the order of several hundred times G and, in such cases, the constraint of the warping at the ends will be effective over much larger distances from the ends. Before turning to the equivalent isolator problem, however, in the next section we will consider the buckling problem for this beam example.

7.3 Buckling of Short Beams with Warping Included

The main problem associated with the determination of the buckling load for the short beam with shear and warping included, is the determination of the appropriate equilibrium equations in the buckled configuration Since we have no physically intuitive understanding of Q and R, a direct method is not available and a formal approach must be used, such as that which led to $Q' - R = 0$. To verify the results of the formal approach, we can compare it to the form of the equilibrium equations in Chapter 5 on compression buckling, where plane sections remain plane, which corresponds to $EJ \to \infty$ and $\phi \to 0$, in which case an intuitive approach is possible.

To develop the equations of equilibrium that correspond to Equations (5.2a) and (5.2b) in Chapter 5 when the warping variables Q and R are included, we resort to integration of the stress equations of equilibrium through the thickness.

We consider a differential element of the material with sides $\mathrm{d}x$ and $\mathrm{d}y$ in the undeformed configuratio parallel and perpendicular to the undeformed beam axis as shown in Figure 7.4. In the deformed configuration the edges of the element parallel to the x-axis are parallel to the deformed middle surface of the beam and the edges parallel to the y-axis are rotated through the angles θ and $\theta + (\partial\theta/\partial x)\,\mathrm{dx}$, where θ is the local rotation of the vertical line element given by

$$\theta = -\frac{\partial u}{\partial y} = \psi - \phi f_w'(y) \tag{7.54}$$

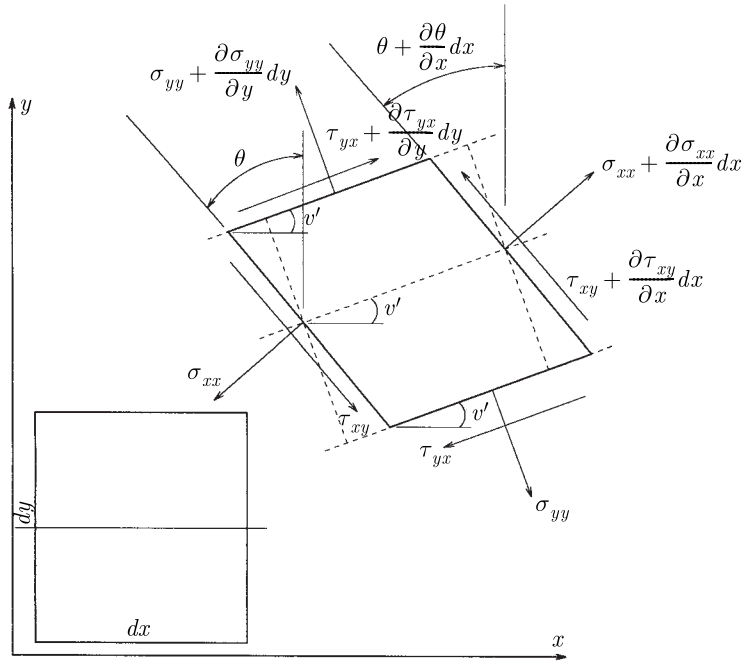

Figure 7.4 Stresses on deformed element when warping is included

The stresses in the deformed configuratio are shown in Figure 7.4. Equilibrium in the x-direction gives

$$\frac{\partial}{\partial x}(\sigma_{xx} - \tau_{xy}\theta) + \frac{\partial}{\partial y}(\tau_{yx} - \sigma_{yy}v') = 0 \tag{7.55}$$

Equilibrium in the y-direction leads to

$$\frac{\partial}{\partial x}(\tau_{xy} + \sigma_{xx}\theta) + \frac{\partial}{\partial y}(\sigma_{yy} + \tau_{yx}v') = 0 \tag{7.56}$$

and moment equilibrium about the left center of the element leads to

$$\tau_{yx} - \tau_{xy} + \sigma_{xx}(v' - \theta) = 0 \tag{7.57}$$

Substitution of Equation (7.57) into Equations (7.55) and (7.56) gives

$$\frac{\partial}{\partial x}(\sigma_{xx} - \theta\,\tau_{xy}) + \frac{\partial}{\partial y}[\tau_{xy} - \sigma_{xx}(v' - \theta) - \sigma_{yy}v'] = 0 \tag{7.58}$$

$$\frac{\partial}{\partial x}(\theta\sigma_{xx} + \tau_{xy}) + \frac{\partial}{\partial y}(\sigma_{yy} + \tau_{xy}v') = 0 \tag{7.59}$$

Integration of both equations over the cross-section $-h \leq y \leq h$ and assuming traction-free surfaces at $y = \pm h$ leads to

$$\frac{\mathrm{d}N}{\mathrm{d}x} = 0 \tag{7.60}$$

$$\frac{\mathrm{d}}{\mathrm{d}x}\left(N\psi - \frac{NB}{A}\phi + V\right) = 0 \tag{7.61}$$

Multiplication of the firs by y and integration over the cross-section leads to

$$\frac{\mathrm{d}M}{\mathrm{d}x} + V - N(v' - \psi) - \frac{N}{A}B\phi = 0 \tag{7.62}$$

Multiplication of the firs by $f_w(y)$ and integration over the cross-section leads to

$$\frac{\mathrm{d}Q}{\mathrm{d}x} - R + \frac{N}{A}B(v' - \psi) + \frac{N}{A}C\phi = 0 \tag{7.63}$$

These equations of equilibrium in the deformed configuration developed by integration over the cross-sectional area of the equations of stress equilibrium can be verifie as before by the use of virtual work. However when the stability of the beam model is considered, it is necessary to include length changes due to second-order effects. The lateral displacement of the beam, $v(x)$ causes an increase in length of any horizontal plane that depends on the slope $v'(x)$ in the form

$$\varepsilon_1 \,\mathrm{d}x = (1 - \cos v')\,\mathrm{d}x = \frac{1}{2}v'^2\mathrm{d}x \tag{7.64}$$

and the shear deformation causes a reduction in length

$$\varepsilon_2 \,\mathrm{d}x = (1 - \cos\gamma_{xy})\,\mathrm{d}x = \frac{1}{2}\gamma_{xy}^2\,\mathrm{d}x \tag{7.65}$$

These two terms contribute to the internal virtual work δW_i such that the f rst variation of the internal virtual work becomes

$$\delta\, W_i = \int_0^l \int_A \left\{\sigma_{xx}\left[\delta\left(\frac{1}{2}v'^2\right) - \delta\left(\frac{1}{2}\gamma_{xy}^2\right)\right]\right\}\mathrm{d}A\,dx \;+ \int_0^l \int_A (\sigma_{xx}\delta\varepsilon_{xx} + \tau_{xy}\delta\varepsilon_{xy})\,\mathrm{d}A\,\mathrm{d}l \tag{7.66}$$

The firs integral can be written as

$$I_1 = \int_0^l \int_A (\sigma_{xx}v'\delta v' - \sigma_{xx}\gamma_{xy}\delta\gamma_{xy})\,\mathrm{d}A\,\mathrm{d}x \tag{7.67}$$

which with $\gamma_{xy} = v' - \psi + \phi f'_w$ and $\delta\gamma_{xy} = \delta v' - \delta\psi + \delta\phi f'_w$ means that

$$\gamma_{xy}\delta\gamma_{xy} = v'\delta v' - \psi\delta v' + \phi f'_w\delta v' - v'\delta\psi + \psi\delta\psi - \phi f'_w\delta\psi + v' f'_w\delta\phi - \psi f'_w\delta\phi + \phi f'_w\delta\phi \tag{7.68}$$

and from this, the firs integral becomes

$$I_1 = \int_0^l \left[\left(\frac{NB}{A}\phi - N\psi \right) \delta v' + \left(N\psi - \frac{NB}{A}\phi - Nv' \right) \delta\psi + \left(\frac{NB}{A}v' - \frac{NB}{A}\psi + \frac{NB}{A}\phi \right) \delta\phi \right] \mathrm{d}x \tag{7.69}$$

The second integral becomes

$$I_2 = \int_0^l (N\delta u'_0 + M\delta\psi' + Q\delta\phi' + V\delta v' - V\delta\psi + R\delta\phi)\, \mathrm{d}x \tag{7.70}$$

Adding the two integrals together and using integration by parts in the usual way, the firs variation of the virtual work takes the form

$$I_1 + I_2 = N\delta u_0 \,|_0^l + \left(-N\psi + \frac{NB}{A}\phi + V \right) \delta v \,|_0^l + M\delta\psi \,|_0^l + \int_0^l N'\delta u_0 \, \mathrm{d}x$$
$$+ \int_0^l \left[\left(-N\psi + \frac{NB}{A}\phi \right)' + V' \right] \delta v \, \mathrm{d}x + \int_0^l \left(-Nv' + N\psi - \frac{NB}{A}\phi - M' - V \right) \delta\psi \, \mathrm{d}x$$
$$+ \int_0^l \left(-\frac{NB}{A}v' + \frac{NB}{A}\psi - \frac{NC}{A}\phi - Q' + R \right) \delta\phi \mathrm{d}x \tag{7.71}$$

It is easy to see that this expression leads to the same equations of equilibrium as before and also provides the appropriate boundary conditions for the beam.

The firs equation, Equation (7.60), reduces to

$$N = -P \tag{7.72}$$

Integration of Equation (7.61) gives

$$V - P\left(\psi - \frac{B}{A}\phi \right) = -H_0 \tag{7.73}$$

and when this is inserted into Equation (7.62), it can be integrated to give

$$M + Pv = H_0 x + M_0 + Pv_0 \tag{7.74}$$

If we set $\phi = 0$, i.e., $\theta = \psi$, then the set of equilibrium equations reduces to the system of Equations (5.2a) and (5.2b), derived by direct application of equilibrium. When the constitutive equations are used, the equilibrium equations become

$$EI\psi' + Pv = H_0 x + M_0 + Pv_0 \tag{7.75}$$

$$GA(v' - \psi) + \left(G + \frac{P}{A}\right) B\phi - P\psi = -H_0 \tag{7.76}$$

$$EJ\phi'' - \left(G + \frac{P}{A}\right) B(v' - \psi) - \left(G + \frac{P}{A}\right) C\phi = 0 \tag{7.77}$$

These three equations can be reduced to a single equation for ϕ or ψ by the following process. We write the three equations in matrix form, using the symbol D in place of the derivative with respect to x, i.e. $\mathrm{D} = \mathrm{d}/\mathrm{d}x$. The equations then become

$$\begin{bmatrix} P & EI\mathrm{D} & 0 \\ GA\mathrm{D} & -(GA+P) & (GA+P)\dfrac{B}{A} \\ -(GA+P)\dfrac{B}{A}\mathrm{D} & (GA+P)\dfrac{B}{A} & EJ\mathrm{D}^2 - (GA+P)\dfrac{C}{A} \end{bmatrix} \begin{bmatrix} v \\ \psi \\ \phi \end{bmatrix} = \begin{bmatrix} H_0 x + M_0 + Pv_0 \\ -H_0 \\ 0 \end{bmatrix} \tag{7.78}$$

The determinant of the 3×3 matrix on the left-hand side is

$$\begin{aligned} &P(GA+P)^2\frac{C}{A} - P(GA+P)EJ\mathrm{D}^2 - EI(GA+P)^2\frac{B^2}{A^2}\mathrm{D}^2 - P(GA+P)^2\frac{B^2}{A^2} \\ &+ EIGA(GA+P)\frac{C}{A}\mathrm{D}^2 - EIGAEJ\mathrm{D}^4 \end{aligned} \tag{7.79}$$

This operator controls the left hand side of the differential equations for the three variables v, ψ, ϕ. The right hand sides of the equations are determined by the determinants of the matrices

$$\begin{bmatrix} H_0 x + M_0 + Pv_0 & EI\mathrm{D} & 0 \\ -H_0 & -(GA+P) & (GA+P)\dfrac{B}{A} \\ 0 & (GA+P)\dfrac{B}{A} & EJ\mathrm{D}^2 - (GA+P)\dfrac{C}{A} \end{bmatrix}$$

which gives the information for v;

$$\begin{bmatrix} P & H_0 x + M_0 + Pv_0 & 0 \\ GA\mathrm{D} & -H_0 & (GA+P)\dfrac{B}{A} \\ -(GA+P)\dfrac{B}{A}\mathrm{D} & 0 & EJ\mathrm{D}^2 - (GA+P)\dfrac{C}{A} \end{bmatrix}$$

which provides this for ψ, and

$$\begin{bmatrix} P & EI\mathrm{D} & H_0x + M_0 + Pv_0 \\ GA\mathrm{D} & -(GA+P) & -H_0 \\ -(GA+P)\dfrac{B}{A}\mathrm{D} & (GA+P)\dfrac{B}{A} & 0 \end{bmatrix}$$

which applies to ϕ.

Using Cramer's rule, we have

$$EJGAEI\frac{\mathrm{d}^4}{\mathrm{d}x^4}\begin{bmatrix} v \\ \psi \\ \phi \end{bmatrix} + \left[EJ(GA+P)P + EI(GA+P)^2\frac{B^2}{A^2} - GAEI(GA+P)\frac{C}{A}\right]\frac{\mathrm{d}^2}{\mathrm{d}x^2}\begin{bmatrix} v \\ \psi \\ \phi \end{bmatrix} + \left[(GA+P)^2\frac{B^2}{A^2}P - (GA+P)^2P\frac{C}{A}\right]\begin{bmatrix} v \\ \psi \\ \phi \end{bmatrix} = \begin{bmatrix} (GA+P)^2\left[\left(\dfrac{B}{A}\right)^2 - \dfrac{C}{A}\right](H_0x + M_0 + Pv_0) \\ (GA+P)^2\left[\left(\dfrac{B}{A}\right)^2 - \dfrac{C}{A}\right]H_0 \\ 0 \end{bmatrix} \tag{7.80}$$

As before, we take $H_0 = 0$ and $\psi = \cos(\pi x/(2l))$ to satisfy the constraints at $x = \pm l$ and determine the buckling load P from

$$EJGAEI\frac{\pi^4}{4l^4} - \left[EJ\left(G + \frac{P}{A}\right)AP + EI\left(G + \frac{P}{A}\right)^2B^2 - GAEI\left(G + \frac{P}{A}\right)C\right]\frac{\pi^2}{4l^2} + \left(G + \frac{P}{A}\right)^2(B^2 - AC)\,P = 0 \tag{7.81}$$

It is convenient to defin the following dimensionless quantities:

(i) the normalized buckling load:

$$p = \frac{P}{GA} \tag{7.82}$$

(ii) the normalized column geometry:

$$\lambda = \frac{\pi h}{2l} \tag{7.83}$$

(iii) the normalized stiffnesses:

$$k_1 = \frac{GB^2h^2}{EAJ} \quad k_2 = \frac{GAh^2}{EI} \tag{7.84}$$

and the parameter $\gamma = AC/B^2$ in terms of which Equation (7.81) becomes

$$\lambda^4 - \{k_1[(1+p)^2 - \gamma(1+p)] + k_2 p(1+p)\}\lambda^2 + k_1 k_2 p(1+p)^2(1-\gamma) = 0 \tag{7.85}$$

It is useful to factor this into the form

$$\{\lambda^2 - k_1[(1+p)^2 - \gamma(1+p)]\}[\lambda^2 - k_2 p(1+p)] - k_1 k_2 p^2(1+p)^2 = 0 \tag{7.86}$$

We note that if $k_1 \to 0$, i.e., $EJ \to \infty$, or no warping, we have

$$\lambda^2 = k_2 p(1+p) \tag{7.87}$$

which is the same result as we had in Chapter 5 for the buckling with no warping; and if $k_2 \to 0$, i.e., $EJ \to \infty$ (no rotation, $\psi \equiv 0$), we have

$$\lambda^2 = k_1[(1+p)^2 - \gamma(1+p)] \tag{7.88}$$

Furthermore, if the quantity γ is allowed to become very large (although in this case it is fixe at 6), we see that

$$\lambda^2 \to k_2 p(1+p) \tag{7.89}$$

Another possible case is $EI \neq 0$ and $EJ \to 0$, which corresponds to the buckling of a beam with no restraint on warping. In this case, $k_1 \to \infty$, and if we divide by k_1, we have

$$\lambda^2 = \frac{k_2 p(1+p)^2(1-\gamma)}{(1+p)^2 - \gamma(1+p)} = \frac{5\,k_2 p(1+p)}{5-p} \tag{7.90}$$

In this case, as $\lambda \to 0$, $p \to \lambda^2/k^2$, i.e.,

$$\frac{P}{GA} \to \frac{\pi^2 EI}{4l^2} \tag{7.91}$$

and as $\lambda \to \infty$,

$$P \to 5\,GA \tag{7.92}$$

The solution for p in terms of λ for the complete solution and the various special cases is shown in Figure 7.5 using the parameters $E = 2.5\,G$ and the values of A, B, C, I, J, as given in Section 7.2. A comparison of the values of p for the case where $\phi = 0$ and the full equation shows that neglecting warping can greatly overestimate the buckling load. Comparison of the case when the warping is unconstrained, i.e., $EJ \to 0$, shows that neglecting the end constraints against warping can greatly underestimate the load. It has to be emphasized, of course, that these results are of very little practical application to real beams since it is almost certain that for most materials the value of the buckling

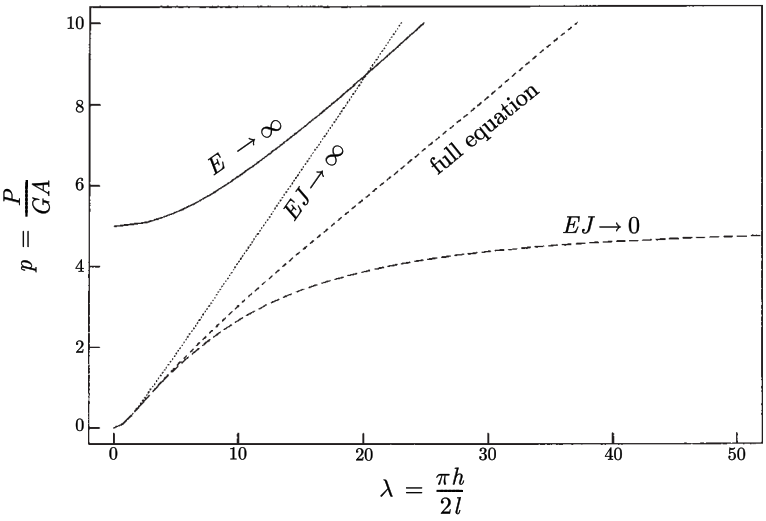

Figure 7.5 Buckling load as a function of beam length for short beam model

stress, P/A, would be too high to be sustainable by the material. The purpose of the analysis has been to demonstrate the structure of the theory and guide its application to the more elaborate problem of the buckling of the isolator.

7.4 Buckling Analysis for Bearing

To make it easier for the reader to draw parallels, the notation used in the buckling analysis for a bearing in this section follows that presented earlier in this chapter. This notation, however, is in some cases different than that presented in earlier chapters in this book. Most importantly, the width of the strip bearing which was $2b$ in earlier chapters (see Figure 2.2) is $2h$ here; the total height of the bearing, i.e., total rubber thickness plus thickness of the steel shims (see Figure 5.3) was h, but is $2l$ here.

In developing the buckling analysis for isolators, it is necessary to extend the equation for the pressure to situations where the displacement fiel in the thickness direction varies in the lateral direction. Because the individual pads are thin compared with their width, and the variation in the displacement in the lateral direction is small, it is assumed that the pressure can be given by the equation

$$\nabla^2 p = \frac{12\,G}{t^3} w \tag{7.93}$$

where $w(x, y)$ is now the displacement in the thickness direction.

It is clear from the analysis of the warping of the short beam that the selection of a warping function, f_w, that permits the uncoupling of the constitutive equations for bending moment M and warping resultant Q, is extremely convenient. To achieve this

for an isolator when the stress in the axial direction is obtained from Equation (7.93) by replacing p by $-\sigma_{xx}$ and w/t by ε_{xx}, we need to select $f_w(y)$ such that

$$\int_A \sigma_{xx} y \mathrm{dA} \tag{7.94}$$

is independent of $\phi(x)$, and

$$\int_A \sigma_{xx} f_w(y)\, \mathrm{d}A \tag{7.95}$$

is independent of $\psi(x)$ when σ_{xx} is given by

$$\nabla^2 \sigma_{xx} = -\frac{12\,G}{t^2}\varepsilon_{xx} \tag{7.96}$$

A suitable selection of $f_w(y)$ is

$$f_w(y) = \frac{y^3}{h^3} - \frac{3}{7}\frac{y}{h} \tag{7.97}$$

and with this, we have

$$u(x, y) = u(x) - \psi(x)y + \phi(x)\left(\frac{y^3}{h^3} - \frac{3}{7}\frac{y}{h}\right) \tag{7.98}$$

$$v(x, y) = v(x) \tag{7.99}$$

from which

$$\varepsilon_{xx} = u' - \psi'(x)y + \phi'(x)\left(\frac{y^3}{h^3} - \frac{3}{7}\frac{y}{h}\right) \tag{7.100}$$

The equation for σ_{xx} becomes

$$\frac{\mathrm{d}^2\sigma_{xx}}{\mathrm{d}y^2} = -\frac{12\,G}{t^2}\left[u' - \psi' y + \phi'\left(\frac{y^3}{h^3} - \frac{3}{7}\frac{y}{h}\right)\right] \tag{7.101}$$

and with $\sigma_{xx} = 0$ at $y = \pm h$, this leads to

$$\sigma_{xx} = -\frac{6\,G}{t^2}h^2\left(\frac{y^2}{h^2} - 1\right)u' + \frac{2\,G}{t^2}h^3\left(\frac{y^3}{h^3} - \frac{y}{h}\right)\psi' - \frac{12\,Gh^2}{20\,t^2}\left(\frac{y^5}{h^5} - \frac{10}{7}\frac{y^3}{h^3} + \frac{3}{7}\frac{y}{h}\right)\phi' \tag{7.102}$$

With the previous definition of M and Q, this leads to

$$N = \frac{4\,Gh^2}{t^2} hu' = EAu' \tag{7.103}$$

$$M = \frac{8\,Gh^2}{15\,t^2} h^3\psi' = EI\psi' \tag{7.104}$$

$$Q = \frac{2\,Gh^2}{1225\,t^2} h\phi' = EJ\phi' \tag{7.105}$$

We calculate the other resultants from

$$\tau_{xy} = G\left(v' - \psi\right) + G\phi\frac{3}{h}\left(\frac{y^2}{h^2} - \frac{1}{7}\right) \tag{7.106}$$

obtaining as before

$$V = GA\left(v' - \psi\right) + GB\phi \tag{7.107}$$

$$R = GB\left(v' - \psi\right) + GC\phi \tag{7.108}$$

where now

$$A = 2\,h \tag{7.109a}$$

$$B = \frac{24}{21} \tag{7.109b}$$

$$C = \frac{552}{245\,h} \tag{7.109c}$$

The structure of the theory for non-buckling problems is now exactly the same as before with the values of the nominal EI and EJ being given in terms of G and the shape factor of a single layer, $S = h/t$, which may be quite large.

For the pure shear of an isolator in the absence of vertical load, the characteristic length of penetration of the restraint produced by the boundary condition at the ends of the bearing, which for the short beam model was

$$l_p \approx \sqrt{\frac{E}{35\,g}} h \tag{7.110}$$

is now given by

$$\left(\lambda l_p\right)^2 = 1 \tag{7.111}$$

where

$$\left(\lambda l_p\right)^2 = \frac{GAGC - (GB)^2}{EJGA} l_p^2 \tag{7.112}$$

with

$$EJ = \frac{2\,Gh^3}{1225t^2} \tag{7.113}$$

Thus

$$\left(\lambda l_p\right)^2 = 980\frac{l_p^2 t^2}{h^2 h^2} \tag{7.114}$$

giving

$$l_p \approx \frac{h}{30}\frac{h}{t} \approx \frac{S}{30}h \tag{7.115}$$

In this case, the penetration length is of the same order as the width of the bearing.

When we turn to the buckling problem, it is necessary to have the stress distribution of σ_{xx} due to the axial load N, denoted here by σ_{xx}^a. From Equation (7.96) and the boundary conditions on σ_{xx} at $y = \pm h$ we have

$$\sigma_{xx}^a = \frac{3N}{4\,h}\left(1 - \frac{y^2}{h^2}\right) \tag{7.116}$$

The equations of equilibrium in the deformed configuratio are as before

$$\frac{\partial}{\partial x}\left(\sigma_{xx} - \theta\tau_{xy}\right) + \frac{\partial}{\partial y}\left(\tau_{xy} - \sigma_{xx}\left(v' - \theta\right) - \sigma_{yy}v'\right) = 0 \tag{7.117}$$

$$\frac{\partial}{\partial x}\left(\theta\sigma_{xx} + \tau_{xy}\right) + \frac{\partial}{\partial y}\left(\sigma_{yy} + \tau_{xy}v'\right) = 0 \tag{7.118}$$

with

$$\theta = \psi - \phi f_w'(y) \tag{7.119}$$

The same process of integration of the firs through the thickness when it is multiplied by 1, y, and $f_w(y)$, and the use of σ_{xx}^a as given above, leads to

$$\frac{\mathrm{d}}{\mathrm{d}x}N = 0 \tag{7.120}$$

$$\frac{\mathrm{d}}{\mathrm{d}x}\left(V + N\psi - \frac{N}{A}\overline{B}\phi\right) = 0 \tag{7.121}$$

$$\frac{\mathrm{d}}{\mathrm{d}x}M + V - N\left(v' - \psi\right) - \frac{N}{A}\overline{B}\phi = 0 \tag{7.122}$$

$$\frac{\mathrm{d}}{\mathrm{d}x}Q - R + \frac{N}{A}\overline{B}\left(v' - \psi\right) + \frac{N}{A}\overline{C}\phi = 0 \tag{7.123}$$

These are the same as before with the difference that the parabolic stress distribution for σ_{xx}^{a} leads to the modificatio of B and C. The constants $\overline{B}$ and $\overline{C}$ are given by

$$\overline{B} = \int_{-h}^{h} \frac{3}{2}\left(1 - \frac{y^2}{h^2}\right) f_w'(y)\,\mathrm{d}y = \frac{12}{35} \tag{7.124}$$

and

$$\overline{C} = \int_{-h}^{h} \frac{3}{2}\left(1 - \frac{y^2}{h^2}\right) f_w'^2(y)\,\mathrm{d}y = \frac{216}{245\,h} \tag{7.125}$$

Returning to Figure 5.2, which shows the generic beam element with end loads, setting $N = -P$ and integrating Equation (7.121) gives

$$V - P\psi + \frac{P}{A}\overline{B}\phi = -H_0 \tag{7.126}$$

When this is used to eliminate V from Equation (7.122), we obtain

$$M' + Pv' = H_0 \tag{7.127}$$

which, when integrated, gives

$$M + Pv = H_0 x + M_0 + Pv_0 \tag{7.128}$$

and when the constitutive relationships for the force resultants are used, the complete system becomes

$$EI\psi' + Pv = H_0 + M_0 + Pv_0 \tag{7.129}$$

$$GA\left(v' - \psi\right) + GB\left(1 + \frac{P}{GA}\frac{\overline{B}}{B}\right)\phi - P\psi = -H_0 \tag{7.130}$$

$$EJ\phi'' - GB\left(1 + \frac{P}{GA}\frac{\overline{B}}{B}\right)\left(v' - \psi\right) - GC\left(1 + \frac{P}{GA}\frac{\overline{C}}{C}\right)\phi = 0 \tag{7.131}$$

Proceeding as before to reduce these to a single equation in ψ, we obtain

$$EIEJGA\psi'''' + \left[EJ\left(G + \frac{P}{A}\right)AP + EI\left(G + \frac{P}{A}\frac{\overline{B}^2}{B}\right)B^2 - GA\left(G + \frac{P}{A}\frac{\overline{C}}{C}\right)C\right]\psi''$$
$$+ \left[\left(G + \frac{P}{A}\frac{\overline{B}}{B}\right)^2 + \left(G + \frac{P}{A}\right)A\left(G + \frac{P}{A}\frac{\overline{C}}{C}\right)C\right]P\psi = \left[\left(G + \frac{P}{A}\right)^2 - \left(G + \frac{P}{A}\right)A\overline{C}\right]H_0 \tag{7.132}$$

As before, we take $\psi = \cos(\pi x/(2l))$ and $H_0 = 0$, as shown in Figure 5.2, and obtain as the equation for P

$$EIEJGA\frac{\pi^4}{16l^4} - \left[EJ\left(G + \frac{P}{A}\right)AP + EI\left(G + \frac{P}{A}\frac{\overline{B}}{B}\right)^2 B^2 - GA\left(G + \frac{P}{A}\frac{\overline{C}}{C}\right)C\right]\frac{\pi^2}{4l^2}$$
$$+P\left[\left(G + \frac{P}{A}\frac{\overline{B}}{B}\right)^2 - \left(G + \frac{P}{A}\right)A\left(G + \frac{P}{A}\frac{\overline{C}}{C}\right)C\right] = 0 \tag{7.133}$$

In this case, it is convenient to use the same set of normalized quantities as earlier, namely,

$$p = \frac{P}{GA} \tag{7.134a}$$

$$\lambda = \frac{\pi h}{2l} \tag{7.134b}$$

$$k_1 = \frac{GB^2h^2}{EAJ} \tag{7.134c}$$

$$k_2 = \frac{GAh^2}{EI} \tag{7.134d}$$

$$\gamma = \frac{AC}{B^2} \tag{7.134e}$$

and to add $\alpha = \overline{B}/B$, $\beta = \overline{C}/C$ in terms of which the equation for relating p and λ becomes

$$\lambda^4 - \left\{k_1\left[(1+\alpha p)^2 - \gamma\,(1+\beta p)\right] + k_2 p\,(1+p)\right\}\lambda^2$$
$$+k_1k_2p\left[(1+\alpha p)^2 - \gamma\,(1+\beta p)\,(1+p)\right] = 0 \tag{7.135}$$

In the derivation so far it has been assumed that the steel reinforcing plates are completely flexibl and provide no resistance to the warping of the cross-section. To include the effect of the plates, it is useful to consider the various terms that contribute to the elastic stored energy of the deformation. These are

(i) bending

$$\frac{1}{2}M\psi' = \frac{1}{2}EI\psi'^2 \tag{7.136}$$

(ii) warping

$$\frac{1}{2}Q\phi' = \frac{1}{2}E\,J\,\phi'^2 \tag{7.137}$$

(iii) shear

$$\frac{1}{2}V\left(v'-\psi\right)+\frac{1}{2}R\phi=\frac{1}{2}GA\left(v'-\psi\right)^2+GB\left(v'-\psi\right)\phi+\frac{1}{2}GC\phi^2 \tag{7.138}$$

When the plates are bent into the shape $\phi(x)f_w(y)$, they add to the stored energy a term W_p (per unit width) of the form

$$W_p=\frac{1}{2}\frac{E_p t_p^3}{12\left(1-\nu_p^2\right)}\phi^2(x)\int_{-h}^{h}\left(f_w''y\right)^2\mathrm{d}y \tag{7.139}$$

where E_p and v_p are the Young's modulus and Poisson's ratio of the plate material and t_p is the plate thickness. For the present form of f_w this becomes

$$W_p=\frac{E_p t_p^3}{\left(1-\nu_p^2\right)}\frac{1}{h^3}\phi^2 \tag{7.140}$$

This contribution must be divided by $t+t_p$ to reduce it to energy per unit width per unit length, and is then added to $GC\phi^2/2$. Thus, the term C in Equation (7.133) is replaced by C^* where

$$C^*=C+\frac{2\,E_p}{G\left(1-\nu_p^2\right)}\frac{t_p^2}{h^3}\frac{1}{t+t_p} \tag{7.141}$$

From the initial definitio of C (Equation 7.109c) we have $C=552/(245h)$, thus

$$C^*=C\left(1+\frac{490}{552}\frac{E_p}{G\left(1-\nu_p^2\right)}\frac{t_p^3}{h^2}\frac{1}{t+t_p}\right) \tag{7.142}$$

The fina form of the equation for p in terms of λ is

$$\begin{aligned}\lambda^4-\left\{k_1\left[(1+\alpha p)^2-\overline{\gamma}\,(1+\beta p)\right]+k_2 p\,(1+p)\right\}\lambda^2\\+k_1k_2p\left[(1+\alpha p)^2-\overline{\gamma}\,(1+\beta p)\,(1+p)\right]=0\end{aligned} \tag{7.143}$$

where

$$\overline{\gamma}=\frac{AC^*}{B^2} \tag{7.144}$$

The solution of this equation for the normalized buckling load as a function of the aspect ratio of the bearing, λ, can be obtained for different values of the reinforcing plate thickness. Examples will be given in the next section.

7.5 Computation of Buckling Loads

In order to use the analysis for the buckling of short uniform beams as a guide in the development of the buckling load for the isolator, it was useful to retain the notation EI and EJ for the bending and warping stiffnesses of the isolator. At this point, it is more convenient to have them expressed in terms of the isolation geometry as follows.

In terms of the half width, h, and the rubber layer thickness, t, we have

$$EI = \frac{8\,Gh^5}{15\,t^2} \tag{7.145}$$

and

$$EJ = \frac{2\,Gh^3}{1225\,t^2} \tag{7.146}$$

from which with

$$A = 2\,h \tag{7.147a}$$

$$B = \frac{24}{21} \tag{7.147b}$$

$$C = \frac{552}{245\,h} \tag{7.147c}$$

$$k_1 = \frac{GB^2h^2}{E\,J\,A} = \frac{400}{S^2} \tag{7.147d}$$

$$k_2 = \frac{GAh^2}{EI} = \frac{15}{4\,S^2} \tag{7.147e}$$

where S is the shape factor of a single layer. The other parameters are

$$\alpha = \frac{\overline{B}}{B} = \frac{3}{10} \tag{7.148a}$$

$$\beta = \frac{\overline{C}}{C} = \frac{9}{23} \tag{7.148b}$$

$$\gamma = \frac{AC}{B^2} = 3.45 \tag{7.148c}$$

and

$$\overline{\gamma} = \gamma\left(1 + \frac{490}{552}\frac{E_p}{G\left(1-\nu_p^2\right)}\frac{t_p^2}{h^2}\frac{t_p}{1+t_p}\right) \tag{7.148d}$$

For purposes of a demonstration example, we will fi the following quantities:

$$
\begin{aligned}
h &= 254\ \text{mm}\,(10\ \text{in}) \\
E_p &= 0.21 \times 10^6\ \text{MPa}\,\left(30 \times 10^6 \text{psi}\right) \\
\nu_p &= 0.3 \\
t &= h/S \\
G &= 0.7\,\text{MPa}\,\left(100\,\text{psi}\right)
\end{aligned}
$$

and evaluate p in terms of λ for a range of shape factors, $S = 5$, 10, 15, 20, and plate thicknesses $t_p = 3.18$ mm (1/8 in), 1.59 mm (1/16 in) and 0.79 mm (1/32 in).

The results of this are shown in Figures 7.6 through 7.9 for values of $\lambda = \pi h/(2l)$ from 1.5 to 4.5, which corresponds to the range of typical isolator geometries. Also included in the diagrams are the normalized buckling loads for the cases of completely rigid plates, which are calculated from

$$\lambda^2 = k_1 \left[(1 + \alpha p)^2 - \overline{\gamma}\,(1 + \beta p)\right] \tag{7.149}$$

and for the cases of completely flexibl plates, which are calculated from Equation (7.135).

The results show that for this choice of isolator and for the typical range of the overall aspect ratio (determined by λ), the influenc of the flexibilit of the reinforcing plates

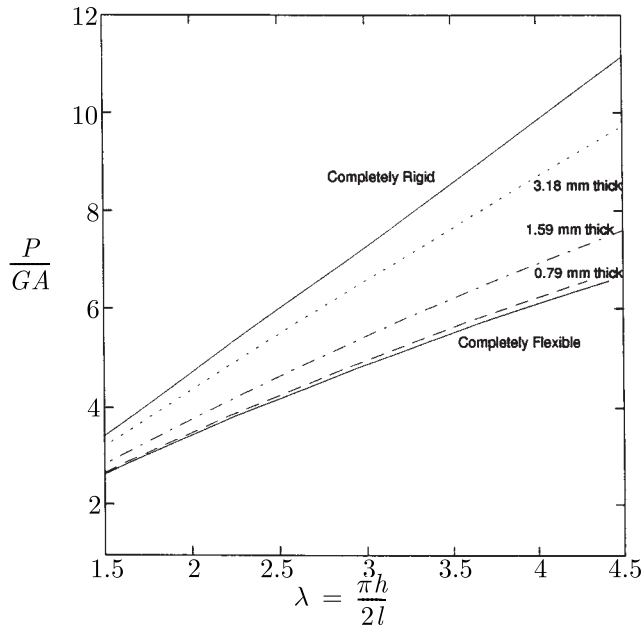

Figure 7.6 Buckling load as a function of bearing height, $S = 5$

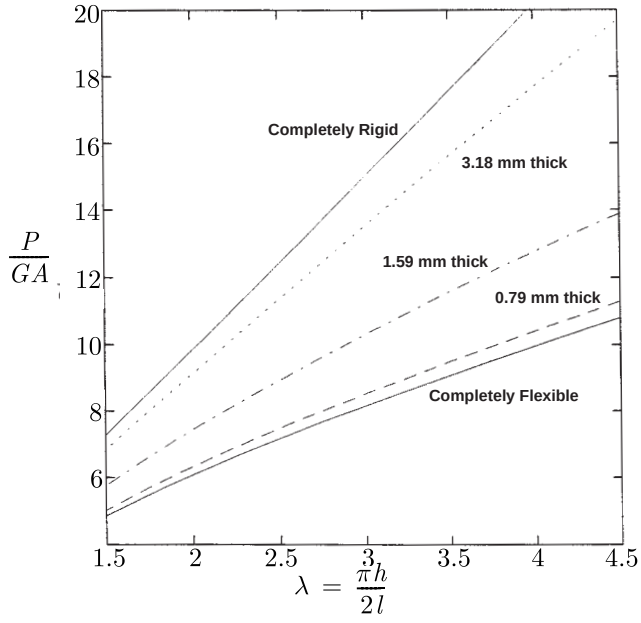

Figure 7.7 Buckling load as a function of bearing height, $S = 10$

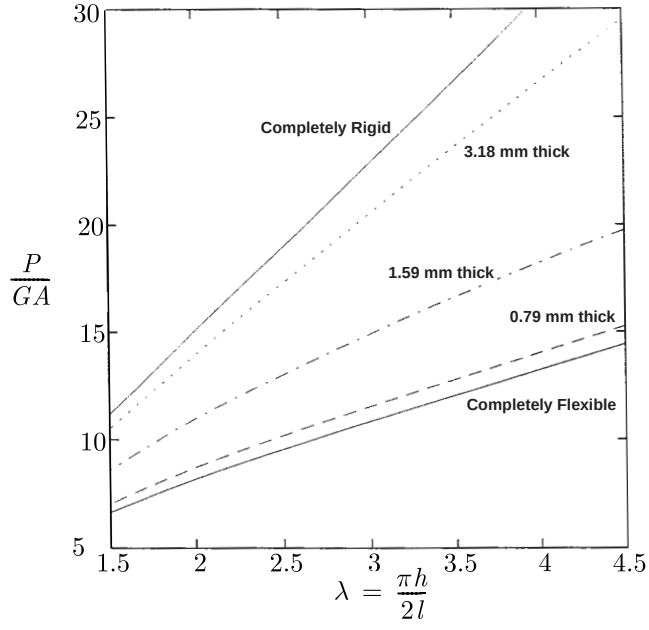

Figure 7.8 Buckling load as a function of bearing height, $S = 15$

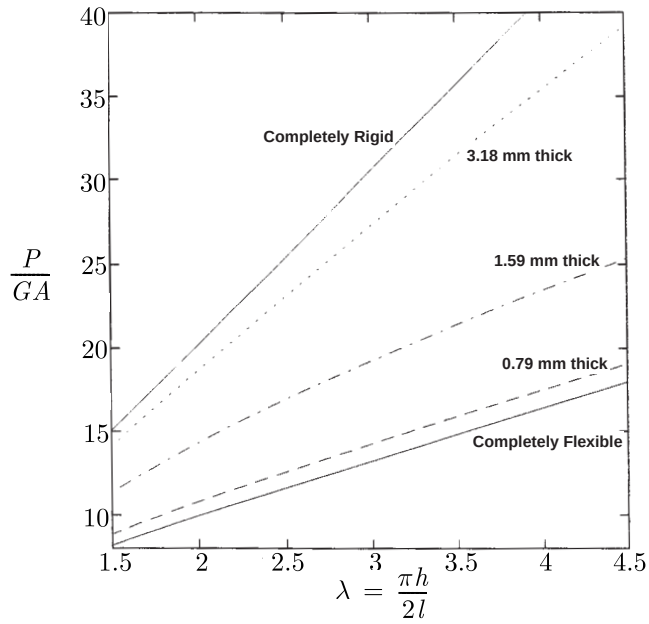

Figure 7.9 Buckling load as a function of bearing height, $S = 20$

is quite significant From completely rigid plates to completely flexibl plates, the drop in the buckling load can be as much as 50%. The most interesting result is that the range of selected plate thicknesses almost completely covers the spread in the buckling load in the sense that the 3.18-mm(1/8 in)-thick plate has almost the same result as the assumed rigid plate, and the 0.79-mm(1/32 in)-thick plate has almost the same result as the assumed fully flexibl plate; thus it would be possible to reduce the thickness below 0.79 mm (1/32 in) with negligible effect on the buckling load. However, there may be practical problems in working with such thin plates. The reinforcing plates have to sustain an axial tension when the isolator carries vertical load, and the capacity of the plate in this mode of response would have to be checked. In addition, the plates are sand-blasted before being bonded to the rubber, and it might not be possible to do this without damaging the plates when they are very thin.

The results of the analysis indicate that although flexibilit of the plates plays a significant role in the behavior of the isolator, it is quantifiable This should be of considerable value in the design of isolators for low-cost applications.

We have shown here an approximate analysis for the buckling load of an multilayer rubber isolator that includes the effect of the flexibilit of the steel reinforcing plates. This analysis has treated the isolator as a short elastic column in which shear deformation and warping of the cross-section are included. The warping of the cross-section is taken to be an independent kinematic quantity and corresponding force resultants have been defined Constitutive equations relating the kinematic quantities that arise in the theory to the force quantities have been developed, and equilibrium equations

have been obtained in the undeformed configuratio for non-buckling problems, and in the deformed configuratio for the buckling problem. Although the theory has been developed for the problem of the buckling of the isolator, a by-product of the analysis is the buckling analysis of short elastic beams of uniform configuratio in which shear and warping are taken into account. Of course, the influenc of shear and warping on the buckling loads of regular beams will not be very important or of practical application, except in extremely short beams where the stresses would be extremely high, and elastic buckling would probably not apply.

The results show that the influenc of warping can be significan for typically sized isolators and for the typical height-to-width ratio. It also shows that to provide an isolator with a buckling load that is negligibly reduced from that obtained from the usual theory with assumed rigid plates, the plates thickness need not be greater than 3.18 mm (1/8 in), and that if the plate thickness is reduced to less than 0.79 mm (1/32 in), there is only a negligible further reduction in the buckling load.

There is increasing interest in several developing countries to use rubber isolators in the earthquake-resistant design of public housing and other local facilities, such as schools and hospitals. For these isolators to be cost-effective in these applications, it will be essential to reduce the steel content, both to reduce cost and to reduce weight to obviate the use of lifting equipment. The results of this analysis show that this should be possible, and this should lead to increased use of this potentially valuable technology in earthquake-prone regions of the developing world.

8

Frictional Restraint on Unbonded Rubber Pads

8.1 Introduction

In Chapter 1 we referred to the patent by the French engineer Eugène Freyssinet on his proposal (1954) for the use of multilayer rubber bearings as bridge supports and his suggestions of several types of steel reinforcement for these bearings. In his patent, it is clear that he envisaged that the rubber layers and the steel plates could be held together only by friction, and in fact he indicated that he thought that friction would be a more reliable method than gluing the rubber and steel together. He also thought, correctly, that the pressure would rise from zero at the edge of a bearing to a maximum at the center, but, mistakenly, that the shear stress between the rubber and steel also varied from zero at the edge to a maximum at the center. We saw in Chapter 2 that this is not the case.

This raises the question as to what the result of using friction and only friction to hold the bearing together can mean for the device. In this chapter, we will examine this through two special cases, namely the long strip pad and the circular pad. The analysis is an extension of the pressure solution for a fully bonded pad, and it will show that the results of Chapter 2 must be modifie if friction is the connecting process, but also that at the high levels of friction that can be attained between rubber and steel, the effect of slip between the rubber and the steel is not very significant In the next chapter, we will describe a theory for a type of unbonded multilayer bearing that is held in place by friction and show test results on such a bearing.

The material in Sections 8.2 and 8.3 firs appeared in the article by Kelly, J. M. and Konstantinidis, D. (2009). "Effect of Friction on Unbonded Elastomeric Bearings." *Journal of Engineering Mechanics* (ASCE), **135**(9), 953–960. DOI 10.1061/(ASCE)EM.1943-7889.0000019. Reproduced with permission from ASCE.

Mechanics of Rubber Bearings for Seismic and Vibration Isolation, First Edition. James M. Kelly and Dimitrios A. Konstantinidis.

8.2 Compression of Long Strip Pad with Frictional Restraint

In this section we are only interested in the theory for a pad in the form of a long strip when the effects of the ends can be neglected, and the strip is taken to be infinite The theory for an arbitrarily shaped pad is given in Chapter 2, and the important points applicable to the analysis of a long strip pad are repeated here for the reader's convenience. We consider a pad of thickness t and width $2b$ and locate a rectangular Cartesian coordinate system, (x, y, z), in the middle surface of the pad, as shown in Figure 8.1(a). Figure 8.1(b) shows the displacements, (u, w), in the coordinate directions under the following assumptions: (i) points on a vertical line before deformation lie on a parabola after loading, and (ii) horizontal planes remain horizontal,

$$\begin{aligned} u(x, z) &= u_0(x)\left(1 - \frac{4z^2}{t^2}\right) \\ w(x, z) &= w(z) \end{aligned} \tag{8.1}$$

This displacement fiel satisfie the constraint that the top and bottom surfaces of the pad are bonded to rigid substrates. The assumption of incompressibility produces a further constraint on the normal components of strain, ε_{xx}, ε_{zz}, in the form

$$\varepsilon_{xx} + \varepsilon_{zz} = \frac{\partial u}{\partial x} + \frac{\partial w}{\partial z} = \frac{\mathrm{d}u_0}{\mathrm{d}x}\left(1 - \frac{4z^2}{t^2}\right) + \frac{\mathrm{d}w}{\mathrm{d}z} = 0 \tag{8.2}$$

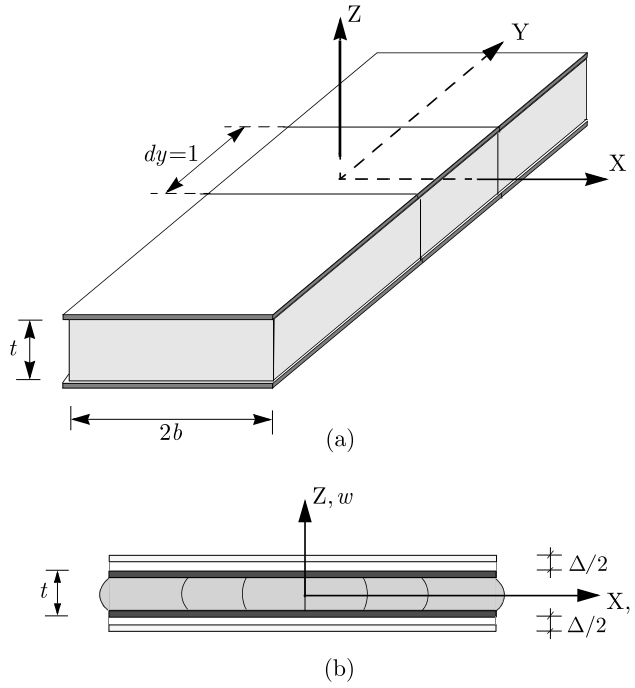

Figure 8.1 Infinitel long rectangular pad showing dimensions

When integrated through the thickness, this gives

$$\frac{\mathrm{d}u_0}{\mathrm{d}x} = \frac{3}{2}\frac{\Delta}{t} = \frac{3}{2}\varepsilon_c \tag{8.3}$$

where Δ is the change of thickness ($\Delta > 0$ in compression), and $\varepsilon_c = \Delta/t$ is the compression strain.

The other assumptions of the theory are that the material is incompressible and that the stress state is dominated by the pressure p in the sense that the normal stress components can be taken as $-p$. The vertical shear stress components are included in the analysis, but the in-plane shear stress is assumed to be negligible. The only equation of stress equilibrium in this case is

$$\frac{\partial \sigma_{xx}}{\partial x} + \frac{\partial \tau_{xz}}{\partial z} = 0 \tag{8.4}$$

which with the assumption that $\sigma_{xx} = \sigma_{zz} = -p$ provides the sole equation of equilibrium

$$\frac{\partial \tau_{xz}}{\partial z} = \frac{\mathrm{d}p}{\mathrm{d}x} \tag{8.5}$$

The assumption of linear elastic behavior means that

$$\tau_{xz} = G\gamma_{xz} = G\left(\frac{\partial u}{\partial z} + \frac{\partial w}{\partial x}\right) = -\frac{8G}{t^2} z u_0 \tag{8.6}$$

This equation together with (8.3) and (8.5) leads to

$$\frac{\mathrm{d}^2 p}{\mathrm{d}x^2} = -\frac{12 G\varepsilon_c}{t^2} \tag{8.7}$$

The boundary condition at the edges of the pad, $p(x = \pm b) = 0$, completes the system for the pressure distribution, $p(x)$. The solution is given by

$$p(x) = \frac{6G\varepsilon_c}{t^2}\left(b^2 - x^2\right) = 6GS^2\varepsilon_c\left(1 - \frac{x^2}{b^2}\right) \tag{8.8}$$

since $S = b/t$. The effective compression modulus E_c of the pad is obtained by integrating $p(x)$ over the area of the pad to determine the resultant load P, i.e., the load per unit length of the strip. The effective compression modulus E_c is then given by

$$E_c = \frac{P}{A\varepsilon_c} = \frac{1}{2b\varepsilon_c}\int_{-b}^{b} p(x)\,\mathrm{d}x = 4GS^2 \tag{8.9}$$

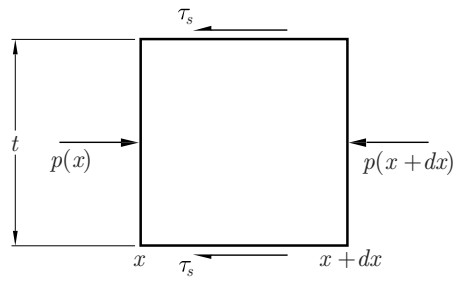

Figure 8.2 Definition of surface shears

The only equation of stress equilibrium in this case remains Equation (8.5). Integration of this through the thickness of the pad with the definitio of the surface shear stresses as shown in Figure 8.2

$$\tau_{xz}\Big|_{z=\frac{t}{2}} = -\tau_s; \quad \tau_{xz}\Big|_{z=-\frac{t}{2}} = \tau_s \tag{8.10}$$

leads, using Equation (8.8), to

$$\tau_s = -\frac{t}{2}\frac{\mathrm{d}p}{\mathrm{d}x} = \frac{6\,G\varepsilon_c}{t}x = 6\,GS\varepsilon_c\frac{x}{b} \tag{8.11}$$

It is clear that the shear stress increases toward the edges, whereas the pressure decreases, and if the constraint is controlled only by friction, that is by

$$\tau_s \leq \mu p \tag{8.12}$$

where μ is the friction coefficient at some point slip must happen. In fact, if the pressure is given by Equation (8.8), τ_s and μp would be equal at

$$\frac{x}{b} = \sqrt{1+\frac{1}{4\,\mu^2 S^2}} - \frac{1}{2\,\mu S} \tag{8.13}$$

For example if $\mu = 1$, then slip occurs for $x = b - t/2$ showing that for the high level of friction typical of rubber against steel, very little slip would take place. On the other hand, if the surface is fully lubricated, such that $\mu = 0$, there will be no shear stress at any point in the pad, and the pressure is given by $E_0\varepsilon_c$, where $E_0 = 3\,G$ is the Young's Modulus of the incompressible material. In most cases of thin bonded pads, this is completely negligible since the E_c of a single bonded layer can be two orders of magnitude larger than this. We will see in the next section that in the case of a pad with partial slip, $E_0\varepsilon_c$ is required as a nonzero boundary condition at the edge of the pad for the homogeneous equation for p.

8.3 The Effect of Surface Slip on the Vertical Stiffness of an Infinit Strip Pad

In order to accommodate the slip at the surface due to the shear stresses overcoming the frictional resistance between the rubber and the steel or concrete, we need to modify the original kinematic assumptions. In this approach, as before, the rubber is assumed incompressible and the pressure is assumed to be the dominant stress component. The kinematic assumption of quadratically variable displacement is supplemented by an additional displacement that is constant through the thickness and is intended to accommodate the squeezing out of the rubber where slip occurs, as shown in Figure 8.3. Thus, in this case the displacement pattern that leads to the pressure solution of Equation (8.8) is replaced by the displacement fiel

$$\begin{aligned} u(x,z) &= u_0(x)\left(1-\frac{4z^2}{t^2}\right)+u_1(x) \\ w(x,z) &= w(z) \end{aligned} \tag{8.14}$$

where $u_1(x) = 0$ for $0 \le x \le x_1$, with x_1 being the location where slip starts.

The constraint of incompressibility consistent with the displacement pattern of Equation (8.14) leads to

$$\frac{\mathrm{d}u_0}{\mathrm{d}x}+\frac{3}{2}\frac{\mathrm{d}u_1}{\mathrm{d}x}=\frac{3}{2}\frac{\Delta}{t}=\frac{3}{2}\varepsilon_c \tag{8.15}$$

The only equation of stress equilibrium in this case is

$$\frac{\partial\sigma_{xx}}{\partial x}+\frac{\partial\tau_{xz}}{\partial z}=0 \tag{8.16}$$

and the assumption of elastic behavior means that

$$\tau_{xz}=G\gamma_{xz} \tag{8.17}$$

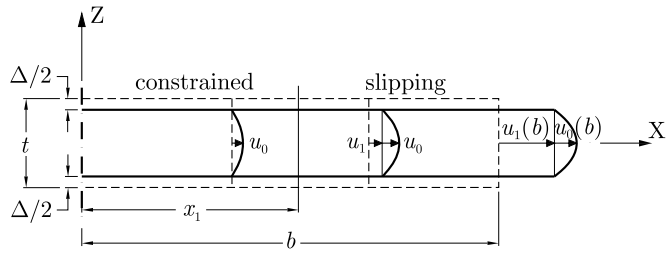

Figure 8.3 Coordinate system and displacement field for a single, infinitel long strip pad with slip

which, with

$$\gamma_{xz} = \frac{\partial u}{\partial z} + \frac{\partial w}{\partial x} = -\frac{8}{t^2} z u_0 \tag{8.18}$$

from Equation (8.14), gives

$$\frac{\partial \sigma_{xx}}{\partial x} = \frac{8\,G}{t^2} u_0 \tag{8.19}$$

which, with the assumption that $\sigma_{xx} = \sigma_{zz} = -p$, provides the sole equation of equilibrium as

$$\frac{\mathrm{d}p}{\mathrm{d}x} = -\frac{8\,G}{t^2} u_0 \tag{8.20}$$

In the region where no slip has occurred, i.e. $0 \le x \le x_1$, the slip displacement is zero and Equation (8.20) can be inverted to give u_0 in terms of pressure and inserted into the incompressibility constraint (Equation 8.15), to give

$$p\,(x) = -\frac{6\,G\varepsilon_c}{t^2} x^2 + Ax + B$$

Symmetry implies that $A = 0$, giving

$$p\,(x) = -\frac{6\,G\varepsilon_c}{t^2} x^2 + B$$

It is convenient to absorb the unknown constant into the other constants and write the pressure as

$$p\,(x) = 6\,G\varepsilon_c \frac{b^2}{t^2}\left(B - \frac{x^2}{b^2}\right) = 6\,GS^2\varepsilon_c\left(B - \frac{x^2}{b^2}\right) \tag{8.21}$$

For $x_1 \le x \le b$, we need to determine $u_1(x)$ subject to the simultaneous requirements that $\tau_s = \mu p$ and $\tau_s = -(t/2)\,\mathrm{d}p/\mathrm{d}x$. This leads to the equation

$$\frac{\mathrm{d}p}{\mathrm{d}x} + \frac{2\,\mu}{t} p = 0 \tag{8.22}$$

which has solution $p(x) = Ce^{-2\mu x/t}$, where C is a constant of integration. To determine it, we use as boundary condition at $x = b$ the fact that $p(b) = E_0\varepsilon_c = 3\,G\varepsilon_c$. Thus for $x_1 \le x \le b$, the pressure is given by

$$p\,(x) = -3\,G\varepsilon_c e^{(2\mu/t)(b-x)} \tag{8.23}$$

and at $x = x_1$, we have continuity in p and $\mathrm{d}p/\mathrm{d}x$ (since τ_s must be continuous across $x = x_1$). From Equations (8.21) and (8.23), we have

$$\begin{aligned} \frac{\mathrm{d}p}{\mathrm{d}x} &= -\frac{12\,G\varepsilon_c}{t^2}x, \quad 0 \le x \le x_1 \\ \frac{\mathrm{d}p}{\mathrm{d}x} &= -3\,G\varepsilon_c\frac{2\,\mu}{t}e^{(2\,\mu/t)(b-x)}, \quad x_1 \le x \le b \end{aligned} \tag{8.24}$$

which in turn gives us the equation for x_1

$$\frac{2\,\mu x_1}{t}e^{(2\,\mu/t)x_1} = \mu^2 e^{(2\,\mu/t)b} \tag{8.25}$$

which can be written in the form

$$2\,\mu S\frac{x_1}{b}e^{2\,\mu S x_1/b} = \mu^2 e^{2\,\mu S} \tag{8.26}$$

The procedure is now to solve for $2\,\mu S x_1/b$ knowing μ and S and then to evaluate $p(x_1)$ from which B can be determined. From this, we calculate τ_s then u_0 from $\tau_s = 4\,\mathrm{G}u_0/t$. Finally the extent of the slip in $x_1 \le x \le b$ is calculated from the equation of incompressibility, Equation (8.15).

We denote $y = 2\,\mu S x_1/b$ and $\lambda = \mu^2 \mathrm{e}^{2\mu S}$ and solve

$$y = \lambda e^{-y} \tag{8.27}$$

The solution of this equation is given by the Lambert W function (Weisstein 2002), $y = W(\lambda)$, and is plotted in Figure 8.4. Since the Lambert W function cannot be expressed in terms of elementary functions, its use here is somewhat limited. Another way to determine y is graphical. Since $\lambda = \mu^2 \mathrm{e}^{2\mu S} > 0$, and the right-hand side of Equation (8.27) always decreases from λ at $y = 0$, and the left-hand side increases from zero, there is always a solution. Figure 8.5 shows this graphical solution for various λ values (descending curves). From the root y, we readily obtain x_1. The two expressions for the pressure at $x = x_1$

$$\begin{aligned} p(x_1^-) &= 6\,GS^2\varepsilon_c\left(B - \frac{x_1^2}{b^2}\right) \\ p(x_1^+) &= 3\,G\varepsilon_c e^{2\,\mu S(1-x_1/b)} \end{aligned} \tag{8.28}$$

are equal because of continuity, giving

$$B = \frac{1}{2\,S^2}e^{2\,\mu S(1-x_1/b)} + \frac{x_1^2}{b^2} \tag{8.29}$$

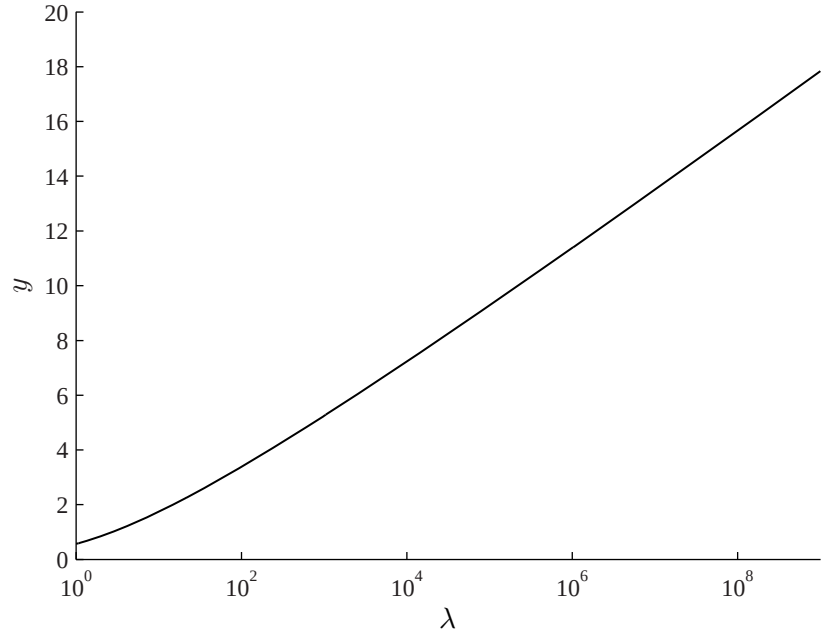

Figure 8.4 The solution for $y = 2\mu S x_1/b$ is given by the Lambert *W* function

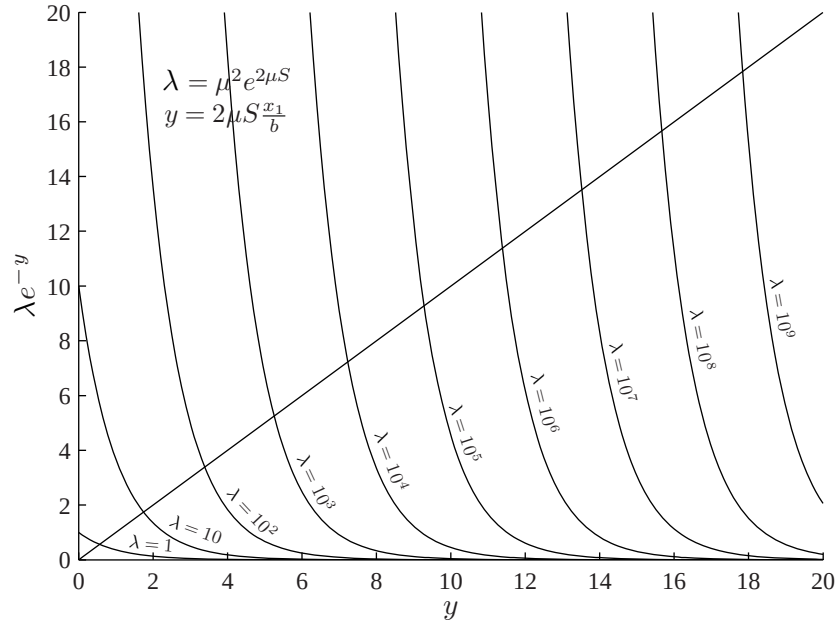

Figure 8.5 Determination of *y* by graphical approach

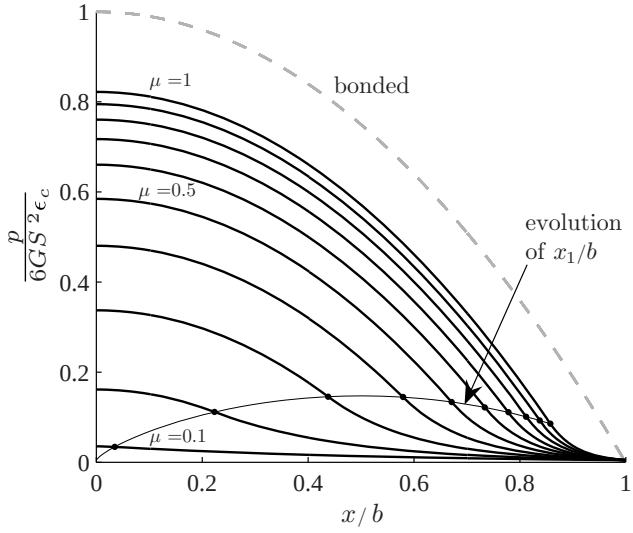

Figure 8.6 Pressure distributions for a strip pad with $S = 10$ and μ ranging from 0.1 to 1 (in increments of 0.1) and for a fully bonded pad

The pressure distribution is then given by

$$\begin{aligned} p(x) &= 6\,GS^2\varepsilon_c\left(B - \frac{x^2}{b^2}\right), \quad 0 \le x \le x_1 \\ p(x) &= 3\,G\varepsilon_c e^{2\,\mu S(1-x/b)}, \quad x_1 \le x \le b \end{aligned} \tag{8.30}$$

Let us take for example the case where $b/t = S = 10$ and $\mu = 0.3$. We get $\lambda = 36.3$, and the result for y is 2.63, from which we have $x_1/b = 0.438$. Equation (8.29) then gives $B = 0.3375$, and the pressure distribution from Equation (8.30) is plotted in Figure 8.6 together with pressure distributions for various other values of μ between 0.1 and 1 and the pressure distribution of a fully bonded pad given by Equation (8.8). We note a considerable reduction in peak pressure with decreasing μ.

The shear stresses that result from this pressure distribution are

$$\begin{aligned} \tau_s &= -\frac{t}{2}\frac{\mathrm{d}p}{\mathrm{d}x} = 6\,GS\varepsilon_c\frac{x}{b}, \quad 0 \le x \le x_1 \\ \tau_s &= -\frac{t}{2}\frac{\mathrm{d}p}{\mathrm{d}x} = 3\,\mu G\varepsilon_c e^{2\,\mu S(1-x/b)}, \quad x_1 \le x \le b \end{aligned} \tag{8.31}$$

In the slipped region, $x_1 \le x \le b$, where $u_1 \neq 0$, use of $\tau_s = 4\,Gu_0/t$ gives

$$u_0 = \frac{3}{4}\,\mu t G\varepsilon_c e^{2\,\mu S(1-x/b)}, \quad x_1 \le x \le b \tag{8.32}$$

We now calculate u_1 from the equation of incompressibility (Equation 8.15), which when integrated from x_1 to $x \geq x_1$ with $u_0(x_1) = (3/2)x_1\varepsilon_c$ and $u_1(x_1) = 0$ gives

$$u_1(x) = \left(x - \frac{\mu t}{2} e^{2\mu S(1-x/b)}\right)\varepsilon_c \tag{8.33}$$

Thus the maximum amount of slip is

$$u_1(b) = \frac{b}{2}\left(2 - \frac{\mu t}{b}\right)\varepsilon_c \tag{8.34}$$

To calculate the value of E_c that is developed when the pad slips, we must integrate the pressure over the range $-b \leq x \leq b$ to determine P and divide by $2b\varepsilon_c$. We have

$$P = 2\varepsilon_c \left[\int_0^{x_1} 6GS^2\left(B - \frac{x^2}{b^2}\right)\mathrm{d}x + \int_{x_1}^{b} 3Ge^{2\mu S(1-x/b)}\mathrm{d}x\right] \tag{8.35}$$

which leads to

$$E_c = \frac{P}{2b\varepsilon_c} = 6GS^2\frac{x_1}{b}\left(B - \frac{x_1^2}{3b^2}\right) + \frac{3G}{2\mu s}\left[e^{2\mu S(1-x_1/b)} - 1\right] \tag{8.36}$$

In the case of $\mu = 0.3$ and $S = 10$ with $B = 0.3375$ and $x_1/b = 0.438$, we have $E_c/(4GS^2) = 0.2149$, which implies a very substantial reduction in the modulus for this value of the coefficien of friction. Similar results for values of μ between 0.1 and 1.0 are given in Table 8.1 and plots of x_1/b and $E_c/(4GS^2)$for these values are shown in Figure 8.7.

Table 8.1 Compression modulus of strip pad for different friction coefficient ($S = 10$)

μ	y	$\frac{x_1}{b}$	B	$\frac{E_c}{4GS^2}$
0.1	0.069	0.035	0.036	0.024
0.2	0.894	0.223	0.162	0.089
0.3	2.626	0.438	0.338	0.215
0.4	4.634	0.579	0.480	0.346
0.5	6.710	0.671	0.585	0.457
0.6	8.803	0.734	0.660	0.544
0.7	10.898	0.778	0.717	0.613
0.8	12.990	0.812	0.761	0.668
0.9	15.076	0.838	0.795	0.712
1.0	17.158	0.858	0.822	0.748

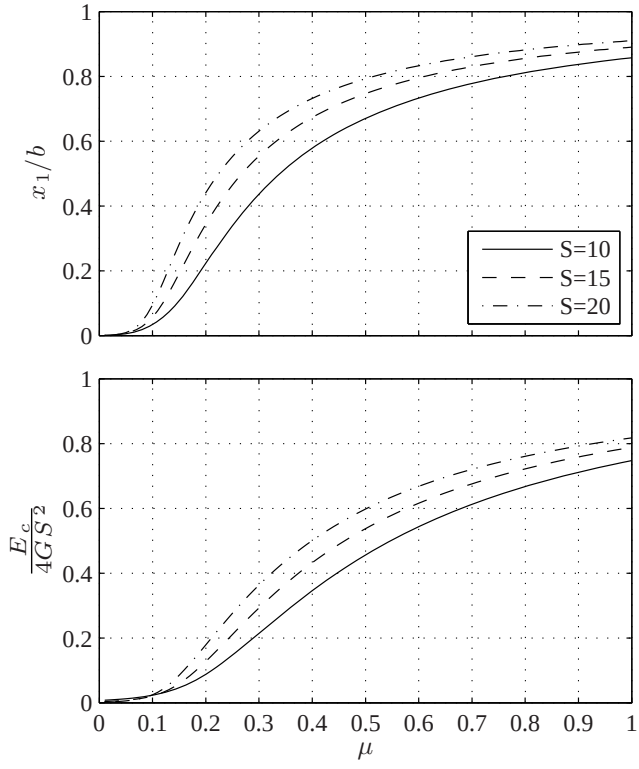

Figure 8.7 *Top*: location where slip initiates for a long strip pad. *Bottom*: compression modulus as a fraction of the compression modulus of a fully bonded strip pad

8.4 The Effect of Surface Slip on the Vertical Stiffness of a Circular Pad

The previous analysis for the unbonded pad in the form of a long strip can be extended to the case of the circular pad of radius R. In this case the displacement pattern that is the starting point of the analysis is

$$\begin{aligned} u(r,z) &= u_0(r)\left(1-\frac{4z^2}{t^2}\right)+u_1(r) \\ w(r,z) &= w(z) \end{aligned} \tag{8.37}$$

where $u_1(r)=0$ for $0 \le r \le r_1$, with r_1 being the radius at which the slip starts.

The strains in the rubber in polar coordinates (r,θ,z) are

$$\begin{aligned} \varepsilon_r &= \frac{\partial u}{\partial r} \quad \varepsilon_\theta = \frac{u}{r} \quad \varepsilon_z = \frac{\partial w}{\partial z} \\ \gamma_{rz} &= \frac{\partial u}{\partial z} \quad \gamma_{\theta z}=0 \quad \gamma_{r\theta}=0 \end{aligned} \tag{8.38}$$

The three normal strains when computed using Equation (8.37) are

$$\varepsilon_r = \frac{\mathrm{d}u_0}{\mathrm{d}r}\left(1 - \frac{4z^2}{t^2}\right) + \frac{du_1}{dr} \qquad \varepsilon_\theta = \frac{u_0}{r}\left(1 - \frac{4z^2}{t^2}\right) + \frac{u_1}{r} \qquad \varepsilon_z = \frac{\mathrm{d}w}{\mathrm{d}z} \tag{8.39}$$

The constraint of incompressibility $\varepsilon_r + \varepsilon_\theta + \varepsilon_z = 0$ consistent with the displacement pattern of Equation (8.37) leads, after integration through the thickness, to

$$\frac{1}{r}\frac{\mathrm{d}}{\mathrm{d}r}(ru_0) + \frac{3}{2}\frac{1}{r}\frac{\mathrm{d}}{\mathrm{d}r}(ru_1) = \frac{3}{2}\varepsilon_c \tag{8.40}$$

The only shear stress component is $\gamma_{rz} = \partial u/\partial z = -8u_0 z/t^2$, and the assumption of elastic behavior means that

$$\tau_{rz} = G\gamma_{rz} = -\frac{8G}{t^2}zu_0 \tag{8.41}$$

The equations of stress equilibrium in polar coordinates are

$$\begin{aligned} \frac{\partial \sigma_r}{\partial r} + \frac{\partial \tau_{rz}}{\partial z} + \frac{\sigma_r - \sigma_\theta}{r} &= 0 \\ \frac{\partial \tau_{rz}}{\partial r} + \frac{\partial \sigma_z}{\partial z} + \frac{\tau_{rz}}{r} &= 0 \end{aligned} \tag{8.42}$$

which with the assumption that the normal stresses are all equal to the negative pressure $-p$, reduces the firs to

$$\frac{\partial \tau_{rz}}{\partial z} = \frac{\mathrm{d}p}{\mathrm{d}r} \tag{8.43}$$

and the second can be used to determine the distribution of pressure through the thickness of the pad. Equation (8.43) with the result from Equation (8.41) gives

$$\frac{dp}{dr} = -\frac{8G}{t^2}u_0 \tag{8.44}$$

In the region where no slip has occurred, i.e., $0 \le r \le r_1$, the slip displacement is zero, and Equation (8.44) can be inverted to give u_0 in terms of p and inserted into the incompressibility constraint (Equation 8.40), to give

$$p(r) = -\frac{3G\varepsilon_c}{t^2}r^2 + A\ln r + B$$

Regularity at $r = 0$ implies that $A = 0$, giving

$$p(r) = -\frac{3G\varepsilon_c}{t^2}r^2 + B \tag{8.45}$$

It is convenient to absorb the unknown constant into the other constants and write the pressure as

$$p(r) = 3G\varepsilon_c \frac{R^2}{t^2}\left(B - \frac{r^2}{R^2}\right) \tag{8.46}$$

If there were no slip anywhere, we could use $p(R) = 0$ to determine B and get $p(r) = (3G\varepsilon_c/t^2)(R^2 - r^2)$, which is the same result we obtained in Chapter 2 for the bonded circular pad. It is convenient to express this in terms of the shape factor S, which for the circular pad is $R/(2t)$, with which Equation (8.46) becomes

$$p(r) = 12GS^2\varepsilon_c\left(B - \frac{r^2}{R^2}\right) \tag{8.47}$$

The maximum value of the pressure when there is no slip is $12GS^2\varepsilon_c$ which we will use later for comparison purposes.

For $x_1 \le r \le R$, we need to determine $u_1(r)$ subject to the simultaneous requirements that $\tau_s = \mu p$ and $\tau_s = -(t/2)\mathrm{d}p/\mathrm{d}r$. This leads to the equation

$$\frac{\mathrm{d}p}{\mathrm{d}r} + \frac{2\mu}{t}p = 0 \tag{8.48}$$

This equation has the solution $p(r) = Ce^{-2\mu r/t}$, where C is a constant of integration. To determine it, we use as the boundary condition at $r = R$ the fact that $p(R) = E_0\varepsilon_c = 3G\varepsilon_c$. Thus for $r_1 \le r \le R$, the pressure is given by

$$p(r) = 3G\varepsilon_c e^{(2\mu/t)(R-r)} \tag{8.49}$$

and at $r = r_1$, we have continuity in p and $\mathrm{d}p/\mathrm{d}r$ (since τ_s must be continuous $r = r_1$). Differentiating Equations (8.46) and (8.49) and equating them, we obtain

$$\left.\frac{\mathrm{d}p}{\mathrm{d}r}\right|_{r=r_1} = -\frac{6G}{t^2}r_1\varepsilon_c = -3G\varepsilon_c\left(\frac{2\mu}{t}\right)e^{(2\mu/t)(R-r_1)} \tag{8.50}$$

which in turn gives

$$\frac{2\mu r_1}{t}e^{(2\mu/t)r_1} = 2\mu^2 e^{(2\mu/t)R} \tag{8.51}$$

or, in terms of S,

$$4\mu S\frac{r_1}{R}e^{4\mu Sr_1/R} = 2\mu^2 e^{4\mu S} \tag{8.52}$$

Letting $y = 4\mu Sr_1/R$ and $\lambda = 2\mu^2 e^{4\mu S}$, this equation reduces to

$$y = \lambda e^{-y} \tag{8.53}$$

which has the same form as in the case of the strip pad, except that y and λ are define differently. As discussed earlier, the solution to this equation is the Lambert W function, $y = W(\lambda)$, although it is more practical to obtain the solution graphically. Once y has been determined, r_1/R is also known. $p(r_1^+)$ can then be computed from Equation (8.49). From continuity, $p(r_1^-) = p(r_1^+)$, therefore Equations (8.47) and (8.49) give

$$B = \frac{1}{4\,S^2} e^{4\,\mu S(1-r_1/R)} + \frac{r_1^2}{R^2} \tag{8.54}$$

Let us take for example the case where $S = 10$ and $\mu = 0.3$. We have $\lambda = 0.18e^{12}$, and the result for y is 8.18, from which we have $r_1/R = 0.682$. Substituting into Equation (8.54) gives $B = 0.5787$. The corresponding pressure distribution is plotted in Figure 8.8. We note that $p_{\max} = p(0) = 694\,G\varepsilon_c$, and if fully bonded this would be $p_{\max} = 12\,GS^2\varepsilon_c = 1200\,G\varepsilon_c$, implying that slip for this value of friction has reduced the peak pressure by almost one half. The figu e also shows pressure distributions for various other values of μ between 0.1 and 1 and the pressure distribution of a fully bonded pad.

The shear stresses corresponding to the pressure distributions given by Equations (8.47) and (8.49) are

$$\begin{aligned} \tau_s &= -\frac{t}{2}\frac{\mathrm{d}p}{\mathrm{d}r} = 6\,G\frac{r}{t}\varepsilon_c = 12\,GS\varepsilon_c\frac{r}{R}, \quad 0 \le r \le r_1 \\ \tau_s &= -\frac{t}{2}\frac{\mathrm{d}p}{\mathrm{d}r} = 3\,\mu G\varepsilon_c e^{4\,\mu S(1-r/R)}, \quad r_1 \le r \le R \end{aligned} \tag{8.55}$$

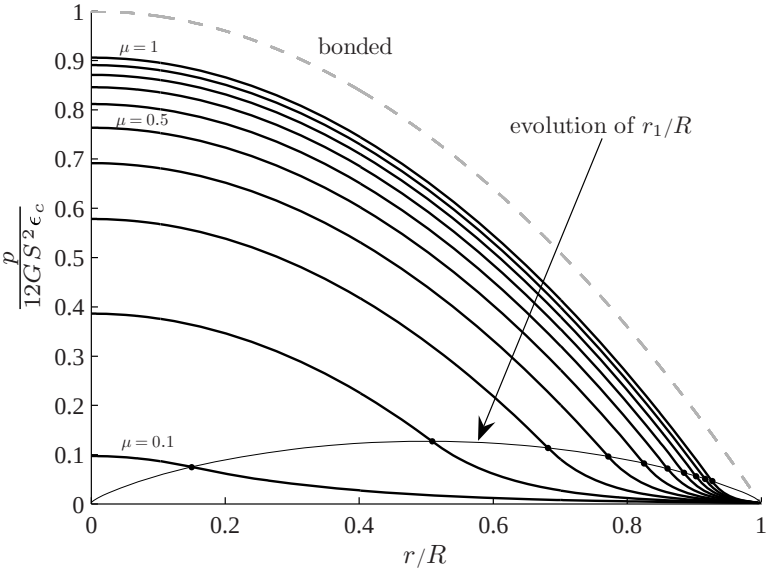

Figure 8.8 Pressure distributions for a circular pad with $S = 10$ and μ ranging from 0.1 to 1 (in increments of 0.1) and for a fully bonded pad

In the slipped region, $r_1 \le r \le R$, where $u_1 \neq 0$, use of $\tau_s = 4Gu_0/t$ gives

$$u_0 = \frac{3}{4}\mu t\varepsilon_c e^{4\mu S(1-r/R)}, \quad r_1 \le r \le R \tag{8.56}$$

We now calculate u_1 from the equation of incompressibility (Equation 8.40), which when integrated from to r_1 to $r \ge r_1$ with $u_0(r_1) = (3/4)\, r_1\varepsilon_c$ and $u_1(r_1) = 0$ gives

$$u_1(r) = \frac{\varepsilon_c}{2}\left(r - \mu t e^{4\mu S(1-r/R)}\right), \quad r_1 \le r \le R \tag{8.57}$$

Thus the maximum amount of slip is

$$u_1(R) = \frac{\varepsilon_c}{2}(R - \mu t) \tag{8.58}$$

To calculate the value of E_c that is developed when the pad slips we must integrate the pressure over the range $0 \le r \le R$ to determine P and divide by $A\varepsilon_c = \pi R^2\varepsilon_c$. We have,

$$P = 2\pi\varepsilon_c\left[\int_0^{r_1} 12GS^2\left(B - \frac{r^2}{R^2}\right) r\,\mathrm{d}r + \int_{r_1}^{R} 3Ge^{4\mu S(1-r/R)} r\,\mathrm{d}r\right] \tag{8.59}$$

which leads to

$$\frac{E_c}{6GS^2} = \int_0^{r_1} 4\left(B - \frac{r^2}{R^2}\right)\frac{r}{R^2}\mathrm{d}r + \int_{r_1}^{R}\frac{1}{S^2}e^{4\mu S(1-r/R)}\frac{r}{R^2}\mathrm{d}r \tag{8.60}$$

The result is

$$\frac{E_c}{6GS^2} = 2B\frac{r_1^2}{R^2} - \frac{r_1^4}{R^4} + \frac{1}{S^2}\frac{(1+4\mu S r_1/R)\,e^{4\mu S(1-r_1/R)} - (1+4\mu S)}{(4\mu S)^2} \tag{8.61}$$

In the case of $\mu = 0.3$ and $S = 10$ with $B = 0.5787$ and $r_1/R = 0.682$, we have $E_c/(6GS^2) = 0.350$, which implies a significan reduction in the modulus for this value of friction coefficient Similar results for values of μ between 0.1 and 1.0 are given in Table 8.2 and plots of r_1/R and $E_c/(6GS^2)$ for these values are shown in Figure 8.9.

The analysis in this chapter has concentrated on a single pad, either long strip or circular, that is held in place between rigid surfaces only by friction. One purpose of this has been to quantify the suggestion of Freyssinet that friction might be more reliable than gluing the rubber to steel when constructing a multilayer bearing. He seemed not to be confiden in the glues that were available for this purpose at that time. Of course the subsequent development of bonding compounds with very reliable properties has eliminated this concern. There may, however, be a few situations where unbonded single layers are used in technical applications.

Table 8.2 Compression modulus of circular pad for different friction coefficient ($S = 10$)

μ	y	$\frac{r_1}{R}$	B	$\frac{E_c}{6\,GS^2}$
0.1	0.600	0.150	0.097	0.031
0.2	4.071	0.509	0.386	0.172
0.3	8.183	0.682	0.579	0.350
0.4	12.347	0.772	0.692	0.489
0.5	16.503	0.825	0.763	0.590
0.6	20.644	0.860	0.812	0.664
0.7	24.770	0.885	0.846	0.719
0.8	28.884	0.903	0.871	0.762
0.9	32.986	0.916	0.891	0.795
1.0	37.080	0.927	0.906	0.822

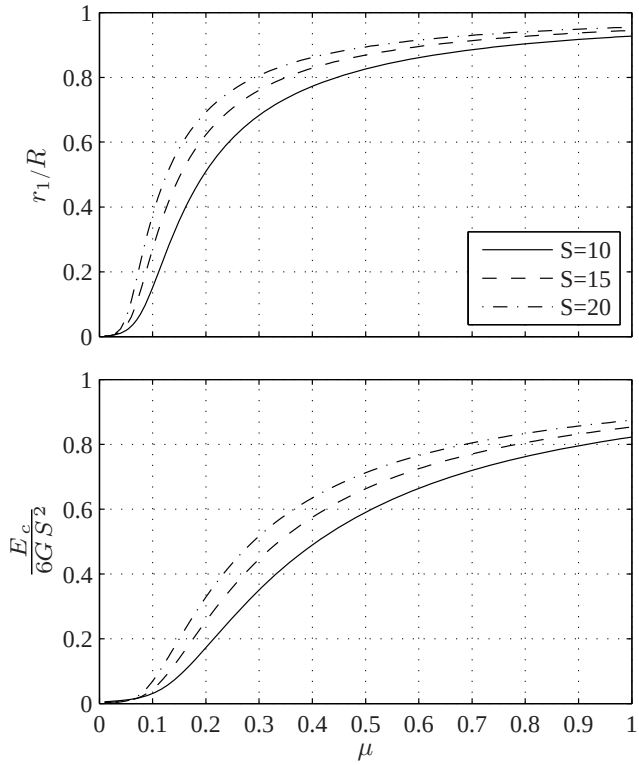

Figure 8.9 *Top*: location where slip initiates for a circular pad. *Bottom:* compression modulus as a fraction of the compression modulus of a fully bonded circular pad

The real value of the analysis in this chapter is to a type of bearing that we will cover in detail in the following chapter. We will extend the analysis of this chapter to a type of multilayer bearing where the reinforcing steel sheets are bonded to the rubber, but the top and bottom of the bearing are held in place only by friction. Eliminating the heavy end-plates leads to a potential seismic or vibration isolator that is much lighter than a conventional isolator and possibly much less expensive. The theory for the single pad is extended in the next chapter to this type of bearing. A very common application of this unbonded bearing is to accommodate non-seismic lateral motions due to traff c loads and thermal expansions and contractions in highway bridges.

9

Effect of Friction on Unbonded Rubber Bearings

This chapter describes the mechanics of a type of multilayer rubber bearing that is currently used very widely as a standard thermal expansion bridge bearing, but could also be used as a lightweight low-cost rubber isolator for application to housing, schools and other public buildings in highly seismic areas of the developing world. A characteristic of these bearings is that the reinforcing steel shims (normally thick and inflexibl in conventional seismic isolators) are thin and flexible In an effort to determine the ultimate lateral displacement of these bearings, the analysis assumes that the steel shims are in fact completely without flexura stiffness, which is in contrast to the analysis done for conventional rubber isolators, where the steel shims are typically assumed to be perfectly rigid, both in extension and flexu e. The assumption that the shims are perfectly flexibl is not entirely accurate, but it allows us to determine a lower bound to the ultimate lateral displacement of the bearing.

Another very important characteristic of the bearings examined in this chapter is that they do not have thick steel end-plates, which reduces their weight, but also means that they are not bonded to the upper and lower support surfaces; thus, they are held in place only by friction. This at firs sight might seem to be a deficienc of this design, but it has the advantage that it eliminates the presence of tensile stresses in the bearings. It is these tensile stresses and the bonding requirements that arise from them that lead to the high costs of the conventional rubber isolation bearings.

An approximate theoretical analysis of the ultimate displacement of these bearings suggests, and test results confirm that it is possible to produce an unbonded strip- or rectangular-shaped isolator that matches the behavior of a conventional seismic isolator. The unbonded isolator is significantl lighter, and, because it can be made by a much

---

The material in Section 9.4 firs appeared in the article by Kelly, J. M. and Konstantinidis, D. (2009). "Effect of Friction on Unbonded Elastomeric Bearings." *Journal of Engineering Mechanics* (ASCE), **135(**9), 953–960. DOI 10.1061/(ASCE)EM.1943-7889.0000019. Reproduced with permission from ASCE.

Mechanics of Rubber Bearings for Seismic and Vibration Isolation, First Edition. James M. Kelly and Dimitrios A. Konstantinidis.

less labor-intensive manufacturing process, it is significantl cheaper than a conventional seismic isolator. A further advantage of a strip isolator is that it can be easily used in buildings with masonry walls.

9.1 Introduction

Recent earthquakes in India, Turkey and South America have emphasized the fact that the major loss of life in earthquakes happens when the event occurs in developing countries. Even in relatively moderate earthquakes in areas with poor housing, many people are killed by the collapse of brittle, heavy, unreinforced masonry or poorly constructed concrete buildings. Modern structural control technologies, such as active control or energy dissipation devices, can do little to alleviate this, but it is possible that seismic isolation could be adopted to improve the seismic resistance of poor housing and other buildings such as schools and hospitals in developing countries.

The theoretical basis of seismic isolation (Kelly 1997) shows that the reduction of seismic loading produced by the isolation systems depends primarily on the ratio of the isolation period to the fixed-bas period. Since the fixed-bas period of a masonry-block or brick building may be of the order of 0.1 s, an isolation period of 1.0 s or longer would provide a significan reduction in the seismic loads on the building and would not require a large isolation displacement. For example, the current code for seismic isolation (ICC 2009) has a formula for minimum isolator displacement, which, for a 1.5-s system, would be around 15 cm (6 in).

The problem with adopting seismic isolation in developing countries is that conventional isolators are large, expensive, and heavy. An individual isolator can weigh one ton or more and cost as much as $10 000. To extend this valuable earthquake-resistant strategy to housing and commercial buildings, it is necessary to reduce the cost and weight of the isolators. The primary weight in an isolator is due to the end-plates and the steel reinforcing plates which are used to provide the vertical stiffness of the rubber–steel composite element. A typical rubber isolator has two large end-plates, each at least 25 mm (1 in) thick, and 20–30 or more thin reinforcing plates, each typically 3.18 mm (1/8 in) thick. The high cost of producing the isolators results from the labor involved in preparing the steel plates and laying-up of the rubber sheets and steel plates for vulcanization bonding in a mold. The steel plates are cut, sand-blasted, acid-cleaned, and then coated with bonding compound. Next, the compounded rubber sheets with the interleaved steel plates are put into a mold and heated under pressure for several hours to complete the manufacturing process. The research outlined in this chapter suggests that both the weight and the cost of isolators can be reduced by using thinner steel reinforcing plates, no end-plates and no bonding to the support surfaces. Since the demands on the bonding between the rubber and the reinforcing plates are reduced, a simpler and less expensive manufacturing process can be used.

The manufacturing process for conventional isolators has to be done very carefully because the testing requirements in the current codes for seismic isolation require that the isolators be tested under very extreme loading conditions prior to use. The bond between the rubber and the steel reinforcement and between the rubber and the

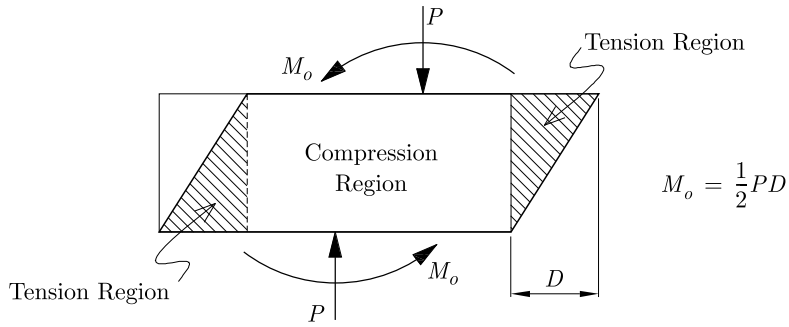

Figure 9.1 Tensile-stress regions produced by the presence of unbalanced moments in a bonded bearing

end-plates must be very good to survive these tests. The effect of a large shear displacement of the isolator is to generate an unbalanced moment that must be equilibrated by tensile stresses, as shown in the diagram in Figure 9.1. The compression load is carried through the overlap region between top and bottom surfaces, and the unbalanced moment is carried by tension stresses in the regions outside the overlap.

Bridge bearings are much less expensive than seismic bearings for buildings. The in-service demands that the former are expected to satisfy are of course much lower, but tests on the response of unbonded rubber bridge bearings to seismic level displacements (Konstantinidis *et al.* 2008) have shown that even if such large displacements are applied to them, they can deform without damage. The primary reason for this is the fact that the top and bottom surfaces can roll off the support surfaces (Figure 9.2), and no tension stresses are produced. The unbalanced moments are resisted by the vertical load through offset of the force resultants on the top and bottom surfaces (Figure 9.3).

The bearings in the tests survived very large shear strains, comparable to those expected of conventional seismic isolators under seismic loading. However, their cost is in the hundreds of dollars as compared to the cost of conventional isolators in the thousands of dollars. In this chapter, we will describe the various aspects of this type

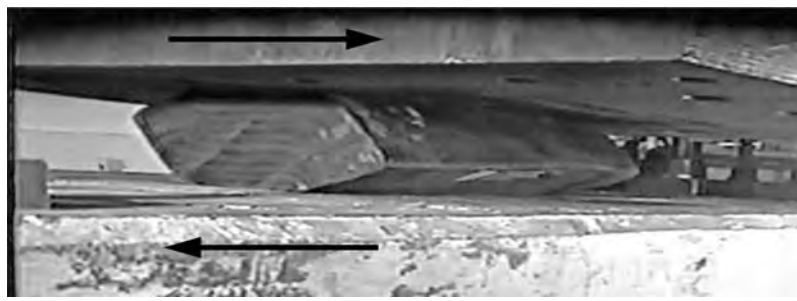

Figure 9.2 The corners of an unbonded rubber bearing rolling off the top and bottom supports as the bearing is sheared (to a displacement approximately 1.5 times the total rubber thickness of the bearing) in the direction pointed by the arrows

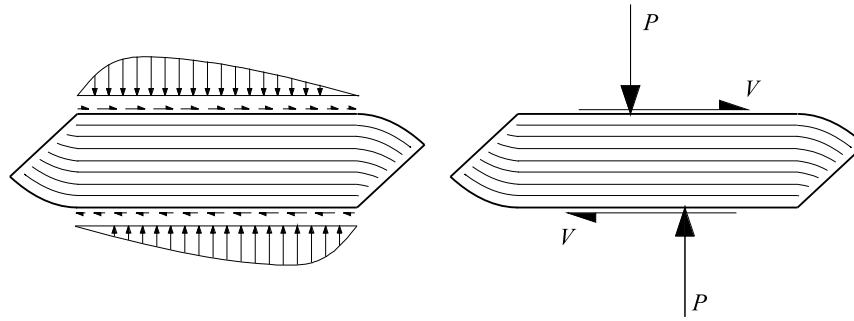

Figure 9.3 *Left*: Normal and shear stress distributions on the top and bottom faces of the unbonded bearing in its deformed shape. *Right*: The moment created by the offset of the resultant compressive loads, *P*, balances the moment created by the shear, *V*

of thermal expansion bridge bearing, which could be used as a lightweight, low-cost rubber seismic isolator for application to housing, schools and other public buildings in earthquake prone areas of the developing world. The most important aspect of these bearings is that, not having end-plates, they are not bonded to the upper and lower support surfaces and are held in place only by friction.

In the later part of the chapter, we examine the behavior of unbonded rubber bearings under vertical load and show that slip between the unbonded surfaces and rigid supports above and below can have a significan influenc on the vertical stiffness and the internal pressure distribution.

9.2 Bearing Designs and Rubber Properties

Figure 9.4 is a photograph of a typical unbonded multilayer rubber bearing, and Figure 9.5 shows its cross-section. The particular bearing was manufactured by Scougal Rubber Corporation. The rubber compound is Neoprene (polychloroprene) with a specifie hardness of 55 on the Shore A scale. Each intermediate rubber layer is 12 mm (0.47 in) thick, while the top and bottom rubber layers are 6 mm (0.24 in) thick. A 3-mm (0.12 in) protective cover surrounds the bearing on the sides. The bearings are laminated with 1.9-mm-thick (14-ga) A1011 steel shims. Table 9.1 shows detailed geometric properties for two typical-size rubber bridge bearings.

9.3 Ultimate Displacement of Unbonded Bearings

The highly favorable response of an isolator which is not bonded to the top or bottom plates is due to the elimination of tension in the rubber. In a bonded bearing under the simultaneous action of shear and compression, the presence of an unbalanced moment at both top and bottom surfaces produces a distribution of tensile stresses in the triangular region outside the overlap between top and bottom (Figure 9.1). The compression load is carried through the overlap area, and the triangular regions created by the shear

Figure 9.4 A 120-mm-tall unbonded multilayer rubber bearing (plan dimensions: 375 × 575 mm).

displacement provide the tensile stresses to balance the moment. These tensile stresses must be sustained by the rubber and also by the bonding between the rubber and the steel reinforcing plates. The provision of these bonding requirements is the main reason for the high cost of current designs of isolator bearings for buildings. With the elimination of these tension stresses, the bonding requirements for unbonded bridge bearing are reduced.

In unbonded multilayer rubber bridge bearings, the steel reinforcing plates are relatively thin as compared with the reinforcing in current designs of building seismic isolators. This flexibilit allows the unbonded surfaces to roll off the loading surfaces and thus relieves the tensile stresses that would be produced if the top and bottom surfaces of the bearing were bonded. This in turn puts much lower demands on the internal bonding between the rubber layers and reinforcing steel plates.

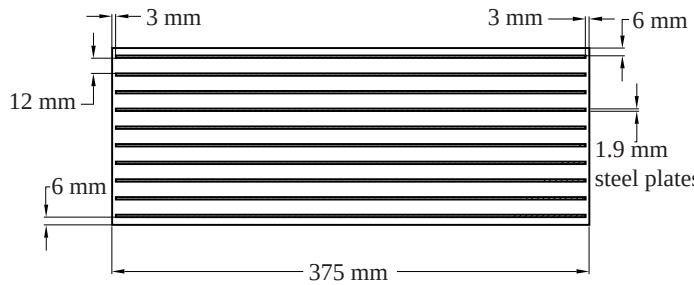

Figure 9.5 Cross-section of 120-mm-tall unbonded steel-laminated rubber bearing

Table 9.1 Geometric characteristics of the steel–laminated rubber bearings

Bearing designation	Rubber height [mm (in)]	Number of steel shims	Total height [mm (in)]	Width [mm (in)]	Depth [mm (in)]
S-48	48.0 (1.89)	4	55.6 (2.19)	375.0 (14.76)	575.0 (22.64)
S-120	120.0 (4.72)	10	139.0 (5.47)	375.0 (14.76)	575.0 (22.64)

Experimental results (Konstantinidis *et al.* 2008) show that the roll-off response is limited by the fact that the free edge of the bearing rotates from the vertical towards the horizontal with increasing horizontal displacement, and the limit of this process is reached when the originally vertical surfaces at each side come in contact with the horizontal support surfaces at both top and bottom. Further horizontal displacement beyond this point can only be achieved by slip. The friction factor between rubber and other surfaces can often take very large values, possibly as high as 1, and slip can produce damage to the bearing through tearing of the surface, distortion of the reinforcing steel and heat generated by the sliding motion. Thus the maximum displacement for a bearing of this type can be specifie as that which transforms the vertical free edge to a horizontal plane. In the normal situation, where the bearing thickness is small in comparison with the plan dimension in the direction of loading, this can be estimated by studying only the deformation of one side and neglecting the interaction between the deformations at each end.

The basic assumptions used in the development of the prediction of the limiting shear deformation are:

(1) the material is incompressible;
(2) the plates are completely flexible
(3) the free surface of the roll-off portion is stress free.

The firs two are reasonable for the rubber and reinforcement of these bearings, and the third means that the displacement when the vertical surface touches the horizontal support is the length of the curved arc of the free surface.

The geometry assumed in the derivation is shown in Figure 9.6. The thickness of the bearing is 1, the length of the horizontal surface is a, and we assume that the curved free

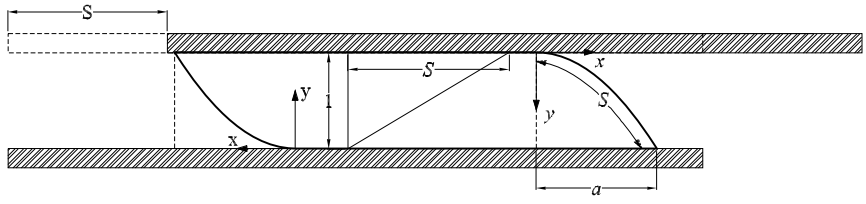

Figure 9.6 Schematic of the deformed unbonded bearing

surface is a parabolic arc; then in the coordinate system (x, y) shown in Figure 9.6, the curved surface is given by

$$y = \frac{x^2}{a^2}, \quad \text{or} \quad x = a\sqrt{y} \tag{9.1}$$

The area of the region enclosed by the curved arc of length S is

$$A = \int_0^1 \mathrm{d}y \int_0^{a\sqrt{y}} \mathrm{d}x = \frac{2}{3}a \tag{9.2}$$

The requirement of incompressibility means that the volume before deformation and after are preserved. Thus,

$$\frac{1}{2}S = \frac{2}{3}a \quad \text{or} \quad a = \frac{3}{4}S \tag{9.3}$$

The curved arc length S is given by

$$\mathrm{d}S = \sqrt{\mathrm{d}x^2 + \mathrm{d}y^2} \tag{9.4}$$

where

$$\mathrm{d}y = \frac{2x}{a^2}\mathrm{d}x \tag{9.5}$$

and

$$S = \int_0^a \sqrt{1 + \frac{4x^2}{a^4}}\mathrm{d}x \tag{9.6}$$

Using the change of variable $u = 2x/a^2$, we have

$$S = \frac{a^2}{2}\int_0^{2/a} \sqrt{1 + u^2}\mathrm{d}u \tag{9.7}$$

Letting $u = \sinh t$, we have

$$S = \frac{a^2}{2}\int_0^{\sinh^{-1}(2/a)} \cosh^2 t \mathrm{d}t \tag{9.8}$$

Since $\cosh^2 t = (\cosh(2t) + 1)/2$, this leads to

$$S = \frac{a^2}{4}[\sinh t \cosh t + t]_0^{\sinh^{-1}(2/a)} \tag{9.9}$$

and with $\cosh t = \sqrt{1 + \sinh^2 t}$, we have

$$S = \frac{a^2}{4}\left(\frac{2}{a}\sqrt{1 + \frac{4}{a^2}} + \sinh^{-1}\left(\frac{2}{a}\right)\right) \tag{9.10}$$

The incompressibility condition requires that $S = 4a/3$, leading to an equation for a in the form

$$\sinh^{-1}\left(\frac{2}{a}\right) = \frac{16}{3a} - \frac{2}{a}\sqrt{1 + \frac{4}{a^2}} \tag{9.11}$$

Replacing $2/a$ by t and inverting the equation leads to a transcendental equation for t in the form

$$t = \sinh\left[\left(\frac{8}{3} - \sqrt{1 + t^2}\right)t\right] \tag{9.12}$$

which after solving for t gives a and, in turn, S. The solution to a high degree of accuracy is $t = 1.60$, $a = 1.25$ and $S = 1.67$. This is the overall shear strain. Since the steel will not deform in shear, the shear in the rubber is increased by the ratio of the total thickness (steel plus rubber) to rubber thickness. For the bridge bearings in (Konstantinidis *et al.* 2008), the rubber and steel thicknesses are 12 mm (0.48 in) and 1.9 mm (0.004 in), respectively. Thus the limiting shear strain based on the thickness of rubber is 1.92. The conclusion is that in broad terms these bearings with small thickness compared with their plan dimension can experience a displacement of twice the thickness of rubber before they run the risk of damage by sliding. This is quite comparable to the shear maxima usually imposed on building bearings in current practice in the United States, although it is somewhat less than that permitted in Japan. It is also worth noting that this is a lower bound to the maximum displacement since the reinforcement is not completely flexibl and the bending stiffness will allow the bearing to displace further.

9.4 Vertical Stiffness of Unbonded Rubber Bearings with Slip on their Top and Bottom Supports

Friction in rubber is relatively high, but there is always the possibility that some level of lubrication can be introduced either intentionally or by accident. This results in a reduction of frictional resistance that develops in the support–rubber interface, and thus it is important to be able to predict the effect of slip in these bearings. This section presents an analysis of the mechanics of the bearing with slip, and this will include the effect on the internal pressure in the bearing and the reduction of the vertical stiffness caused by slip. Also, the maximum amount of slip at the unbonded surfaces will be calculated.

In addition to the unbonded surfaces, another aspect of these bearings that distinguishes them from other isolation bearings is that the outer layers are only half the thickness of the inner layers. This means that if the friction is high enough to simulate the fully bonded situation at the top and bottom surfaces, these two outer layers will each be four times stiffer than each inner layer. On the other hand, if the top and bottom surfaces are fully lubricated to the extent that there is no shear stress on either surface, the two outer layers will act as if they were a single inner layer since the analysis for the fully bonded inner layer has zero shear stress on the center of the layer. Thus, the two layers together will have the stiffness of an inner layer. Frictional slip will cause the stiffness of these two outer layers to vary between these two extreme values.

In the analysis that follows, only the outer layers are considered, and the compression modulus, E_c, of the two-outer-layer system is determined. Then the vertical stiffness of the outer layers is $E_c A/t$, and once the vertical stiffness of the inner layers is computed using the formulas presented in Chapter 2, the total vertical stiffness of the bearing can be computed by treating the inner and outer layers as springs in series.

To determine the effect of slip on the vertical stiffness of the two outer layers of the bearing the inner layers are replaced by a central line. The deformation is divided into two parts: (a) the parabolic displacement fiel assumed for the fully bonded bearing; and (b) an additional linear displacement pattern that varies from zero at the inner surface to $u_1(x)$ at the outer edges to characterize the slip. Symmetry in both horizontal and vertical directions is assumed and deformation in the y direction is neglected.

This displacement fiel is shown in Figure 9.7 and takes the form

$$u(x,z) = u_0(x)\frac{2z}{t}\left(1-\frac{2z}{t}\right) + u_1(x)\frac{2z}{t}$$
$$w(x,z) = w(z) \tag{9.13}$$

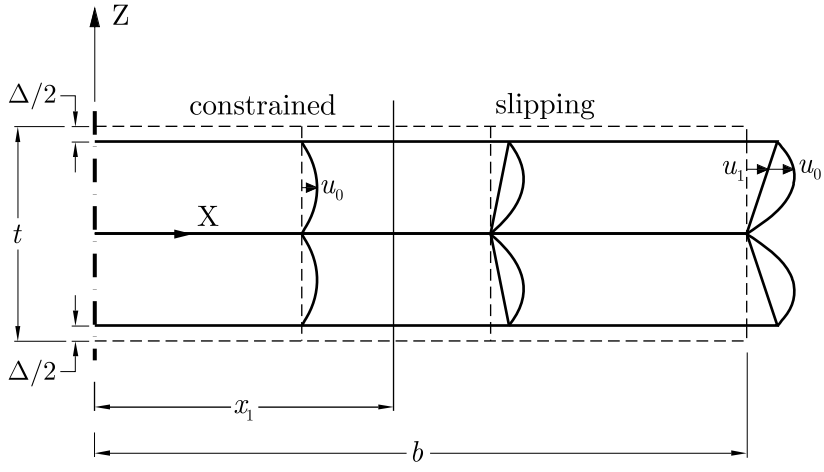

Figure 9.7 Coordinate system and displacement field for bearing with two slipping outer layers

The normal strains are given by

$$\varepsilon_{xx} = \frac{\partial u}{\partial x} = \frac{\mathrm{d}u_0}{\mathrm{d}x}\frac{2z}{t}\left(1 - \frac{2z}{t}\right) + \frac{\mathrm{d}u_1}{\mathrm{d}x}\frac{2z}{t}$$
$$\varepsilon_{zz} = \frac{\partial w}{\partial z} = \frac{\mathrm{d}w}{\mathrm{d}z} \tag{9.14}$$

The material is assumed to be incompressible so that

$$\varepsilon_{xx} + \varepsilon_{zz} = \frac{\mathrm{d}u_0}{\mathrm{d}x}\frac{2z}{t}\left(1 - \frac{2z}{t}\right) + \frac{\mathrm{d}u_1}{\mathrm{d}x}\frac{2z}{t} + \frac{\mathrm{d}w}{\mathrm{d}z} = 0 \tag{9.15}$$

Integration of this through the half thickness $0 \le z \le t/2$ gives

$$\frac{\mathrm{d}u_0}{\mathrm{d}x}\frac{t}{12} + \frac{\mathrm{d}u_1}{\mathrm{d}x}\frac{t}{4} = -w\left(\frac{t}{2}\right) + w(0) = \frac{\Delta}{2} \tag{9.16}$$

or

$$\frac{\mathrm{d}u_0}{\mathrm{d}x} + 3\frac{\mathrm{d}u_1}{\mathrm{d}x} = 6\varepsilon_c \tag{9.17}$$

where the compression strain $\varepsilon_c = \Delta/t$ is positive in compression. The only significan shear strain is given by

$$\gamma_{xz} = \frac{\partial u}{\partial z} + \frac{\partial w}{\partial x} = \left(\frac{2}{t} - \frac{8z}{t^2}\right)u_0 + \frac{2}{t}u_1 \tag{9.18}$$

and the shear stress is $\tau_{xz} = G\gamma_{xz}$. The important shear stresses are the surface stresses, which will be denoted by τ_s and define by $\tau_s = -\tau_{xz}|_{z=t/2}$ and $\tau_s = \tau_{xz}|_{z=-t/2}$ and the inner shear stresses at the bonded surface, which will be denoted by $\tau_l = \tau_{xz}|_{z=0}$, as shown in Figure 9.8. These two shear stresses can be expressed in terms of the displacement variables u_0 and u_1 by

$$\tau_s = \frac{2G}{t}(u_0 - u_1); \qquad \tau_l = \frac{2G}{t}(u_0 + u_1) \tag{9.19}$$

The normal stresses σ_{xx}, σ_{yy} and σ_{zz} are all represented by the pressure $p(x) = -\sigma_{xx} = -\sigma_{yy} = -\sigma_{zz}$. The surface shear stress (Figure 9.8) is define in the negative x-direction

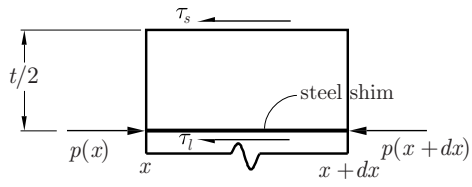

Figure 9.8 Definition of surface shears

on the top surface and in the positive direction on the bottom surface, as shown in the diagram, to allow us to make use of symmetry.

The assumption that all the normal stress components are equal to the negative pressure reduces the equations of stress equilibrium to the single equation

$$\frac{\partial \tau_{xz}}{\partial z} = \frac{\mathrm{d}p}{\mathrm{d}x} \tag{9.20}$$

and integration of this through the upper half layer $0 \le z \le t/2$ gives

$$\int_0^{t/2} \frac{\partial \tau_{xz}}{\partial z} \mathrm{d}z = \frac{t}{2}\frac{\mathrm{d}p}{\mathrm{d}x} = -(\tau_s + \tau_l) \tag{9.21}$$

which is also shown in the diagram. From this equation and the fact that for both the non-slip and slipped regions, $\tau_s + \tau_l = 4Gu_0/t$, we have a connection between the pressure and the displacement fiel valid everywhere in the form

$$\frac{\mathrm{d}p}{\mathrm{d}x} = -\frac{8\,G}{t^2}u_0 \tag{9.22}$$

We assume that slip occurs at $x = x_1$ and assume symmetry and continuity at $x = 0$ and $x = x_1$. In the non-slip region $0 \le x \le x_1$, we have $u_1 = 0$, and with the above equation, we have

$$u_0 = -\frac{t^2}{8\,G}\frac{\mathrm{d}p}{\mathrm{d}x} \tag{9.23}$$

Substitution into the equation of incompressibility, which now takes the form $\mathrm{d}u_0/\mathrm{d}x = 6\varepsilon_c$, gives

$$\frac{\mathrm{d}^2 p}{\mathrm{d}x^2} = -\frac{48\,G\varepsilon_c}{t^2} \tag{9.24}$$

from which

$$p(x) = -\frac{24\,G\varepsilon_c}{t^2}x^2 + Ax + B$$

Symmetry dictates that $A = 0$, and, if there were no slip, we could use a boundary condition at $x = b$ to determine B. In this case, we cannot use such a condition and must leave B as an unknown. It is convenient to absorb it into the other constants and write $p(x)$ and $\mathrm{d}p/\mathrm{d}x$ as

$$p(x) = 24\,GS^2\varepsilon_c\left(B - \frac{x^2}{b^2}\right), \quad 0 \le x \le x_1 \tag{9.25}$$

$$\frac{\mathrm{d}p}{\mathrm{d}x} = -\frac{48\,G\varepsilon_c}{t^2}x, \quad 0 \le x \le x_1 \tag{9.26}$$

The displacement fiel in this region is simply $u_0 = 6x\varepsilon_c$ and $u_1 = 0$. We note that at $x = x_1$ the value of the surface shear stress is related to the pressure through $\tau_s = \mu p$, where μ is the coefficien of friction, so that from Equations (9.17) and (9.22)

$$\frac{48\,G\varepsilon_c}{t}x_1 = 24\mu G\varepsilon_c\frac{b^2}{t^2}\left(B - \frac{x_1^2}{b^2}\right)$$

or

$$x_1 = \frac{\mu b^2}{2t}\left(B - \frac{x_1^2}{b^2}\right) \tag{9.27}$$

which shows that the location of the slip is not affected by the level of the compression strain.

For the region $x_1 \le x \le b$, where $u_1 \neq 0$, the equation of incompressibility becomes

$$\frac{\mathrm{d}u_0}{\mathrm{d}x} + 3\frac{\mathrm{d}u_1}{\mathrm{d}x} = 6\varepsilon_c \tag{9.28}$$

This can be integrated over the region $x_1 \le x \le b$ using the fact that continuity requires that $u_0(x_1) = 6x_1\varepsilon_c$ and $u_1(x_1) = 0$, giving

$$u_0(x) + 3u_1(x) = 6x\varepsilon_c \tag{9.29}$$

In addition, over the slipped region, we have $\tau_s = \mu p$ and also $\mathrm{d}p/\mathrm{d}x = -2(\tau_s + \tau_l)/t$, which taken together give

$$\frac{\mathrm{d}p}{\mathrm{d}x} + \frac{2\mu}{t}p = -\frac{2}{t}\tau_l = -\frac{4\,G}{t^2}(u_0 + u_1) \tag{9.30}$$

We can replace u_1 using the integrated form of the equation of incompressibility, leading to

$$\frac{\mathrm{d}p}{\mathrm{d}x} + \frac{2\mu}{t}p = -\frac{4\,G}{t^2}\left(\frac{2}{3}u_0 + 2x\varepsilon_c\right) \tag{9.31}$$

which, in turn, by replacing u_0 from Equation (9.22), gives

$$\frac{\mathrm{d}p}{\mathrm{d}x} + \frac{3\mu}{t}p = -\frac{12\,G\varepsilon_c}{t^2}x \tag{9.32}$$

Using the integrating factor $e^{3\mu x/t}$, this can be written in the form

$$\frac{\mathrm{d}}{\mathrm{d}x}(e^{3\mu x/t}\,p) = -\frac{12\,G\varepsilon_c}{t^2}xe^{3\mu x/t} \tag{9.33}$$

Integration from x to b gives

$$e^{3\mu b/t}\,p(b) - e^{3\mu x/t}\,p(x) = -\frac{12\,G\varepsilon_c}{t^2}\int_x^b x' e^{3\mu x'/t}\mathrm{d}x' \tag{9.34}$$

If we assume that $p(b) = 0$ (in this case we do not need to use the Young's Modulus, E_0, to provide the boundary condition) and carry out the integration, the result for $p(x)$ takes the form

$$p(x) = \frac{4\,G\varepsilon_c}{3\mu^2}\left[(3\mu S - 1)e^{3\mu S[1-(x/b)]} - \left(3\mu S\frac{x}{b} - 1\right)\right],\ x_1 \le x \le b \tag{9.35}$$

from which we have

$$\frac{\mathrm{d}p}{\mathrm{d}x} = -\frac{4\,G\varepsilon_c}{\mu t}[1 + (3\mu S - 1)e^{3\mu S[1-(x/b)]}] \tag{9.36}$$

At this point, we can use continuity across $x = x_1$ of the pressure and its derivative to determine the two unknowns B and x_1. At $x = x_1$, we have

$$\frac{\mathrm{d}p}{\mathrm{d}x}(x_1^-) = -\frac{48\,G\varepsilon_c x_1}{t} \tag{9.37}$$

$$\frac{\mathrm{d}p}{\mathrm{d}x}(x_1^+) = -\frac{4\,G}{\mu t}[1 + (3\mu S - 1)e^{3\mu S[1-(x_1/b)]}] \tag{9.38}$$

Setting the two equal to each other and definin $y = 3\mu S x_1/b$, we obtain the identity

$$(4y - 1)e^y = (3\mu S - 1)e^{3\mu S} \tag{9.39}$$

After solving this identity for y, we readily obtain x_1/b, which depends only on the coefficien of friction and the shape factor $S = b/t$. The constant B is then obtained by equating $p(x_1^-)$ and $p(x_1^+)$,

$$24\,GS^2\varepsilon_c\left(B - \frac{x_1^2}{b^2}\right) = \frac{4\,G\varepsilon_c}{3\mu^2}\left[(3\mu S - 1)e^{3\mu S[1-(x_1/b)]} - \left(3\mu S\frac{x_1}{b} - 1\right)\right]$$

which reduces to

$$B = \frac{x_1^2}{b^2} + \frac{1}{18\mu^2 S^2}\left[(3\mu S - 1)e^{3\mu S[1-(x_1/b)]} - \left(3\mu S\frac{x_1}{b} - 1\right)\right] \tag{9.40}$$

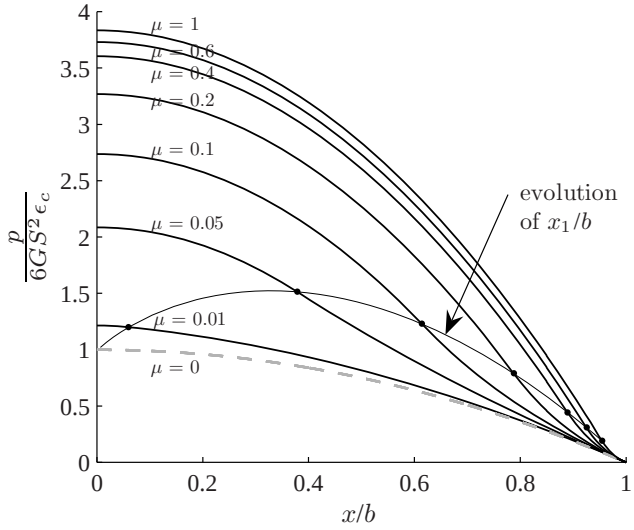

Figure 9.9 Pressure distributions for bearing ($S = 10$) with slip on the top and bottom surfaces

and leads to the result for the pressure in the non-slip region in the from

$$p(x) = 24\,GS^2\varepsilon_c\left(B - \frac{x^2}{b^2}\right), \quad 0 \le x \le x_1 \tag{9.41}$$

In Figure 9.9, pressure distributions are shown for a bearing with $S = 10$ and slip on the top and bottom surfaces for various values of μ.

To calculate the value of E_c, we integrate the pressure over the range $-b \le x \le b$ to determine P and then divide by $A\varepsilon_c = 2b\varepsilon_c$. From Equations (9.35) and (9.41), we have

$$P = 2\left\{\int_0^{x_1} 24\,GS^2\varepsilon_c\left(B - \frac{x^2}{b^2}\right)\mathrm{d}x + \int_{x_1}^{b}\frac{4\,G\varepsilon_c}{3\mu^2}\left[(3\mu S - 1)e^{3\mu S[1-(x/b)]} - \left(3\mu S\frac{x}{b} - 1\right)\right]\mathrm{d}x\right\} \tag{9.42}$$

which leads to

$$\begin{aligned} E_c = {} & 24\,GS^2\frac{x_1}{b}\left(B - \frac{x_1^2}{3b^2}\right) + \frac{4\,G}{9\mu^3 S}(1 - 3\mu S)(1 - e^{3\mu S[1-(x_1/b)]}) \\ & - \frac{2\,G}{3\mu^2}\left[\frac{x_1}{b}\left(2 - 3\mu S\frac{x_1}{b}\right) - (2 - 3\mu S)\right] \end{aligned} \tag{9.43}$$

Table 9.2 lists values of x_1/b and $E_c/4\,GS^2$ for $S = 10$ and various values of μ, and Figure 9.10 shows these quantities as a function of μ for $S = 10$, 15, and 20.

Table 9.2 Compression modulus for bearing with slip on the top and bottom surfaces ($S = 10$)

μ	y	$\frac{x_1}{b}$	B	$\frac{E_c}{4GS^2}$
0.01	0.018	0.060	0.303	1.122
0.05	0.568	0.378	0.522	1.733
0.10	1.842	0.614	0.684	2.359
0.20	4.725	0.788	0.817	2.985
0.30	7.687	0.854	0.872	3.271
0.40	10.668	0.889	0.902	3.433
0.50	13.657	0.911	0.920	3.536
0.60	16.650	0.925	0.933	3.607
0.70	19.645	0.936	0.942	3.660
0.80	22.641	0.943	0.949	3.700
0.90	25.638	0.950	0.954	3.731
1.00	28.635	0.955	0.959	3.757

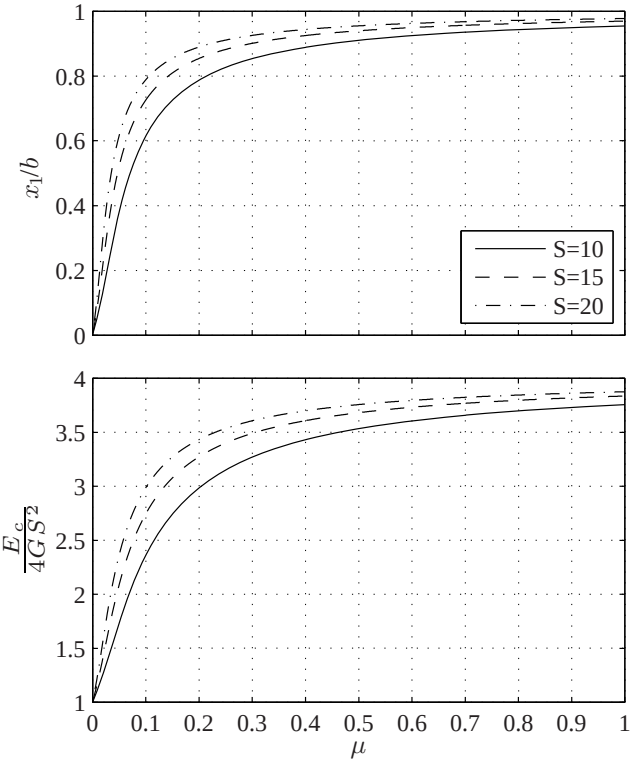

Figure 9.10 *Top*: location where slip initiates for a bearing with slip on the top and bottom surfaces. *Bottom*: compression modulus as a fraction of the compression modulus of a fully bonded pad

This chapter has provided an analysis of a type of rubber bearing that is not bonded to the supports above and below it, but held in place solely by friction. These bearings have been previously tested and survived very large shear strains (of the order of 200% or larger, Konstantinidis *et al.* 2008). While the seismic performance objectives that unbonded bearings are expected to achieve are not as high as those of isolation bearings, their low cost and light weight makes them very appealing for use as a low-cost alternative to seismic isolators for schools, housing and other public buildings in highly seismic areas of the developing world, where conventional seismic isolators are not affordable (Kelly and Konstantinidis 2007).

The effect of the frictional resistance of the top and bottom supports on the pressure distribution and the compression modulus of an unbonded bearing under compressive load were firs examined by Kelly and Konstantinidis (2009b) in an effort to predict the behavior of a type of rubber bridge bearing permitted in California for use as a thermal expansion bridge bearing. The analysis shows that friction has an important effect on both the maximum pressure and the compression modulus.

Appendix

Elastic Connection Device for One or More Degrees of Freedom

Mr Eugène Freyssinet, resident in France (Seine)

Mechanics of Rubber Bearings for Seismic and Vibration Isolation, First Edition. James M. Kelly and Dimitrios A. Konstantinidis.

RÉPUBLIQUE FRANÇAISE

MINISTÈRE
DE L'INDUSTRIE ET DU COMMERCE

SERVICE
de la PROPRIÉTÉ INDUSTRIELLE

BREVET D'INVENTION

Gr. 5. — Cl. 3. N° 1.110.285

Classification internationale : F 06 *d*

Dispositif de liaison élastique à un ou plusieurs degrés de liberté.

M. EUGÈNE FRÈYSSINET résidant en France (Seine).

Demandé le 25 mai 1954, à 16h 47m, à Paris.

Délivré le 12 octobre 1955. — Publié le 10 février 1956.

(Brevet d'invention dont la délivrance a été ajournée en exécution de l'article 11, § 7, de la loi du 5 juillet 1844 modifiée par la loi du 7 avril 1902.)

Les réalisations techniques ressortissant à la mécanique nécessitent fréquemment des liaisons entre pièces rigides autorisant, suivant un ou plusieurs degrés de liberté, des déplacements relatifs de ces pièces. On sait réaliser au moyen de pièces mécaniques usinées, faisant intervenir le frottement entre surfaces graissées ou le roulement d'organes intermédiaires, des liaisons à nombre limité de degrés de liberté. L'obtention de plusieurs degrés de liberté à la fois nécessite des ensembles parfois très complexes. Ces réalisations, à l'aide de pièces mécaniques, sont néanmoins considérées comme indispensables lorsque les efforts mis en jeu sont importants ou qu'une grande précision est exigée dans les déplacements relatifs des pièces.

Cependant, on a déjà proposé, en cas d'efforts relativement faibles et aussi lorsque la précision des déplacements n'est pas requise, d'obtenir des liaisons permettant des déplacements limités, par interposition entre les pièces rigides de masses de gomme du type caoutchouc. Ces gommes, travaillant par distorsion, permettent des déplacements relatifs avec de faibles frottements et procurent en outre l'avantage d'un rappel élastique des pièces après déplacement vers leur position d'origine. Les liaisons ainsi réalisées ont en outre l'avantage, sans aucun entretien, d'être à l'abri des grippages auxquels sont sujettes des liaisons réalisées avec des organes mécaniques.

Le but de la présente invention est la réalisation de liaisons entre pièces rigides permettant à ces pièces des déplacements relatifs limités avec au moins un degré de liberté et mettant en œuvre des gommes déformables par distorsion, mais, contrairement aux liaisons par gomme élastique connues, ces liaisons peuvent être soumises à des efforts pratiquement illimités et permettent d'assurer une précision de déplacement radial relatif entre pièces aussi grande que l'on désire.

Il devient ainsi possible d'appliquer de telles liaisons dans les techniques mettant en jeu des efforts énormes, comme c'est le cas dans les travaux publics ou bien en mécanique de haute précision où les tolérances dimensionnelles sont très réduites. Néanmoins, l'invention permet ces résultats avec des prix de revient très économiques tant pour les matières premières utilisées que pour les frais de main-d'œuvre et d'usinage.

Selon l'invention, entre les surfaces sensiblement parallèles appartenant à deux pièces rigides, entre lesquelles on désire établir une liaison, est interposé un bloc formé de plaques de gomme entre lesquelles sont intercalées des feuilles inextensibles dont les faces, sensiblement parallèles aux surfaces des pièces rigides, possèdent un fort coefficient de frottement au contact desdites plaques.

Le fort coefficient de frottement peut être obtenu par collage entre les feuilles inextensibles et les plaques de caoutchouc ou, de préférence, en utilisant des feuilles inextensibles à forte rugosité superficielle telles que des tôles perforées gaufrées ou ondulées ou encore des grillages.

De préférence, le bloc formé par l'assemblage des plaques de caoutchouc et des feuilles inextensibles alternées est comprimé dans la direction perpendiculaire aux surfaces de feuilletage, soit par une compression préalable, soit par les charges appliquées aux pièces rigides y compris le poids propre de ces pièces.

On montrera dans la suite du mémoire que la déformation que peut subir un tel bloc sous cette compression dépend dans une faible mesure du module d'élasticité de la gomme, qu'il est possible d'admettre sur un tel bloc des charges unitaires sans aucune mesure avec les limites d'écrasement propre à la gomme, mais que, néanmoins, un tel bloc permet essentiellement, dans des directions tangentielles au feuilletage, des déplacements des deux pièces rigides par distorsion de la gomme qui les sépare dans les mêmes conditions que si cette gomme n'était pas feuilletée.

Les déplacements autorisés par un tel bloc feuil-

Prix du fascicule : 100 francs.

leté, interposé entre surfaces parallèles, correspondent essentiellement à la possibilité pour deux surfaces parallèles de glisser l'une contre l'autre en restant en contact sur toute leur étendue.

Géométriquement, les surfaces qui satisfont parfaitement à cette condition sont le plan, les surfaces de révolution (y compris la sphère) et les surfaces hélicoïdales. Néanmoins, étant donné que les déplacements sont limités, d'autres surfaces de définition géométrique plus complexe peuvent être choisies pour les surfaces des pièces rigides, si l'approximation de parallélisme correspondant au déplacement maximum envisagé reste acceptable.

Avec les surfaces qui satisfont rigoureusement à la condition de parallélisme pendant le déplacement relatif, il est possible d'obtenir les déplacements suivants :

Deux surfaces planes parallèles autorisent des translations dans toutes les directions de leur plan et aussi des rotations autour d'un axe quelconque perpendiculaire à ce plan;

Deux surfaces de révolution parallèles permettent une rotation autour de leur axe commun et éventuellement une translation le long de cet axe si ces surfaces sont des cylindres ou portions de cylindre; dans le cas de deux sphères, l'axe de rotation relatif est quelconque pourvu qu'il passe par le centre commun à ces sphères;

Deux surfaces hélicoïdales permettent un déplacement en hélice, c'est-à-dire, la combinaison d'une translation et d'une rotation.

Il a été supposé implicitement, dans ce qui précède, que la distribution des contraintes dans le bloc feuilleté restait la même au cours du déplacement et que, par conséquent, ce bloc ne se déformait que par distorsion de la gomme. On peut cependant aussi dans le déplacement faire varier la répartition des contraintes dans le bloc feuilleté et faire travailler ce bloc également par déformation élastique, ce qui procure des degrés de liberté supplémentaires. Ainsi, un bloc en forme de prisme droit, feuilleté parallèlement à ses bases, peut autoriser non seulement des translations parallèles à ces bases ou des rotations perpendiculaires à celles-ci, mais, aussi, des rotations dont une composante axiale est parallèle au plan des bases, rotation qui amène en angle dièdre les plans desdites bases. On peut faciliter les déplacements de ce genre en donnant à un tel bloc prismatique une section rectangulaire allongée dans la direction de l'axe de rotation prévu.

Une des applications principales de l'invention est la réalisation de coussinets d'appui des ouvrages d'art sur leurs supports, afin de permettre des déplacements de ces ouvrages soit pour des causes internes (dilatations), soit pour des causes externes (ouvrages mobiles, tels que ponts levants ou tournants, vannes de barrages, etc.).

Pour de tels ouvrages l'invention permet de substituer à des pièces métalliques très lourdes, d'usinage et d'entretien délicat, des organes faciles à mettre en place, qui ne requièrent pas, à l'exécution et à la pose, une extrême précision et qui fonctionnent avec sécurité même en l'absence d'entretien. En outre, l'invention permet la réalisation de joints mécaniques de grande précision dans les machines et appareils, spécialement dans le domaine de la machine-outil et des véhicules, chaque fois que des déplacements relatifs d'amplitude limitée sont nécessaires.

La description qui va suivre en regard du dessin annexé, donné à titre d'exemple non limitatif, fera bien comprendre comment l'invention peut être réalisée, les particularités qui ressortent tant du dessin que du texte faisant, bien entendu, partie de ladite invention :

La fig. 1 est une figure schématique permettant de comprendre le principe de l'invention;

La fig. 2 est une élévation schématique d'un dispositif de liaison conforme à l'invention;

La fig. 2*a* montre ce même dispositif après distorsion;

Les fig. 3 et 4 illustrent deux exemples de réalisation de dispositifs selon l'invention;

Les fig. 5 et 6 montrent en coupe schématique des dispositifs permettant des translations rectilignes;

Les fig. 7 et 7*a* montrent avant et après déformation un dispositif permettant une rotation d'axe parallèle au plan du feuilletage;

Les fig. 8 et 9 montrent en élévation deux ouvrages d'art auxquels sont appliqués des dispositifs selon l'invention;

La fig. 10 est une vue en coupe axiale d'un dispositif selon l'invention formant crapaudine;

Les fig. 11 et 12 montrent respectivement, en élévation et en plan, un dispositif selon l'invention permettant un mouvement hélicoïdal;

La fig. 13 est l'élévation d'un palier permettant une rotation limitée d'axe parfaitement déterminé.

On sait que certains corps tels que les caoutchoucs naturels et artificiels, ainsi que de nombreuses résines synthétiques ou matières plastiques, peuvent être déformés à volume pratiquement constant soit par allongement ou raccourcissement, soit par distorsion, et que ces corps ont, pour de telles déformations, la propriété de se comporter sensiblement comme des liquides au point de vue de la transmission des pressions. De tels corps ont en outre la faculté d'adhérer à certaines surfaces telles que l'acier ou le béton, autrement dit de créer par leur contact avec de telles surfaces un très fort coefficient de frottement qu'il est possible d'accroître par collage ou par augmentation de la rugosité des surfaces de contact.

Considérons donc un bloc parallélépipédique 1

(fig. 1) d'une telle matière, disposé (pour simplifier les raisonnements) entre deux surfaces planes et parallèles 2 et 3, puis comprimé entre ces surfaces par une certaine force F qui amène la surface 2 en 2*a* et donne au bloc 1 la forme 1*a*. En appelant S la surface du bloc, *h* son écrasement et E le module de raccourcissement de la matière, le rapport F/h n'est nullement égal au produit SE. En effet, la matière du bloc étant pratiquement incompressible, la déformation de ce bloc n'est possible que par un déplacement interne de la matière qui tend à faire glisser ledit bloc au contact des surfaces 2*a* et 3 et, en raison des frottements, incurve les faces latérales de ce bloc. Ainsi un filet de matière initialement rectiligne *a*, *b*, *c* glisse légèrement (d'autant moins que l'adhérence est plus forte) par ses extrémités au contact des surfaces 2*a* et 3 et s'incurve en s'allongeant pour prendre la forme *a'*, *b'*, *c'* développant ainsi sur la masse du bloc une pression élémentaire centripète qui dépend du frottement, qui est proportionnelle à son allongement et inversement proportionnelle à son rayon de courbure. Il naît ainsi dans la masse du bloc un champ de pressions centripètes qui donne une pression résultante *p*, laquelle croît de zéro à la périphérie à une valeur maximum au centre; les frottements en *a* et *c*, fonction de cette pression, croissent également avec celle-ci et atteignent au centre des faces du bloc leur valeur maxima.

La résistance à l'aplatissement est donc, non pas SE, mais SE + Σ pds et si la plus petite dimension en plan du bloc est beaucoup plus grande que son épaisseur, le second terme est beaucoup plus important que le premier d'autant plus que le coefficient de frottement de la gomme sur la surface des pièces rigides 2 et 3 est plus fort.

Si l'on suppose divisée par deux l'épaisseur du bloc 1, on voit, en supposant les mêmes valeurs du frottement, que la pression *p* se trouve doublée puisque le rayon de courbure des filets de gomme se trouve divisé par deux. De plus, la valeur *p*, c'est-à-dire du frottement $p\varphi$, qui de ce fait était atteinte à une certaine distance ρ de la périphérie est maintenant atteinte à une distance $\frac{\rho}{2}$ de cette même périphérie. Les pressions dans la zone centrale prendront donc des valeurs beaucoup plus grandes et Σ pds sera beaucoup plus que doublé.

Si on considère donc, au lieu du bloc homogène de gomme 1, un bloc formé de deux plaques d'épaisseur moitié séparées par une feuille de matière inextensible à fort coefficient de frottement au contact de ces plaques, l'introduction de cette feuille aura pour effet de multiplier au moins par quatre la résistance à la déformation de ce bloc composite par rapport au bloc homogène.

La division du bloc par neuf feuilles intermédiaires en dix plaques de gomme égales multipliera de même cette résistance par un chiffre supérieur à 100.

Cette résistance, sans rapport aucun avec la résistance intrinsèque de la gomme à l'écrasement, peut donc croître sans autres limites que la résistance aux efforts d'expansion des feuilles intermédiaires et l'abaissement du coefficient de frottement avec la pression, abaissement qui n'est pratiquement obtenu que sous des pressions unitaires extrêmement élevées.

On peut ainsi réaliser un bloc tel que celui montré schématiquement sur la fig. 2, comprenant des plaques de gomme minces 6 séparées par des feuilles inextensibles 5, ayant un fort coefficient de frottement au contact de ces plaques.

Si, comme le montre la fig. 2*a*, on provoque un déplacement relatif des pièces 2 et 3 dans une direction parallèle au feuilletage, ce déplacement se produit par distorsion dans toute l'étendue des plaques 6 s'il y a effectivement adhérence entre les plaques et les feuilles.

La force qui s'oppose à ce déplacement est toujours $\frac{SE.d}{e}$ en appelant *e* l'épaisseur totale et *d* l'amplitude du déplacement. Il est indifférent en effet que l'épaisseur totale *e* soit en une ou plusieurs plaques, puisque la division en plaques modifie également *d* et *e*. De plus, dans le cas d'un bloc homogène, la valeur de l'effort nécessaire au déplacement est majoré par la présence dans le bloc d'une zone marginale dans laquelle la distorsion de la gomme est irrégulière, tandis que la division en plaques divise en même temps par un même facteur la largeur de cette zone marginale.

Afin d'obtenir un fort coefficient de frottement des plaques de gomme au contact des feuilles inextensibles, on pourrait utiliser des feuilles inextensibles lisses et coller à la surface de celles-ci lesdites plaques de gomme. Dans ce cas, cependant, la sécurité en service dépendrait dans une grande mesure de la qualité et de l'uniformité du collage et cette sécurité pourrait disparaître sous l'effet du décollement.

Il est par conséquent préférable, pour assurer une liaison à fort coefficient de frottement entre les plaques et les feuilles, de munir celles-ci de rugosités susceptibles de s'accrocher dans la surface de la gomme.

A cette fin, comme le montre la fig. 3, les feuilles inextensibles peuvent être des grillages métalliques formés par exemple de fils tissés ou de métal déployé. Dans le cas de fils, il peut y avoir intérêt à utiliser des grillages à mailles nouées ou soudées pour éviter les glissements des fils au contact les uns des autres.

On peut aussi, comme le montre la fig. 4, utiliser des feuilles inextensibles 8 formées de tôles plis-

sées ou gaufrées ou encore des tôles perforées par de nombreuses ouvertures de forme quelconque.

Toutefois, alors que l'utilisation de feuilles lisses collées aux plaques de gomme permet, au moins théoriquement, de réduire autant qu'on le désire l'épaisseur de ces plaques de gomme, l'utilisation de feuilles comportant des rugosités limite la réduction d'épaisseur des plaques de gomme. Il est nécessaire, en effet, que cette épaisseur soit telle qu'elle remplisse l'intervalle entre les feuilles même lorsque deux des creux les plus profonds de ces feuilles sont en regard l'un de l'autre. Il convient donc que l'épaisseur des plaques de gomme soit au moins égale au double de la hauteur des reliefs des feuilles. Pour fixer les idées avec des feuilles comportant des reliefs de l'ordre de 3 mm, l'épaisseur des plaques de gomme devra être d'au moins 6 mm.

L'exemple de réalisation suivant fera bien comprendre les avantages économiques de l'invention. Considérons, sur la fig. 8, le pont 9, reposant sur les culées 10 et sur la pile intermédiaire par des blocs feuilletés 12 réalisés conformément à l'invention et destinés à permettre la libre dilatation du tablier du pont sur ses appuis. Supposons pour fixer les idées que la charge appliquée à l'un des blocs feuilletés de culée soit de 100 tonnes.

Si on accepte un taux de contrainte (considéré comme normal pour du caoutchouc) de 10 kg/cm², il faudrait, si le bloc 12 était massif, donner à la surface de base de ce bloc 10 000 cm², soit un mètre carré. Si l'on admet, en outre, que le caoutchouc utilisé à un coefficient de distorsion tel que l'effort pour obtenir un déplacement horizontal égal à son épaisseur soit aussi de 10 kg/cm² et si l'on impose une limite à l'effort nécessaire pour réaliser un déplacement déterminé, par exemple une tonne par centimètre de déplacement, ce bloc devrait avoir une épaisseur de 10 cm.

Un tel appui serait en principe satisfaisant, mais il serait d'un prix et d'un encombrement prohibitifs.

Par contre, si l'on substitue à ce bloc de caoutchouc massif de 100 dm³ de volume (soit 130 kg) trois plaques de 0,40 m × 0,40 m × 0,006 m, séparées par des plaques adhérentes et inextensibles, la section horizontale de caoutchouc à déformer sera réduite dans le rapport de 1 à 0,16; comme le rapport des épaisseurs de caoutchouc à déformer est alors de 10 cm à 1,8 cm, la résistance aux déformations par distorsion dans le sens horizontal sera modifiée dans le rapport $\frac{0{,}16 \times 10}{1{,}8}$, c'est-à-dire qu'il sera sensiblement le même que précédemment. Néanmoins, la résistance aux déformations verticales est considérablement accrue et surtout le poids de caoutchouc utilisé passe de 130 kg à 3,700 kg. La valeur et le poids des deux tôles intercalaires est infime, car l'effort de traction auquel ces tôles sont soumises est de l'ordre de 500 kg.

Un tel dispositif, constitué par un feuilletage plan disposé entre surfaces planes parallèles, permet des déplacements parallèles aux plans de feuilletage dans toutes les directions, le coefficient de distorsion, c'est-à-dire le rapport de la réaction de déplacement à l'amplitude de ce déplacement, pour une surface donnée de plaque, diminuant au fur et à mesure que l'épaisseur totale des plaques utilisées augmente.

Mais on peut obtenir des coefficients de distorsion très différents dans chacune des deux directions perpendiculaires au plan de feuilletage en utilisant des surfaces d'appui et des feuilles intermédiaires non planes.

Ainsi, sur la fig. 5, les surfaces d'appui 2 et 3 sont en forme de cylindres et entre ces surfaces les plaques de gomme 6 et les feuilles 5 sont également en forme de cylindres parallèles à ces surfaces 2 et 3. Sur la fig. 6, les surfaces 2 et 3 sont cannelées dans la direction perpendiculaire à cette figure et les plaques 6 et feuilles 5 sont également cannelées.

De tels blocs feuilletés permettent évidemment des translations relatives des surfaces 2 et 3 dans la direction perpendiculaire à ces figures, mais s'opposent pratiquement aux translations dirigées dans le plan de ces figures. La raideur transversale de telles liaisons peut être augmentée en tant que de besoin en accroissant la hauteur des cannelures et nervures correspondantes et inversement. Il est ainsi possible de régler le coefficient de distorsion transversale à toute valeur désirée jusqu'à la rigidité pratiquement complète.

Des dispositifs de liaison élastiques, tels que montrés sur les fig. 5 et 6, peuvent par exemple trouver leur application dans des réalisations du genre de celui qui est montré sur la fig. 8. On peut désirer par exemple supprimer les réactions transversales au droit de la pile intermédiaire 11, grâce à des réactions transversales fournies par les culées 10 et à la raideur du tablier 9. A cette fin, les dispositifs 12 d'appui sur les culées 10 peuvent être réalisés comme montré sur les fig. 5 et 6, les nervures étant orientées dans la direction longitudinale du pont.

On peut aussi avoir besoin d'ajouter aux libertés de déformation longitudinales et transversales une certaine liberté de déformation angulaire autour d'un axe parallèle au plan déterminé par ces directions de déformation. Pour cela, comme le montre la fig. 7, on peut utiliser des blocs feuilletés de faible largeur l, dont la longueur L est augmentée de façon à conserver au bloc la surface totale nécessaire. Un tel bloc peut ainsi se déformer non seulement comme il a été précédemment indiqué par des translations relatives de ses faces parallè-

lement à leur plan, mais aussi comme montré par la fig. 7*b* par pivotement autour d'un axe parallèle à la plus grande dimension de ce bloc.

Une rotation systématique autour d'un axe est de préférence obtenue en utilisant des surfaces d'appui et un feuilletage de révolution autour de l'axe de rotation désiré.

Ainsi, le pont 13 montré sur la fig. 9 peut reposer par la surfac cylindrique convexe 16 sur la surface cylindrique concave 18 de l'appui 15 par l'intermédiaire d'un bloc feuilleté 17 en forme de portion de cylindre analogue à celui que montre la fig. 5, mais qui, cette fois, est utilisé à des fins différentes.

Un tel pont peut basculer sous l'action de forces extérieures autour de l'axe commun des surfaces de révolution 16, 17 et 18. Cependant, si l'on suppose que ces surfaces sont des portions de calottes sphériques, ce pont peut non seulement basculer mais aussi tourner autour de l'axe vertical passant par le centre commun à ces différentes sphères et, plus généralement, effectuer une rotation autour d'un axe quelconque passant par ce centre commun.

Dans ce cas, on peut accepter des valeurs très élevées pour les distorsions et, par exemple, obtenir des rotations de 45° environ avec des épaisseurs totales de caoutchouc de l'ordre du tiers du rayon de la surface concave d'appui.

Le pivot et le mécanisme de basculement d'un tel pont peuvent être exécutés entièrement en béton modelé au gabarit, sans aucune partie métallique usinée, étant donné la valeur relativement faible des contraintes locales de pression. Bien entendu, le centre de gravité de la masse pivotante peut être placé à la volonté du constructeur au-dessus, au-dessous ou bien au niveau du centre ou de l'axe de rotation.

La fig. 10 concerne le cas où l'on désire seulement une possibilité de rotation d'axe vertical. La pièce rigide 2 comporte une calotte sphérique convexe 19 et une surface tronconique de révolution 21; la pièce 3 comporte une calotte sphérique concave 20 et une surface tronconique 22 parallèle à la surface 21. Entre les surfaces d'appui sont disposés les blocs feuilletés 23 et 24, le premier en forme de calotte sphérique, le second en forme de tronc de cône. L'épaisseur du second est d'ailleurs plus forte que celle du premier. Bien entendu, l'orientation des calottes et des troncs de cône peut être inversée entre les pièces 2 et 3.

Comme le montrent les fig. 11 et 12, les pièces 2 et 3 et le bloc feuilleté qui les sépare peuvent aussi être organisés pour permettre un déplacement hélicoïdal relatif de ces pièces (sur les fig. 11 et 12, pour la clarté, la pièce 2 est supposée transparente).

Ces deux pièces de formes cylindriques comportent deux surfaces hélicoïdales d'appui 25 et 26 identiques ayant un développement d'un tour environ, mais qui sont décalées l'une par rapport à l'autre de l'angle α.

Entre ces deux hélicoïdes 25 et 26 est disposé le bloc feuilleté hélicoïdal formé de plaques et de feuilles hélicoïdales, parallèles aux surfaces 25 et 26. Le développement total de ce bloc est égal à un tour diminué de l'angle α, son épaisseur est telle que par distorsion du caoutchouc les surfaces hélicoïdales, qui le limitent, peuvent glisser l'une par rapport à l'autre de l'angle α tant dans un sens que dans l'autre. Les deux pièces 2 et 3 peuvent ainsi se déplacer l'une par rapport à l'autre d'un mouvement hélicoïdal relatif d'amplitude 2α. Une tige centrale de guidage 28 (qui peut être solidaire de l'une ou de l'autre pièce) empêche les déplacements latéraux relatifs. Un tel dispositif peut être appliqué à une presse à balancier.

Enfin, la fig. 13 montre un palier permettant le guidage en rotation et éventuellement en translation d'amplitude limitée d'un axe 29. Cet axe est entouré d'un manchon 30 formé de minces couches de gomme séparées par des feuilles inextensibles. La feuille inextensible peut être une bande de métal enduite d'un côté d'une couche de gomme qui est roulée très serrée autour de l'axe 29. Le manchon ainsi obtenu formant coussinet est fortement serré dans un palier 31. On peut obtenir ainsi un guidage pratiquement sans jeu latéral de l'axe 29 dans son palier pour des amplitudes de rotation et de translation longitudinales importantes, puisque celles-ci sont déterminées essentiellement par l'épaisseur totale de gomme utilisée.

Il va de soi que des modifications peuvent être apportées aux modes de réalisation qui viennent d'être décrits, notamment par substitution de moyens techniques équivalents, sans que l'on sorte pour cela du cadre de la présente invention.

RÉSUMÉ

La présente invention comprend notamment :

1° Un dispositif de liaison élastique à un degré de liberté au moins entre deux pièces rigides, dispositif suivant lequel entre surfaces sensiblement parallèles, appartenant auxdites pièces rigides, est interposé un bloc formé d'un empilement de plaques de matière de la nature du caoutchouc entre lesquelles sont intercalées des feuilles inextensibles dont les faces possèdent un fort coefficient de frottement au contact desdites plaques.

2° Formes de réalisation du dispositif spécifié sous 1°, pouvant présenter les particularités suivantes, prises séparément ou selon les diverses combinaisons possibles :

a. Le bloc feuilleté formé par les plaques et les feuilles intercalaires est comprimé perpendiculairement aux surfaces de feuilletage;

b. Les feuilles intercalaires sont en métal et comportent des rugosités superficielles;

c. Les feuilles spécifiées sous *b* sont des grillages;

d. Les feuilles spécifiées sous *b* sont des tôles plissées, gaufrées ou perforées;

e. Les surfaces parallèles des pièces rigides sont des plans;

f. Les surfaces parallèles des pièces rigides sont des surfaces de révolution coaxiales;

g. Les surfaces parallèles des pièces rigides sont des hélicoïdes de même axe et même pas;

h. Les surfaces parallèles des pièces rigides sont des calottes sphériques concentriques;

i. Les surfaces parallèles des pièces rigides comportent l'une, au moins une nervure, et l'autre, au moins une cannelure de forme correspondante emboîtées l'une dans l'autre;

j. Le bloc feuilleté comprend des plaques et des feuilles planes de forme rectangulaire de longueur très supérieure à la largeur, ledit bloc étant, suivant sa plus grande dimension, orienté dans la direction d'un axe éventuel de rotation;

k. Le bloc feuilleté est obtenu par enroulement simultané autour d'une surface cylindrique d'une bande de métal et d'une bande de gomme qui adhèrent entre elles.

3° L'application des dispositifs de liaison élastique, spécifiés sous 1° et 2°, aux ouvrages d'art mobiles par rapport à leurs appuis et en particulier aux ponts, soit pour la réalisation d'appuis permettant les dilatations, soit pour permettre le déplacement de ces ouvrages à l'aide de forces extérieures.

4° L'application des dispositifs de liaison élastiques, spécifiés sous 1° et 2°, à la mécanique de précision en vue de permettre des déplacements relatifs, limités mais guidés, de deux pièces l'une par rapport à l'autre.

EUGÈNE FREYSSINET.

Par procuration :
J. CASANOVA (Cabinet ARMENGAUD jeune).

Pour la vente des fascicules, s'adresser à l'IMPRIMERIE NATIONALE, 27, rue de la Convention, Paris (15e).

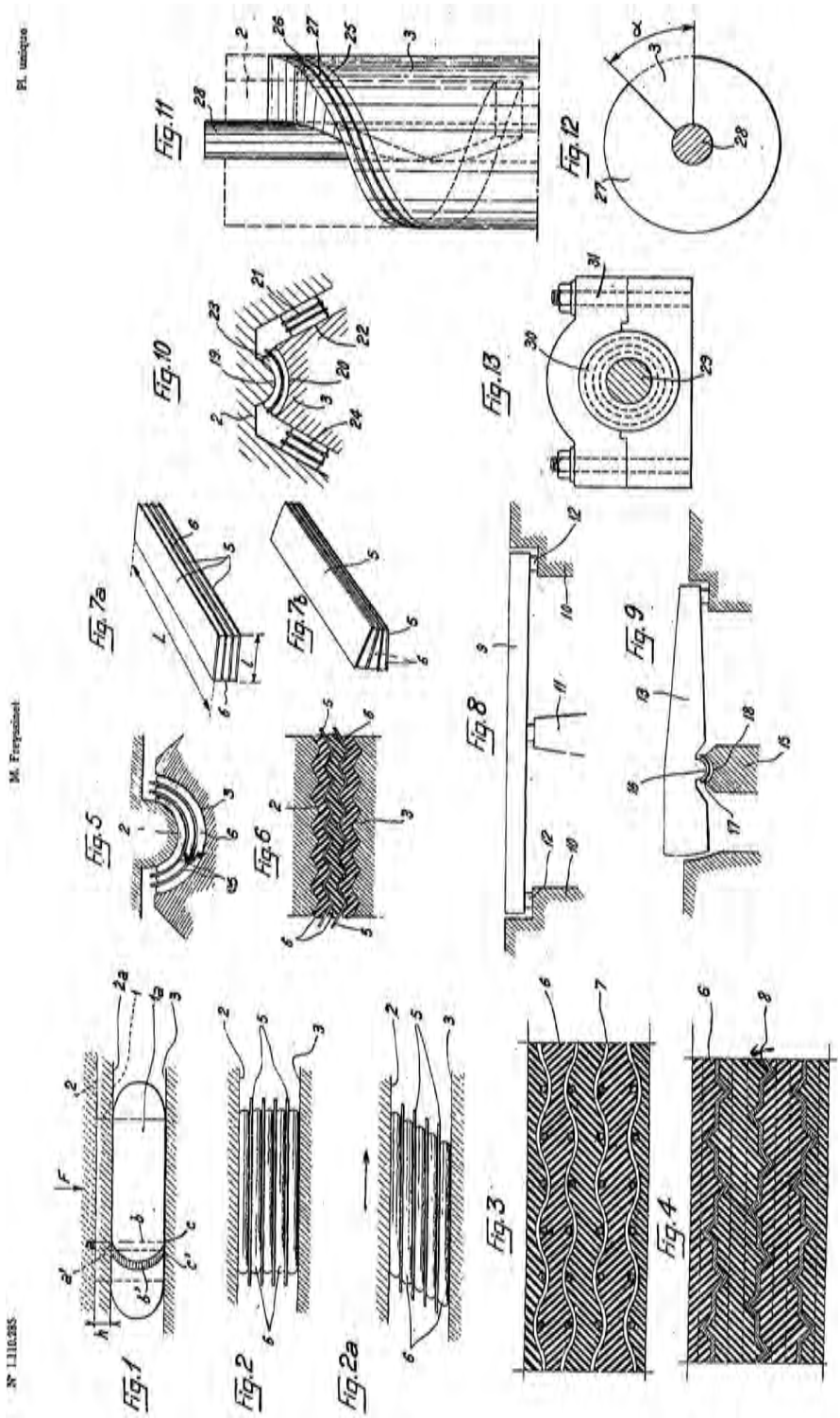
Pl. unique
M. Ferguisset
N° 1.116.285
Fig.1
Fig.2
Fig.2a
Fig.3
Fig.4
Fig.5
Fig.6
Fig.7a
Fig.7b
Fig.8
Fig.9
Fig.10
Fig.11
Fig.12
Fig.13

Application on 25 May 1954, 16h 47m, in Paris
Issued on 12 October 1955.—Published 10 February 1956

(Patent of invention, the grant has been issued pursuant to Article 11, § 7, of the Law of 5 July 1844 amended by the Act of 7 April 1902.)

Mechanical construction projects frequently require connections between rigid parts that allow relative displacements, with one or more degrees of freedom, between these parts. One can provide these by means of machined mechanical components, eliminating by lubrication the friction between bearing surfaces or by intermediate roller bearings, providing connections with a limited number of degrees of freedom. Obtaining several degrees of freedom at a time can often require very complex assemblies. The connections that use machined components are nevertheless regarded as essential when the structures are important or when a high degree of accuracy is required in providing relative displacements between the parts.

However, it has already been proposed that in the case of relatively low forces and also when the precision in the displacement is not required, that connections allowing limited displacements can be provided, by interposing rubber-like components between the rigid parts. These rubber parts working through the distortion of the rubber, allow relative movements with low friction and provide the added advantage of an elastic recovery after displacement from their original position. This type of connection has another advantage in the fact that they need no maintenance and are protected from the type of seizure to which links made with mechanical parts are subject.

The purpose of the present invention is the realization of connections between rigid parts that allow displacements on boundaries with at least one degree of freedom by the use of rubber components that are deformed by distortion, but, unlike the conventional connections using rubber, these connections can have virtually unlimited size and can ensure precise radial relative displacements to parts as large as we desire.

It thus becomes possible to apply such connections in projects involving huge efforts, as is the case in public works or in high-precision machines with very small dimensional tolerances. Nevertheless, the invention allows these results to be achieved with costs that are very economic both in terms of the raw materials used and for labor costs and machining.

According to the invention, a block formed of rubber plates within which are interspersed inextensible sheets whose surfaces are parallel to the surfaces of the rigid parts and which have a large coefficien of friction in contact with the rubber plates, is interposed between the substantially parallel surfaces of two rigid parts to which one wishes to establish a connection.

The high coefficien of friction can be obtained by bonding between the inextensible sheets and the plates of rubber or, preferably, by using an inextensible sheet surface with a strong surface roughness such as embossed, perforated or corrugated sheets or yet again gratings.

Preferably, the block formed by the assembly of the alternating plates of rubber and inextensible sheets is compressed in the direction perpendicular to the surfaces of the sheets, either by a prior compression or by the loads applied to the rigid parts including the weight of these parts.

It will be shown later in the memoir that the deformation that can be sustained by such a block under the applied compression depends only to a small degree on the elasticity modulus of the rubber, and that it is possible to apply to such a block loads, within the extent of crushing of the rubber, that, nevertheless, allows in directions tangential to the lamination, displacements between the two rigid parts by distortion of the rubber that separates them, in the same way as would happen if this rubber was not laminated by the sheets.

The displacements permitted by such a laminated block, interposed between parallel surfaces, correspond mainly to the possibility of two parallel surfaces to slide one versus the other while remaining in contact over all of their extent.

Geometrically, the surfaces that perfectly satisfy this condition are the plane, the surfaces of revolution (including the sphere) and the helicoidal surfaces. Nevertheless, should the movements be limited, other surfaces of more complex geometric definitio can be chosen for the surfaces of the rigid parts, if the approximation of parallelism corresponding to the maximum displacement remains acceptable.

With surfaces that meet the strict requirement of parallelism during the relative displacement, it is possible to obtain the following displacements:

Two parallel fla surfaces allow for translations in all directions in their plane and also rotations around any axis perpendicular to their plane;

Two parallel surfaces of revolution can rotate around their common axis and possibly a translation along this axis if these surfaces are cylinders or portions of a cylinder; in the case of two spheres, the axis of relative rotation is any axis provided it passes through the common center of these two spheres;

Two helicoidal surfaces permit a helical displacement, i.e., the combination of a translation and a rotation.

It was implicitly assumed in the above that the distribution of stresses in the laminated block remained the same during the motion and, therefore, this block is distorted by the deformation of the rubber. One can however also vary the distribution of stresses in the laminated block during the displacement by means of elastic deformation, thus providing additional degrees of freedom. Thus, a prismatic block, laminated parallel to its bases, can allow not only translations parallel to these bases or rotations perpendicular to them, but also rotations with an axial component parallel to the plane of these bases, a rotation which allows a dihedral angle between the planes of these bases. It may facilitate a displacement of this kind by giving to such a prismatic block a rectangular section aligned in the direction of the preferred axis of rotation.

One of the main applications of the invention is the realization of support pads for structures that allow for displacements of these structures by internal causes (expansion) or by external causes (moving structures such as turning or lifting bridges, dam gates, etc.).

For such works the invention allows the substitution for heavy metal components which have machining and maintenance requirements by components that are easy to install, do not need extreme precision in their execution and installation and that will work reliably, even in the absence of maintenance. In addition, the invention allows the realization of high-precision mechanical joints in machines and equipment, especially in

the fiel of machine tools and vehicles, when relative displacements of limited amplitude are required.

The description, which follows regarding the attached drawings, but not limited by these examples, will help to understand how the invention can be realized and describe the features that will emerge in the development of the text, as part of the invention:

Fig. 1 is a schematic for understanding the principle of the invention;
Fig. 2 is a schematic elevation of a bearing conforming to the invention;
Fig. 2a shows the same device after deformation;
Fig. 3 and Fig. 4 illustrate two examples of devices based on the invention;
Fig. 5 and Fig. 6 show schematic cross-sections of devices allowing translations in a single direction;
Fig. 7 and Fig. 7*a* show before and after deformation of a device allowing a rotation about an axis parallel to the plane of lamination;
Fig. 8 and Fig. 9 show elevations of two structures to which are applied devices based on the invention;
Fig. 10 is an axial cross-section of a device based on the invention;
Fig. 11 and Fig. 12 show respectively, in plan and elevation, a device according to the invention allowing helicoidal movement;
Fig. 13 is the elevation of a bearing allowing a limited rotation about a fully determined axis.

We know that certain materials such as natural and artificia rubbers, and many synthetic resins or plastics, can be deformed at virtually constant volume by lengthening or shortening, or distortion, and that these bodies have, for such deformations the property of behaving much like a liquid in terms of transmission of pressure. Such materials also have the facility of adhering to certain surfaces such as steel or concrete, in other words creating on such contact surfaces a strong coefficien of friction that can be increased by gluing or by increasing the roughness of the surfaces in contact.

Consider a parallelepiped block 1 (Fig. 1) of such a material, lying (to simplify the reasoning) between two fla and parallel surfaces 2 and 3, then compressed between these surfaces by a certain force F which moves the surface 2 to 2a and gives block 1 the shape 1a. Calling S the surface of the block, h the shortening and E the elastic modulus of the material, the ratio F/h is not equal to the product SE. Indeed, the material of the block being virtually incompressible, the deformation of this block is only possible by an internal displacement of matter which tends to slide the contact surfaces 2a and 3 and, because of friction, curves the lateral faces of the block. Thus an element of material initially rectangular a, b, c with small slip (smaller if the adherence is stronger) at its ends at the contact surfaces 2a and 3, curves to take the shape a', b', c' and thus develops within the block a centripetal state of stress which depends on friction, and which is proportional to its elongation and inversely proportional to its radius of curvature. This creates in the body of the block a state of stress that gives a resultant pressure p, which varies from zero at the periphery to a maximum value at the center and the

frictional stress on the surfaces a and c, caused by this pressure, also grow with this and reach their maximum value at the center of the block.

The resistance to the flattenin is not SE, but $SE + \Sigma$ and if the smallest dimension in the plane of the block is much larger than its thickness, the second term is much larger than the firs providing the coefficien of friction of rubber on the surface of the rigid parts 2 and 3 is large.

If we assume that the thickness of the block 1 is halved, we see, assuming the same values of friction that the pressure p is doubled since the radius of curvature of element of rubber is divided by two. Moreover, the value p, i.e., friction $p\varphi$ which before was reached at a certain distance ρ from the periphery, is now reached at a distance $\rho/2$ from the same periphery. The pressure in the central zone will therefore be much larger and Σ will be much more than double.

If one considers, instead of a homogeneous rubber block 1, a block formed from two plates of half thickness separated by a sheet of inextensible material with a high coefficien of friction in contact with these plates, the presence of this sheet will have a multiplier effect of at least four in the resistance to deformation of this block compared with the homogeneous composite block.

The division of the block by nine intermediate sheets giving ten equal plates of rubber can also increase the resistance by a factor of more than 100.

This resistance, unrelated to the intrinsic strength of the rubber against compression, can be increased without limit other than the resistance to efforts to stretch the intermediate leaves and the lowering of the coefficien of friction with pressure, which reduction is only obtained under extremely high pressures.

One can create a block of rubber plates, as shown schematically in Fig. 2, separated by 6 thin inextensible sheets 5 with a high coefficien of friction in contact with these plates.

If, as shown in Fig. 2a, there is a relative displacement between parts 2 and 3 in a direction parallel to the lamination, this displacement is produced by deformation over the entire set of 6 plates providing there is adherence between the plates and sheets.

The force which opposes this displacement is always $(SE.d)/e$, where e is the total thickness and d the amplitude of the displacement. It does not matter in fact that the total thickness e is in one or several plates, since the division into plates also modifie equally d and e. Moreover, in the case of a homogeneous block, the value of the force necessary to cause the displacement is bounded in the block by the presence of a marginal zone in which the distortion of the rubber is irregular, while the division into separate plates divides at the same time the width of the marginal zone by the same factor.

To obtain a high coefficien of friction for the rubber plates in contact with the inextensible sheets one could use smooth inextensible sheets and glue their surfaces to the rubber plates. In this case, however, reliability in use will depend to a large extent on the quality and consistency of the gluing and that reliability could disappear under the effect of loss of quality of the glue.

It is therefore preferable to ensure that a bearing has a high coefficien of friction between the plates and the sheets and they have enough roughness between the surfaces of the rubber and the sheets.

To this end, as shown in Fig. 3, the inextensible sheets can be metal gratings formed for example by woven wire or of expanded metal. In the case of wire, it may of interest to

use a grating of forged or welded mesh to avoid slippage of the wires where they contact each other. It may also be useful, as shown in Fig. 4, to use inextensible sheets 8 formed of folded or embossed sheets or sheets punctured by numerous openings of any shape.

However, while the use of sheets glued to the smooth slabs of rubber permits, at least theoretically, the reduction as much as wished in the thickness of these rubber plates, using roughened sheets limits the amount of reduction of the thickness of the rubber plates. It is necessary, indeed, that this thickness is such that it fill the gap between the sheets, even when two of the deepest hollows in the sheets are opposite each other. Therefore, the thickness of the rubber plates must be at least twice the height of the relief of the sheets. To fi ideas, for a sheet with a relief of about 3 mm, the thickness of plates of rubber should be at least 6 mm.

The following example of realization will help to understand the economic benefit of the invention. Consider, in Fig. 8, a bridge deck 9, supported on the abutments 10 and on the intermediate pier, by laminated blocks 12 made in accordance with the invention to allow the free expansion of the bridge deck on its supports. Suppose, to fi ideas, that the load applied to one of the laminated blocks is 100 tons.

If we accept a level of compression (regarded as normal for rubber) of 10 kg/cm^2, the base area of this block 12 should be 10 000 cm^2 or one meter square. If it is assumed, moreover, that the rubber used has a shear modulus also 10 kg/cm^2 and if one imposes a limit to the force to produce a horizontal displacement equal to its thickness, for example, of one tonne per centimeter displacement, this block should have a thickness of 10 cm.

Such a bearing would in principle be satisfactory, but it would be prohibitive both in price and the space it would require.

In contrast, if we replace this solid block of rubber of 100 dm^3 in volume (130 kg) by three plates 0.40 m $\times$ 0.40 m $\times$ 0.006 m, separated by adhering inextensible sheets, the horizontal section of rubber that deforms is reduced in the ratio from 1 to 0.16, and the thickness of deforming rubber is reduced from 10 cm to 1.8 cm, the resistance to deformation in the horizontal direction will be amended in the ratio (0.16 $\times$ 10)/1.8, i.e., it is substantially the same as before. Nevertheless, the resistance to vertical deformations is significantl increased and in particular the weight of rubber used is reduced from 130 kg to 3.700 kg. The value and weight of both the interlayer sheets is negligible because the tensile force to which these sheets are subject is of the order of 500 kg.

Such a device is a laminated component placed between parallel fla surfaces, allowing displacements parallel to the plane of the lamination in any direction and the coefficien of distortion, i.e., the ratio of the displacement reaction to the amplitude of this movement, for a given surface of the plate, decreases as the total thickness of the plates increases.

But one can get coefficient of distortion that are very different in the two directions perpendicular to the plane of lamination by using seat surfaces and intermediate sheets that are not planes.

Thus, in Fig. 5, the support surfaces 2 and 3 are in the form of cylinders and the surfaces between the rubber plates 6 and the sheets 5 are in the form of cylinders parallel to the surfaces 2 and 3. In Fig. 6, the surfaces 2 and 3 are grooved in the direction perpendicular to this figu e and plates 6 and sheets 5 are equally grooved.

Such laminated blocks can obviously permit relative translations on surfaces 2 and 3 in the direction perpendicular to this figu e, but resist translations directed in the plane of this figu e. The transverse stiffness of such connections can be increased as necessary by increasing the height of ribs and corresponding grooves and vice versa. It is thus possible to adjust the coefficien of transverse distortion to any value until the desired rigidity is achieved.

The elastic bearing devices such as shown in Fig. 5 and 6, for example, may fin their application in examples of the kind shown in Fig. 8. One can for example wish to disconnect the transverse reactions to the right of the intermediate pier 11, from the transverse reactions provided by the abutments 10 and the stiffness of the deck 9. To this end, the devices 12 carried on the abutments 10 can be realized as shown on Fig. 5 and Fig. 6, the grooves being oriented in the longitudinal direction of the bridge.

One may also need to add to the freedom of longitudinal and transverse deformation a certain freedom of angular deformation about an axis parallel to the plane determined by these directions of deformation. To do this, as shown in Fig. 7, we can use narrow laminated blocks with a short width l, the length L of which being increased so as to keep the required block area. Such a block can be deformed not only as mentioned above by relative translations of its faces parallel to their plane, but as shown by Fig. 7*b* by pivoting about an axis parallel to the longest dimension of this block.

Rotation around an axis of a preference is obtained using seat surfaces and a lamination of revolution around the desired axis of rotation.

Thus, the bridge 13 shown in Fig. 9 can reposition through the convex cylindrical surface 16 on the concave cylindrical surface 18 of support 15 through a laminated block 17 in the form of a portion of a cylinder similar to that shown in Fig. 5, but which this time, is used for a different purpose.

Such a bridge can open by the action of external forces around the common axis of revolution of the surfaces 16, 17 and 18. However, if one assumes that these surfaces are portions of spherical caps, the bridge can not only open, but also rotate around the vertical axis passing through the common center of these different spheres and, more generally, rotate around any axis passing through the common center. In this case one must accept very high values for the distortion of the rubber and, for example, obtain rotations about 45 degrees with a total thickness of rubber of the order of a third of the radius of the concave surface of the support.

The pivot and the mechanism of opening the deck may be made entirely of standard concrete, without any machined metal part, given the relatively low value of the local pressure. Of course, the center of gravity of the pivoting mass can depend on the choice of the manufacturer either above, below or at the level of the center of the axis of rotation.

Fig. 10 concerns the case where we need to consider only the possibility of rotation about a vertical axis. The rigid part 2 is a convex spherical surface 19 and a cone of revolution 21 and the part 3 includes a concave spherical cap 20 and a conical surface 22 parallel to the surface 21. Between the support surfaces are laminated blocks 23 and 24, the firs in the form of a spherical shell, the second in the form of truncated cone. The thickness of the second is larger than the first Of course, the orientation of the shell and the truncated cone can be inverted between the parts 2 and 3.

As shown in Fig. 11 and Fig. 12, parts 2 and 3 and the laminated block which separates them are arranged to allow a helicoidal motion between these parts (on Fig. 11 and Fig. 12, for clarity, the piece 2 is supposed transparent). The two cylindrical forms have two identical helicoidal support surfaces 25 and 26 with a development of a turn, but are shifted one relative to the other by the angle α.

Between these two helicoids 25 and 26 is a laminated block with the shape of helicoidal plates and helicoidal sheets, parallel to surfaces 25 and 26. The total development of this block is equal to a turn diminished by the angle α, its thickness is such that by deformation of the rubber the two helicoidal surfaces can slide one with respect to the other by the angle α one in one direction and the other in the opposite direction. The two pieces 2 and 3 can thus move one in relation to the other through a relative helicoidal movement of amplitude 2α. A central guide rod 28 (which can be attached to one or the other piece) prevents lateral relative displacements. Such a device may be applied to a press.

Finally, Fig. 13 shows a bearing permitting guided rotation and possibly translation of a limited amplitude along the axis 29. This axle is surrounded by a sleeve 30 of thin rubber layers separated by inextensible sheets. The inextensible sheets may be strips of metal bonded on one side to a layer of rubber rolled tightly around the axle 29. The sleeve thus obtained forms a pad that is held in place by the clamp 31. One can get guidance with virtually no lateral play on the axis 29 by this bearing for a specifie amplitude of rotation and longitudinal translation, since these are essentially determined by the total thickness of rubber used.

It goes without saying that changes may be made to the ways of realizing the examples described above, particularly by substitution of technically equivalent methods, without it affecting the scope of the present invention.

Summary

The present invention includes:

1. A device of elastic connection to at least one degree of freedom between two rigid parts, this device being placed between the substantially parallel surfaces of the rigid parts and taking the form of a block of stacked plates of a material with the nature of rubber between which are inter-layered inextensible sheets whose surfaces have a high coefficien of friction in contact with the rubber plates.
2. The various ways in which device specifie in item 1 can be developed, either separately or in combinations, to provide the following features are:
   a. The laminated block formed by the plates and the inter-layered sheets is compressed perpendicular to the surfaces of these sheets;
   b. The interlayer sheets are metal and include surface roughness;
   c. The inextensible sheets specifie under *b* are gratings;
   d. The sheets specifie in *b* are folded, embossed or perforated sheets;
   e. The parallel surfaces of the rigid parts are planes;
   f. The parallel surfaces of the rigid parts are coaxial surfaces of revolution;

g. The parallel surfaces of the rigid parts are helicoidal surfaces of the same axis and the same pitch;
h. The parallel surfaces of the rigid parts are concentric spherical caps;
i. The parallel surfaces of rigid parts have on one part, at least one rib and on the other at least one groove corresponding to that rib allowing them to nest into one another;
j. The laminated block includes plates and sheets of rectangular shape, of which the length far exceeds the width, with its greatest dimension, directed along an eventual axis of rotation;
k. The laminated block is obtained by the simultaneous winding of a metal strip and a strip of rubber which are bonded to each other around a cylindrical surface.

3. The application of these elastic connections, as specifie in items 1 and 2, to structures that can move with respect to their supports, and especially to bridges, are for the provision of supports allowing expansion, or to allow the displacement of these structures with the help of external forces.
4. The application of these devices of elastic connection, as specifie in items 1 and 2, with mechanical precision to two parts with a view to allow for relative displacements, limited but guided, of the two parts with respect to each other.

References

Anderson, T. L. (1989). "Seismic Isolation for the Los Angeles County Fire Command and Control Facility." *Proceedings of the Structures Congress of the American Society of Civil Engineers*, Vol. 1, pp 615–624. San Francisco, California, May 1–5, 1989.

Bouchon, M. (1988). "Nuclear Spent Fuel Storage Pools on Aseismic Bearing Pads." *Proceedings of the Ninth World Conference on Earthquake Engineering (9WCEE)*, Vol V, pp 533–538. Tokyo-Kyoto, Japan, August 2–9, 1988.

Chalhoub, M. S. and Kelly, J. M. (1987). "Reduction of the Stiffness of Rubber Bearings due to Compressibility." *Report No. UCB/SEMM-86/06*, Department of Civil Engineering, University of California, Berkeley.

Chalhoub, M. S. and Kelly, J. M. (1991). "Analysis of Infinite-Strip-Shape Base Isolator with Elastomer Bulk Compression." *Journal of Engineering Mechanics* (ASCE), **117**(8), 1791–1805.

Constantinou M. C., Kartoum A., and Kelly, J. M. (1992). "Analysis of Compression of Hollow Circular Elastomeric Bearings." *Engineering Structures*, **14**(2), 103–111.

Crockett, J. H. A. (1983). "Early Attempts, Research and Modern Techniques for Insulating Buildings." *Proceedings of the International Conference on Natural Rubber for Earthquake Protection of Buildings and Vibration Isolation*, pp 15–44. Kuala Lumpur, Malaysia, February 22–25, 1982.

Derham, C. J. and Kelly, J. M. (1985). "Combined Earthquake Protection and Vibration Isolation of Structures." *Natural Rubber Technology*, **16**, 3–11.

Derham, C. J. and Waller, R. A. (1975). "Luxury without Rumble." *The Consulting Engineer*, **39**(7), 49–53.

Fuller, K. N. G., Gregory, M. J., Harris, J. A., Muhr, A. H., Roberts, A. D., and Sevenson, A. (1988), "Engineering Use of Natural Rubber." In: Roberts, A. D., ed. *Natural Rubber Science and Technology*, Oxford University Press, New York, New York.

Freyssinet, E. (1954). "Dispositif de liaison élastique à un ou plusieurs degrés de liberté" (translated as "Elastic Device of Connection to One or More Degrees of Freedom"), French patent no. 1.110.285 Class F06 d 25/5/54, Ministry of Industry and Commerce, France.

Freyssinet International (1977). "Congress Centre in Berlin." Freyssinet International, Vol. 159.

Garevski, M., Kelly, J. M., and Bojadziev, M. (1998). "Experimental Dynamic Testing of the First Structure in the World Isolated by Rubber Bearings." *Proceedings of the Eleventh European Conference on Earthquake Engineering*. Paris, France, September 6–11, 1998.

Mechanics of Rubber Bearings for Seismic and Vibration Isolation, First Edition. James M. Kelly and Dimitrios A. Konstantinidis.

Gent, A. N. (1964). "Elastic Stability of Rubber Compression Springs." *Journal of Mechanical Engineering Science*, **6**(4), 318–326.

Gent, A. N. (1990). "Cavitation in Rubber: A Cautionary Tale." *Rubber Chemistry and Technology*, **63**, G49–G53.

Gent, A. N. (2001). "Elasticity." In: Gent A. N., ed. *Engineering with Rubber: How to Design Rubber Components*, 2nd edn, Hanser Gardner, Cincinnati, Ohio.

Gent, A. N. and Lindley, P. B. (1959a). "Internal Rupture of Bonded Rubber Cylinders in Tension." *Proceeding of the Royal Society of London*, Ser. A, **249**, 195–205.

Gent, A. N. and Lindley, P. B. (1959b). "The Compression of Bonded Rubber Blocks." *Proceedings of the Institution of Mechanical Engineers*, **173**(3), 111–122.

Gent, A. N. and Meinecke, E. A. (1970). "Compression, Bending and Shear of Bonded Rubber Blocks." *Polymer Engineering and Science*, **10**(1), 48–53.

Grootenhuis, P. (1983). "Vibration isolation of buildings—some basic principles." *Proceedings of the International Conference on Natural Rubber for Earthquake Protection of Buildings and Vibration Isolation*, pp 1–14. Kuala Lumpur, Malaysia, 1982.

Haringx, J. A. (1949). "On Highly Compressible Helical Springs and Rubber Rods, and Their Application for Vibration-Free Mountings, III." *Philips Research Reports*, **4**, 206–220.

HKS (2001). ABAQUS, Version 6.2 [computer software]. Hibbitt, Karlsson & Sorensen Inc., Pawtucket, Rhode Island.

ICC (2009). *2009 International Building Code* (IBC 2009), International Code Council (ICC), Washington, D.C.

Kamada, T. and Fujita, T. (2007). "Current Status of Seismic Isolation and Vibration Control to Buildings, Cultural Heritage and Industrial Facilities in Japan." *Proceedings of the ASSISi 10th World Conference on Seismic Isolation, Energy Dissipation and Active Vibrations Control of Structures*. Istanbul, Turkey, May 28–31, 2007.

Kelly, J. M. (1991). "Dynamic and Failure Characteristics of Bridgestone Isolation Bearings." *Report No. UCB/EERC-1991/04*, Earthquake Engineering Research Center, University of California, Berkeley.

Kelly, J. M. (1997). *Earthquake-Resistant Design with Rubber*, 2nd edn, Springer-Verlag, London, England.

Kelly, J. M. (2003). "Tension Buckling in Multilayer Elastomeric Bearings." *Journal of Engineering Mechanics* (ASCE), **129**(12), 1363–1368.

Kelly, J. M. and Konstantinidis, D. (2007). "Low-Cost Seismic Isolators for Housing in Highly-Seismic Developing Countries." *Proceedings of the ASSISi 10th World Conference on Seismic Isolation, Energy Dissipation and Active Vibrations Control of Structures.* Istanbul, Turkey, May 28–31, 2007.

Kelly, J. M. and Konstantinidis, D. (2009a). "Steel Shim Stresses in Multilayer Bearings under Compression and Bending." *Journal of Mechanics of Materials and Structures*, **4**(6), 1109–1125.

Kelly, J. M. and Konstantinidis, D. (2009b). "Effect of Friction on Unbonded Elastomeric Bearings." *Journal of Engineering Mechanics* (ASCE), **135**(9), 953–960.

Kelly, J. M. and Takhirov, S. M. (2001). "Analytical and Experimental Study of Fiber-Reinforced Elastomeric Isolators." *Report No. PEER-2001/11*, Pacifi Earthquake Engineering Research Center, University of California, Berkeley.

Kelly, J. M. and Takhirov, S. M. (2004). "Analytical and Numerical Study on Buckling of Elastomeric Bearings with Various Shape Factors." *Report No. UCB/EERC-2004/03*, Earthquake Engineering Research Center, University of California, Berkeley.

Kelly, J. M. and Takhirov, S. M. (2007). "Tension Buckling in Multilayer Elastomeric Isolation Bearings." *Journal of Mechanics of Materials and Structures*, **2**(8), 1591–1605.

Kircher, C. A., Delfosse, G. C., Schoof, C. C., Khemici, O., and Shah, H. C. (1979). "Performance of a 230 KV ATB 7 Power Circuit Breaker Mounted on GAPEC Seismic Isolators." *Report No. JABEEC 40*, The John A. Blume Earthquake Engineering Center, Stanford University, California.

Koh, C. G. and Kelly, J. M. (1987). "Effects of Axial Load on Elastomeric Isolation Bearings." *Report No. UCB/EERC-1986/12*, Earthquake Engineering Research Center, University of California, Berkeley.

Konstantinidis, D., Kelly, J. M., and Makris, N. (2008). "Experimental Investigation on the Seismic Response of Bridge Bearings." *Report No. UCB/EERC-2008/02*, Earthquake Engineering Research Center, University of California, Berkeley.

Lindley, P. B. (1966). "Load-Compression Relationships of Rubber Units." *Journal of Strain Analysis*, **1**(3), 190–195.

Lindley, P. B. (1978). "Engineering Design with Natural Rubber." NR Technical Bulletin, 4th edn, The Malaysian Rubber Producers' Research Association, Brickendonbury, Hertford, England.

McLachlan, N. W. (1955). *Bessel Functions for Engineers*, 2nd edn, Clarendon Press, Oxford, England.

Naeim, F. and Kelly, J. M. (1999). *Design of Seismic Isolated Structures: From Theory to Practice*, John Wiley & Sons, New York, New York.

Plichon, C., Gueraud, R., Richli, M. H., and Casagrande, J. F. (1980). "Protection of Nuclear Power Plants against Seism." *Nuclear Technology*, **49**(2), 295–306.

Postollec, J.-C. (1982). "Les Fondations Antisismiques de la Centrale Nucléaire de Cruas-Meysse." *Travaux*, No. 569, September, pp 75–83.

Prager, W. and Hodge, P. G. (1951), *Theory of Perfectly Plastic Solids*, John Wiley & Sons, New York, New York.

Renault, J., Richli, M., and Pavot, B. (1979). "Première Application des Appuis Anti-Sismiques à Friction: La Centrale Nucléaire de Koeberg" (translated as "First Application of Antiseismic Friction Bearings: Koeberg Nuclear Plant"). *Annales de l'Institut Technique du Bâtiment et des Travaux Publics*, No. 371, pp 69–90.

Rocard, Y. (1937). "*Note sur le Calcul des Propriétès Élastique des Supports en Caoutchouc Adhérent*" *Journal de Physique et de Radium*, **8**, 197–203.

Snowden, J. C. (1979). "Vibration Isolation: Use and Characterization." *NBS Handbook 128*, U.S. National Bureau of Standards, Washington, DC.

Taniwangsa, W., Clark, P. W., and Kelly, J. M. (1996). "Natural Rubber Isolation Systems for Earthquake Protection of Low-Cost Buildings." *Report No. UCB/EERC-95/12*, Earthquake Engineering Research Center, University of California, Berkeley.

Tarics, A. G., Way, D., and Kelly, J. M. (1984). "The Implementation of Base Isolation for the Foothill Communities Law and Justice Center." *Report to the National Science Foundation and the County of San Bernardino*, Base Isolation Consultants Inc., San Francisco, California.

Terashima, N. and Miyazaki, M. (2001). "Design Example of Base-Isolated Artificia Ground." *Kenchiku-Gijutsu*, 172–175 (in Japanese).

Timoshenko, S. P. and Goodier, J. N. (1970). *Theory of Elasticity*, 3rd edn, McGraw-Hill, New York, New York.

Tsai, H.-C. and Kelly, J. M. (2002). "Stiffness Analysis of Fiber-Reinforced Rectangular Seismic Isolators." *Journal of Engineering Mechanics* (ASCE), **128**(4), 462–470.

Tyler, R. G. (1991). "Rubber Bearings in Base-Isolated Structures: A Summary Paper." *Bulletin of the New Zealand National Society for Earthquake Engineering*, **24**(3), 251–274.

Walters, M. T., Honeck, B., and Elsesser, E. (1995). "Use of Seismic Isolation in New and Retrofi Construction." *Proceedings of the Joint ASME/JSMR Pressure Vessels and Piping Conference*, pp 221–228. Honolulu, Hawaii, July 23–27, 1995.

Weisstein, E. W. (2002). *CRC Concise Encyclopedia of Mathematics*, 2nd edn, Chapman & Hall/CRC, Boca Raton, Florida.

Yang, T. Y., Konstantinidis, D., and Kelly, J. M. (2010). "The Influenc of Isolator Hysteresis on Equipment Performance in Seismic Isolated Buildings." *Earthquake Spectra*, **26**(1), 275–293.

Youssef, N. (2001). "Viscous Dampers at Multiple Levels for the Historic Preservation of Los Angeles City Hall." *The Structural Design of Tall Buildings*, **10**(5), 339–350.

Photograph Credits

The authors are grateful for permission to reproduce photographs for the following fig res.

1.1 By Hans-Georg Weimar. License: Creative Commons Attribution Version 2.0 Germany. Accessed November 19, 2010, http://commons.wikimedia.org/wiki/File:ICC_Berlin_pixelquelle.jpg.
1.2 Reproduced by permission of Freyssinet, Inc.
1.3 Courtesy of James M. Kelly. NISEE Online Archive, University of California, Berkeley.
1.4 Courtesy of James M. Kelly. NISEE Online Archive, University of California, Berkeley.
1.5 Courtesy of James M. Kelly. NISEE Online Archive, University of California, Berkeley.
1.6 Courtesy of James M. Kelly. NISEE Online Archive, University of California, Berkeley.
1.7 Courtesy of James M. Kelly. NISEE Online Archive, University of California, Berkeley.
1.8 Courtesy of James M. Kelly. University of California, Berkeley.
1.9 By Brion Vibber. Licensed: Creative Commons Attribution-Share Alike 1.0 Generic license. Accessed December 21, 2010, http://upload.wikimedia.org/wikipedia/commons/4/48/Los_Angeles_City_Hall_%28color%29_edit1.jpg.
1.10 Courtesy of James M. Kelly. University of California, Berkeley.
1.11 Courtesy of Ian D. Aiken. SIE, Inc.
1.12 Courtesy of James M. Kelly. University of California, Berkeley.
1.13 Courtesy of James M. Kelly. University of California, Berkeley.
1.14 Courtesy of James M. Kelly. University of California, Berkeley.

Mechanics of Rubber Bearings for Seismic and Vibration Isolation, First Edition. James M. Kelly and Dimitrios A. Konstantinidis.

Author Index

Mechanics of Rubber Bearings for Seismic and Vibration Isolation, First Edition. James M. Kelly and Dimitrios A. Konstantinidis.

Subject Index

Mechanics of Rubber Bearings for Seismic and Vibration Isolation, First Edition. James M. Kelly and Dimitrios A. Konstantinidis.